Synthesis of ligands for self-assembly of discrete metallo-supramolecular complexes

Dissertation

zur

Erlangung des Doktorgrades (Dr. rer. nat.)

der
Mathematisch-Naturwissenschaftlichen Fakultät

der

Rheinischen Friedrich-Wilhelms-Universität Bonn

vorgelegt von

Sophie Hytteballe

aus

Svendborg, Dänemark

Bonn, Juni 2014

Angefertigt mit Genehmigung der Mathematisch-Naturwissenschaftlichen Fakultät der Rheinischen Friedrich-Wilhelms-Universität Bonn

1. Gutachter: Prof. Dr. Arne Lützen

2. Gutachter: Prof. Dr. Sigurd Höger

Tag der Promotion: 19. März 2015

Erscheinungsjahr: 2016

Abstract

Different aspects of self-assembly and self-sorting of metallo-supramolecular have been investigated in this thesis. Starting with self-sorting, four different 9,9'-spirobifluorene derivatives substituted with pyridine were synthesized as racemates as well as in enatiomerically pure form and used to investigate self-discrimination and self-recognition during the assembly of two different rhombic systems consisting of two ligands and two metal ions; Pd- or Pt-corner (M_2L_2). The two systems differ in the lengths of the spacer between the spirobifluorene and the metal-binding pyridine, the smaller one having no spacer and the long one having an ethynylspacer.

For the ligand with the shorter spacer a crystal structure of the homochiral complex was obtained, confirming the preference for self-recognition of the system, which was also observed in the NMR- and mass spectra. In the case of the larger ligand no self-sorting behavior was observed. The ability of the larger ligand to form a catenane was established by mass, ^{1}H-NMR-spectroscopy and crystallography.

The small spirobifluorene based ligand was used with Pd(II)to form a M_6L_{12}-sphere, and several attempts were made to confirm the presence of the M_6L_{12}-species. A smaller M_2L_4-cage was formed with a third synthesized spirobifluorene derivative and confirmed by mass spectroscopy.

Two ligands with both a soft and a hard metal-binding site were synthesized and used in complexation experiments with Ti(IV), Pd(II) and Pt(II) in order to obtain a self-assembled supramolecular multicomponent complex. We succeeded in performing the first complexation steps with both ligands, preparing for the final complexation event.

Lastly, a ligand based on a thiophene core with bipyridine as the metal binding unit was synthesized and tested for its ability to form a triple helix with Fe(II) and undergo spin crossover.

Acknowledgement

This thesis would not have come to completion without the help and support of a special group of people.

Firstly, I would like to thank my advisor Prof. Dr. Arne Lützen for giving me the opportunity to do my thesis in his group and for support and advice throughout the completion of my thesis.

I also want to thank Prof. Dr. Höger, Prof. Dr. Mader and Prof. Dr. Steffens for accepting the task of being the opponents for my dissertation.

The mass measurements would not have been possible without the help of both Dipl. Chem. Rainer Hovorka and Dipl. Chem Yvonne Lorenz, who have spent days, nights and weekends measuring, evaluating and discissing the results.

For the crystallization and measurements of my at times very extensives complicated complexes, I would like to thank both Dipl. Chem. Georg Meyer-Eppler and Prof. Dr. Kari Rissanen. Dr. Gregor Schnakenburg, M. Sc. Filip Topic and Charlotte Rödde have my gratitude for the measurements of the crystal structures of the ligands.

For the measurement of standard NMR-spectra I would like to thank Claus Schmidt, Ulrike Weynand and Hannelore Spitz. Marianne Engeser and the department for mass spectrometry are thanked for the measurements of standard mass spectra.

For the possibility to perform light scattering measurements I would like to thank Prof. Dr. Carsten Schmuck. Also, special thanks go to Dipl. Chem. Patryciusz Piotrowski, who took the time needed to introduce and perform the dynamic light scattering-measurements with me.

The members of the Lützen group have played a very important part in the years of my thesis. I would like to thank Dipl. Chem. Christopher Kremer for great discussions in the laboratory, both scientific and non-scientific. Also, I would like to thank Dr. Christoph Gütz for his commitment and helpfulness. My lab colleagues Dipl. Chem. Kim Hintze, Dipl. Chem. Tatiana Rothe and Dipl. Chem. Verena Göker deserve my gratitude for creating a great atmosphere in the lab. Also, thanks to Dipl. Chem. Christian Benkhäuser and Dr. Andreas Osadnik for great discussions in the office during the last months of my thesis.

The coffee breaks would not have been the same without Dr. Andrea Liesenfeld, Dr. Anke Laures, Dipl. Chem. Lea Küchler, Dipl. Chem. Caroline Stobe and M.Sc. Martin Berg. Dominik Müller is thanked for his great storytelling abilities

A special thanks goes out to Dr. Ivonne Wallmann, who has supported me during difficult times, and who was always ready to distract me with food and wine.

Last but definitely not least, I would like to thank my family and especially my parents, without whom I would not have gotten so far in life.

“Problems worthy of attack prove their worth by fighting back.”

Piet Hein

Publication List:

Rainer Hovorka, Georg Meyer-Eppler, Torsten Piehler, Sophie Hytteballe, Marianne Engeser, Filip Topic´, Kari Rissanen, Arne Lützen, "*Unexpected Self-Assembly of a Homochiral Metallosupramolecular M_4L_4 Catenane"*
Chem. Eur. J. **2014**, *20,* 13253 – 13258*, [DOI: 10.1002/chem.201403414]*

R. Hovorka, S. Hytteballe, T. Piehler, G. Meyer-Eppler, F. Topić, K. Rissanen, M. Engeser, A. Lützen, *"Self-assembly of metallosupramolecular rhombi from chiral concave 9,9'-spirobifluorene-derived bis(pyridine) ligands"*
Beilstein J. Org. Chem, **2014***, 10,* 432-441, *[DOI:10.3762/bjoc.10.40]*

N. Dalla Favera, U. Kiehne, J. Bunzen, S. Hytteballe, A. Lützen, C. Piguet, *"Intermetallic Interactions Within Solvated Polynuclear Complexes: A Misunderstood Concept"*
Angew. Chem. **2010**, *122*, 129-132, *[DOI: 10.1002/ange.200904614]*

Angew. Chem. Int. Ed. **2010**, *49*, 125-128*. [DOI: 10.1002/anie.200904614]*.

Presentations:

S. Hytteballe, *"Trögers Twist, Selbstorganisierende Helikate" Doktorandenworkshop SFB 624*, Bad Honnef, **17.06.2010**

S. Hytteballe, *"Heteronuclear Metal complexes"Arbeitsgruppentreffen Albrecht, Engeser, Lützen, Schalley*, Rursee, **13.09-15.09.11**

Poster presentations:

S. Hytteballe, U. Kiehne, N. Della Favera, C. Piguet, A. Lützen
"Synthesis and self-assembly of Tröger´s Base derived bis(bipyridyl) ligands"
EuChemMS, Nürnberg, 29.08.-02.09.**2010**

S. Hytteballe, U. Kiehne, N. Della Favera, C. Piguet, A. Lützen
"Synthesis and self-assembly of Tröger´s Base derived bis(bipyridyl) ligands"
ORCHEM, Weimar, 13.-15.09.**2010**

C. Gütz, S. Hytteballe, L. Küchler, A. Lützen
"Self-assembly of chiral metallosupramolecular aggregates"
SFB 624 Symposium, Bonn*,* 22-23.09.**2011***,*

S. Hytteballe, T. Piehler, R. Hovorka, A. Lützen
"Self-assembly of polynuclear supramolecular metal-complexes containing pyridine-ligands"
EuCheMS, Prag, 26.-30.08 **2012**

Index

Abbreviations

ALOX	= aluminum oxide
BINOL	= 1,1'-bi-2-naphthol
COSY	= correlation spectroscopy
CPDIPS	= [(3cyanopropyl) diisopropylsilyl]-acetylene
D	= diffusion coefficient
DLS	= dynamic light scattering
DNA	= deoxyribonucleic acid
DMF	= dimethylformamide
DMSO	= dimethyl sulfoxide
DOSY	= diffusion ordered spectroscopy
dppf	= 1,1'-bis(diphenylphosphino)ferrocene
dppp	= 1,3-bis(diphenylphosphino)propane
EDTA	= ethylenediaminetetraacetic acid
EI	= electron ionization
ESI	= electrospray ionization
FT	= fourier transformation
h	= hours
HETTAP	= heterochiral terpyridine and phenanthroline complex formation
ICR	= ion cyclotron resonance
IRMPD	= infrared multiphoton dissociation
NMR	= nuclear magnetic resonance
MOM	= methoxymethyl ether
MS	= mass spectrometry
RT	= room temperature
SCO	= spin crossover
$T_{½}$	= transition temperature
TBAF	= tetra-*n*-butylammonium fluoride
Tf	= triflate
THF	= tetrahydrofurane
TIPS	= triisopropylsilyl
TLC	= thin layer chromatography
TMS	= trimethylsilyl
TOF	= time-of-flight
UV	= ultraviolet

1 Introduction

Organic chemistry is centered on carbon-atoms and the covalent bonds they form, but its concepts are not able to describe the bonding observed in inorganic complexes such as hexol (($[Co(NH_3)_4(OH)_2]_3Co(SO_4)_3$) to its full extent. Until the late 19th century, chemists had been struggling to explain the difference in bonding behavior of the chloride anions of $Co(NH_3)_6Cl_3$ and $Co(NH_3)_5Cl_3$. When treated with aqueous silver nitrate, three chloride ions of $Co(NH_3)_6Cl_3$ could be precipitated as silver chloride, whereas only two chloride ions could be precipitated from $Co(NH_3)_5Cl_3$.[1] In 1893 Alfred Werner presented his theory suggesting that despite cobalt's valence of three, six ammonia or water molecules were bound directly to the metal in an octahedral fashion. Removing one ammonia molecule from $[Co(NH_3)_6]Cl_3$ resulted in one chloride-ion taking its place as a metal ligand resulting in $[Co(NH_3)_5Cl]Cl_2$. Alfred Werner spent the rest of his career proving his theory experimentally and eventually received the Nobel Prize in chemistry in 1913.[1,2]

The theory of Alfred Werner revolutionized inorganic chemistry and laid the basis for the development of coordination chemistry, which by now has advanced into an interdisciplinary science connecting organic chemistry and biochemistry with inorganic chemistry. One of the resulting disciplines is supramolecular chemistry, which combines organic ligands and transition metals to form large non-covalently bound architectures.[3]

Supramolecular chemistry was first described by J.M. Lehn in 1978, who defined it as the "chemistry of molecular assemblies and of the intermolecular bond".[4] Starting with the accidental synthesis of dibenzo[18]crown-6 and the subsequent discovery of its ability to bind potassium ions by Pedersen,[5] supramolecular chemistry has undergone an enormous development and has become an important area of chemical research,[6,7] spanning areas such as molecular informatics, artificial molecular machines, and catalysis.[8–11]

Metal-ligand bonds play an important role in the assembly of supramolecular entities, together with other non-covalent bonds. Hydrogen bonds, π-π-stacking and hydrophobic effects, to only mention a few, all help assemble and stabilize a non-covalent association of two molecules into a supramolecular structure.[12] Even though non-covalent bonds are generally much weaker than covalent bonds, the number of bonds stabilizes the assembly while allowing it to be dynamic in its response to changes in the environment.[3,12]

The ability to stabilize yet render space for adaptability is the reason that supramolecular interactions are wide spread in nature and are the basis of the evolution of life. Without the formation of micelles and membranes and the resulting compartmentalization of eukaryotes, life as we know it would not have been possible.[13] Many cellular components such as

enzymes, DNA and microtubules form via self-assembly and depend on the dynamic nature of supramolecular chemistry.[14] The advantages of cellular machinery based on non-covalent bonds are many, for instance the energy needed to form and break non-covalent bonds is much lower than the corresponding energies for covalent bonds. Such abilities are highly sought after when chemists design new artificial products, which is why chemists often turn to nature for inspiration and nature has many stories to tell.

The DNA-strand is the carrier of gene information and is itself a supramolecular aggregate. The assembly of two single stranded DNA molecules into a supramolecular double helix relies not only on hydrogen bonding between the base pairs (through Watson-Crick base pairing) but also on hydrophobic forces. These forces keep the base pairs in the center of the helix while leaving the charged phosphate groups on the outside. When adding two complementary DNA-strands to an aqueous solution they will self-assemble into a stable double helix. The strands can be separated or denatured by heating the solution, yet upon cooling the strands will self-assemble again.[15] The self-organization and the reversibility of the process form the basis of storage and replication of genetic information.

Another important part of the cell's machinery are the enzymes, which are made out of one or more strands of amino acids that are bent into the specific shape by the use of a mixture of disulfide bonds, hydrogen bonding, dispersion forces, and hydrophobic effects. In many cases the functional enzyme consists of several subunits of proteins which are held together by non-covalent forces. Out of many possible forms an enzyme with the correct amino acid sequence under the right conditions always reaches its functional or native state. Due to the dynamic and reversible nature of non-covalent forces the enzyme is able to run through the different possible conformations without getting stuck in a local minimum. When correctly folded, the enzyme can exhibit a remarkable selectivity towards a singular biomolecule catalyzing a specific reaction yielding only one regio - and/or stereoisomer again by supramolecular forces. By heating a human enzyme or changing the pH of its environment, the enzyme can be denatured and lose its function. However, when restoring the optimal conditions, the enzyme will often renature and regain its function.[15]

An example of an enzyme catalyzing such a regioselective reaction is human chymotrypsin, a serine protease found in the digestive tract. Chymotrypsin catalyzes the cleavage of peptide bonds specifically after large hydrophobic side-chains. The active site of the enzyme is equipped with a serine (Ser 195), an asparagine (Asp 102), and a histidine (His 57) which form the active triad, which is the site where the peptide bond is cleaved. Moreover, chymotrypsin has a hydrophobic pocket near the active site perfectly engineered to accommodate aromatic side chains of amino acids such as phenylalanine, trypsin or tryptophan or large hydrophobic groups such as methionine.[16] Nature has designed chymotrypsin to fulfill one specific task: to hydrolyze peptide bonds after specific amino acids. Supramo-

lecular chemistry attempts to transfer the abilities seen in molecular machines to synthetic systems able to perform functions not previously available outside the biological realm.[17]

1.1 Essential Structural Understanding

Cooperativity can be described as the effect when the binding of one ligand to a receptor influences the binding of the next ligand.[18] This effect is wide spread in nature, and can be divided into positive and negative cooperativity. Positive cooperativity arises when binding of one ligand to an acceptor with multiple binding sites increases the affinity of the acceptor for a second ligand. In the case of negative cooperativity, binding of one ligand leads to decreased binding affinity for subsequent ligands.[14] An example of positive cooperativity in nature is the binding of oxygen to hemoglobin. Able to bind four molecules of O_2 per hemoglobin, binding of one O_2 induces an allosteric change in the other binding sites, increasing the affinity of the protein for the next O_2-molecule. Due to cooperative binding hemoglobin is able to transport 1.7 times the amount of O_2 compared to non-cooperative binding.[14]

The metal-ligand bonds in supramolecular assemblies can also be examined for their ability to show cooperativity. When Lehn and coworkers examined a supramolecular assembly system consisting of two tridentate tris-bipyridine ligands and three Ag(I)-ions forming a double helix, they came to the conclusion that the assembly showed positive cooperativity.[19] This result was rather surprising since one would expect the repulsive forces of the charged metal-ions as well as the interligand repulsion in the complex to have a negative influence on the formation of the helix. About ten years later Ercolani was able to refute the results by Lehn using the site binding model, which clearly separated the intermolecular and intramolecular processes of self-assembly.[18] However, Piguet *et al*. discovered an attractive intermetallic interaction related to the solvation energy ($\Delta E_{exp,sol}^{CuCu}$), when trying to fit the experimental data of Lehn's helix-system to the site binding model indicating that positive cooperative effects are not impossible in multimetallic complexes.[20] Further examinations of this effect prompted the need for a system where only the intermetallic distance changed, such as the Tröger's Base derivatives synthesized by Lützen *et al.* (Figure 1.1).[21,22]

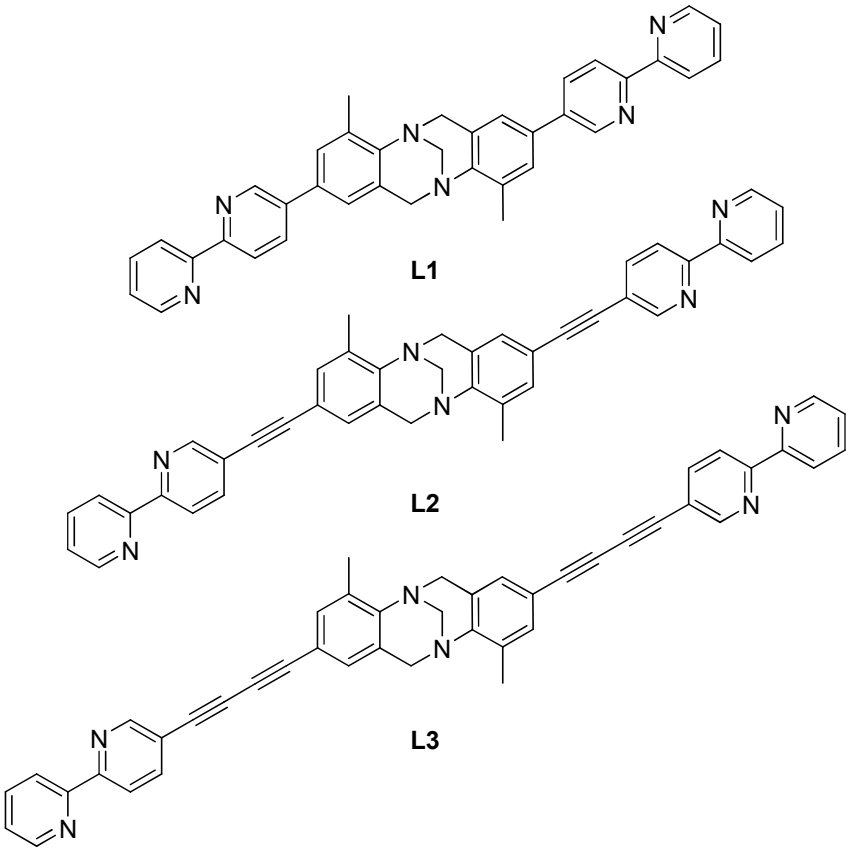

Figure 1.1 Tröger's Base derivatives synthesized by Lützen et al. for helicate complexes.

In cooperation with Piguet and coworkers measurements of the effective concentration of the helices formed by **L1**, **L2** and **L3** with Ag(I) or Cu(I) by UV-titration were performed which indicated a very high degree of preorganization. In fact the effective concentration for the complex formed by Cu(I) and **L1** is the largest reported to date for a helix. A much more interesting and counterintuitive result is that when the intermetallic distance in the helices increases, the intermetallic repulsion increases as well. The result is that the complex formed by **L1** is more stable than the one formed by **L3**. By taking not only the coulombic contribution into account, as in the gas phase, but also the solvation energies represented by the Born equation produces Equation 1.1 which correlates the difference in intermetallic interactions between the ligands $\left(\Delta E^{M,M}_{\mathbf{Lk},\,sol}\text{-}\Delta E^{M,M}_{\mathbf{L1},sol}\right)$ and is able to reproduce the results obtained by UV-titration.[23]

$$\Delta E^{M,M}_{\boldsymbol{Lk},sol} - \Delta E^{M,M}_{\boldsymbol{L1},sol} = \Delta\Delta G^{\boldsymbol{L1},\boldsymbol{Lk}}_{Coulomb} + \Delta\Delta_{solv} G^{\boldsymbol{L1},\boldsymbol{Lk}}_{Complex} + 2\Delta\Delta_{solv} G^{\boldsymbol{L1},\boldsymbol{Lk}}_{ligand}$$

*Equation 1.1: Difference in intermetallic interactions between ligands **L1** and **L**k (k=2,3), where the term $\Delta\Delta G^{\boldsymbol{L1},\boldsymbol{Lk}}_{Coulomb}$ describes the difference in formation free energies for the complexes between ligand **L1** and **L**k (k=2,3), the term $\Delta\Delta_{solv} G^{\boldsymbol{L1},\boldsymbol{Lk}}_{Complex}$ decribes the difference in solvation free energies of the complex when the ligands are increasing in size from **L1** and **L**k (k=2,3) and the term $2\Delta\Delta_{solv} G^{\boldsymbol{L1},\boldsymbol{Lk}}_{ligand}$ describes the difference in solvation free energies for the free ligands **L1** and **L**k (k=2,3).*

So not only does the solvation energy play a role in the self-assembly of the helices synthesized by Lützen, it actually dominates coulombic effect when elongating the spacer between the Tröger's Base and the metal-binding unit from **L1** to **L3**.

Understanding the forces that control the self-assembly of supramolecular entities can help explain why systems, that are very similar on a molecular level, behave differently on a macroscopic level. In the end, this could take supramolecular chemistry towards successful design and engineering of functional aggregates.

2 Scope of the thesis

The goal of the thesis is to reach a better understanding of supramolecular forces which govern the different functionalities displayed by supramolecular aggregates.

It is possible to form helices diastereoselectively using chiral ligands. However, helices can also bear intrinsic properties not exhibited by the uncomplexed ligands. Examples of this could be host-guest-recognition, catalysis, or change of electronic characteristics. Among the latter is the phenomenon of spin crossover, which describes the change in spin state of a metal-ion when subjected to change in pressure or temperature. Spin crossover can also be facilitated by distortion of the ligand field of the metal using rigid ligands. Part of this thesis focuses on the synthesis of ligands able to bind Fe(II) in a distorted octahedral ligand field and examination of the spin crossover abilities of the resulting complexes.

Using one ligand with one metal-ion can only result in a limited number of supramolecular structures and further restricts the complexity of the architectures of the assemblies. If instead a multicomponent system is used with more than one ligand of more than one metal ion, it is possible to form different complex structures using the same components simply by changing the solvent or the counterion. The synthesis of such a multicomponent system is a target of this thesis.

Another interesting feature of certain self-assembled systems is their ability to display self-sorting and discriminate between ligands, which differ either in their structure or chirality. Part of this thesis therefore aims atthe synthesis and investigation of M_2L_2-systems, which are able to discriminate between different enantiomers of the same ligand. Starting from M_2L_2-complexes, the next step is to increase the size of the complex, aiming at producing M_2L_4- and M_6L_{12}-complexes.

Different ligands adapted to the desired complexation approach according to modeling studies will be synthesized and tested for their ability to form complexes as mentioned above. NMR- and mass spectroscopy will be used to identify the formed complexes.

3 Spin crossover

3.1 Background

Similar to biological multicomponent systems, supramolecular self-assembled aggregates can bear functions not seen for the separate components. An example is the catalytic activity displayed by supramolecular cages,[24] another is the occurrence of spin crossover (SCO) in supramolecular entities.[25–27]

Spin crossover was first described by Cambi and Malatesta in 1937 when they examined a Fe(II)-complex.[28] The fact that a Fe(II)-complex was the center of the discovery of the SCO-phenomenon is very indicative of the importance of Fe(II) in the field. Although complexes of many first row d^4-d^7-configured transition metals are able to display SCO in an octahedral ligand field, the most examples are found with complexes with d^6 Fe(II). Due to the relatively high spin pairing energy (compared to other d^6-ions) the high spin configuration of Fe(II) is more accessible (Figure 3.1).[29] The difference between the spin pairing energy and the ligand field splitting energy in a given complex determines whether SCO occurs or not.

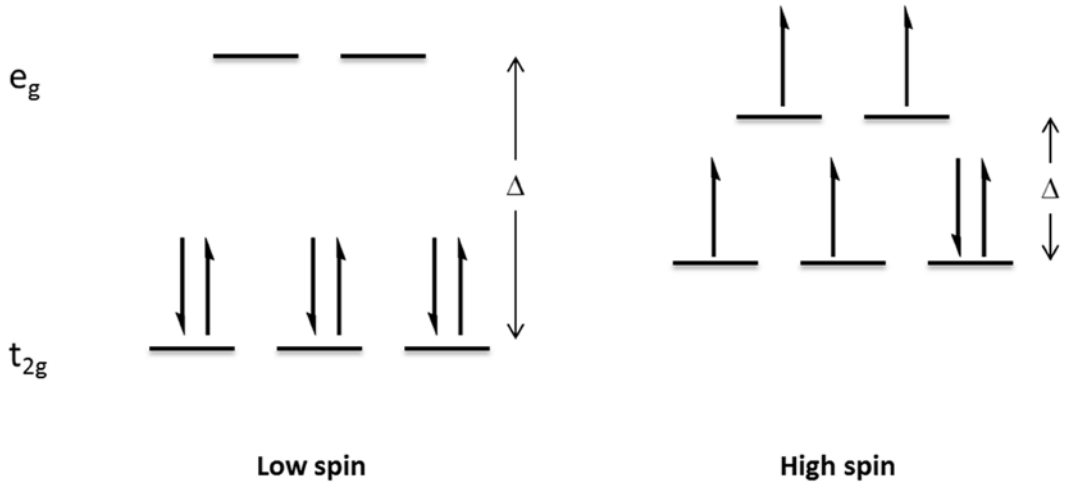

Figure 3.1 Diagram of the electronic configuration in the low spin and high spin state in an octahedral ligand field

As shown in Figure 3.1, the transition from low spin (LS) to high spin (HS) in an octahedral ligand field results in the transfer of two electrons from the t_{2g} to the e_g atomic orbital. This shift of electrons results in a series of electronic and macroscopic changes. The most obvious is the color change which accompanies the transition between the spin states and which can be very significant in Fe(II)-complexes. It is a simple method to determine whether SCO has happened or not. Another effect of the SCO is the change in magnetic behavior of the complex. In the low spin configuration all electrons are paired and the mol-

ecule is therefore diamagnetic. When the high spin configuration is obtained the complex becomes paramagnetic due to the four unpaired electrons. The population of the antibonding e_g-orbitals is also the origin of another effect of the SCO, the increase of the molecular volume through elongation of the metal-ligand-bond.[29]

However, if the energy needed to pair two electrons in one orbital (pairing energy) is lower than the energy required to push one electron into the higher orbital (field splitting energy) SCO will not occur. Different methods changing external factors can be used to facilitate the spin transfer and decrease the difference between the pairing and field splitting energy. Adding extra energy by raising the temperature can in some cases induce a SCO from low spin to high spin. Since the low spin state has a shorter metal-ligand distance than the high spin state, increasing the pressure stabilizes the low spin configuration. Lastly steric effects can help distort the ligand field, destabilizing the low spin configuration.[29]

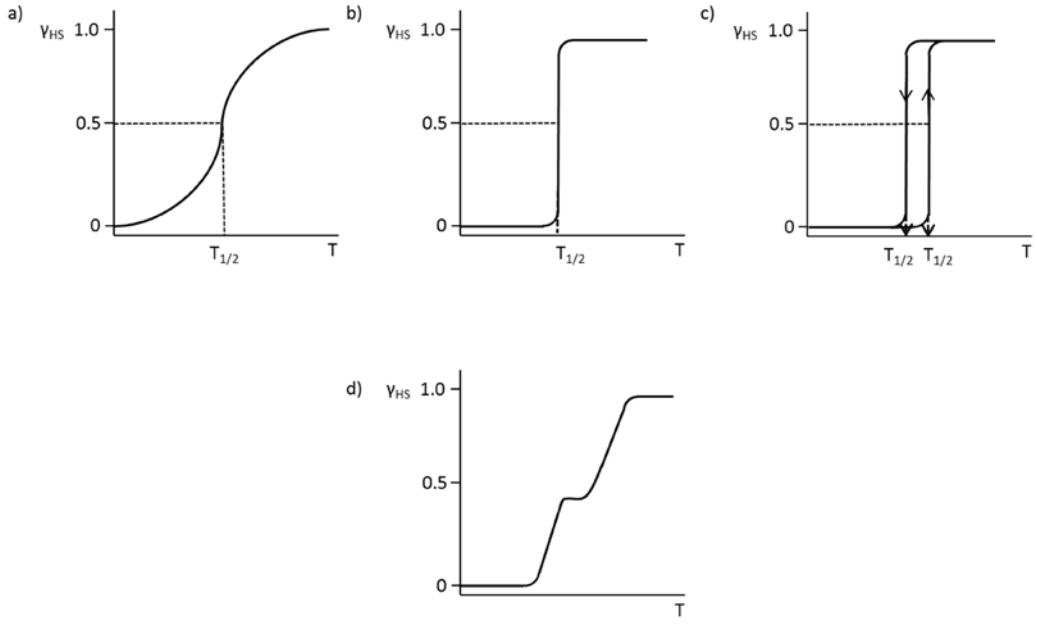

Figure 3.2 Different types of spin transition curves a) gradual b) abrupt c) with hysteresis d) two-step. The high-spin fraction (γ_{HS}) is depicted on the y-axis, the temperature is on the x-axis.

When measuring the SCO, the changes in magnetism and volume are exploited. The change from dia- to paramagnetic can be followed using magnetic susceptibility ($\chi(T)$), a proportionality constant describing the magnetization of the complex in response to a magnetic field, versus temperature. This results in spin transition curves such as those shown in Figure 3.2. The fraction of high spin (γ_{HS}) is calculated from the magnetic susceptibility and is plotted on the y-axis versus the temperature on the x-axis.[29]

The temperature at which the fraction of high spin to low spin is 0.5 is called the transition temperature ($T_{½}$) and describes the thermal dependence of an SCO-system. The most

common type of transition curve is the gradual transition shown in Figure 3.2a. A gradual transition indicates that the cooperativity between the metal centers is low, i.e. the spin transition in one complex does not or hardly affect the neighboring complex. A high cooperativity results in an abrupt spin transition curve, as shown in Figure 3.2b. Hysteresis occurs if the complex can be brought back to its original spin state at two different transition temperatures (Figure 3.2c), as a consequence of very high cooperativity. This cooperativity can be a result of covalent bonds between the metal centers, the formation of hydrogen bonds or π-π-stacking effects. The bistability of compounds of this type is very important when considering application of supramolecular complexes exhibiting SCO. Another important phenomenon within SCO is the stepwise spin transition as shown in Figure 3.2d. This kind of stepwise SCO is often seen in dinuclear complexes, where the transition to high spin of one metal-center stabilizes the low spin configuration of the other metal-center in the complex.[29]

Bistability or even tristability, as seen in complexes with a two-step transition curve, is the basis for the application of SCO-compounds in information storage.[30,31] Other applications for compounds able to undergo SCO, include switching devices, displays and temperature sensors.[30–32]

By combining the SCO-concept with supramolecular chemistry, capabilities typical for supramolecular assemblies can influence the SCO-properties and help fine tune the transition temperature. An example of this behavior is the tetrahedral capsule synthesized by Nitschke *et al*.; Mixing a tripodal imine-ligand with Fe(II) resulted in the formation of a tetrahedral supramolecular capsule, which can undergo SCO and encapsulate different guest molecules such as Br^- and CS_2. Addition and encapsulation of the guest molecules caused a small stabilization of the high spin state of the complex.[26] Batten and coworkers were able to form a supramolecular nanoball, which packs inefficiently in solid state leaving interstitial cuboctahedral cavities in the crystal lattice which can be occupied by different solvents. The nanoporous material is able to respond to temperature changes and irradiation and with SCO. Furthermore, the nature of the solvent has a great impact on the spin transition from broadening to complete loss of SCO-behavior.[33] Hannon *et al*. were able to form a triple helical cylinder complex with Fe(II), which display full spin transition curves when combined with the anions PF_6^- and BF_4^-. When ClO_4^- is used as anion, the two metal centers in the complex become non-equivalent and the result is a two-step spin transition curve indicating a stable HS-LS-state.[27]

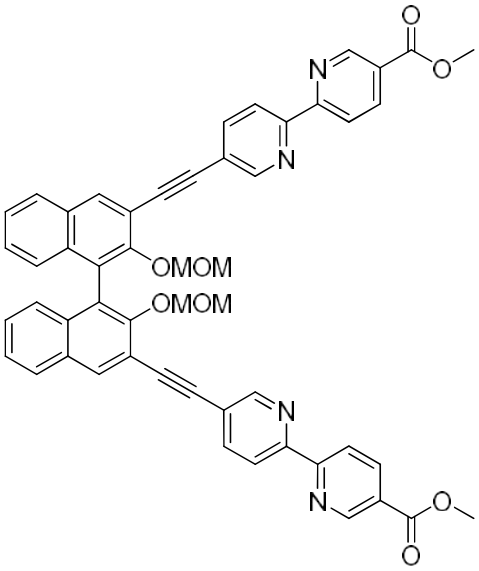

Figure 3.3 SCO-ligand synthesized by Bunzen

In our own group, Dr. Jens Bunzen observed the formation of a high spin complex when mixing the enantiomerically pure ligand (both (*R*) or (*S*)) in Figure 3.3 with Fe(II) in CD_2Cl_2/DMSO-d_6 (3:1). Instead of a red/brown solution typical for low spin Fe(II)-complexes the solution turned green indicating a high spin complex. This observation was confirmed by ^{1}H-NMR-spectroscopy and mass-spectroscopy, which suggested the formation of an M_2L_3-complex with Fe(II). Changing the solvent to CD_2Cl_2/CD_3CN (3:1) resulted in a red solution of the low spin complex.[34] The electron withdrawing carboxymethyl-group combined with the rigid angle induced by the BINOL therefore seemed capable of distorting the ligand field of the Fe(II)-ion resulting in a high spin complex.

3.2 Synthesis of the ligands

The goal is to develop a system able to participate in spin crossover and which, ideally, undergoes hysteresis. The ligand synthesized by Bunzen forms a high spin complex with Fe(II), however, it does not exhibit hysteresis. Nevertheless, we were hoping to be able to design a library of ligands based on the BINOL-ligand.

We decided to keep the metal binding 5-carboxymethyl-5'-ethynyl-2,2'-bipyridine in our series of ligands using the synthesis previously performed by J. Bunzen.[34] However instead of BINOL, simpler and cheaper core units would be used, since a large, enantiomerically pure core is not necessary for the SCO to occur.

The central unit connecting the substituted bipyridines is expected to induce an angle between the two metal binding sites of the ligand, that could potentioally distort the ligand field of the metal to such an extent, that the metal would adopt the high spin configuration.

Just like the ligand by Bunzen (Figure 3.3) the core and the bipyridine were connected via an ethynyl spacer using the *Sonogashira*-reaction. Five membered heterocycles, such as furane, thiophene and pyrrole, were chosen as core molecules. By substituting the heterocycles in different positions, it is possible to vary the angles of the ligands (Figure 3.4).

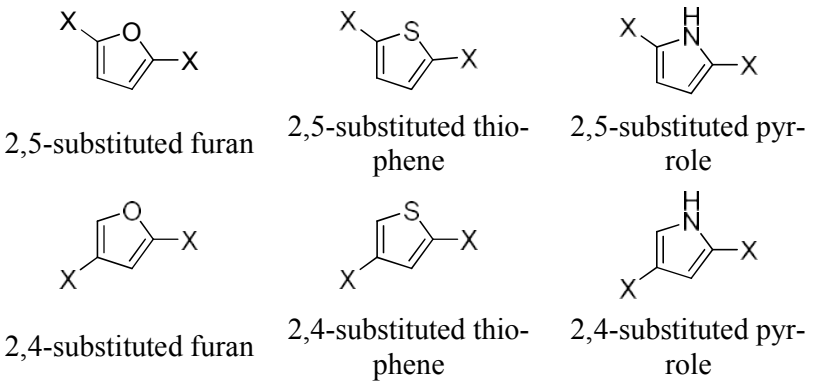

Figure 3.4 Core units for ligand for SCO

Dihalogenated heterocycles are needed for the cross-coupling reaction. 2,5-Diiodothiophene and 2,4-dibromothiphene are both commercially available, but this was not the case for the furane- or pyrrole-derivatives, which therefore had to be synthesized in the lab.

L. Volbach attempted synthesizing different di-brominated and di-iodinated furanes and pyrroles, however this proved to be rather difficult and partly because the poor stability of the final products.[35] Therefore, we started looking for other five-membered heterocyclic systems with the possibility to be substituted in the 2,5- and 2,4-positions. In the search we came upon 1,3-thiazole, which, according to Grubb *et al*., can be dihalogenated in good yields starting from commercially available 2-amino-1,3-thiazole or 1,3-thiazolidine-2,4-dione (Scheme 3.1 and Scheme 3.2).[36]

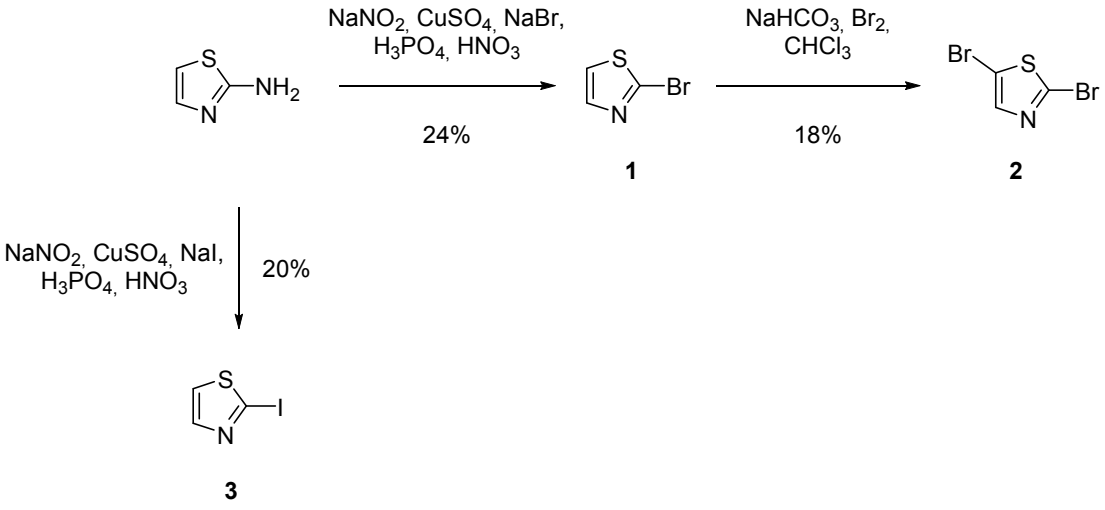

Scheme 3.1 Synthesis of core molecules starting from 2-amino-1,3-thiazole

Grubb *et al*. performed the synthesis on a large scale in order to use the synthesis in an industrial context.[36] However, the synthesis was scaled down from 25 g of starting material

to 1-5 g. This had a great influence on the yields of the reactions, since significant amounts of product are lost especially during work-up and purification.

2-Bromo-1,3-thiazole, **1**, was synthesized by a variation of the *Sandmeyer*-reaction and purified by steam distillation (Scheme 3.1). During the steam distillation we ended up having about 1.5 g of the product **1** in about 500 mL of solvent. When trying to extract such a small amount of product from a comparably large amount of solvent much of the product stays in the reaction mixture, lowering the yield significantly. This explains why the yield did not reach the yield of 86% presented in the literature.[36] A corresponding reaction was carried out using NaI instead of NaBr resulting in 2-iodo-1,3-thiazole **3** in a yield of 20%. The low yield is due to the instability of the product, which is light-sensitive. Careful shielding from light should result in an increase of the yield of the reaction.

Bromination of **1** (Scheme 3.1) proceeded without problems until the work-up. Grubb *et al*. used vacuum sublimation to purify 2,5-dibromo-1,3-thiazole **2**, which was a white solid.[36] In our case sublimation of the crude product resulted in an oil, which according to NMR-spectra is the desired product **2** in a yield of 18%. The reaction was only performed once, in order to assess if the method is applicable for our purposes. As an alternative work-up method column chromatography is suggested, since sublimation on such small amounts is not feasible.

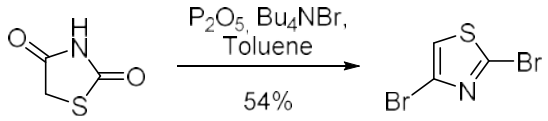

4

*Scheme 3.2 Synthesis of core molecule **4** based on 1,3-thiazolidine-2,4-dione*

The synthesis of **4** was performed according to the protocol of Grubb *et al.*[36] and can be seen in Scheme 3.2. Starting from 1,3-thiazolidine-2,4-dione the deoxygenation followed by bromination resulted in **4** in a yield of 54%. Again, the crude product was purified by sublimation resulting in a low yield compared to the literature.[36]

The metal-binding unit is based on a bipyridine with an electron withdrawing ester group and an ethynyl spacer. 2-aminopyridine was iodinated by a comproportionation of I_2 and HIO_4 resulting in 5-iodo-2-aminopyridine **5** in a yield of 81% (Scheme 3.2). Next, a variation of the *Sandmeyer*-reaction resulted in the 5-iodo-2-bromopyridine **6** which has two halogens with a different reactivity towards *Sonogashira*-conditions.[37–39] Trimethylsilylacetylene was therefore selectively coupled to the 5-position to obtain **7** in a yield of 76%.

Next, **7** was coupled to methyl-2-chloropyridine-5-carboxylate by a *Negishi*-coupling[40] under the conditions previously used by J. Bunzen[34] resulting in bipyridine **8** (Scheme 3.3). Deprotection with KF produced **9**, which can participate in *Sonogashira*-reactions.

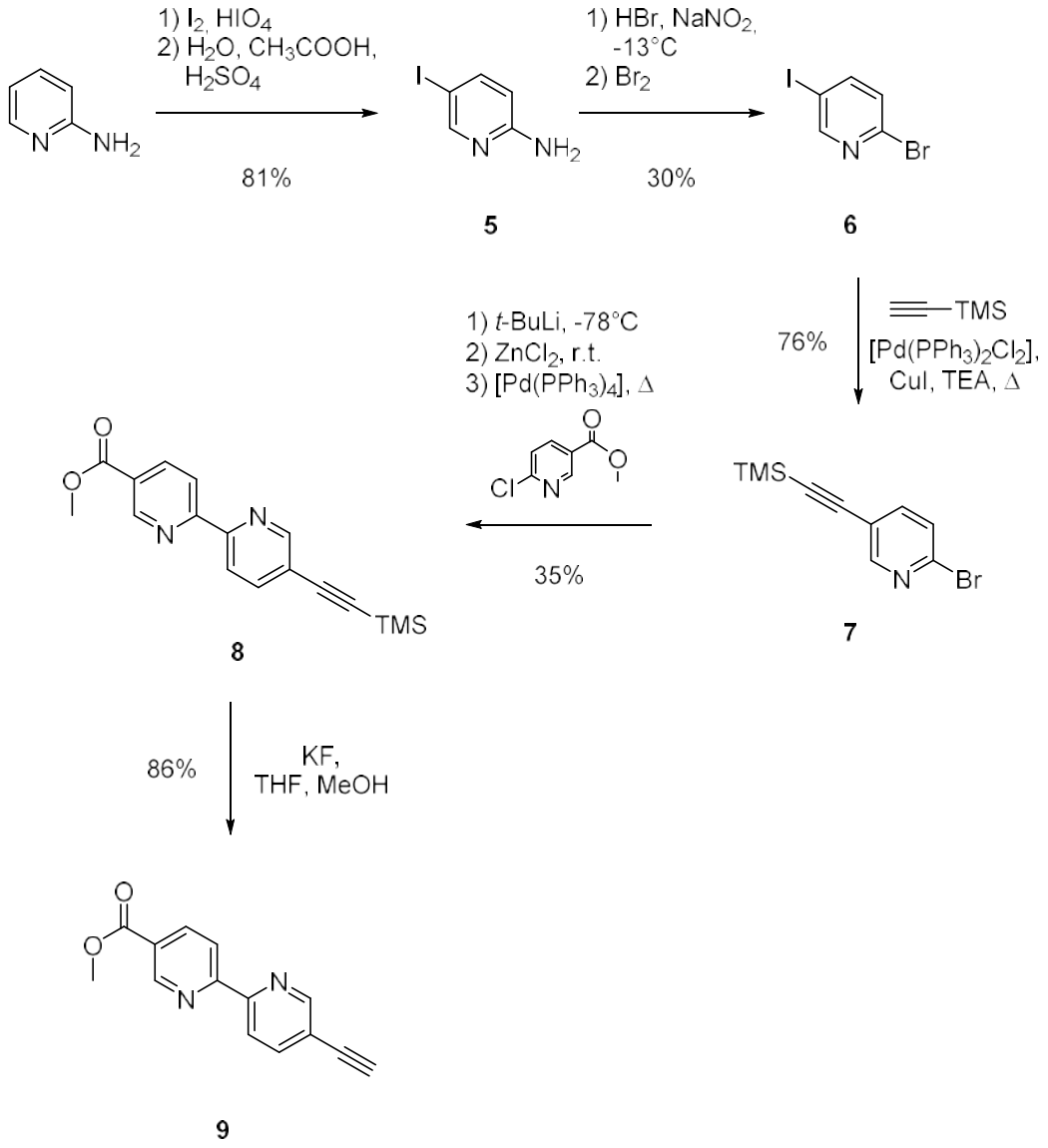

*Scheme 3.3 Synthesis of the metal-binding unit **9***

The synthesis of ligand **10** with 2,5-diiodothiophene was attempted by L. Volbach using the conditions described in Scheme 3.4. However, it was only possible to isolate the mono-substituted product. When performing the reaction again it was noticed that a yellow precipitate formed during the course of the reaction, which glows under UV-light. An attempt to purify the crude product via column chromatography only resulted in the mono-substituted product as previously described; however, examining the remaining crude product at the top of the column with UV-light indicated that the product might be present in the crude remnant. The remnant was extracted with methanol and acetone, but neither

solvent was able to resolve the product. Instead, it was speculated that it might be possible to filter off the precipitate directly after the reaction.

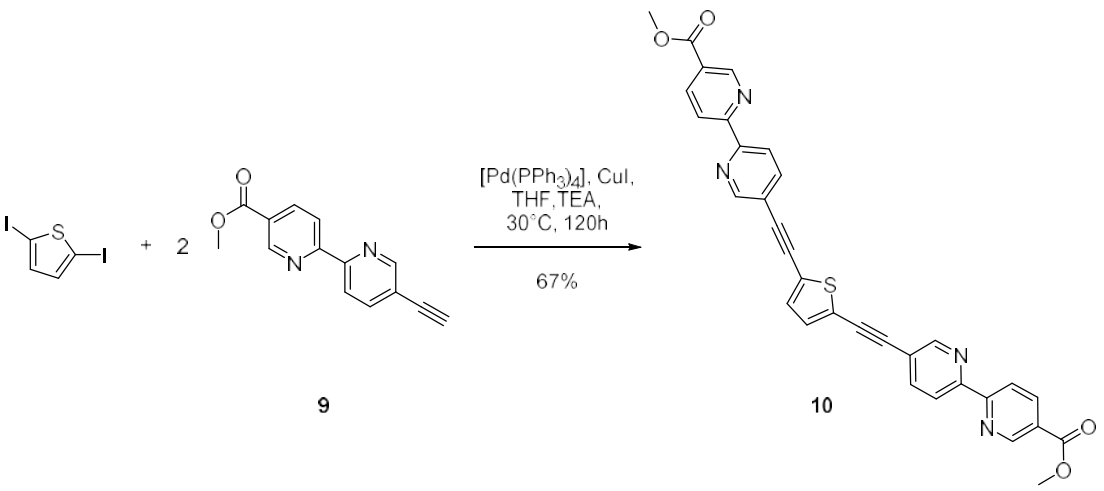

*Scheme 3.4 Synthesis of ligand **10***

Therefore, the reaction was carried out again, and the yellow precipitate was filtered off. However, finding a solvent able to dissolve ligand **10**, in order to perform NMR-spectroscopy, proved to be rather difficult. In the end, the pyridines were protonated using deuterated trifluoroacetic acid finally obtaining the desired ^{1}H-NMR-spectrum, which, along with the ESI-MS spectrum, confirmed the synthesis of **10**, which was used in complexation studies.

To further purify the product, it was heated in THF and filtered off while warm. A CHN-analysis was performed revealing that the product was still impure. Due to its poor solubility it is very difficult to further purify **10**.

An alternative could be to add hexyloxy-groups at the 3- and 4-positions of the thiophene in order to increase the solubility. Also, exchange of the ester-group for another electron-drawing groups which is more soluble such as a cyano-group could alter the solubility. To obtain a ligand with a different angle between the metal binding sites, the reaction should be carried out with 2,4-dibromothiophene. Since bromines have a lower reactivity in *Sonogashira*-reactions, it might be necessary to adjust the conditions. However, as the solubility problems are expected to be the same, it would be important to solve these problems first.

Furthermore, 2,5-dibromo-1,3-thiazole **2** and 2,4-dibromo-1,3-thiazole **4** should be tested in a *Sonogashira*-reaction with **9**, taking into account both the decreased reactivity of the bromines as well as the solubility-issues.

3.3 Complexation

To investigate the SCO-abilities of ligand **10**, we decided to follow the method used by Bunzen to form the high spin SCO-system with the spirobifluorene ligand.[34] We therefore mixed ligand **10** with $Fe(BF_4)_2 \cdot 6H_2O$ in two different solvent mixtures: CD_2Cl_2/CD_3CN and CD_2Cl_2/DMSO-d_6 both in a ratio of 3:1. A photo of the resulting mixtures is shown in Figure 3.5. On the left picture one can see the result of the complexation in CD_2Cl_2/CD_3CN, which instantaneously produced a deep red solution, indicating the formation of a low spin Fe(II)-complex. On the other hand using CD_2Cl_2/DMSO-d_6 as solvent, resulted in a yellow suspension of ligand **10**, and it is therefore reasonable to assume, that no complexation has occurred.

Both solutions were measured by ^{1}H-NMR-spectroscopy. However, the spectrum of the yellow solution showed no ligand peaks at all, supporting the assumption that no complex has formed in CD_2Cl_2/DMSO-d_6. The complex mixture in CD_2Cl_2/CD_3CN-complex, on the other hand, produced one set of peaks in ^{1}H-NMR-spectrum between 9 and 3 ppm, (Figure 3.6). Unfortunately, it is not possible to compare the complex-spectrum directly with the ^{1}H-NMR-spectrum of the free ligand, since the pure ligand is only soluble in CF_3COOD. Nevertheless, thorough investigation of the complex ^{1}H-NMR-spectrum reveals, that the integrals match with the ligand. When the peak at 3.76 ppm, which corresponds to the methoxygroup, was integrated to 6, the protons in the aromatic region integrated to 14, which matched the number of aromatic protons in the ligand. The broadness of the signals is also an indication of a complexation event. Therefore, we can assume that a complexation has happened.

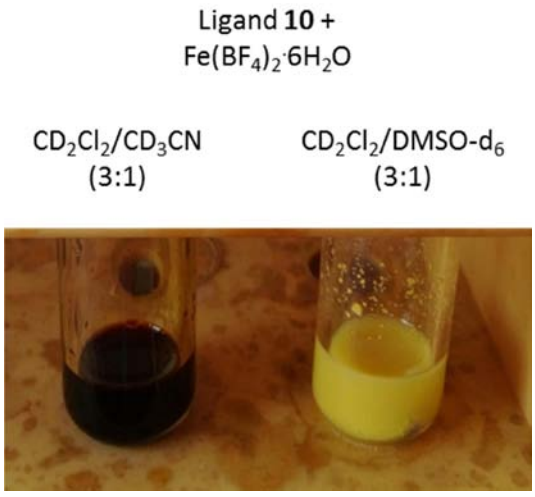

*Figure 3.5 Photo of ligand **10** with $Fe(BF_4)_2 \cdot 6H_2O$ in two different solvent mixtures.*

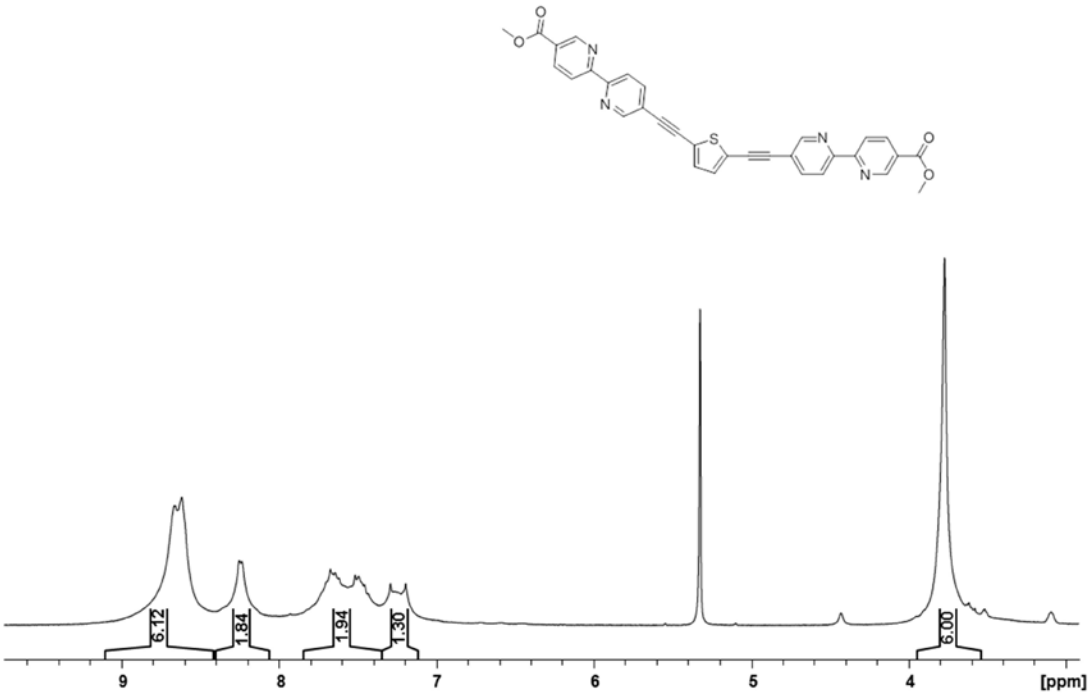

*Figure 3.6 ^{1}H-NMR-spectrum of ligand **10** with $Fe(BF_4)_2 \cdot 6H_2O$ in CD_2Cl_2/CD_3CN*

To confirm the formation of the Fe(II)-helicate, mass spectra were measured (Figure 3.7). When describing mass spectra, the general notation metal:ligand:anion/cation is used. In the case of the helix formed by ligand **10** and Fe(II) with BF_4^- as the anion the notation would be 2:3:1(BF_4^-). In some cases an uncharged solvent molecule is loosely attached to the solvent. If one molecule of acetonitrile was attached the notation would be 2:3:1(BF_4^-) + CH_3CN.

The base peak in the resulting mass spectrum is at 445.3 m/z and, carries a charge of +4, which matches the calculated spectrum and isotope pattern for a 2:3:0-helix. No other significant peaks are found in the spectrum, thereby confirming the formation of a Fe(II)-triple helix.

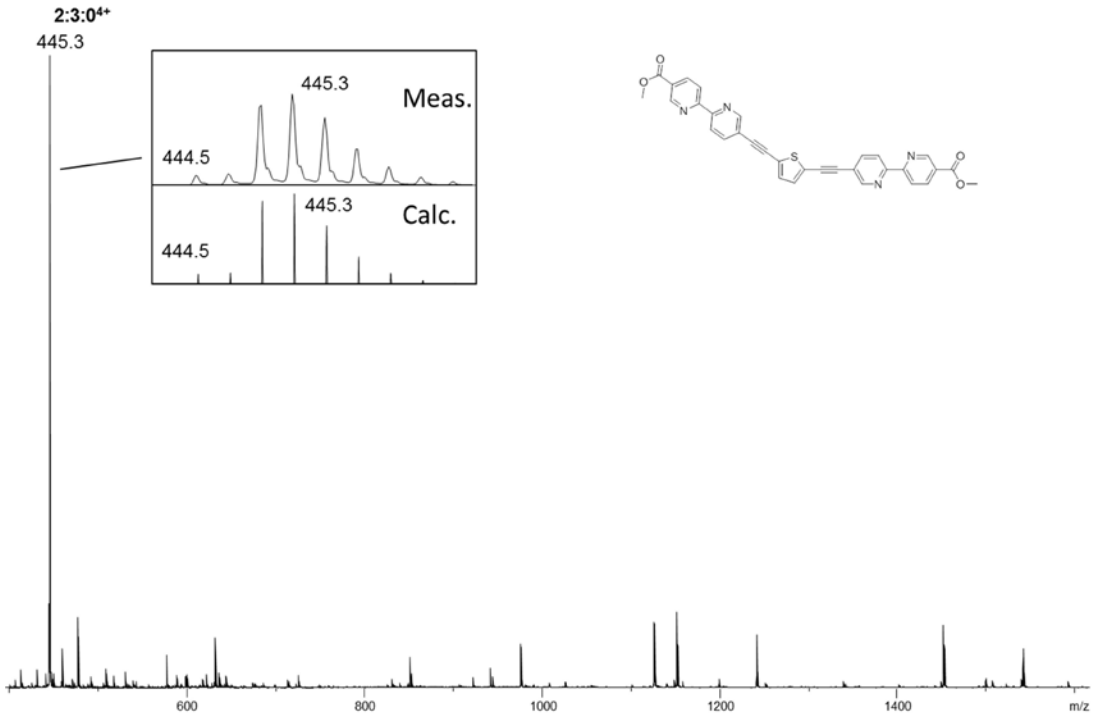

*Figure 3.7 ESI mass spectrum (positive mode) of ligand **10** with $Fe(BF_4)_2 \cdot 6H_2O$ in CD_2Cl_2/CD_3CN. The notation corresponds to Metal:Ligand:Anion.*

The complex mixture in CD_2Cl_2/CD_3CN produces a red complex at room temperature. Heating to 40°C does not change the color and thus does most likely not prompt a spin change. It is however remarkable, that changing the solvent from CD_2Cl_2/CD_3CN to CD_2Cl_2/DMSO-d_6 completely changes the complexation abilities.

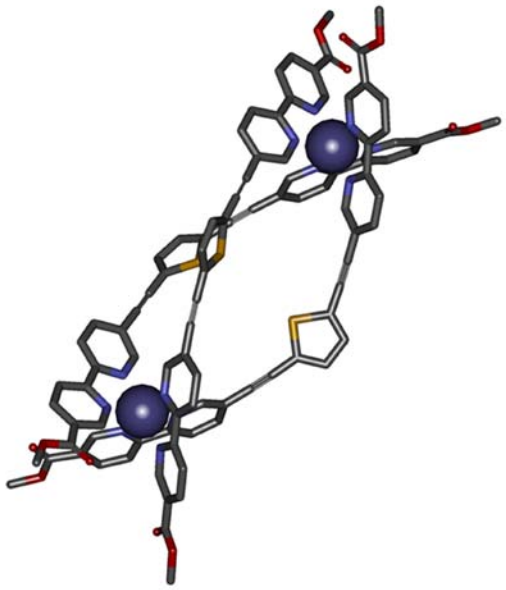

*Figure 3.8 PM6-modelled structure of Ligand **10** with $Fe(BF_4)_2 \cdot 6H_2O$ (Λ,Λ)*

Since Fe(II) has an octahedral coordination geometry, the complex can form three different stereoisomers: (Δ,Δ), (Δ,Λ) or (Λ,Λ). In the case of (Δ,Δ) and (Λ,Λ) the complex would be symmetric and the number of signals in the ^{1}H-NMR-spectrum would be the same as in the uncomplexed ligand. If, the configuration around the metal centers is (Δ,Λ), two sets of signals could be seen in the spectrum. From the ^{1}H-NMR-spectrum obtained of the complex, it is difficult to determine whether one or two sets of signals are present (Figure 3.6). The only signal that can be positively identified is the methyl ester-signal at 3.75 ppm. Only one peak is seen, indicating the formation of a symmetric

complex. However, as can be seen in the modeled structure of the complex (Figure 3.8), the methyl ester is rather far away from the metal center, and is probably not affected much by the conformation around the Fe(II). A crystal structure could elucidate the conformation, but so far no crystals have been obtained from the crystallization attempts of the complex.

3.4 Conclusion

We were able to form a triple helix from ligand **10** and Fe(II) and confirm its formation by mass spectrometry. So far, it has not been possible to produce the complex in the high spin configuration due to solubility problems. These problems can be overcome by testing different solvents and possibly modifying the ligand by adding substituents in the 3-position of the thiophene. This should not interfere with the complexation abilities of the ligand, as the protons of the thiophene point outwards on the complex as illustrated in Figure 3.8.

4 Self-Sorting

4.1 Background

Just as the constitution of the folded enzyme predetermines the amino acid sequence, chemists can design a molecule featuring the information needed to form a specific supramolecular entity. The design can be in the form of a specific number of binding sites or sterically rigid bonds or groups. These programmed interactions take us from mere self-assembly to self-sorting, which again can be divided into narcissistic (self-recognition) and social self-sorting (self-discrimination).[41,42]

The term self-recognition was first introduced by Lehn to describe the phenomenon observed when mixing the bipyridine-ligands in Figure 4.1 with Cu(I) and Ni(II).[43] Even when mixing both chelating ligands with both ions, only the homoleptic double and triple helicates are formed with no detectable crossover products. The coordination number and the geometry of the two metals along with the difference in the flexibility of the linker in the two ligands ensure complete self-recognition.

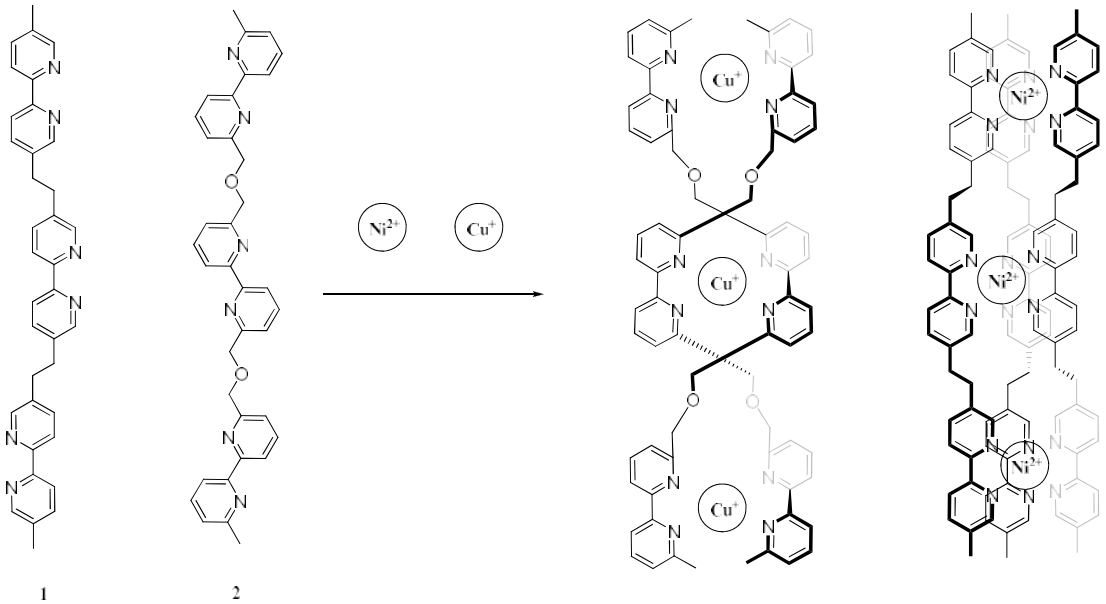

Figure 4.1 Two different tris-bipyridine ligands form two homoleptic complexes with Ni^{2+} and Cu^{+}

However, self-sorting does not only occur with constitutionally different ligands but also with ligands differing only in their chiral conformation. An example of chiral self-recognition is the system by Lützen (Figure 1.14), build up from the C_2-symmetric Tröger's base. The racemic Tröger's base derivatives (**L1**, **L2** and **L3**) were complexated with Ag(I) resulting in discrete dinuclear helices without formation of any polymeric or

oligomeric complexes as confirmed by mass spectroscopy. ^{1}H-NMR-measurement further indicated formation of only homoleptic complexes with the same configuration around the metal center even as the distance between the chiral center and the metal binding unit was increased from a C–C single bond to a butadienyl group.[22]

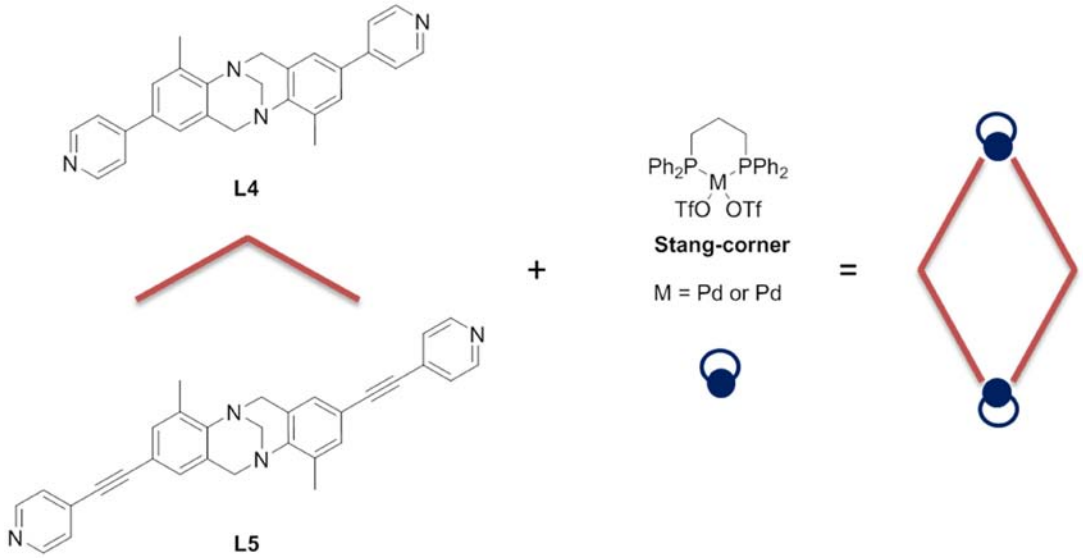

Figure 4.2 Illustration of the complexes synthesized by Lützen et al. using Trögers Base derivatives as ligands together with the Stang-corner

Employing square planar *cis*-protected Pd(II) and Pt(II) complexes of the Stang-type[44] (also referred to as the Pd- and Pt-corners) together with ligands **L4** and **L5** (Figure 4.2) results in complexation and formation of discrete dinuclear rhombs. Yet crystal structures of the complexes reveal that the complexation is stereoselective resulting only in the heterochiral complexes. This is one of the rare examples of self-discriminatory behavior displayed by supramolecular assemblies.[45]

The selectivity of the aforementioned ligands in complex solution can be ascribed to the inherent chirality of the Tröger's base. Synthesized in 1887 by Julius Tröger[46], the (Figure 4.3) unique structure of the Tröger's Base is rigid with an angle ranging from 80° to 114°.[47,48] Due to the methylene bridge between the amines inversion around the nitrogen atoms is prevented, so the molecule is chiral.[49] The chirality is the origin of the Tröger's Base popularity as a part of supramolecular aggregates with applications in catalysis and as receptors.[50–52]

Figure 4.3 Tröger's Base

4.2 Synthesis of the ligands

The Tröger's base is not the only chiral molecule able to control the stereochemistry of its complexes. The spirobifluorene, first synthesized by Clarkson and Gomberg in 1930, contains a spiro carbon, which connects the two separate π-systems, and is not chiral if not substituted (Figure 4.4).[53] By substituting the spirobifluorene in the 2,2'-position with crown ethers Prelog founded the basis of the use of D_2-symmetric spirobifluorenes in chiral recognition.[54–58]

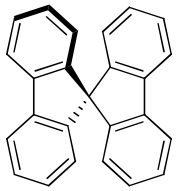

Figure 4.4 Non-substituted Spirobifluorene

Since the spirobifluorene can be easily halogenated in the 2,2'-positions and thereby become chiral, we decided to base further investigations into self-sorting on the spirobifluorene. Similarly to the complexation with the Tröger's base derivatives, we wanted to look closer at the self-sorting behaviour of ligands with different spacer lengths. To this end two target molecules, **Spf1** and **Spf2**, were designed (Figure 4.5). The two ligands differ only in the length of the spacer between the chiral spirobifluorene core and the metal binding pyridine.

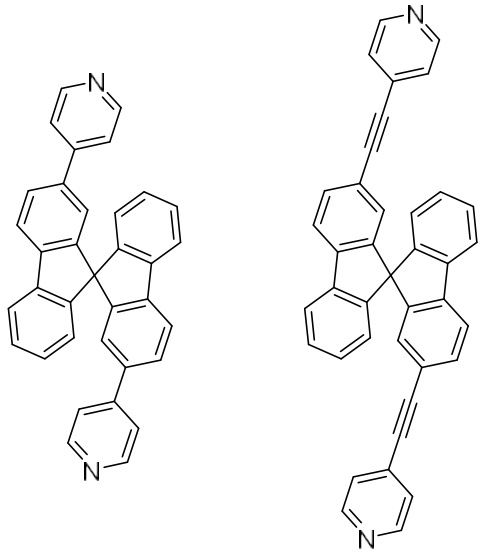

Sbf1 **Sbf2**

Figure 4.5 Spirobifluorene target molecules

The synthesis of the spirobifluorene core (**III** in Scheme 3.1) is known from the literature[53] and has been a standard synthesis in the Lützen group. The synthesis begins with a *Sandmeyer* reaction performed on 2-aminobiphenyl resulting in 2-iodobiphenyl (**II**) (Scheme 4.1). Next, a *Grignard* reaction was carried out using 9-fluorenone, followed by condensation using HCl, yielding the spirobifluorene core (**III**).

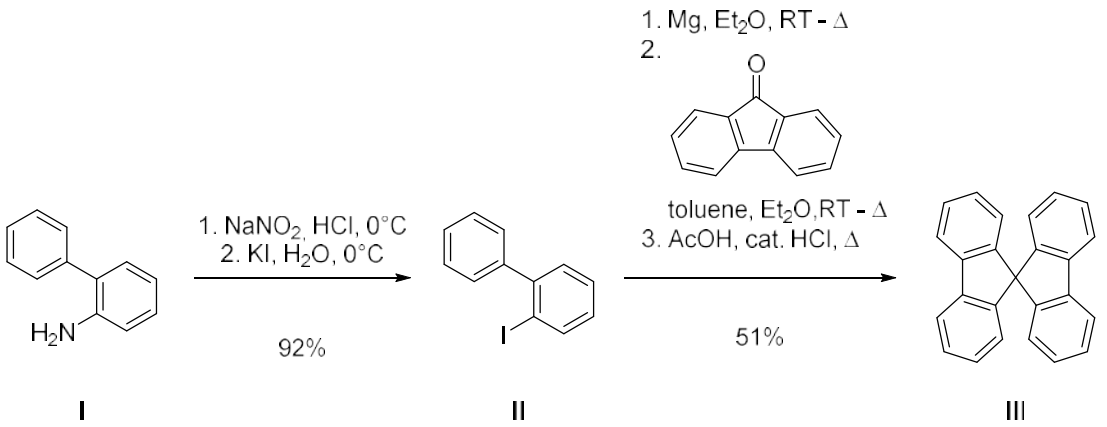

*Scheme 4.1 Synthesis of 9,9'-spirobifluorene **III***

Functionalization of **III** in the 2 and 2'-position to obtain the racemic D_2-symmetric spirobifluorene was performed via 2,2'-diamino-9,9'-spirobifluorene (**VI**) as shown in Scheme 4.2.

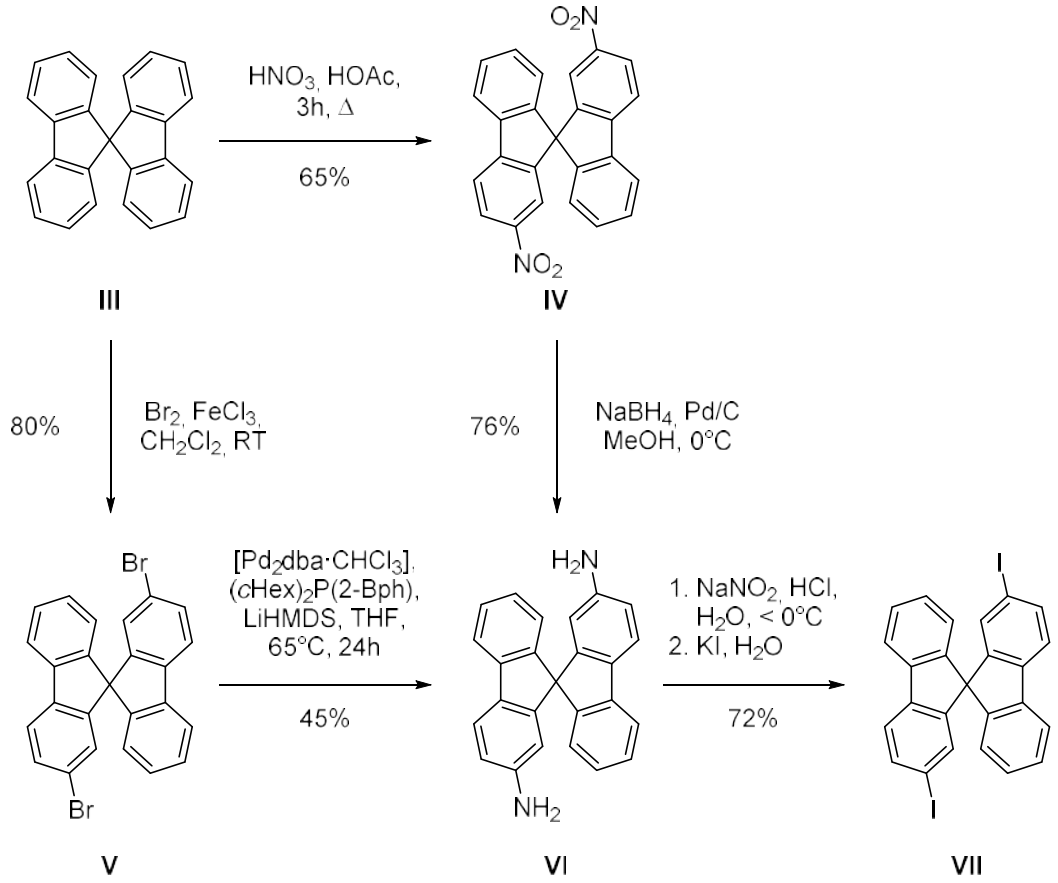

*Scheme 4.2 Synthesis of racemic 2,2'-diiodo-9,9'-spirobifluorene **VII**.*[59]

2,2'-diamino-9,9'-spirobifluorene (**VI**) can be synthesized via two different routes from 9,9'-spirobifluorene (**III**). Electrophilic aromatic substitution results in the bromo- and the nitro-derivatives **IV** and **V** respectively.[60,61] **V** can be converted into **VI** using palladium as

a catalyst and LiHMDS as the ammonia equivalent[62], while **IV** can be reduced using $NaBH_4$ to obtain **VI**. Lastly, a *Sandmeyer* reaction results in 2,2'-diiodo-9,9'-spirobifluorene **VII**. However, separation of the functionalized spirobifluorenes (**IV**-**VII**) into its enantiomers failed. Attempts to separate diastereomers formed with enantiomerically pure BINOL-derivatives were also unsuccessful.[59]

Instead, it was decided to try the method of Toda which we elaborated further in our group, where the 2,2'-dihydroxy-9,9'-spirobifluorene (**X** in Scheme 4.3) is separated by clathrate formation. The synthesis of **X** from **III** is shown in Scheme 4.3.

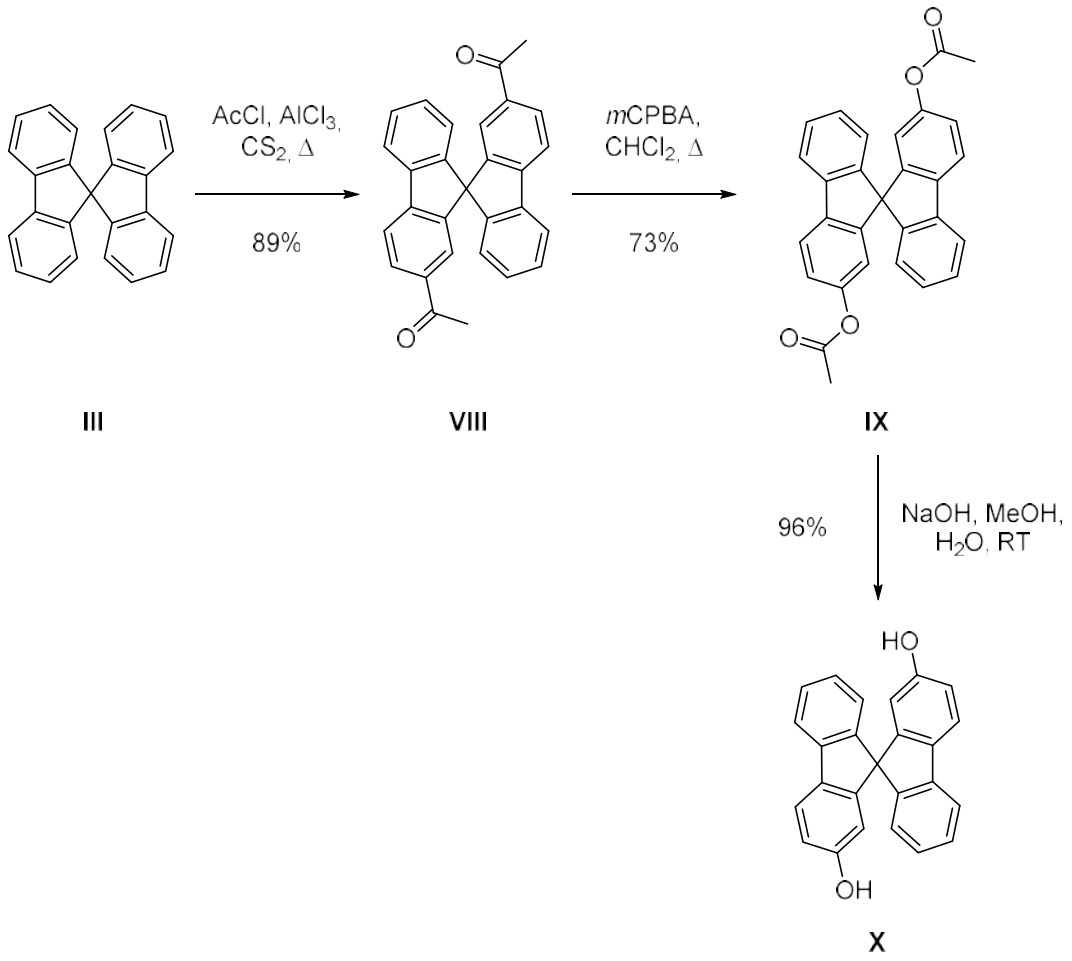

*Scheme 4.3 Synthesis of 2,2'-dihydroxy-9,9'-spirobifluorene **X***

Functionalization of **III** is done via acylation of the 2,2'-positions using acetyl chloride and results in racemic **VIII**. Next, a *Baeyer-Villiger* oxidation was performed producing the ester **IX**, which can be hydrolyzed into 2,2'-dihydroxy-9,9'-spirobifluorene (**X**).[59]

Spirobifluorene **X** can be separated into both enantiomers using (*R*,*R*)-(+)-2,3-dimethoxy-*N*,*N*,*N*',*N*'-tetracyclohexylsuccindiamide. However, we also found that it is possible to perform the separation of **X** on HPLC using *CHIRALPAK®IA* and $CHCl_3$/*i*PrOH (95:5) as the

eluent.[63] The enantiomerically pure 2,2'-dihydroxy-9,9'-spirobifluorene **X** was kindly made available for further synthesis by Dipl. Chem. Caroline Stobe.

The next synthetic step is common to all ligands, the formation of the 2,2'-ditriflate-9,9'-spirobifluorene. Employing triflic anhydride in CH_2Cl_2 and triethylamine, the reaction was performed on both entantiomers to produce spirobifluorene (*R*)- and (*S*)-**11** in good yields (Scheme 4.4).[59]

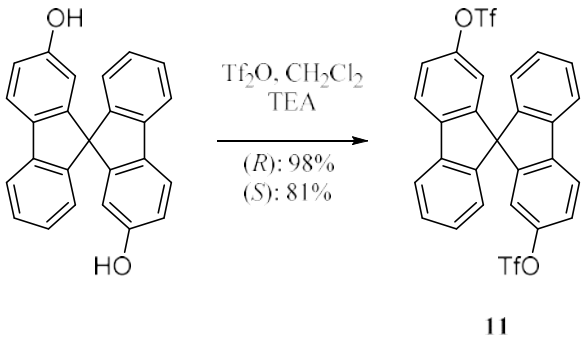

11

*Scheme 4.4 Synthesis of the spirobifluorene **11***

The triflate is crucial for the following synthesis, since it is a far better leaving group than the hydroxyl-ion due it being mesomerically-stabilized. From compound **11** it is possible to perform a *Suzuki*-reaction using the 4-pyridineboronic acid pinacol ester, as shown in Scheme 4.5.[64,65]

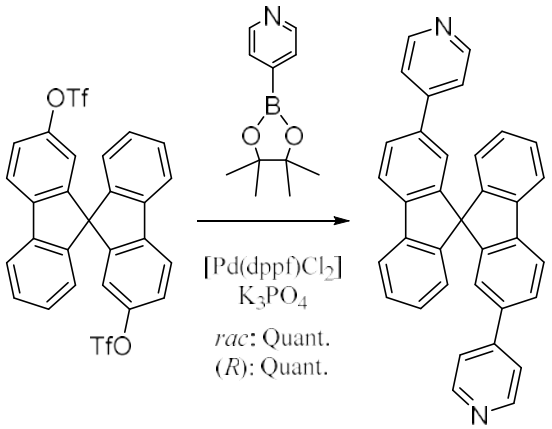

11 **12**

*Scheme 4.5 Synthesis of ligand **12***

The *Suzuki*-cross-coupling is catalyzed by Pd(0). However, we often use a Pd(II)-catalyst, since Pd(0) is air-sensitive, which complicates handling even when working under an argon-atmosphere. In this case Pd(dppf)Cl_2 is used which is reduced to Pd(0) *in situ*.[66] We also used the pyridineboronic acid pinacol esters instead of the boronic acid, as the boronic acid esters are much more stable than their corresponding acids.

The reaction to obtain ligand **12** was initially performed on racemic **11** with three equivalents of 4-pyridineboronic acid pinacol ester in quantitative yield. However, when employing the same conditions on the (*R*)-enantiomer only the mono-substituted product was obtained. Using five equivalents of the pinacol ester finally resulted in the formation of the product in quantitative yield.

Ligand **15**, with the ethynyl spacer, can be obtained using two different synthetic routes as shown in Scheme 4.6.

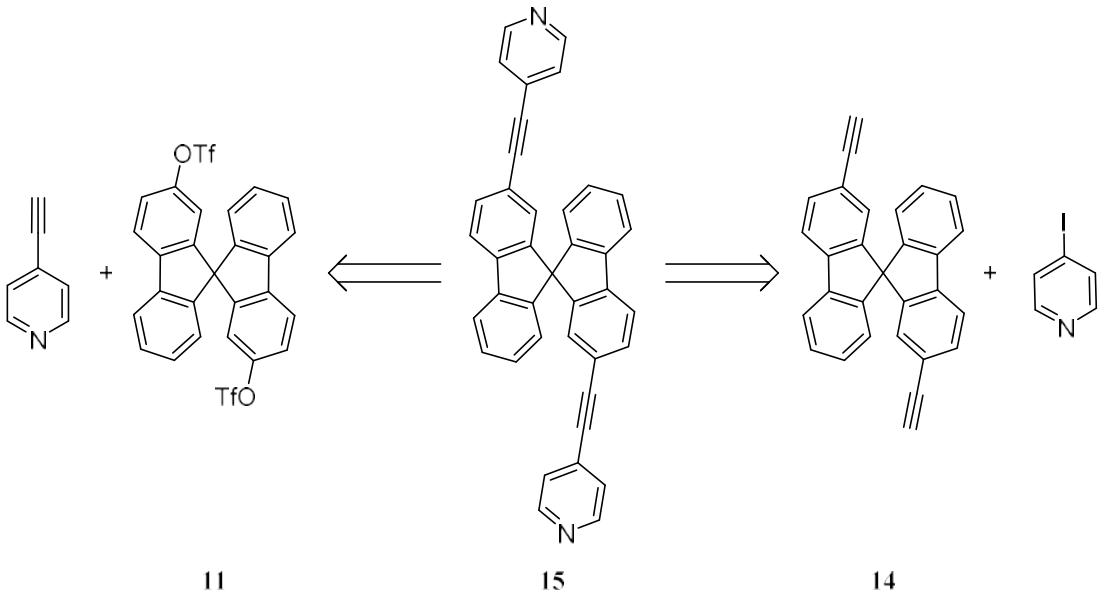

*Scheme 4.6 Retrosynthesis of ligand **15***

Either we can separate ligand **15** between the spirobifluorene and the ethynyl spacer resulting in 4-ethynylpyridine and spirobifluorene **11**. Or the separation can be performed between the pyridine and the ethynyl spacer leaving us with 2,2'-diethynyl-9,9'-spirobifluorene **14** and 4-iodopyridine. Since we already have synthesized **11** it is tempting to use it in a *Sonogashira*-reaction with 4-ethynylpyridine. However, in order to obtain the 4-ethynylpyridine one has to perform several synthetic steps involving the 4-iodopyridine, which is known to be very light- and heatsensitive. We therefore preferred to attach the ethynyl spacer on the spirobifluorene, which is very stable and not prone to degradation. The synthesis of ligand **15**, which was obtained in an overall yield of 24% from **11** for the (*R*)-enantiomer, can be seen in Scheme 4.7. The synthesis of the racemic product **13** was performed by Niklas Struch.

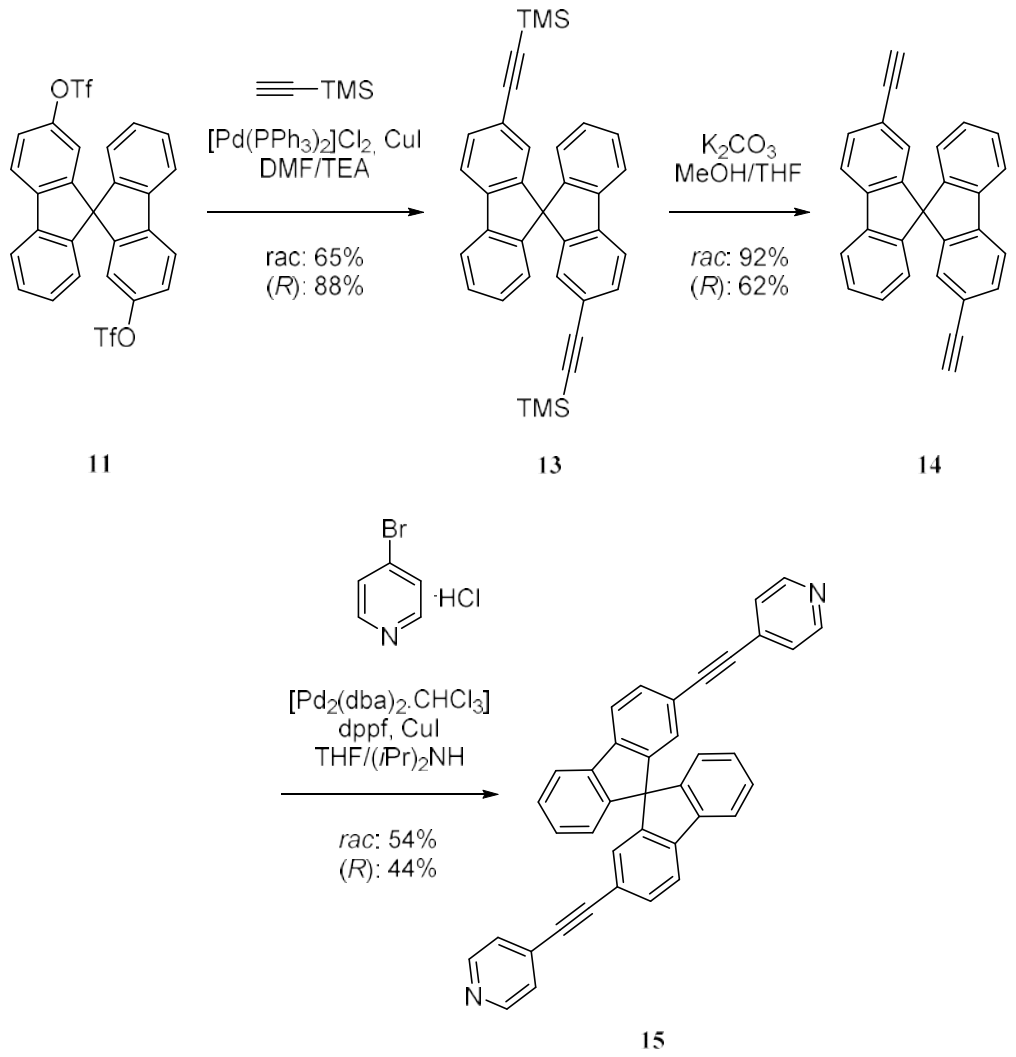

*Scheme 4.7 Synthesis of Ligand **15** from **11***

Starting with a two-fold *Sonogashira*-reaction using commercially available trimethylsilylacetylene the spacer was added to (*R*)-**11** affording (*R*)-**13** in 88% yield.[67] The following deprotection with K_2CO_3 gave unexpected low yields, even though only one spot was observed on the reaction-TLC. After the first purification by column chromatography product **14** was obtained in a yield of 50%. Examination of the aqueous phase by TLC showed that it contained UV-active components, and extraction of the aqueous phase with CH_2Cl_2 produced the desired spirobifluorene **14** in a total yield of 62%. Finding **14** in the aqueous phase is rather unexpected, since the compound is devoid of heteroatoms. The possibility that the ethynyl has not been protonated after deprotection is unlikely, since methanol is more acidic than ethynyl.

The last step in the synthesis of ligand **15** was first performed with 4-iodopyridine as previously carried out by Piehler, but did unfortunately not produce the desired product. Instead the starting material was recovered. We ascribed this to the poor stability of the

4-iodopyridine. A more stable though less reactive alternative to the iodo-derivative is the 4-bromopyridine, which was used in the form of the HCl-salt increasing the stability of the reactant. The *Sonogashira*-reaction requires harsher conditions to compensate for the low reactivity of 4-bromopyridine. However, at elevated temperatures 4-bromopyridine might decompose, so a temperature of 60°C was chosen as a compromise. The use of four equivalents of 4-bromopyridine with 7% of Pd-catalyst resulted in ligand **15** in a yield of 54%, with remnants of both starting materials still present in the reaction.

We also synthesized the pseudo enantiomer[I] of ligands **15** and **12**, by adding methylgroups to the 7,7'-position resulting in ligand **20** and **21** (Scheme 4.8).

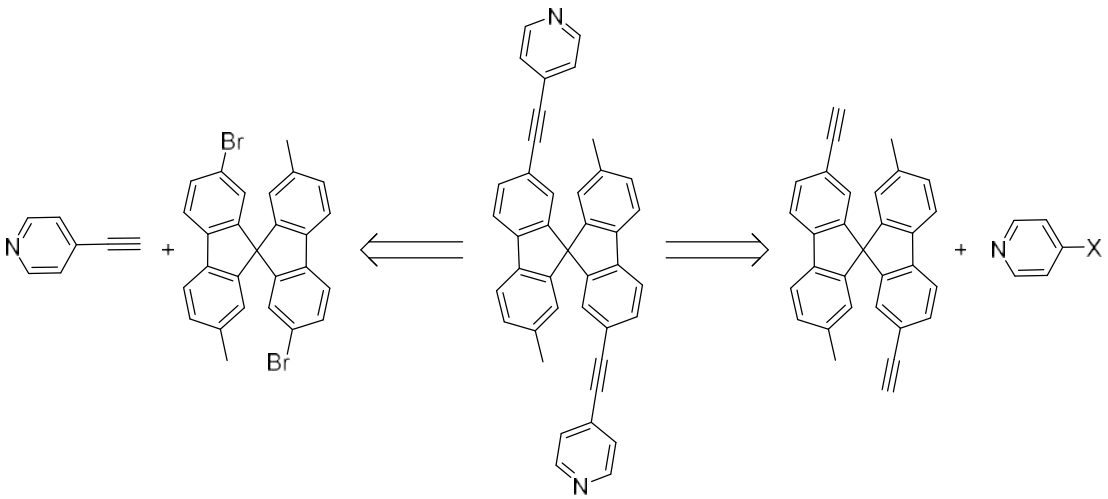

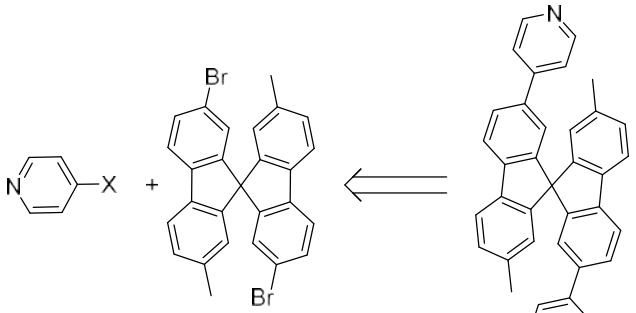

*Scheme 4.8 Retrosynthesis of ligands **20** and **21***

[I] Pseudo enantiomers are two ligands with opposite chirality as expected for enantiomers, but differ in for example substitution.

We started from spirobifluorene **11** and performed a *Kumada*-coupling, which resulted in spirobifluorene **16** with two methyl-groups in quantitative yields (Scheme 4.9).[68]

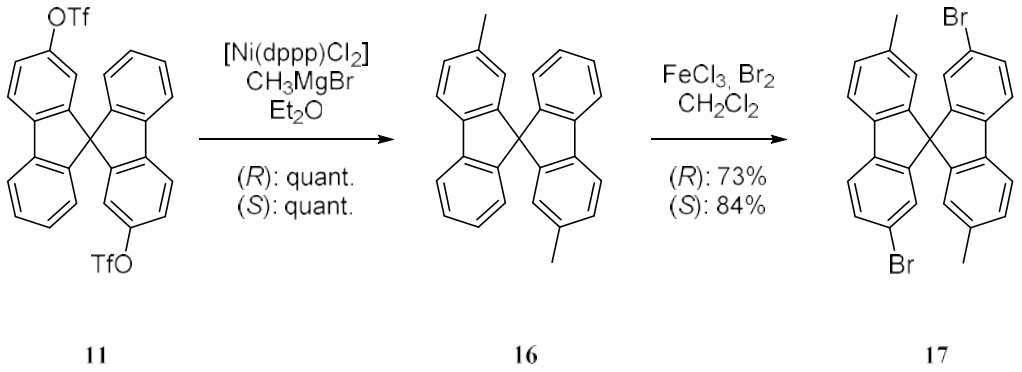

*Scheme 4.9 Synthesis of spirobifluorene **17***

The reactivity of the 9,9'-spirobifluorene resembles that of the fluorene closely, which makes it possible to selectively perform an electrophilic aromatic substitution in the 2,2'-position resulting in the spirobifluorene **17**.[60]

Only one reaction route is possible for the synthesis of ligand **21** as shown in Scheme 4.8 Ligand (*S*)-**21** was obtained in a yield of 69% from **17** using 4-pyridineboronic acid pinacol ester in a *Suzuki*-reaction. This reaction was performed by Thorsten Piehler.

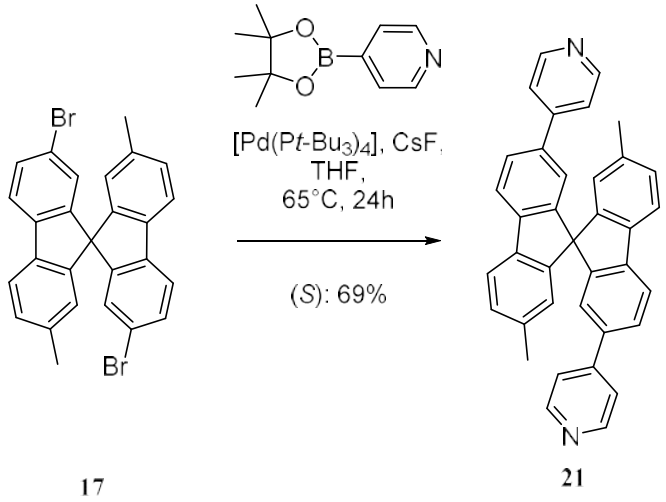

*Scheme 4.10 Synthesis of ligand (S)-**21** from **17** performed by Piehler*

However, two routes are available for the synthesis of the ligand **20** (Scheme 4.8). We can use spirobifluorene **17** in a *Sonogashira-Hagihara*-coupling with 4-ethynylpyridine, or we add the ethynyl spacer to the spirobifluorene resulting in the molecule **19**, which can be reacted with 4-iodopyridine.

Previously, the *Sonogashira*-reaction had been carried out by Piehler, who used **17** and the HCl-salt of 4-etynylpyridine under varying conditions, however with no result as shown in Scheme 4.11.

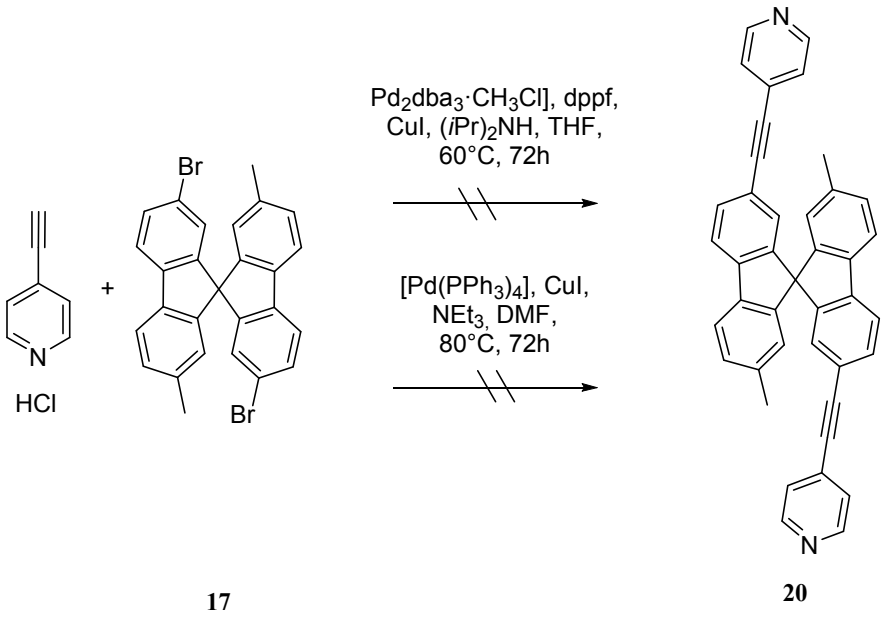

17 **20**

*Scheme 4.11 Attempts to synthesize ligand **20** from spirobifluorene **17** by Piehler*

We therefore decided to perform the synthesis of ligand **20** analogous to the synthesis of ligand **15**, as shown in Scheme 4.12.

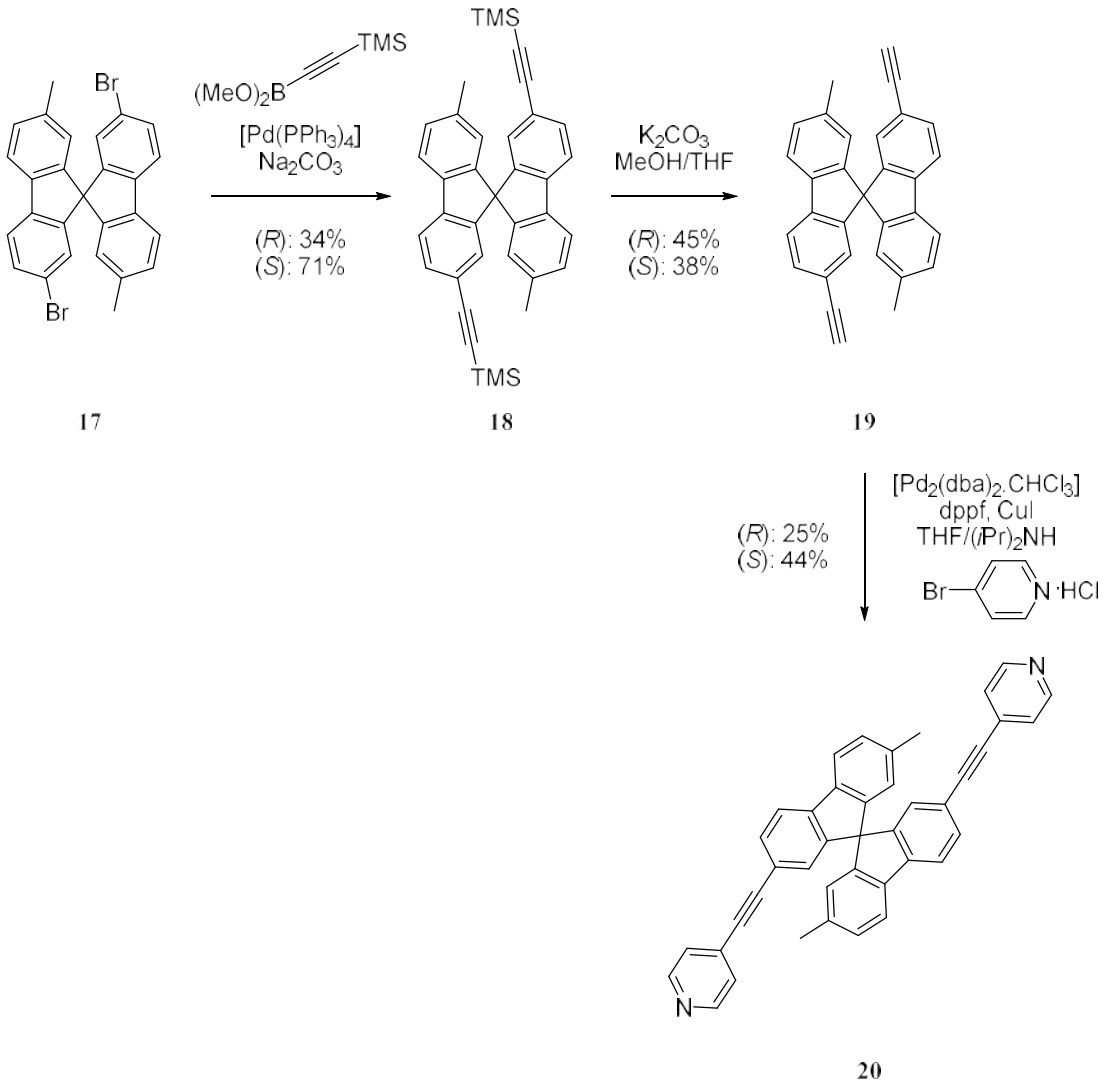

*Scheme 4.12 Synthesis of ligand **20** from **11***

Starting from spirobifluorene **17**, a double *Suzuki*-coupling was carried out, utilizing a TMS-ethynylboronic acid methylester synthesized from $B(OMe)_3$ and TMS-acetylene deprotonated by *n*-butyllithium. Using 250 mg of (*R*)-**17** and resulted in **18** in a yield of 34%. The low yield may be explained by inaccuracy during the transfer of the TMS-ethynylboronic acid methylester to the reaction. When performing the reaction of the (*S*)-enantiomer of **18** the synthesis was carried out more carefully, resulting in a yield of 71%. Deprotection proved to be an unexpectedly difficult task. The reaction resulted in five spots on the TLC, which were difficult to separate. Consequently, significant amount of product was lost during the chromatographic separation.

Lastly a *Sonogashira*-coupling analogous to the one carried out in Scheme 4.6 was performed on **19** resulting in the ligand **20**. Again we had problems with the reactivity of the 4-bromopyridine and consequently significant amounts of both reactants were recovered after column chromatography. In addition a very small amount of reactant was used in the

synthesis of the (*R*)-enantiomer, further lowering the yield. The desired (*S*)-enantiomer **20** was obtained in an overall yield of 10% over five steps.

The four enantiomerically pure 9,9'-spirobifluorene-ligands (*R*)-**12**, (*R*)-**15,** (*S*)-**20** and (*S*)-**21** as well as the racemic ligands were selected for further investigation in complexation studies.

4.3 Complexation

For the complexation of the spirobifluorene ligands (*R*)-**12**, (*R*)-**15** (*S*)-**20** and (*S*)-**21**, the *Stang*-corners[44] Pd(dppp)$(OTf)_2$ and Pt(dppp)$(OTf)_2$ were used. The *Stang*-corners induce a 90° angle into the resulting complexes due to the cis-directionality of the Pt(II) – and Pd(II)-species.

4.3.1 Small spirobifluorene rhombs

We investigated complexes of both the (*R*)-enantiomer but also the racemic ligand **12** with the Pd- or Pt-corner. Employing the enatiomerically pure ligand can only result in the homochiral complexes. When the racemic ligand is used three different complexes can arise as shown in Figure 4.6.

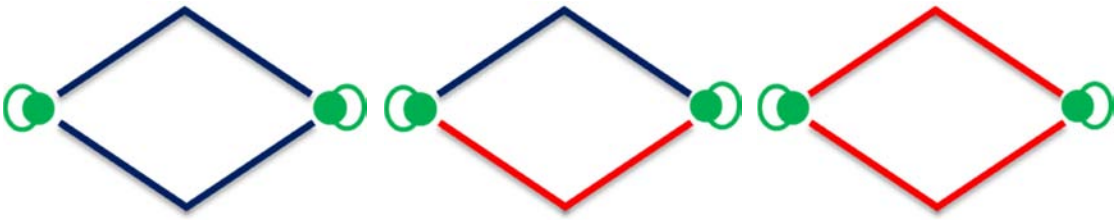

*Figure 4.6 Illustration of the possible 2:2-complexes of racemic ligand **12***

The *R*,*R*- and the *S*,*S*-complexes are enantiomers, while the *R*,*S*-complex is a diastereomer of the two others. The ratio of the three determines whether self-recognition, self-discrimination or no self-sorting effects are taking place. In the case of pure self-recognition, only the two homochiral complexes would be present. Therefore the ^{1}H-NMR-spectrum would be symmetrical, that is, only one set of signals would be present. If on the other hand pure self-discrimination is happening, the ^{1}H-NMR-spectrum would have two sets of signals of equal intensity, corresponding to each of the enantiomers comprising the 2:2-complex. In the case of no self-sorting effects one would expect three sets

of signals: One set from the two homochiral complexes and another from the heterochiral complex in a statistical ratio of 2(homo):2(hetero). Since the two homochiral complexes are enantiomers, they are chemically and magnetically equivalent and result in only one set of signals. One rarely sees pure self-recognition or self-discrimination. More often the ligand shows a preference by deviating from the statistical ratio of no self-sorting and the relative intensities of the signals in the ^{1}H-NMR-spectrum can be used to assess the self-sorting behaviour of the ligand.

Complexes of ligand **12** and the Pd- or Pt-corner have been investigated in CD_2Cl_2/CD_3CN (3:1) by Piehler and Hovorka. The complexations were repeated with the help of R. Hovorka[69] and spectra of the mixture of (*R*)-**12** with $[Pd(dppp)](OTf)_2$ is shown in Figure 4.7.

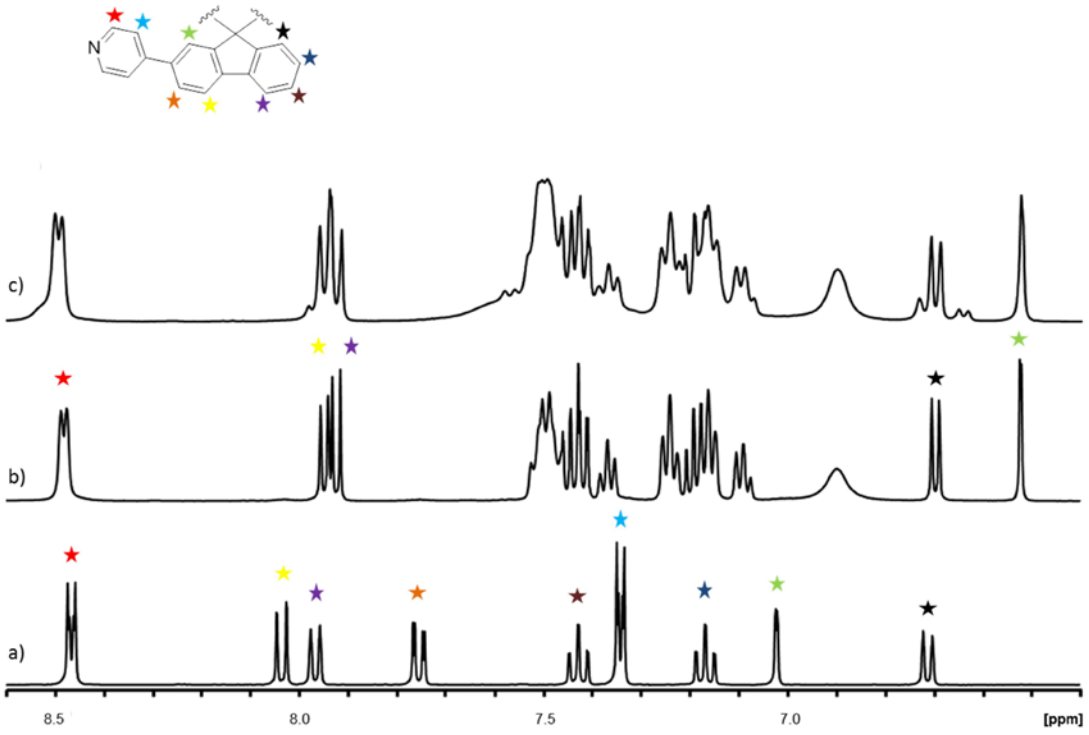

*Figure 4.7 ^{1}H-NMR-spectrum of a) ligand rac-**12** b) ligand (R)-**12** with $Pd(dppp)(OTf)_2$ c) ligand rac-**12** with $Pd(dppp)(OTf)_2$ all in CD_2Cl_2/CD_3CN (3:1).*

The complex spectra are compared to the ^{1}H-NMR-spectrum of the racemic ligand **12**. Using H,H-COSY it was not possible to assign all protons with certainty. The second proton of the pyridine (marked with a light blue star) and protons 3 and 6 of the spirobifluorene (marked with an orange and a brown star respectively) could not be found in the ^{1}H-NMR-spectra of the complex.

Comparing the spectrum of the free ligand with the spectrum of the mixture of the enantiomerically pure ligand (Figure 4.7a and b respectively) all the signals have shifted upon

addition of the Pd-corner indicating that complexation has taken place. However, only one set of signals is present in both spectra indicating the selective formation of one distinct species. Interestingly, the proton in the 2-position of the pyridine (red star) hardly shifts at all in response to complexation, even though it is closest to the pyridine-N, which complexates to the metal. Similar spectra are obtained when using $[Pt(dppp)](OTf)_2$ (spectra not shown).

Comparing the spectrum of the complexated ligand (*R*)-**12** with the complexated racemic ligand **12** (Figure 4.7b and c respectively) the spectra differ from each other indicating that this is not an example of pure self-recognition. Instead, there seems to be a preference towards the homochiral complex, since the intensities of the homochiral complex are much larger than the intensities of the heterochiral complex (Figure 4.7c).

Next, we performed a DOSY-experiment (diffusion ordered spectroscopy) of the mixture of ligand *rac*-**12** and $Pt(dppp)(OTf)_2$ to assess how many different species are present in the solution (See Figure 4.8). In a ^{1}H-DOSY-NMR experiment the diffusion coefficient (D) is derived from the attenuation of the NMR-signals undergoing a pulsed field gradient experiment. Since the attenuation is proportional to the diffusion coefficient, the hydrodynamic radius can be obtained by inserting the measured diffusion coefficient into the Stokes-Einstein equation (Equation 4.1).

$$r = \frac{k_b \times T}{6\pi\eta D}$$

Equation 4.1 Stokes-Einstein equation, where r is the hydrodynamic radius, k_b is the Boltzmann constant, T is the temperature, η is the viscosity of the solvent and D is the diffusion coefficient.

However, there are some limitations to the method. Since the hydrodynamic radius obtained is an expression of the diffusion, large molecules with large cavities, able to let the solvent pass through the molecule, will diffuse faster and result in a smaller hydrodynamic radius. Also, the accuracy of the method is impaired when using mixtures of solvents, since their viscosity cannot be precisely estimated. Nevertheless, when taking these limitations into account, it is possible to derive valuable information from a ^{1}H-DOSY-NMR-experiment.

As can be seen in the spectrum (Figure 4.8) the ^{1}H-NMR-peaks of the complex only produce one set of signals in the ^{1}H-DOSY-NMR, telling us, that only species of one size are present in the solution even when the racemic ligand **12** is used.

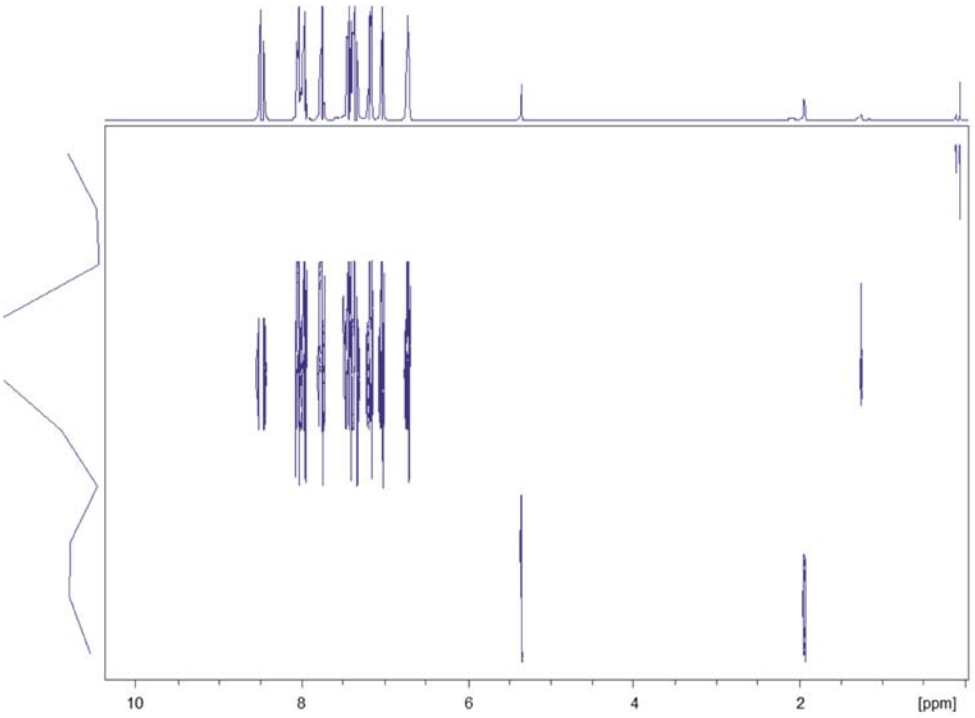

*Figure 4.8 ^{1}H-DOSY-NMR-spectrum of ligand rac-**12** with Pt(dppp)(OTf)$_2$ in CD_2Cl_2/CD_3CN (3:1).*

The signals of the homo – and the heterochiral complexes are very similar and overlap in most cases, which is why it is difficult to assess the exact ratio of the two species. We therefore looked to the ^{31}P-NMR-spectra, which are simpler and therefore easier to compare. The resulting spectra are shown in Figure 4.9.

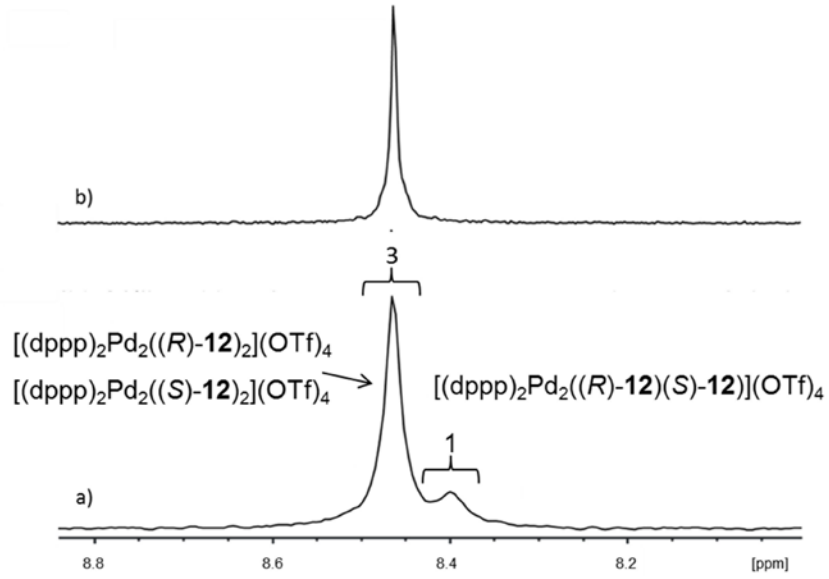

*Figure 4.9 ^{31}P-NMR-spectrum of a) ligand rac-**12** with Pd(dppp)(OTf)$_2$ b) ligand (R)-**12** with Pd(dppp)(OTf)$_2$ in CD_2Cl_2/CD_3CN (3:1).*

The spectrum of the enantiomerically pure ligand mixed with Pd-corner (Figure 4.9b) shows only one peak as expected. When using the racemic ligand two peaks in the ratio of

3:1 are present. The larger peak originates from the two homochiral species $[(dppp)_2Pd_2((R)\text{-}\mathbf{12})_2](OTf)_4$ and $[(dppp)_2Pd_2((S)\text{-}\mathbf{12})_2](OTf)_4$, since we established from the ^{1}H-NMR-spectrum that the homochiral species was predominant. The small peak originates from the heterochiral species $[(dppp)_2Pd_2((R)\text{-}\mathbf{12})(S)\text{-}12)](OTf)_4$.The ratio is 3:1 and the same ratio is also found in the ^{31}P-NMR-spectrum of a mixture of *rac*-**12** with $[Pt(dppp)](OTf)_2$ as shown in Figure 4.10.

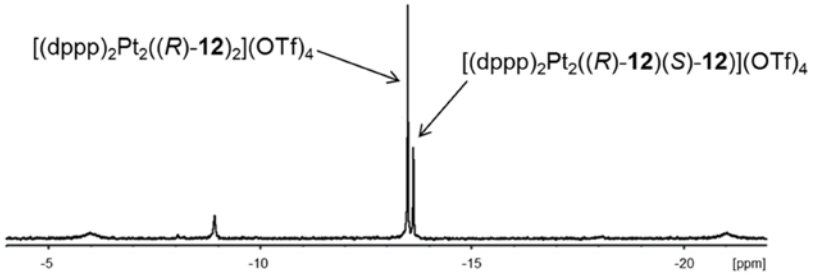

*Figure 4.10 ^{31}P-NMR-spectrum of ligand rac-**12** with Pd(dppp)(OTf)$_2$ in CD_2Cl_2/CD_3CN (3:1).*

The ^{1}H-NMR-spectra indicate strongly, that ligand **12** has a preference for self-recognition. To confirm this mass measurement with ligand **12** were performed. The spectrum is shown in Figure 4.11.

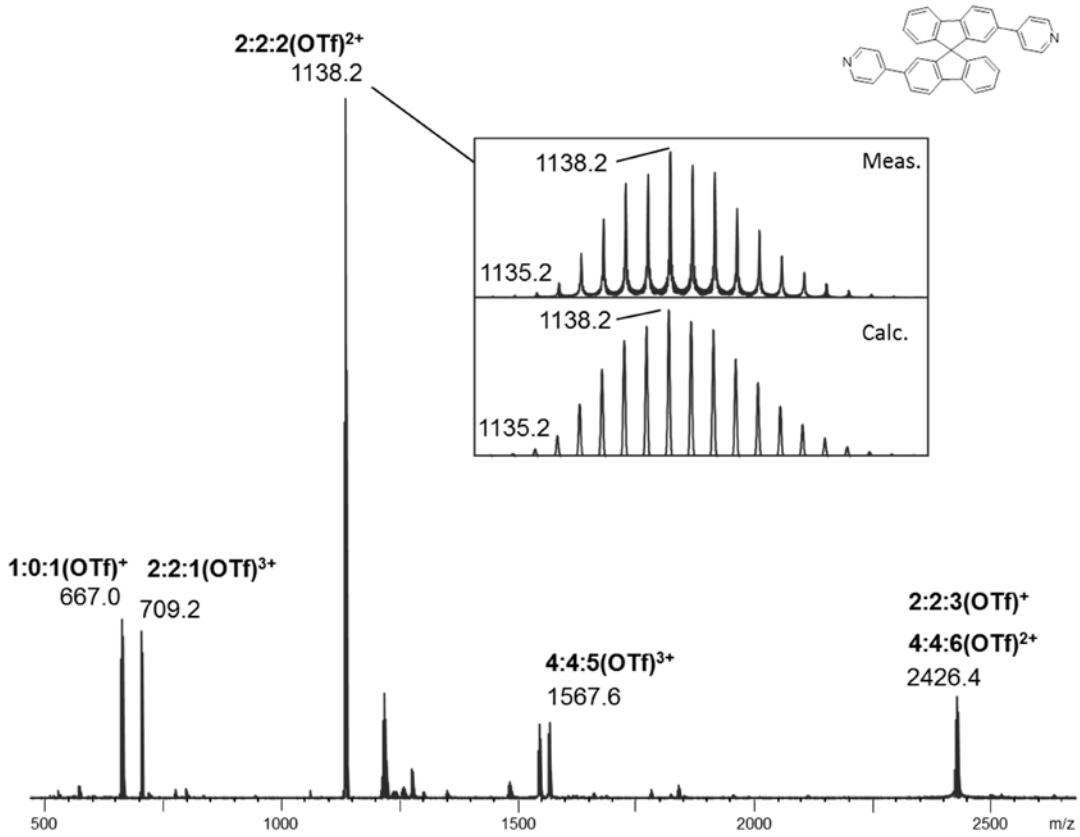

*Figure 4.11 ESI mass spectrum (positive mode) of ligand (R)-**12** with Pd(dppp)(OTf)$_2$ CD_2Cl_2/CD_3CN (3:1) diluted in acetone. The notation corresponds to Metal:Ligand:Anion.*

The base peak of the spectrum is at 1138.2 m/z corresponding to the 2:2-aggregate with two triflate-anions. Peaks at 709.2 and 2426 m/z also originate from the 2:2-aggregate confirming the selective formation of the desired 2:2-rhomb.

It is not possible to see the difference between the different stereoisomers and therefore we used the pseudoenantiomer ligand (*S*)-**21** together with ligand (*R*)-**12**. The two additional methyl-groups on ligand **21** make it possible to distinguish between the (*R*)- and the (*S*)-enantiomer through the m/z-values.

First we wanted to test whether ligand **21** was able to form the desired 2:2-rhombs and therefore mixed ligand (*S*)-**21** with $Pt(dppp)(OTf)_2$ in a stoichiometry of 1:1. A ^{1}H-NMR-spectrum (Figure 4.12) and a mass spectrum (Figure 4.13) were recorded and both confirmed the formation of the desired 2:2-rhomb.

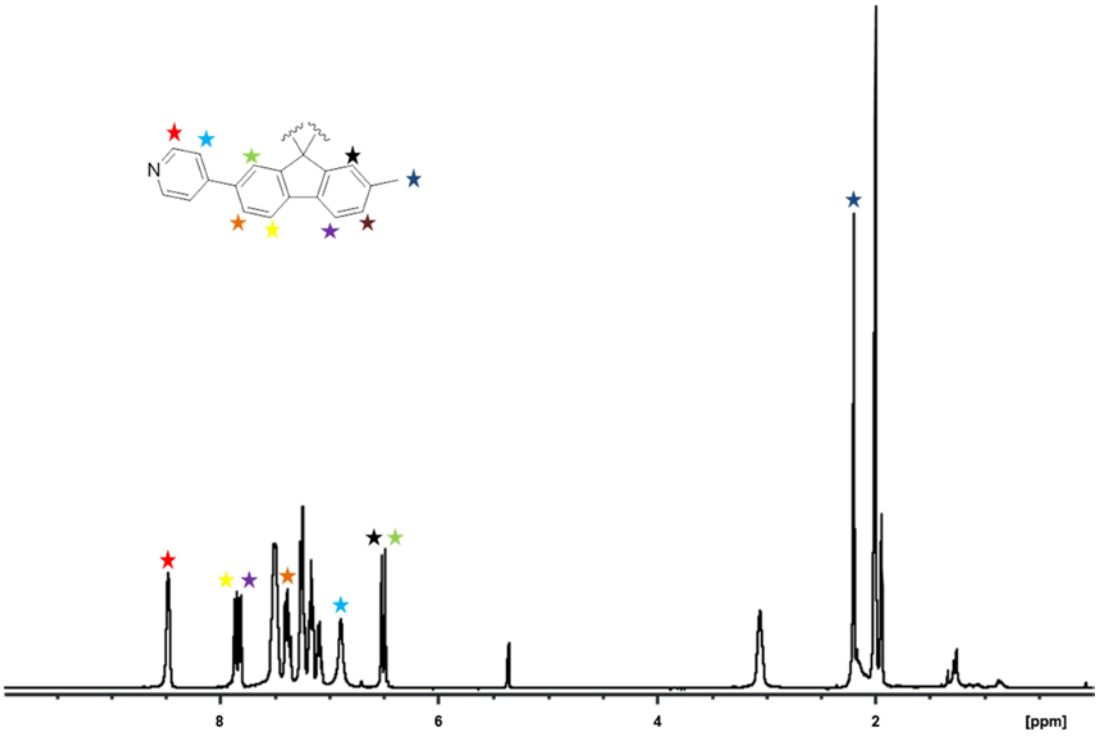

*Figure 4.12 ^{1}H-NMR-spectrum of ligand (S)-**21** withPd(dppp)(OTf)$_2$ in CD_2Cl_2/CD_3CN (3:1).*

Only one set of peaks is seen in the ^{1}H-NMR-spectrum confirming than only one species has been formed.

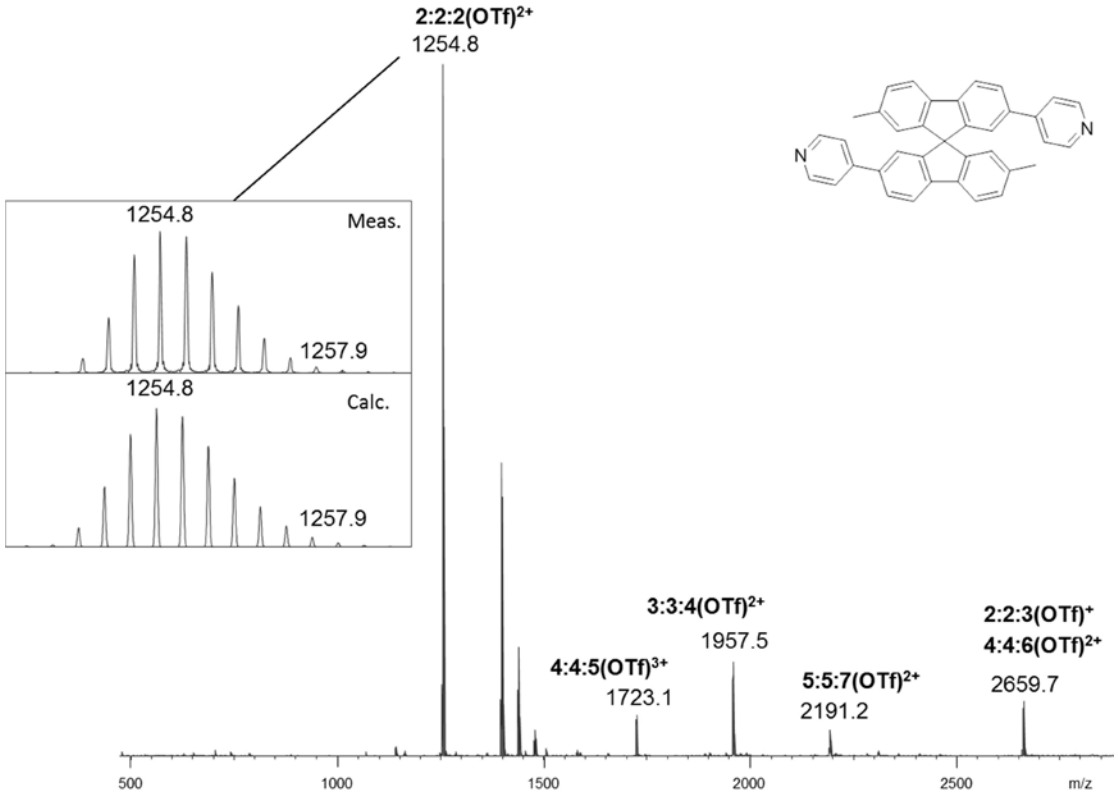

*Figure 4.13 ESI mass spectrum (positive mode) of ligand (S)-**21** with Pt(dppp)(OTf)$_2$ in CD_2Cl_2/CD_3CN (3:1) diluted in acetone. The notation corresponds to Metal:Ligand:Anion.*

The base peak in the spectrum is at 1254.8 m/z and corresponds to the desired 2:2-rhomb with two triflate-anions. In addition, peaks at 1723.1, 1957.5 and 2191.2 m/z originate from non-specific aggregates. Since the ability of ligand **21** to form the 2:2-rhombs had been confirmed, we decided to mix ligand (*S*)-**21** and ligand (*R*)-**12**.

Ligand (*S*)-**21**, ligand (*R*)-**12** and Pt(dppp)(OTf)$_2$ (or Pd(dppp)(OTf)$_2$) were mixed in a ratio of 1:1:2 in CD_2Cl_2/CD_3CN (3:1). The resulting mass spectrum is shown in Figure 4.14.

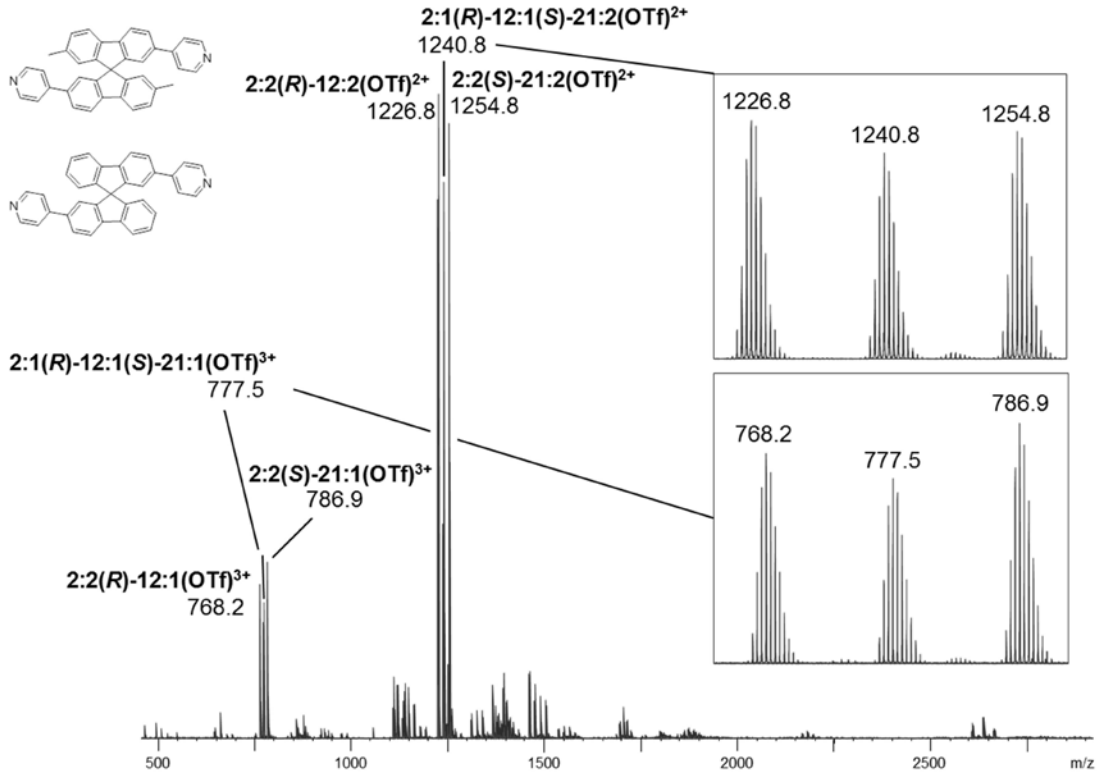

*Figure 4.14 ESI mass spectrum (positive mode) of ligand (R)-**12** and ligand (S)-**21** with Pt(dppp)(OTf)$_2$ in CD_2Cl_2/CD_3CN (3:1) diluted in CH_3CN. The notation corresponds to Metal:Ligand:Anion.*

The spectrum shows one large set of three peaks at 1226.8, 1240.8 and 1254.8 *m/z* corresponding to the three possible 2:2-stereoisomers. The presense of the three different complexes confirms that the self-assembly process is not completely diastereoselective. Since the ratio of the peaks differ from the statistical 1:2:1-ratio in the favor of the homochiral species, this further confirms the findings from the NMR-spectra.

The ratio between the peaks is about 1:0.9:1, strongly favoring the two homochiral species over the heterochiral one.

Furthermore, Dipl. Chem. Georg Meyer-Eppler was able to obtain a crystal structure of the homochiral rhomb from the racemic ligand **12** after stirring for 24 h. This result is significant since normally, the heterochiral complex crystallizes somewhat easier than the homochiral assemblies. The crystal structure of the rhomb is shown in Figure 4.15.

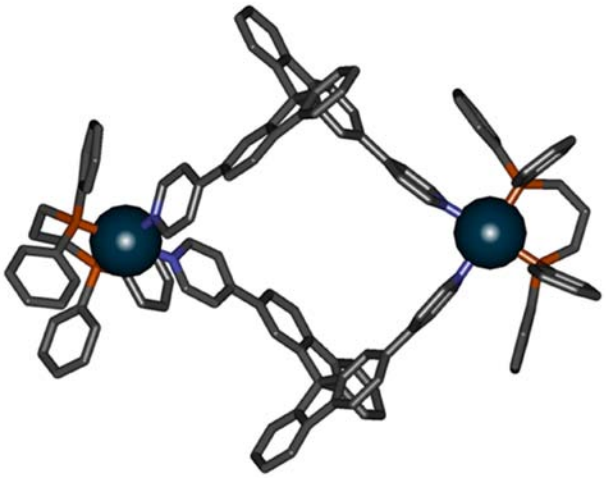

*Figure 4.15 Crystal structure of the homoleptic complex of (S)-**12** and Pd(dppp)(OTf)$_2$ from rac-**12**. Color code: dark grey: carbon, light grey, hydrogen, red: phosphorous, light blue: nitrogen, dark blue: palladium*

The selective formation of 2:2-rhombs of ligand **12** and the Pd- and Pt-corners was confirmed by mass spectrometry and ^{1}H-NMR-spectroscopy. Furthermore, we were able to elucidate the self-sorting behavior of ligand **12** using ^{1}H- and ^{31}P-NMR-spectroscopy and confirm this by mass spectrometry using the pseudoenantiomer **21**. The self-recognition abilities of ligand **12** were further supported when a crystal structure of the homochiral complex was obtained from the racemic mixture.

4.3.2 Large spirobifluorene rhombs

We have established that ligand **12** displays self-recognition during the formation of dinuclear metallosupramolecular rhombs upon coordination to *cis*-protected palladium(II) or platinum(II)-ions and the findings from the ^{1}H-NMR-spectrum and mass spectra were confirmed by a crystal structure.

Next, we were interested in investigating the complexation of ligand **15**, which has an additional ethynyl spacer between the spirobifluorene and the pyridine. Therefore, ligand (*R*)-**15** was complexated with Pd(dppp)(OTf)$_2$ in CH_2Cl_2/CH_3CN (3:1) and characterized by mass spectrometry and NMR-spectroscopy to investigate the behavior of this larger ligand upon coordination.[70]

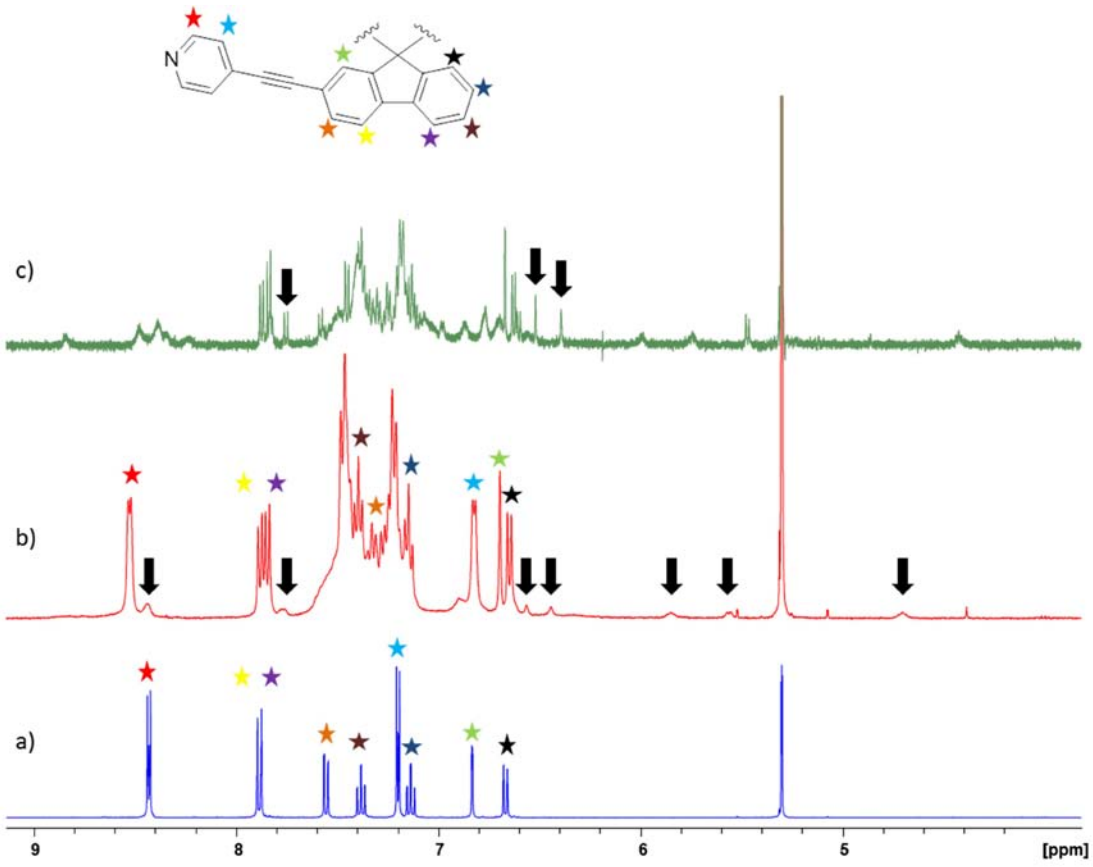

*Figure 4.16 ^{1}H-NMR-spectra of a) Ligand (R)-**15** in CD_2Cl_2/CD_3CN (3:1) b) Ligand (R)-**15** with Pd(dppp)$(OTf)_2$ in CD_2Cl_2/CD_3CN (3:1) at RT c) Ligand (R)-**15** with Pd(dppp)$(OTf)_2$ in CD_2Cl_2/CD_3CN (3:1) at 243K. The black arrows indicate parts of a second, smaller set of signals.*

The ^{1}H- and ^{31}P-NMR-spectra of the complexation of ligand (*R*)-**15** with Pd(dppp)$(OTf)_2$ can be seen in Figure 4.16 while the ^{31}P-NMR-spectra are shown in Figure 4.17. Both spectra were measured at room temperature as well as at 243 K. The signals were assigned using H,H-COSY-NMR. It was not possible to assign proton 3 of the spirobifluorene (orange star) with certainty. Also assignment of the protons in spectrum c at low temperature was not possible.

Starting with ^{1}H-NMR-spectrum of the complex of (*R*)-**15** with Pd(dppp)$(OTf)_2$ at room temperature (Figure 4.16b), we see one dominating set of well-resolved signals. This set contains the same number of signals compared to the spectrum of the free ligand (Figure 4.16a). Several signals are shifted upfield after complexation. As seen before, the protons in the 1-position closest to the pyridine-nitrogen have not shifted much (marked with a red star), as opposed to the proton 1 on the spirobifluorene (green star) and the proton in the 2-position of the pyridine (light blue star). This strongly indicates that the complexation has resulted in a symmetrical complex. The same experiment had previously been performed by Piehler and Hovorka, who came to the same conclusion.

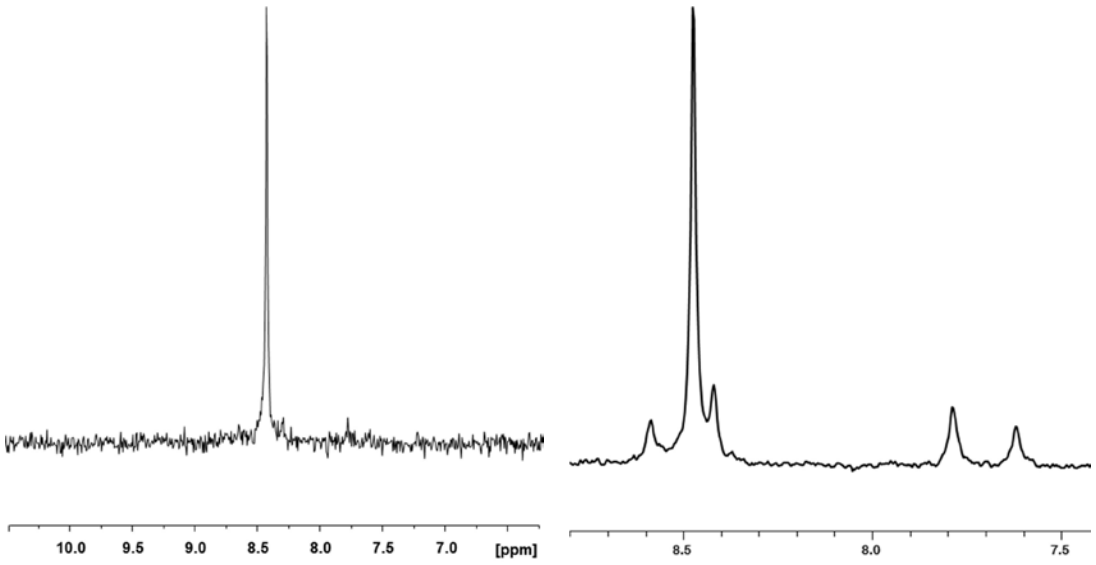

*Figure 4.17 ^{31}P-NMR-spectrum of Ligand (R)-**15** with Pd(dppp)(OTf)$_2$ in CH_2Cl_2/CH_3CN (3:1) at RT (left) and at 243 K (right).*

In addition small, broad peaks in the ^{1}H-NMR-spectrum are observed (marked with black arrows in Figure 4.16b). This second set of signals was not present in the spectra of the pure ligand (*R*)-**15**. When lowering the temperature to 243 K (Figure 4.16c) these peaks are enlarged and become sharper. Only one peak is visible in the ^{31}P-NMR-spectrum of (*R*)-**15** with Pd(dppp)(OTf)$_2$ at room temperature (Figure 4.17 left), but upon cooling another set of signals appears (Figure 4.17 right). The signal in the ^{31}P-NMR-spectrum appears to split up into two doublets, indicating the presence of two sets of magnetically different phosphorous-atoms. It therefore seems that a second, less symmetric species is present in the mixture. Moreover, this second species seems to be in equilibrium with the symmetric complex.

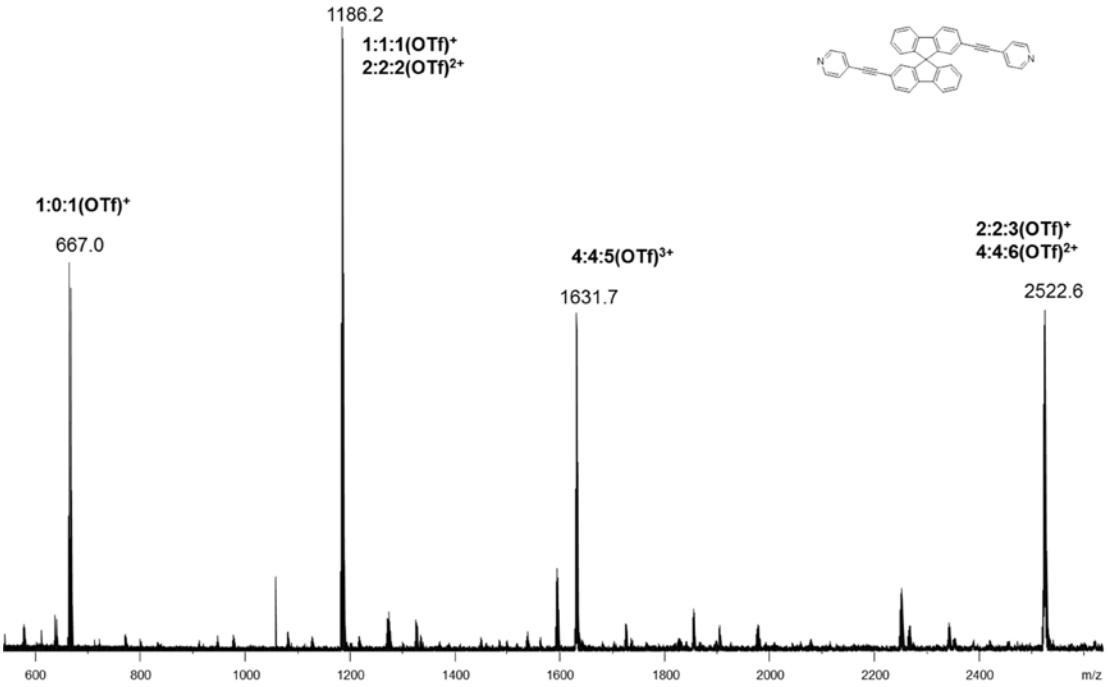

*Figure 4.18 ESI mass spectrum (positive mode) of ligand (R)-**15** with Pd(dppp)(OTf)$_2$ in CH_2Cl_2/CH_3CN (3:1). The notation corresponds to Metal:Ligand:Anion.*

To identify the second species and confirm the formation of the desired 2:2-complex, mass spectroscopy measurements were performed. The resulting mass spectrum can be seen in Figure 4.18. The base peak at 1186.3 m/z originates from the 1:1- as well as the 2:2-complex with triflate as the anion as judged from the isotope pattern and the charge of the peaks. This confirms the formation of the supramolecular rhomb. Interestingly, the rather large peak at 1631.7 m/z results from a 4:4:5-complex. A peak at 2522.6 m/z corresponds to the 2:2:3-complex. Underneath this same peak a 4:4-complex with six triflate-ions is also found. This 4:4-species was also seen in the measurements performed by Piehler and Hovorka, confirming the reproducibility of this experiment. This 4:4-species is not simply a non-specific aggregate as we have seen before, but judging from the ^{1}H- and ^{31}P-NMR-spectra the 4:4-complex originates from a defined structure, which is in equilibrium with the 2:2-complex.

The mass spectrum reveals that the second set of signals in the ^{1}H-NMR-spectrum could originate from the 4:4-complex observed in the mass spectrum. This leaves three structural possibilities for the 4:4-complex: a catenane (two interlocked rings[71]), a macrocycle or a sandwich-complex (Figure 4.19).

Figure 4.19 Illustration of the possible structures for 4:4-complex c) catenane b) sandwich complex and c) macrocycle

Starting with the macrocycle, this structure is not planar but folded into itself, resulting in magnetically different P-atoms. If the two 2:2-rhombs in the sandwich complex are layered exactly on top of each other, we would expect two signals in the ^{31}P-NMR-spectrum. However, if the 2:2-rhombs are not arranged directly on top of each other, this could result in the emergence of more than two ^{31}P-signals. A catenane-complex would also result in at least two different P-atoms, however similar metallosupramolecular catenanes have previously only been observed in aqueous solution as a result of the hydrophobic effect.[72–75]

Mass spectrometry combined with IRMPD[II]-measurements was used to distinguish between the three structures. When irradiating the complex with a laser, the weakest bond is expected to break first. In case of a sandwich complex one would expect to find a 2:2:2- or 2:2:3-complex after the first irradiation. If instead a macrocycle has been formed, the emergence of a 2:3-complex with an undefined number of anions would be a proof of its existence, since this fragment cannot arise from the two other structures. The absence of the fragments mentioned above would be an indication of the formation of a catenane.

The IRMPD-measurements were performed by Piehler and Hovorka on the 4:4:5-ion. It was hoped that the formation of the macrocycle and the sandwich complex could be ruled out. However, it is difficult to distinguish between fragmentation of the catenane and the sandwich complex, since both are expected to produce a 2:2-complex with and unknown number of anions. After irradiation of the 4:4:5-complex for two seconds, one of the Pd-corners and an anion was separated from the complex resulting in a 3:4:4 - and a 1:0:1-fragment. Three seconds of irradiation resulted in the separation of one ligand from the 3:4:4-fragment to produce a 3:3:4-fragment. Further irradiation of the fragment, lead to the alternating separation of one metal and one ligand. Since no separation of a 2:2:2-fragment was observed, a sandwich-structured complex is highly unlikely. Furthermore, we cannot with certainty rule out the formation of a macrocycle, because the fragmentation pattern does not allow the formation of a 3:2-complex.

We therefore still needed more information to determine the structure of the 4:4-complex, so crystallization attempts were made in different solvents by me in cooperation with Dipl. Chem. Georg Meyer-Eppler. It is important to emphasize, that the chances of obtaining crystals of the 4:4-species compared to the 2:2-species are relatively slim considering the

[II] Infrared multiphoton dissociation

ratio between the two complexes. Nevertheless, using ethylacetate as the antisolvent we were able to obtain a crystal structure, which proved the 4:4-complex to be a catenane. The crystal structure is shown in the space filling and the stick model in Figure 4.20. The two rhombs are placed almost parallel and fit exactly into each other with the spirobifluorene core filling out the cavities perfectly. From the crystal structure, one could assume that π-π-stacking plays a role in the interaction of the two rhombs (Figure 4.20, purple and yellow respectively). The stick model also suggests that the protons from the spirobifluorene interact with the π-system of the pyridine. The dense packing of the catenane might also explain why it crystallizes better than the rhombic structure.

From the crystal structure we can explain the signals in the ^{1}H- and ^{31}P-NMR-spectra. The four ligands comprising the catenane can be divided into two outer and two inner ligands in environments differing from the environment in the 2:2-rhomb, resulting in two different sets of signals shifted compared to the signals from the rhomb. The phosphorous-ions become magnetically different upon cooling. The 1,3-bis(diphenylphosphino)propane-ligand (dppp) on adjacent palladium(II)-ions needs to twist in order to accommodate the benzene rings. At room temperature the two adjacent dppp-ligands are able rotate around the Pd-P-bond and the P-ions are therefore indistinguishable from each other. Upon cooling the rotation decreases and the ligands are locked in an unsymmetrical position resulting in two magnetically different P-atoms. The crystal structure also demonstrates that the formation of the catenane is not a result of hydrophobic effects, but instead of a template effect.[70]

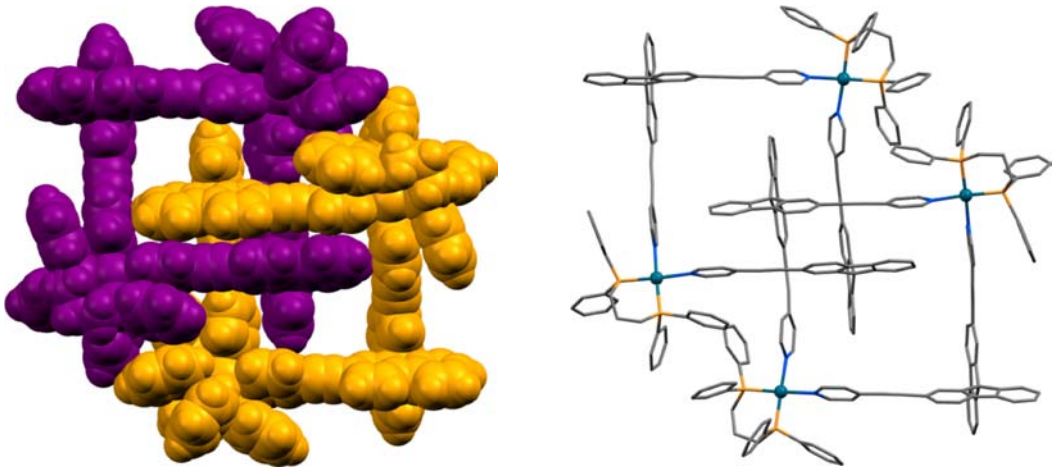

*Figure 4.20 Crystal structure of the catenane of ligand (R)-**15** with Pd(dppp)(OTf)$_2$, on the left in the space filling model and on the right in the stick model. Color code: grey: carbon, yellow: phosphorous, blue: nitrogen, green: palladium*

We also wanted to investigate the self-sorting behavior of ligand (*R*)-**15** during formation of the 2:2-rhomb by the means of pseudoenantiomer ligand (*S*)-**20** (Figure 4.21). Due to the extra methylgroups in ligand (*S*)-**20**, the two enantiomers can be distinguished from each other.

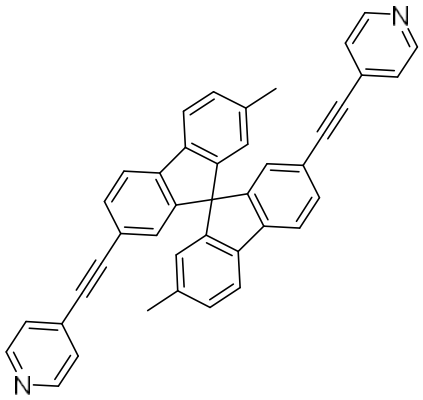

20

*Figure 4.21 Pseudoenantiomer of ligand **15***

We started with establishing the ability of ligand **20** to form a rhombic structure, to ensure its usefulness together with ligand (*R*)-**15**. Therefore (*S*)-**20** was mixed with $Pd(dppp)(OTf)_2$ in CD_2Cl_2/CD_3CN (3:1) and stirred for 24 hours. The resulting ^{1}H-NMR-spectrum (Figure 4.22b) was compared to the spectrum of the free ligand (Figure 4.22a).

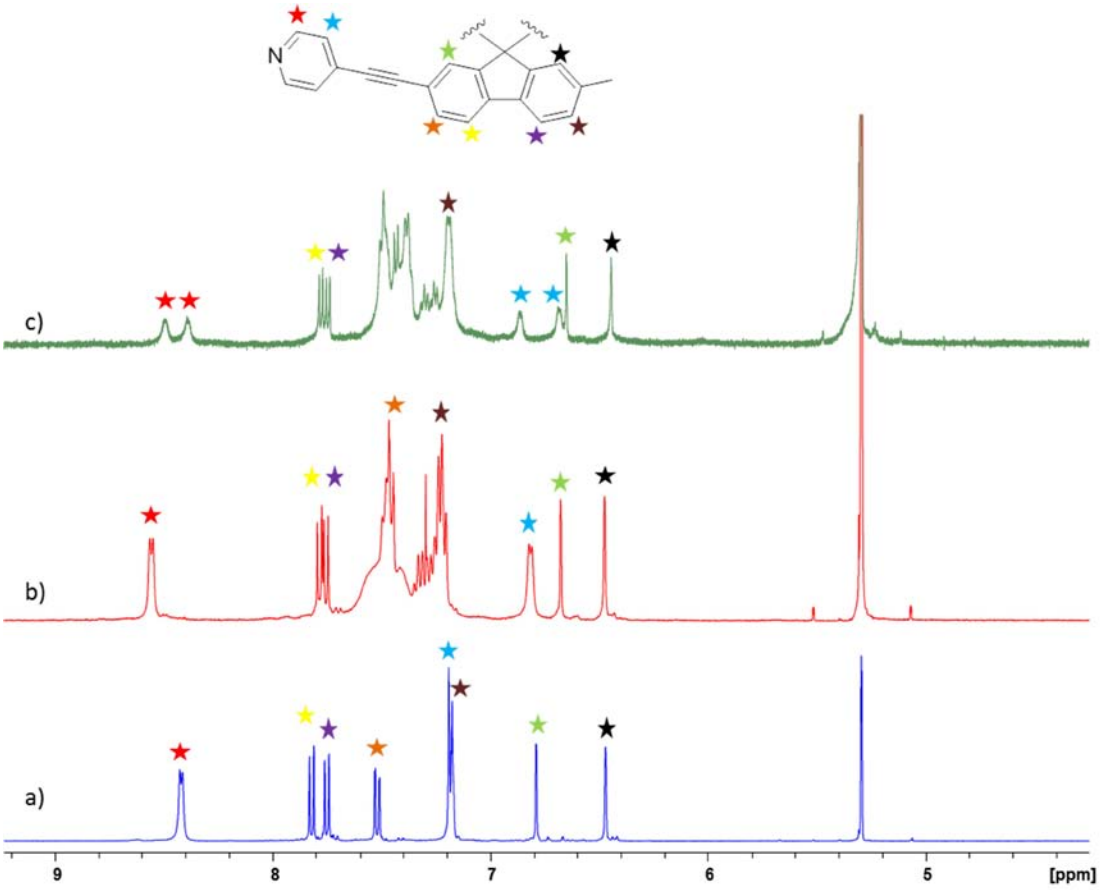

*Figure 4.22 ^{1}H-NMR-spectra of a) Ligand (S)-**20** in CD_2Cl_2/CD_3CN (3:1) b) Ligand (S)-**20** with Pd(dppp)$(OTf)_2$ in CD_2Cl_2/CD_3CN (3:1) at RT c) Ligand (S)-**20** with Pd(dppp)$(OTf)_2$ in CD_2Cl_2/CD_3CN (3:1) at 233 K*

The number of signals in the red and blue spectra is constant, while many signals are shifted, indicating the formation of only one species. A rather large upfield shift of about 0.1 ppm is seen for the peak belonging to the proton next to the pyridine-N (at 8.5 ppm. marked with a red star), further confirming the complexation of the pyridine-entity to the Pd-corner. Generally, the changes in shifts are very similar to the ones seen in the complexation of ligand (*R*)-**15** (Figure 4.16). The peaks were assigned via H,H-COSY-NMR. It was not possible to assign proton 3 and 6 (marked with an orange and a brown star respectively) with certainty. More importantly, no peaks indicating the formation of a catenane are present. This confirms the observation from the crystal structure of the catenane of (*R*)-**15**

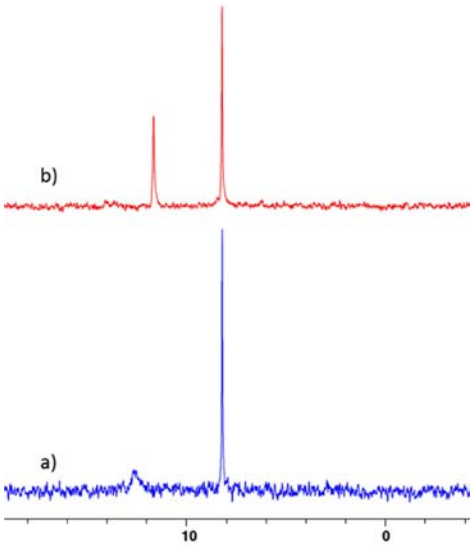

*Figure 4.23 ^{31}P-NMR-spectrum of a) ligand (S)-**20** with Pd(dppp)$(OTf)_2$ at RT b) ligand (S)-**20** with Pd(dppp)$(OTf)_2$ at 243 K*

(Figure 4.20), that the cavity of the catenane is too small to accommodate the methyl groups of (*S*)-**20**.

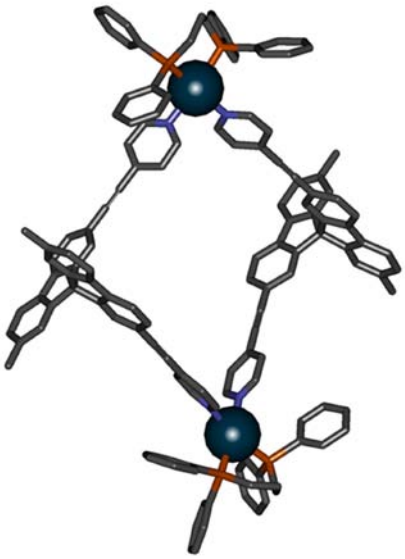

*Figure 4.24 Minimized structure of the complex of ligand (S)-**20** and Pd(dppp)OTf$_2$*

The ^{1}H- and ^{31}P-NMR-spectra were recorded at 233 K (See Figure 4.23c and Figure 4.23b respectively). Interestingly, the two protons at the pyridine in the ^{1}H-NMR-spectrum split up when lowering the temperature to 233 K. Similarly, a second peak emerges in the ^{31}P-NMR-spectrum at low temperatures compared to the spectrum recorded at room temperature. Since none of the other signals display similar behavior, a possible explanation is that the movement around the Pd-N-bond decreases on cooling of the complex, thereby locking the pyridine, which results in two different possible positions for the pyridine-protons as well as the P-atoms. A modeled structure of the complex is shown in Figure 4.24.

To investigate the ability of ligand (*S*)-**20** to form mixed complexes with ligand (*R*)-**15**, a 1:1 mixture of the two ligands with one equivalent of Pd(dppp)(OTf)$_2$ was prepared and ^{1}H- and ^{31}P-NMR-spectra were measured (See Figure 4.25 and Figure 4.26 respectively). In the case of self-recognition, two different supramolecular rhombs would be formed and the mixed spectrum would be a superimposition of the two separate complexes. This will not be the case, if self-discrimination is the major effect during complexation, instead the ^{1}H-NMR-spectrum of the mixed complex would display a new set of signals, which cannot be found in any of the separate complexes. Again, pure self-discrimination or self-recognition is rare, and it is more likely to find a preference towards one of the two. If no self-sorting is taking place we will see an intensity-ratio of homo:hetero:homo of 1:2:1.

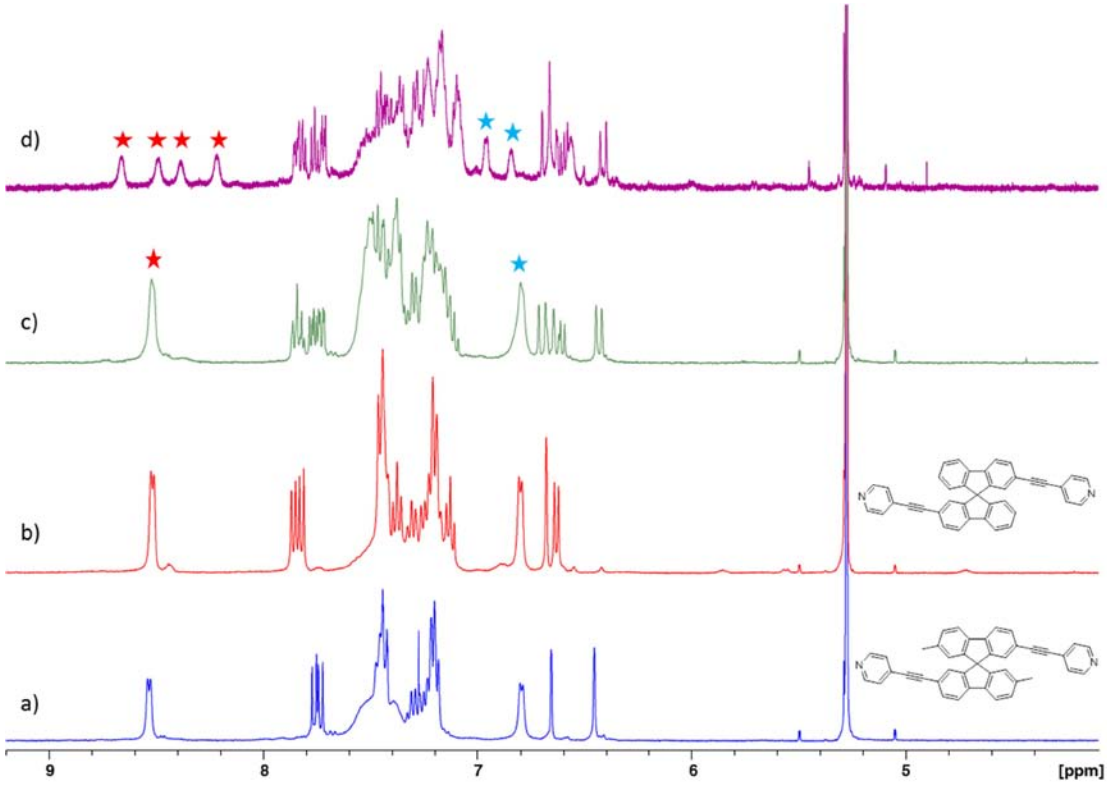

*Figure 4.25 ^{1}H-NMR-spectra of a) Ligand (S)-**20** with Pd(dppp)(OTf)$_2$ in CD_2Cl_2/CD_3CN (3:1) b) Ligand (R)-**20** with Pd(dppp)(OTf)$_2$ in CD_2Cl_2/CD_3CN (3:1) at RT c) Ligands (S)-**20** and (R)-**15** with Pd(dppp)(OTf)$_2$ in CD_2Cl_2/CD_3CN (3:1) at RT d) Ligands (S)-**20** and (R)-**15** with Pd(dppp)(OTf)$_2$ in CD_2Cl_2/CD_3CN (3:1) at 233 K.*

From the ^{1}H-NMR-spectra we can conclude that all three possible complexes have formed since signals originating from the two homochiral complexes can be seen along with signals not belonging to either of the homochiral species. It is also worth noticing that no peaks corresponding to the catenane are present in the mixed structure. Upon cooling to 233 K, the most significant change happens around the peaks corresponding to the pyridine-protons (Figure 4.25d). The signal from proton 2 on the pyridine (marked with a red star) splits into four peaks, while the signal corresponding to proton 3 on the pyridine (marked with a light blue star) splits into at least two peaks. In the ^{31}P-NMR-spectrum two peaks in the relative intensity of 1:0.75 are present (Figure 4.26a), indicating the formation of two species. The two peaks correspond to each of the complexes of ligands (*R*)-**15** and (*S*)-**20**. Apparently, the change in the chemical environment upon formation of the mixed complex is not significant enough to result in a third and fourth signal from the phosphorous. No change is seen in the ^{31}P-NMR-spectrum upon cooling the complex solution (Figure 4.26b).

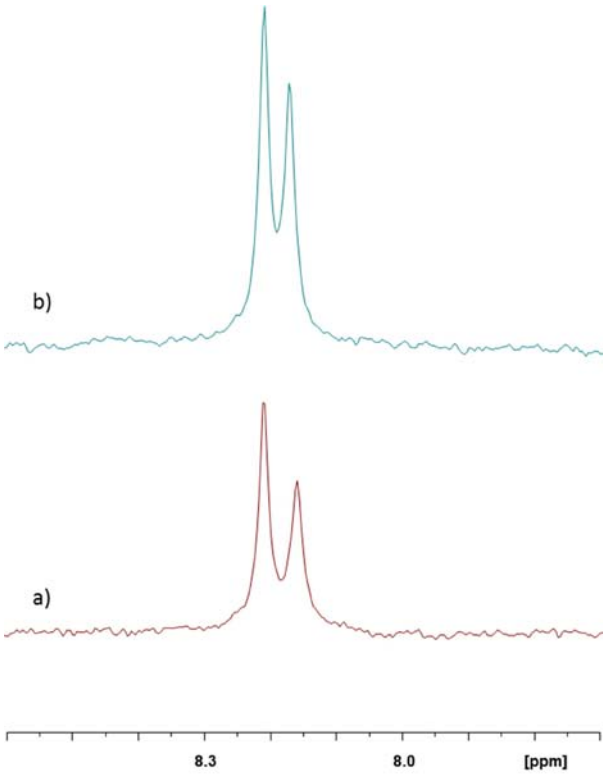

*Figure 4.26 ^{31}P-NMR-spectrum of a) Ligands (S)-**20** and (R)-**15** with Pd(dppp)(OTf)$_2$ in CD_2Cl_2/CD_3CN (3:1) at RT b) Ligands (S)-**20** and (R)-**15** with Pd(dppp)(OTf)$_2$ in CD_2Cl_2/CD_3CN (3:1) at 233 K*

In order to investigate whether self-discrimination or self-recognition is preferred in the self-assembly of ligand **15** and **20**, a closer look was taken at the ^{1}H-NMR-spectra. As mentioned earlier, when no self-sorting is taking place, the ratio of homo:hetero:homo is statistical, making it twice as likely that (*R*)- and (*S*)-enantiomers form a complex in solution than two (*R*)- or two (*S*)-enantiomers. Consequently the ratio of homo:hetero:homo complexes is 1:2:1. In the ^{1}H-NMR-spectrum we would expect to see four sets of signals in total; Two for each of the homochiral complexes and two for the heterochiral complex. Since the two ligands comprising the heterochiral complex are different, we expect to see two sets of signals. This results in a ratio of 1(homo):1(hetero):1(hetero):1(homo) in case of a statistical distribution.

Therefore we were looking for three distinct peaks in the ^{1}H-NMR-spectrum, corresponding to the two homochiral complexes and the heterochiral one. We were able to find a section in the ^{1}H-NMR-spectra between 7.90 and 7.70 ppm (Figure 4.27). Comparing the spectrum of the complex of ligand (*S*)-**20** (Figure 4.27c) and ligand (*R*)-**15** (Figure 4.27a) with the spectrum of the mixed solution (Figure 4.27b), it becomes apparent that an additional sets of doublet of doublets have formed (green star) which cannot be found in either of the spectra of the individual ligands. These peaks must belong to the heterochiral complex. Next to these peaks, two sets of doublets originating from the complex of ligand (*S*)-**20** can be seen (black arrows) indicating that the new set of signals belongs to ligand (*S*)-**20** in the heterochiral complex. The intensities of the sets of doublets are roughly 1:1, indicating that the mixture is statistical for ligand (*S*)-**20**. It was not possible to find a similar set of signals for ligand (*R*)-**15** and the heterochiral complex, therefore it is not possible to perform the same investigation for the homochiral complex comprised of (*R*)-**15** and the heterochiral complex.

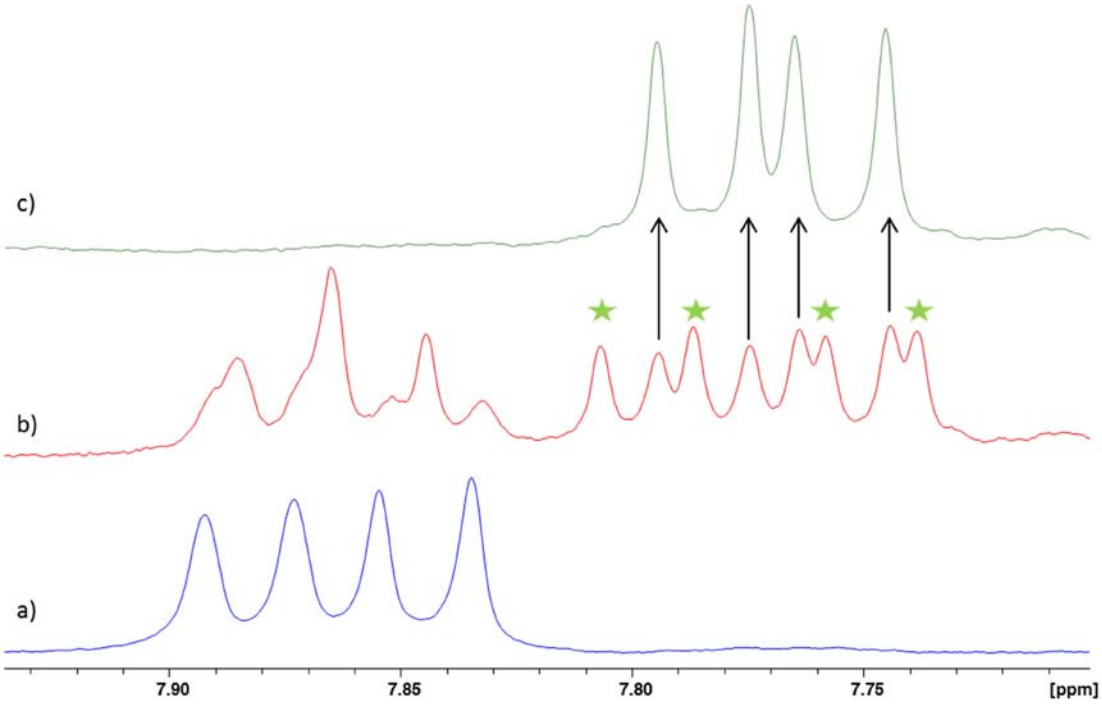

*Figure 4.27 Section of the ^{1}H-NMR-spectra of a) Ligand (R)-**15** with Pd(dppp)(OTf)$_2$ in CD_2Cl_2/CD_3CN (3:1) b) Ligands (S)-**20** and (R)-**15** with Pd(dppp)(OTf)$_2$ in CD_2Cl_2/CD_3CN (3:1) c) Ligand (S)-**20** with Pd(dppp)(OTf)$_2$ in CD_2Cl_2/CD_3CN (3:1). The green stars indicate peaks arising from the mixed complex. The black arrows indicate the presence of the peaks originating from ligand (S)-**20** in the mixed spectrum.*

We therefore turned to mass spectrometry, to help get further information on the mixed complex of (*R*)-**15** and (*S*)-**20** as well as the complex of (*S*)-**20**. The mass spectrum of the mixed complex is shown in Figure 4.28.

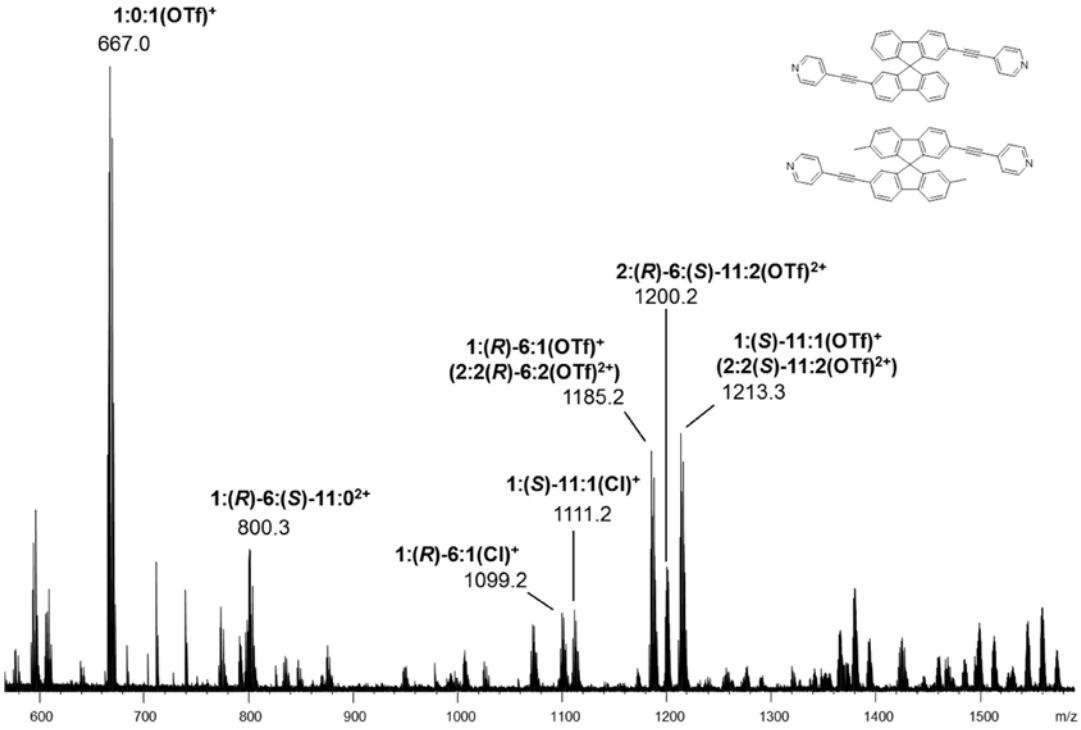

*Figure 4.28 ESI mass spectrum (positive mode) of ligand (R)-**15** and ligand (S)-**20** with Pd(dppp)(OTf)$_2$ in CD_2Cl_2/CD_3CN (3:1). The notation corresponds to Metal:Ligand:Anion.*

In the spectrum we see a series of peaks at 1185.2, 1200.2 and 2213.3 m/z, which are suited to evaluate the self-sorting behavior of ligand (*R*)-**15**. The two larger peaks at 1185.2 and 2213.3 m/z can be assigned to the 1:1-complexes of each of the pseudoenantiomers (*R*)-**15** and (*S*)-**20**. However, underneath the two peaks the doubly charged 2:2-complex of both pseudo enantiomers can be observed. In addition, the signal in between at 1200.2 m/z corresponds to the mixed complex of (*R*)-**15** and (*S*)-**20**. We also observed peaks originating from the 1:2-complex (at 800.3 m/z) as well as both of the 1:1-complexes (1099.2 and 1111.2 m/z), which probably are fragments resulting from the measurement in the mass spectrometer, since the ^{1}H-NMR-spectra do not indicate formation of asymmetric species.

It should be possible to deduce the selectivity of the ligands from their intensity in the mass spectra. Here we look at the three signals at 1185.2, 1200.2 and 1213.2 *m/z*, the only set of all three signals originating from all the three possible 2:2-complexes. However, overlapping the homochiral 2:2-complexes are the corresponding 1:1-complexes. Therefore this should only be a rough estimate

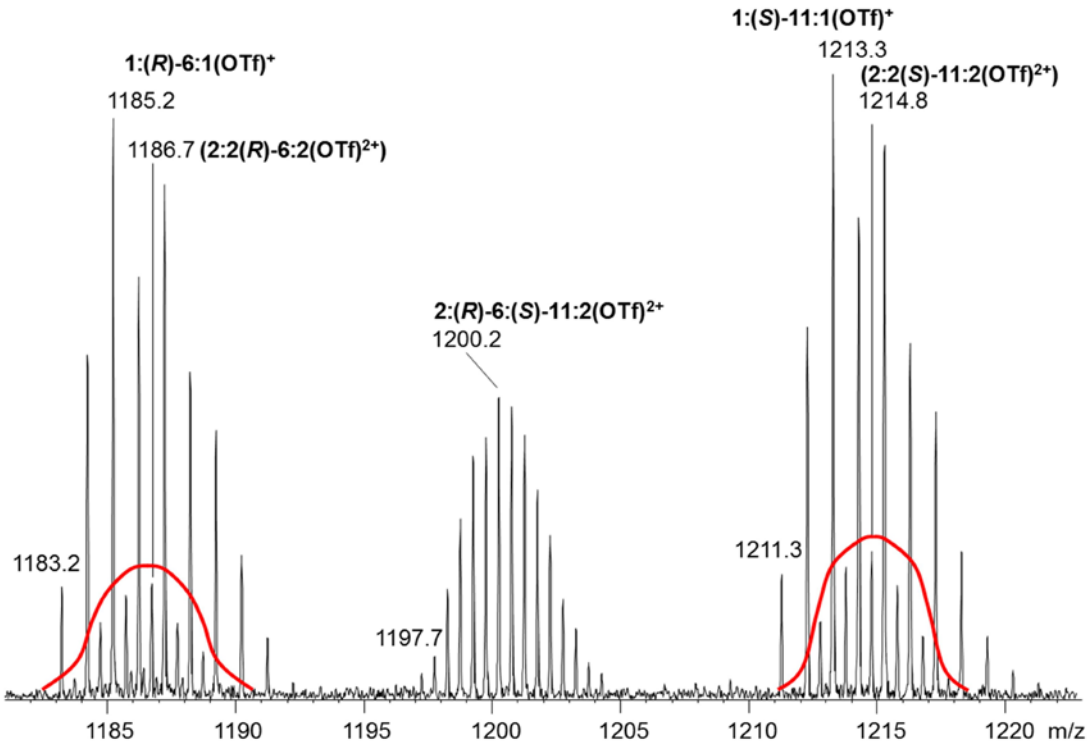

*Figure 4.29 Section of the ESI positive of ligand (R)-**15** and ligand (S)-**20** with Pd(dppp)(OTf)$_2$ in CH_2Cl_2/CH_3CN (3:1). The signalsets from the homochiral complexes are marked in red.*

Figure 4.29 is a detail of the spectrum of the mixed complexes of ligands (*R*)-**15** and ligand (*S*)-**20** showing the peaks corresponding to each of the homochiral and the heterochiral complexes. In addition, the 1:1-complexes of both ligands are also present in the spectrum overlapping the homochiral 2:2-complexes. Therefore comparison of the intensities is not straight forward. The 2:2-complexes are doubly charged and therefore display two peaks per mass in the spectrum, while the 1:1-complexes are singly charged and only display one peak per mass (Figure 4.29). This means, that every second peak originating from the 2:2-complex is covered by a peak from the 1:1-complex. To determine which peak is the highest of the 2:2-complex, a simulation of the peaks of both 2:2-complexes was done in Bruker *Data Analysis 4.0*, which showed that the peaks at 1186.7 and 1214.8 m/z are the highest for the 2:2-complexes of ligand (*R*)-**15** and (*S*)-**20** respectively. The intensities of the peaks at 1186.7 and 1214.8 m/z where compared with the peak from the heterochiral complex at 1200.2 m/z. This resulted in a ratio of 1((*R*)-**15**):2.7((*R*)-**15**/(*S*)-**20**):1.4((*S*)-**20**), which matches the statistical distribution of 1:2:1 expected from the ^{1}H-NMR-spectrum quite well, although the ratio is not a perfect 1:2:1-ratio. An explanation for this could be the additional peaks at 800.3, 1099.2 and 1111.2 m/z in the mass spectrum (Figure 4.28), which all contain one or both ligands. It is possible that these fragments disturb and alter the ratio between the 2:2-rhombs. If no fragments were present it is possible that the ratio would change into the expected 1:2:1-ratio. Further mass measurements would have to be performed in order to verify this assumption and confirm the statistical distribution of the

complexes. However, the experiments so far suggest that ligand **15** displays little self-sorting behavior.

We also investigated the complexation and self-sorting of ligand **15** in other solvents: Acetone-d_6 and DMF-d_7, with interesting results. The complexation in acetone of ligand (*R*)-**15** ^{1}H- and ^{31}P-NMR-spectra were recorded and compared to the uncomplexed ligand (Figure 4.30 and Figure 4.31).

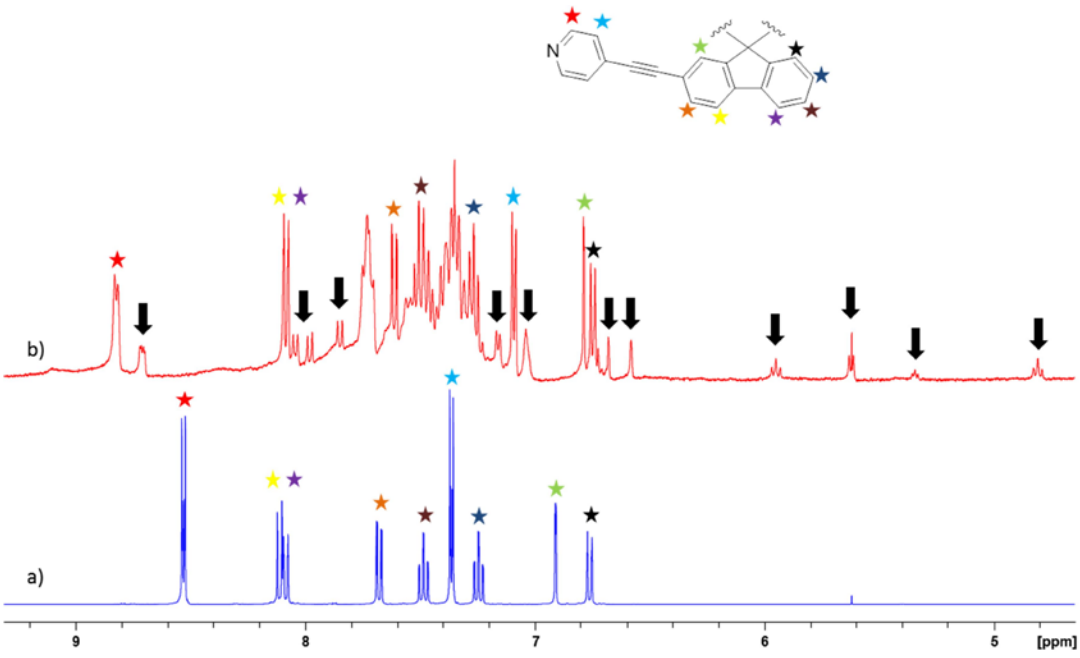

*Figure 4.30 ^{1}H-NMR-spectra of a) Ligand (*R*)-**15** in acetone-d_6 b) Ligand (*R*)-**15** with Pd(dppp)(OTf)$_2$ in acetone-d_6*

The protons closest to the metal-binding pyridine-N are all shifted compared to the free ligand. Similar to what we observed in CD_2Cl_2/CD_3CN a second set of peaks (marked with black arrows) is found in the spectrum, with a relative intensity of 1:0.4 (Figure 4.30b). The second set of signals originating from the catenane seems to have a greater intensity in acetone than in CD_2Cl_2/CD_3CN. This is confirmed by the ^{31}P-NMR-spectrum (Figure 4.31), where the two doublets are present even at room temperature. The protons were assigned using H,H-COSY-NMR. It was not possible to assign proton 6 of the spirobifluorene (marked with a brown star) unambiguously.

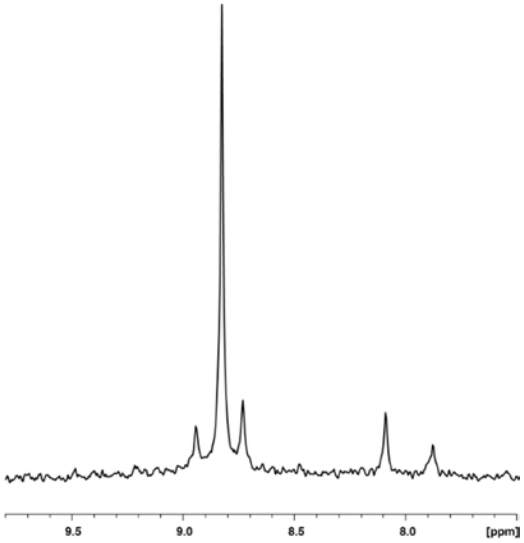

*Figure 4.31 ^{31}P-NMR-spectrum of ligand (R)-**15** with Pd(dppp)(OTf)$_2$ in acetone-d$_6$ at RT*

A mass spectrum was recorded in acetone which is shown in Figure 4.32. Many of the peaks recur compared to the spectrum recorded in CD_2Cl_2/CD_3CN (Figure 4.28). The base peak at 518.1 m/z originates from two species, the 2:2:0^{2+}- and the 1:1:0^{+}-complexes. The peak at 1631.0 m/z corresponds to the 4:4:5^{3+}-complex, the 2:2:2^{2+}- and the 1:1:1^{+}-complex can be found at 1186.2 m/z. When looking very closely at the peak at 1186.2 m/z, it is possible to a very small set of peaks originating from the 4:4:4-complex.

In addition, we see a peak at 1854.3 m/z corresponding to the 6:6:8^{4+}-complex, which probably originates from a non-specific aggregate during the measurement resulting in the loose assembly of a 4:4- and a 2:2-complex. Another possibility is that three 2:2-complexes have assembled, but it is more likely that two species find each other rather than three. The peak at 777.2 m/z could not be identified.

The formation of the desired 2:2-rhomb in acetone-d$_6$ was confirmed. It was also made plausible, that catenane-formation is favored in acetone-d$_6$ compared to the mixture of dichloromethane and acetonitrile.

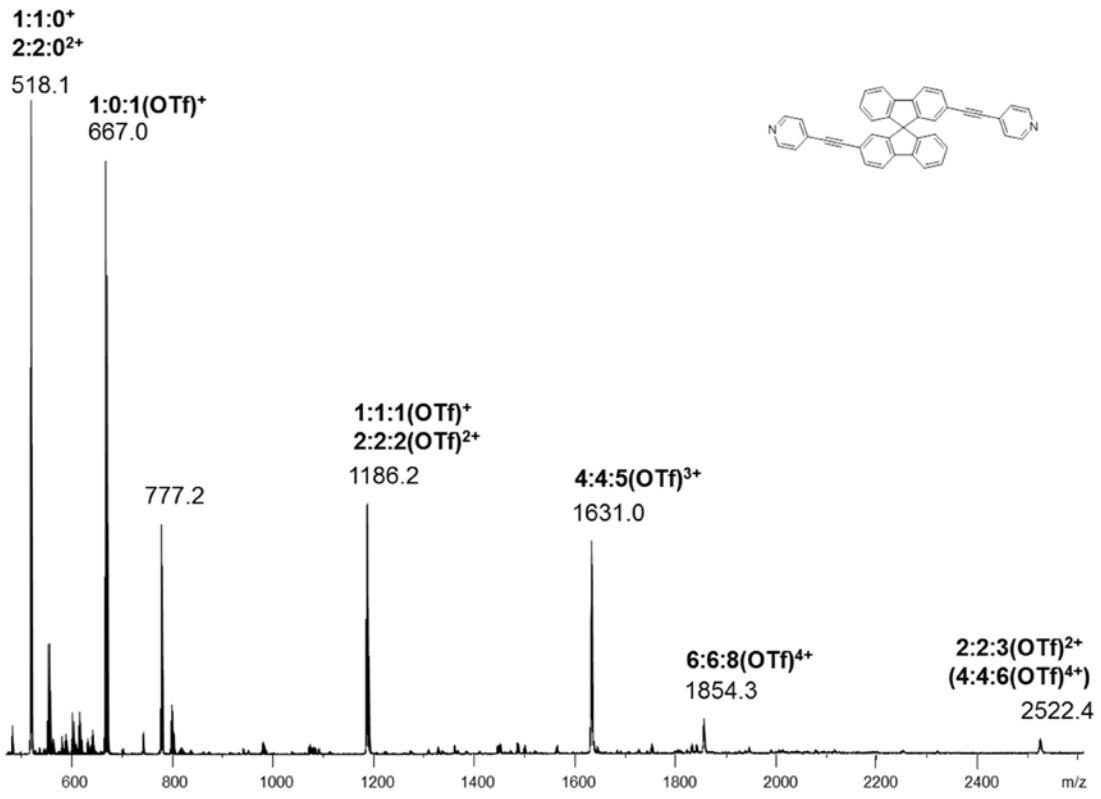

*Figure 4.32 ESI mass spectrum (positive mode) of ligand (R)-**15** with Pd(dppp)(OTf)$_2$ in acetone. The notation corresponds to Metal:Ligand:Anion.*

The complex of ligand (*S*)-**20** with Pd(dppp)(OTf)$_2$ in acetone was also investigated by ^{1}H- and ^{31}P-NMR (See Figure 4.33 for ^{1}H-NMR-spectrum). As in CD_2Cl_2/CD_3CN (Figure 4.22) only one species is formed since only one set of signals can be observed. The ^{31}P-NMR-spectrum shows only one peak, confirming the result from the ^{1}H-NMR-spectrum (Figure 4.33). The shift of proton 1 and 2 on the pyridine (marked with a red and green star respectively) is more significant than in CD_2Cl_2/CD_3CN. The spectrum is well resolved and all peaks could be assigned via H,H-COSY-NMR. Again, no signals corresponding to the catenane are observed, confirming that ligand **20** is not able to form a catenane, due to the two additional methyl groups in the 7,7'-position.

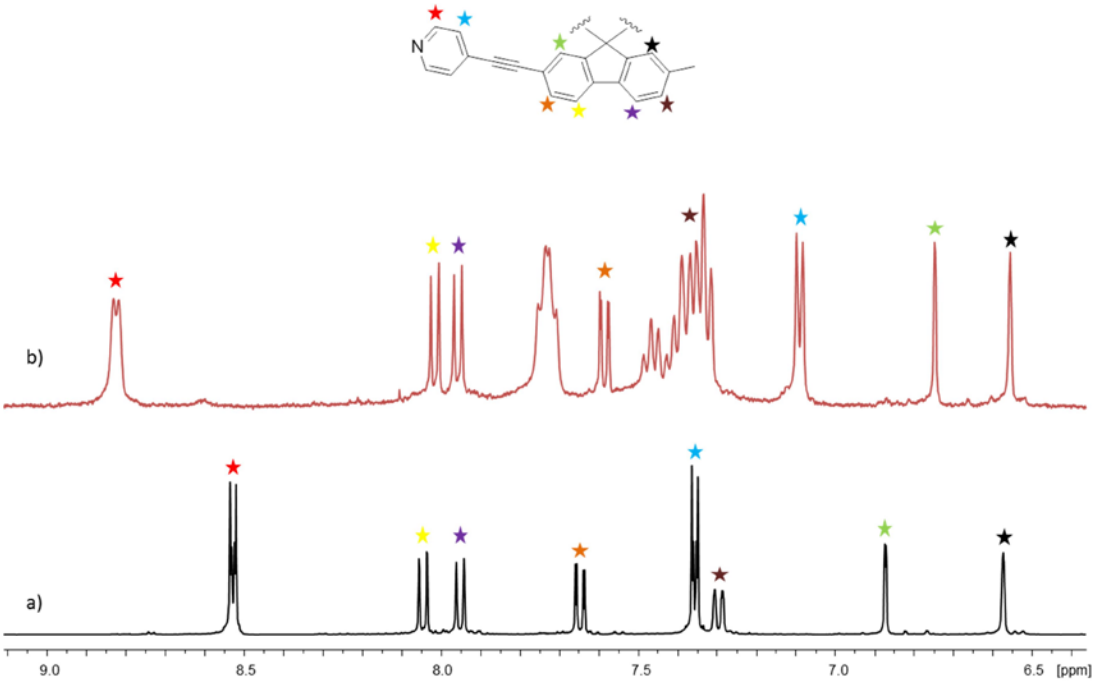

*Figure 4.33 ^{1}H-NMR-spectrum of a) ligand (S)-**20** in acetone-d_6 b) ligand (S)-**20** with Pd(dppp)(OTf)$_2$ in acetone-d_6.*

A mass spectrum of the complex of ligand (*S*)-**20** with the Pd-corner in acetone was obtained and the result is shown in Figure 4.34. The largest peak in the spectrum at 1214.2 m/z originates from the desired 2:2-complex with two triflate anions as well as the 1:1-complex with one triflate anion. It was not possible to identify all peaks in the spectrum, but most seem to be 1:1- or 1:0-complexes with an unknown anion. This is supported by the ^{1}H-NMR-spectrum, which shows no signals corresponding to an asymmetrically substituted ligand.

Interestingly, a peak at 1668.9 m/z can be ascribed to the 4:4:5-complex. As discussed earlier, the crystal structure of ligand (*R*)-**15** (Figure 4.20) indicates that catenane-formation with ligand **20** should be highly disfavored. The ^{1}H-NMR-spectrum (Figure 4.33b) only shows one species and no additional smaller peaks that could indicate the formation of another species. The presence of a 4:4-complex in the mass spectrum is therefore most likely due to non-specific interactions, similar to the 6:6:5-complex that was seen earlier in the spectrum of ligand (*R*)-**15** in acetone (Figure 4.32). This could be confirmed by an MS/MS-experiment, where the ion at 1668.9 m/s was isolated and fragmented. In the case of a non-specific aggregate the weakest bond would brake first resulting in a 2:2:2^{2+}- and a 2:2:3^{3+}-complex. This is still to be done. However, when looking closer at the peak at 1214.2 m/z, no sign of a 4:4:4-complex is seen, as opposed to the corresponding peak in the spectrum of the complex of (*R*)-**15** (Figure 4.32). This strongly indicates, that ligand 20 is not able to form a catenane and that the peak at 1668.9 m/z is a result of non-specific aggregation.

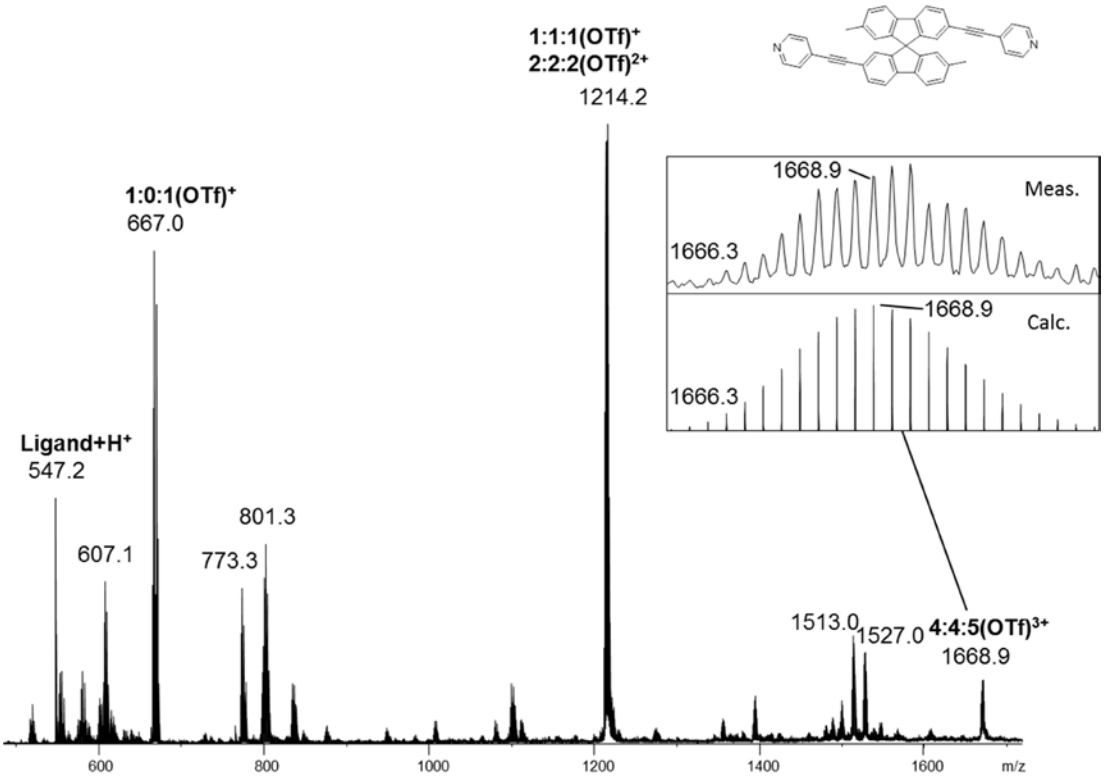

*Figure 4.34 ESI mass spectrum (positive mode) of ligand (S)-**20** with Pd(dppp)(OTf)$_2$ in acetone. The notation corresponds to Metal:Ligand:Anion.*

Together with the ^{1}H-NMR-spectrum the mass spectrum of the Pd-complex of ligand (*S*)-**20** confirms the formation of the 2:2-complex in acetone. Upon mixing the two ligands (*S*)-**20** and (*R*)-**15** in acetone, the ^{1}H-NMR-spectrum suggests that both of the homochiral complexes as well as the heterochiral complex have been formed, since peaks from both the separate complexes can be seen along with peaks belonging to neither species (Figure 4.35). Also we can see signals from the catenane present in the mixture (marked with black arrows) indicating that formation of the catenane is possible even in the presence of ligand **20**.

We also recorded a ^{31}P-NMR-spectrum which is shown in Figure 4.36. Here we see one large peak next to a smaller peak. In addition the two doublets previously seen in the ^{31}P-NMR-spectrum of ligand (*R*)-**15** in CD_2Cl_2/CD_3CN (Figure 4.17) as well as in acetone (Figure 4.31). It seems that ^{31}P-signals for both (*R*)-**15** and (*S*)-**20** as well as the catenane are present, confirming our observations from the ^{1}H-NMR-spectrum.

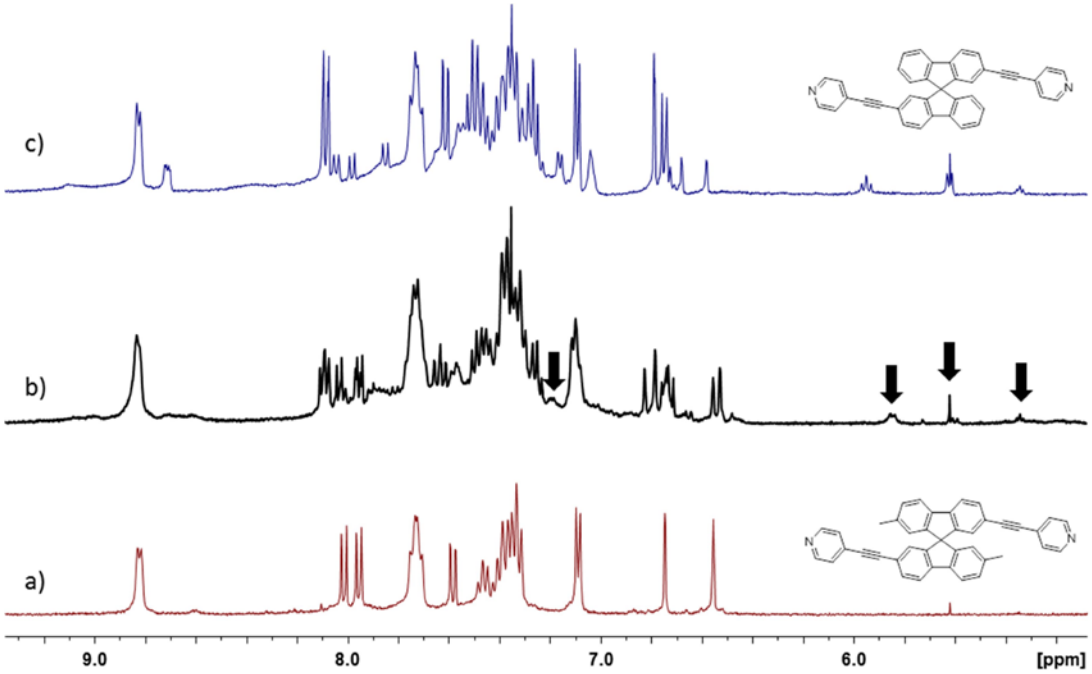

*Figure 4.35 ^{1}H-NMR-spectra of a) ligand (S)-**20** with Pd(dppp)(OTf)$_2$ b) ligands (S)-**20**and (R)-**15** with Pd(dppp)(OTf)$_2$ c) ligand (R)-**15** with Pd(dppp)(OTf)$_2$ all in acetone-d$_6$.*

The solution was measured on the Q-TOF and the resultant spectrum is shown in Figure 4.37. The base peak is at 1200.2 m/z and corresponds to the doubly charged heterochiral 2:2-complex of the two ligands (*S*)-**20** and (*R*)-**15**. On either side of the mixed peak, smaller peaks originating from the homoleptic 2:2- and 1:1-complexes of each ligand can be seen. The mass spectrum confirms the formation of both the two homochiral and the heterochiral complex. However, it was not possible to find a signal corresponding to the catenane in the mass spectrum, which is surprising since both the ^{31}P- and ^{1}H-NMR-spectra indicate its formation. In the future, additional mass measurements on finding the 4:4-complex could confirm the desired outcome.

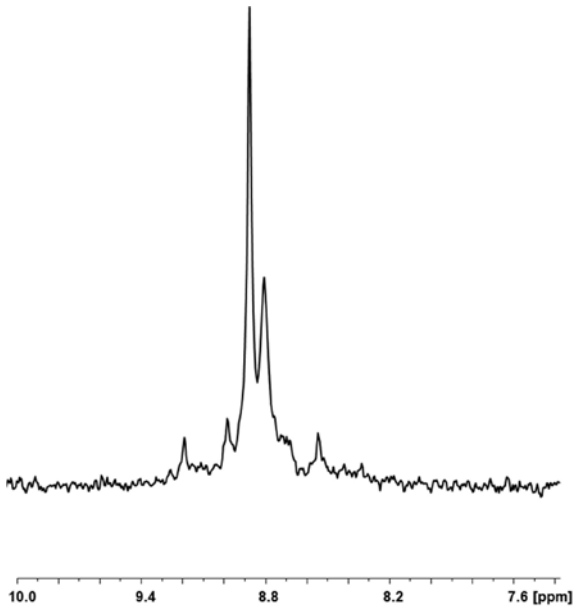

*Figure 4.36 ^{31}P-NMR-spectrum of ligands (S)-**20** and (R)-**15** with Pd(dppp)(OTf)$_2$ in acetone-d$_6$.*

In this case our main objective was to determine the ratios of homo and heterochiral complex. Therefore, we again compared the ^{1}H-NMR-spectra of the single ligands and the mixture. Like before, the challenge was to find three non-overlapping peaks belonging to each species in the mixed spectrum.

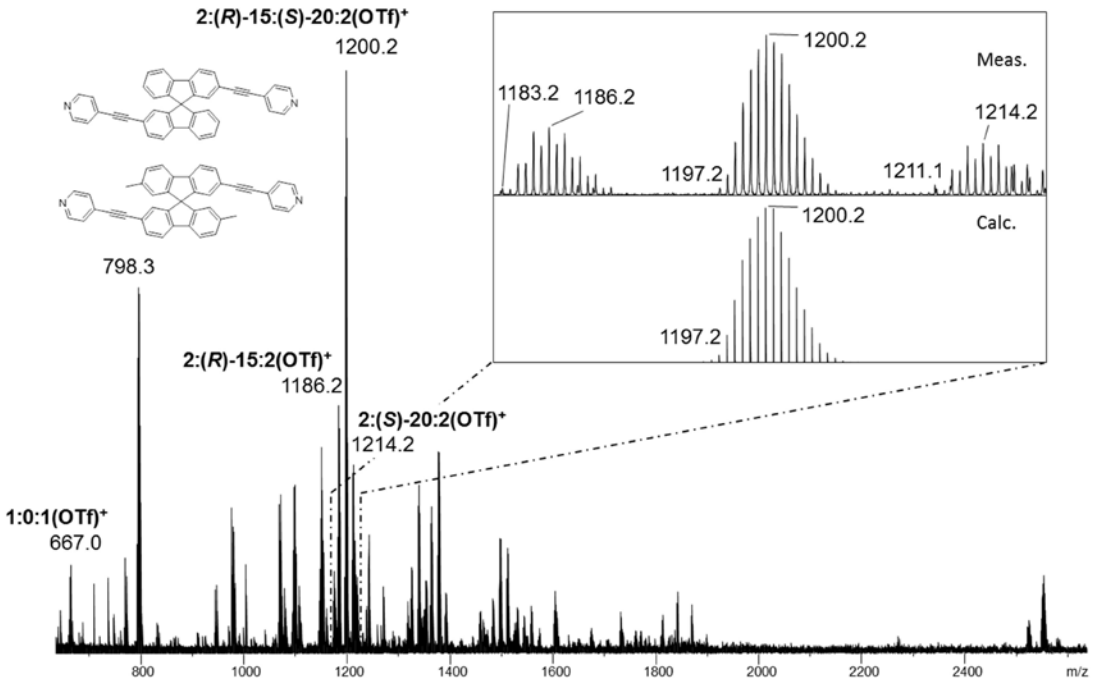

*Figure 4.37 ESI mass spectrum (positive mode) of ligand (R)-**15** and ligand (S)-**20** with Pd(dppp)(OTf)$_2$ in acetone. The notation corresponds to Metal:Ligand:Anion.*

A section of the three spectra is shown in Figure 4.38. This section was chosen because of the few sections, where it was possible to distinguish clearly between signals of the heterochiral and the homochiral complexes. Two peaks were identified in the mixed spectrum (Figure 4.38b), where one belongs to the complex of ligand (*S*)-**20** while the other belongs to the heterochiral complex. When integrating the two peaks the intensity of both equal to one. A ratio of 1:1 of one specific hetero- and homoleptic signal indicates a statistical distribution of the self-recognition and self-discrimination processes. This is the same effect that was seen in CD_2Cl_2/CD_3CN (3:1) (See Figure 4.28).

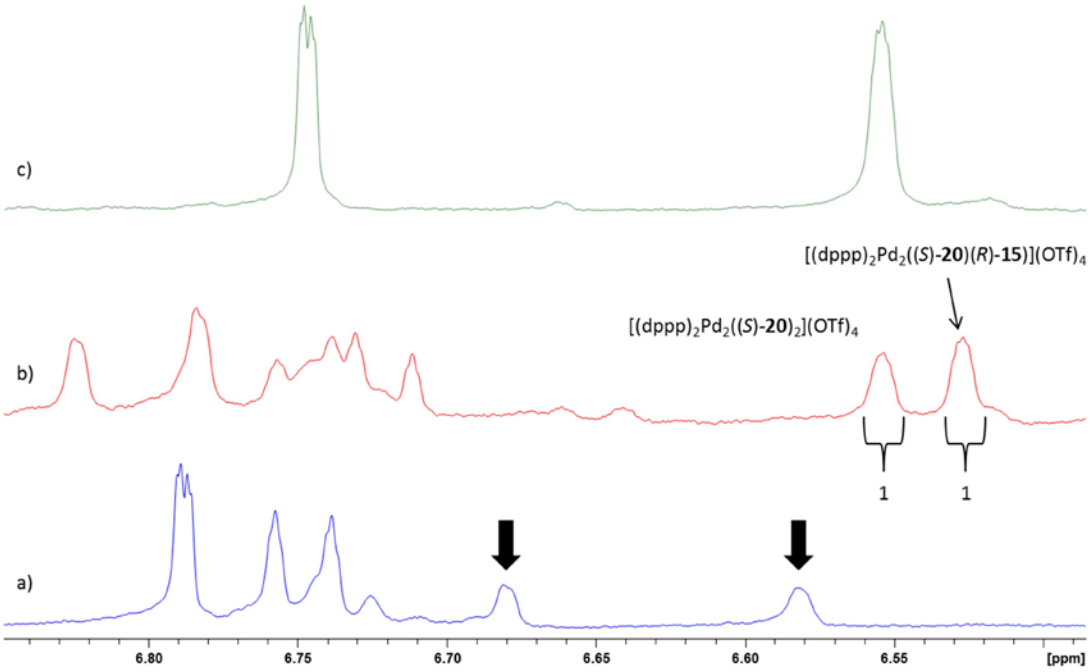

*Figure 4.38 Section of the ^{1}H-NMR-spectra of a) Ligand (R)-**15** with Pd(dppp)(OTf)$_2$ in acetone-d$_6$ b) Ligands (S)-**20** and (R)-**15** with Pd(dppp)(OTf)$_2$ in acetone-d$_6$ c) Ligand (S)-**20** with Pd(dppp)(OTf)$_2$ in acetone-d$_6$. Peaks originating from the catenane are marked with black arrows.*

Again, we were looking for three signals in the mass spectrum resulting from all three possible 2:2-complexes. The section is shown in Figure 4.39. The same method that was used for the complex in CD_2Cl_2/CD_3CN was applied here and the peaks at 1186.7, 1200.2 and 1214.8 m/z were compared. The resultant ratio of 1((*R*)-**15**):3.1((*R*)-**15**/(*S*)-**20**):0.8((*S*)-**20**) indicates self-discriminating behavior of the ligands and differs markedly from the result obtained from the ^{1}H-NMR-spectrum. In this case, it is difficult to assess if the discrepancy is due to fragmentation of the 2:2-complex in the mass spectrum (Figure 4.37). It has not been possible to identify many of the other peaks in the spectrum for example at 798.3 m/z. Nevertheless, the isotope pattern and the charge of +1 indicated a 1:1:1-complex with an unknown anion. Interestingly, no fragments containing the ligand are seen which adds more credibility to this spectrum compared to the one made in CD_2Cl_2/CD_3CN (Figure 4.29). In order to confirm the results obtained from these mass spectra, more mass measurements would have to be made to obtain fully identifiable spectra.

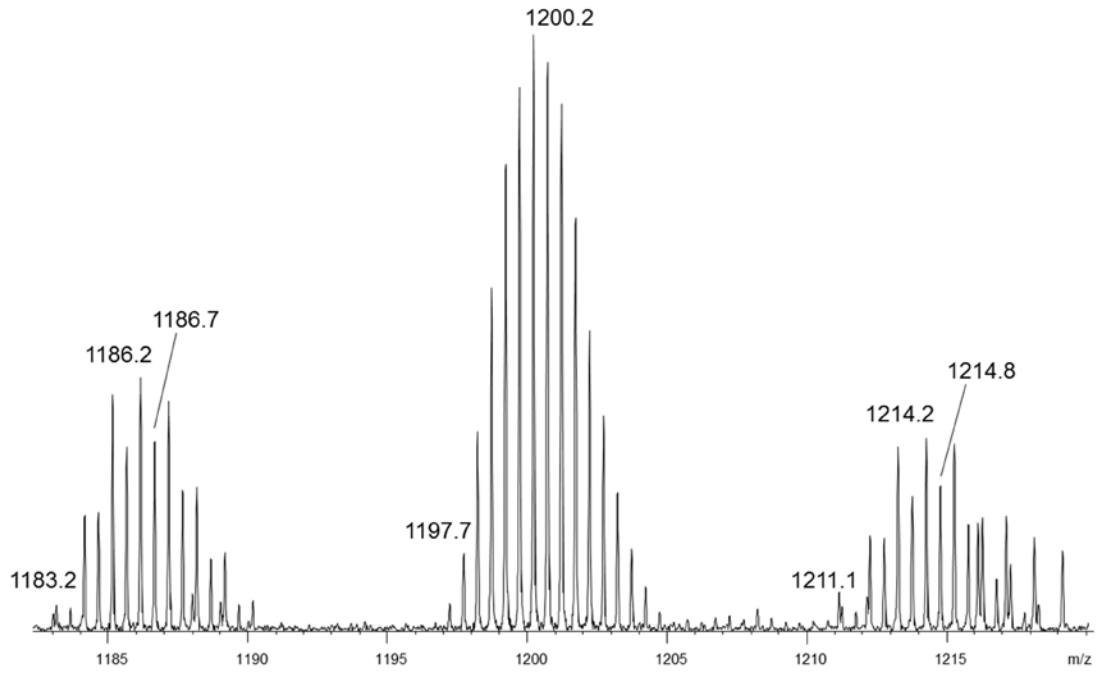

*Figure 4.39 Section of ESI mass spectrum (positive mode) of ligand (R)-**15** and ligand (S)-**20** with Pd(dppp)(OTf)$_2$ in acetone.*

The complexation of ligand (*R*)-**15** and (*S*)-**20** was also measured in DMF-d_7. In the case of the separate complexes of the ligands, the resulting ^{1}H-NMR-spectra were compared to the uncomplexed ligand and both indicated formation of a complex. Only one set of signals was present, however, the signals corresponding to the pyridine protons as well as the signals from the triphenylphosphine of the Pd(II) were broadened indicating a rapid exchange on the NMR time scale. Due to the broadness of the peaks in the ^{1}H-NMR-spectrum it is not possible to conclude about the identity of aggregate in the solution without the help of mass spectroscopy. The ^{1}H-NMR-spectrum of the mixed complex is shown in Figure 4.40c.

What we have seen in the spectra of the separate complexes also holds true for the mixed complex: the protons near the complexation center are unusually broad. Only protons situated far away from the complexing pyridine appear as sharp signals. Apparently, the conformation around Pd-N-bond is very labile on an NMR-time-scale, thereby broadening the signals.

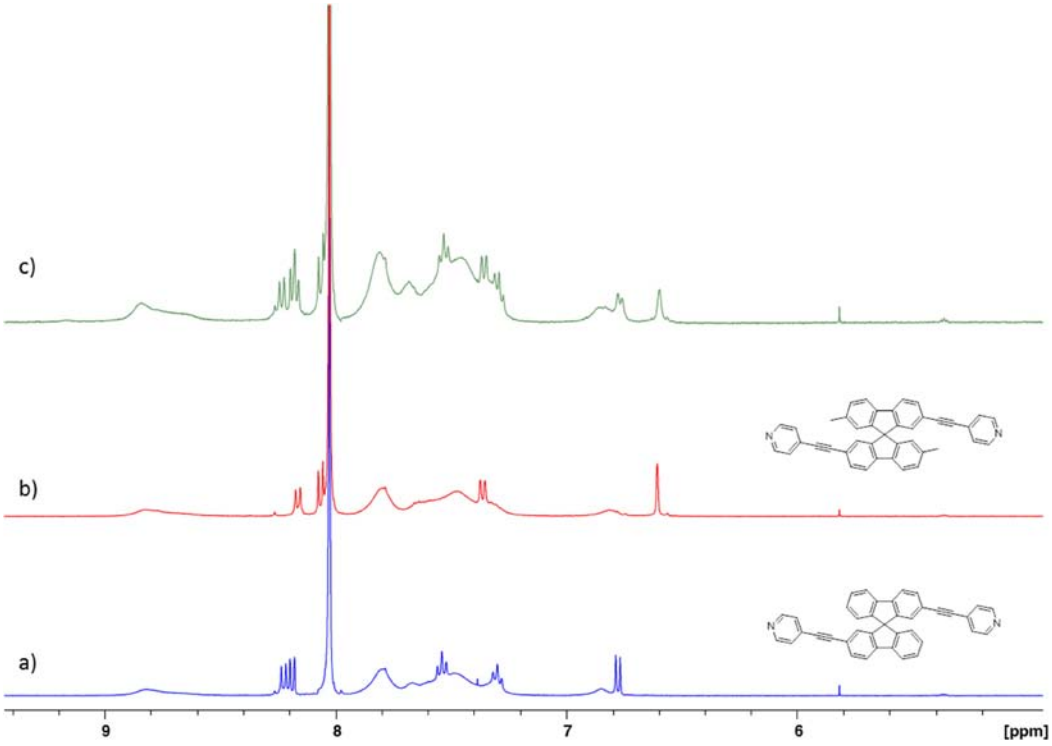

*Figure 4.40 ^{1}H-NMR-spectra of a) ligand (R)-**15** with Pd(dppp)(OTf)$_2$ b) ligand (S)-**20** with Pd(dppp)(OTf)$_2$ c) ligands (S)-**20** and (R)-**15** with Pd(dppp)(OTf)$_2$ all in DMF-d$_7$.*

Looking at the mixed ^{1}H-NMR-spectrum it seems to be a superposition of the ^{1}H-NMR-spectra of the separate ligands (Figure 4.40). However, because of the broadness of the signals it is difficult to make a finite statement about the self-sorting behavior of the ligands in DMF. A mass spectrum could tell us more, but DMF is a difficult solvent to spray into the mass spectrometer due to its high boiling point. Dissolving the complex in CH_3CN or acetone could change the self-sorting behavior. In the future, it would therefore be interesting to investigate self-sorting of ligands **15** and **20** in other solvents such as THF or pure CH_3CN, which both can be sprayed into the mass spectrometer.

4.4 Conclusion

We have been able to reproduce the formation of rhombs of ligand (*R*)-**12**, and confirm the preference of ligand **12** towards formation homochiral aggregates with the help of pseudoenantiomer ligand **21**. ´

Using ligand **15** also resulted in the formation of the desired 2:2-rhombs as well as a 4:4-catenane structure as observed in the ^{1}H-NMR- and mass spectra and confirmed by crystal structure obtained of the catenane of (*R*)-**15**. The formation of the catenane was also investigated in acetone-d_6, and inspection of the ^{1}H-NMR-spectra suggests that the formation of the catenane is favored in acetone. More studies have to be carried out in DMF-d_7 and in other solvents.

The self-sorting behavior of the ligand (*R*)-**15** using the pseudoenantiomer (*S*)-**20** was also investigated in different solvents. In CD_2Cl_2/CD_3CN and acetone-d_6 no selectivity for the enantiomers was observed in the ^{1}H-NMR-spectra. It was not possible to perform mass spectrometry on the complexes in the DMF-solution, due to the high boiling point of the solvent and the solution can therefore not be investigated further. Ideally, crystal structures could help elucidate whether homo- or heterochiral or both complexes have formed. However, several crystallization experiments have been attempted but so far no measurable crystals have been produced.

The change in selectivity going from the small ligand **12** to the large ligand **15** is significant. Increasing the length of the linker changes the selectivity from preferred self-recognition to no selectivity, emphasizing the importance of the linker length in self-sorting. This could be investigated further with crystal structures of the obtained complexes. Also, more flexible linkers could be investigated for their influence on the selectivity.

5 Cage Structures with large chiral cavities

5.1 Background

As described in the previous chapter 4.3.1, substituted spirobifluorenes are able to participate in complex formation forming supramolecular rhombs, which display self-sorting abilities. However, so far only 2:2- or 4:4-complexes of spirobifluorenes have been described. Larger complexes involving more than four ligands present an interesting subject and are presented in the following chapter.

Through the last two decades many different synthesis of large self-assembled metal-based structures have been presented.[76–80] The interest in such large supramolecular structures is not just aesthetical but also has a functional aspect. The formation of larger complexes means the cavities within the aggregate becomes larger and can thus accommodate larger or more guest molecules. Furthermore, functionalization of the cavity with, for example, hydrophobic groups or electron withdrawing substituents can give rise to a binding pocket displaying specificity towards certain molecules or facilitating otherwise unfavorable reactions.

Fujita and coworkers presented a supramolecular cage assembled of six Pd-ions and four tridentate pyridine-ligands. This cage was shown to be able to influence the photodimerization of two molecules of the asymmetric 1-methylacenaphtylene when irradiated resulting only in the syn- and head-to-tail isomers. The supramolecular cage is able to accommodate only two substrates positioned head-to-tail in respect to each other and, in doing so, facilitates the formation of only one isomer.[81] Other uses for self-assembled polyhedral structures could also be imagined such as molecular machines and new materials.[82–84]

The formation of the large supramolecular cages can be predicted and designed with quite some accuracy. Using metals, with their predefined bonding geometries, together with rigid organic ligands often results in the desired and predicted discrete self-assembled structure.[77] This approach, also called the directional-bonding methodology, was tested by Fujita and coworkers when assembling several coordination polyhedra. Using the five different ligands shown in Figure 5.1 together with $Pd(NO_3)_2$, it was possible to assess which ligand angle lead to formation of $M_{24}L_{48}$-polyhedra rather than $M_{12}L_{24}$. Having a cavity-volume of 23000 $Å^3$, the $M_{24}L_{48}$-structure built from the ligand **3** (Figure 5.1) is the largest polyhedral formed to date.[83,85]

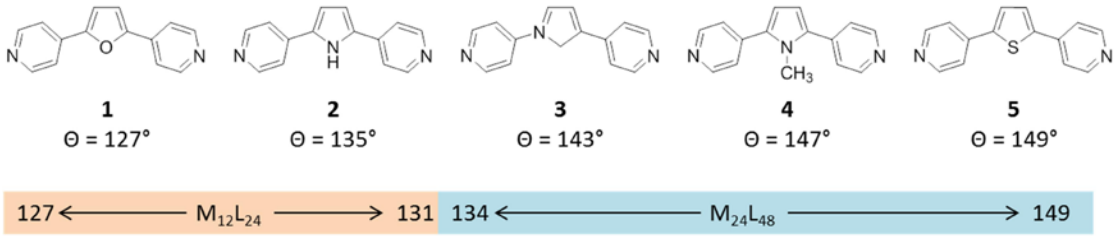

Figure 5.1 Ligands synthesized by Fujita et al including angle spans on the basis of the illustration by Fujita et al. [85]

An example of a chiral molecule with a rigid core is 1,1′-bi-2-naphthol (BINOL), which has been used by the Lützen group to form large complexes. The ligands in Figure 5.2 are based on BINOL and were synthesized by Christoph Gütz.[86] When mixing racemic **BINOL1** with $Pd(CH_3CN)_4(BF_4)_2$ and stirring for two days in CD_2Cl_2:CD_3CN 3:1, only one species, the M_2L_4-cage, was detected in the mass-spectrum. Four possible diastereomeric structures can be formed during complexation. However, comparing the ^{1}H-NMR-spectra of the complex formed using the racemic ligand and the complex formed using the enantiomerically pure ligand, no difference is found in the spectra. All in all the formation of a racemic mixture of the two homochiral complexes was observed revealing a ligand displaying self-recognition.

Figure 5.2 BINOL-Ligands synthesized by Gütz

The BINOL-core can also be used to form even larger complexes, as exemplified by **BINOL2** (Figure 5.2). Formation of M_6L_{12} was confirmed in DOSY and ESI-MS after heating of **BINOL2** with $Pd(CH_3CN)_4(BF_4)_2$ in DMSO-d_6. In this case, however, no stereoselectivity was observed in the self-assembly process.[86]

5.2 Synthesis of the ligands

Just like the BINOLs the substituted spirobifluorenes have a rigid core and a defined angle and therefore fulfill the demand for a predefined bonding geometry. Furthermore, the spirobifluorenes are also chiral and could be able to form complexes displaying self-sorting. Therefore synthesis of ligands based on spirobifluorene, that are potentially able to form large supramolecular assemblies with Pd(II) and the formation of these was a key subject during this study.

We therefore looked for a spirobifluorene ligand, which would be able to form an M_6L_{12}-cage. First, we examined the ligands already available such as ligand **12**, **15** and **20**. Modeling studies suggested, that ligand **12** should be well suited to form a cube with square planar Pd(II) without distortion of neither the coordination geometry of the metal nor the ligand itself (Figure 5.3).

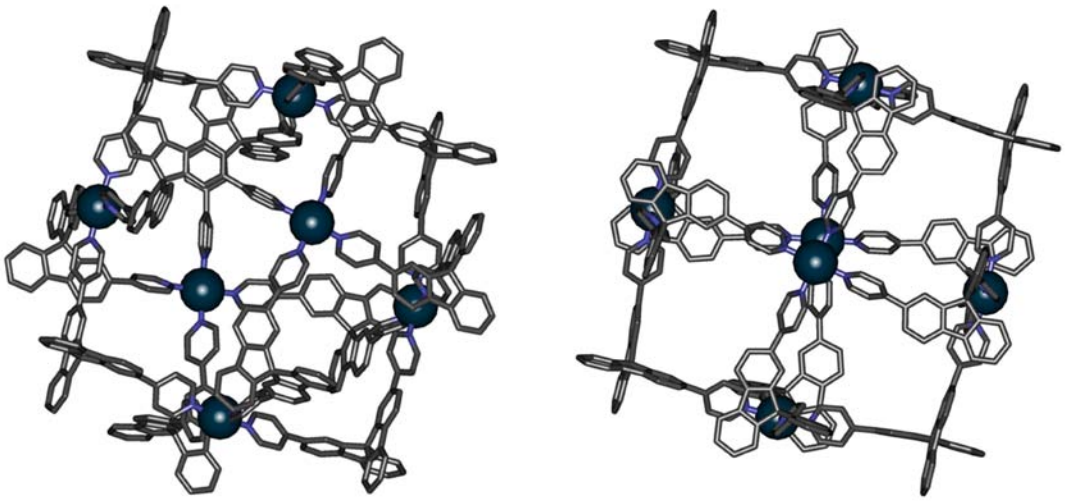

*Figure 5.3 PM6-minimized structure of the M_6L_{12}-cube of ligand (R)-**12***

Ligand **12** was described previously and the synthesis is described in chapter 4.2.

We also aimed at forming a simpler M_2L_4-cage also using the spirobifluorene core. To this end, a different angle between the metal-binding entities than the 90° in the previously synthesized ligands is needed. Using a 3-pyridine instead of a 4-pyridine in the synthesis of ligand **12** results in ligand **22** which is shown in Figure 5.4. The angle changes to about 86°, however the bonding angle to the metal ion is changed drastically as can be seen in the modeled structures of the complex with Pd(II) in Figure 5.5. The angle between the spirobifluorene core and the two metal centers is ca. 67° from the modeled structures.

*Figure 5.4 Ligand **22***

The synthesis of ligand **22** starts from **11**, which has previously served as a starting material for the other spirobifluorene ligands and is performed analogously to the synthesis of ligand **12**.

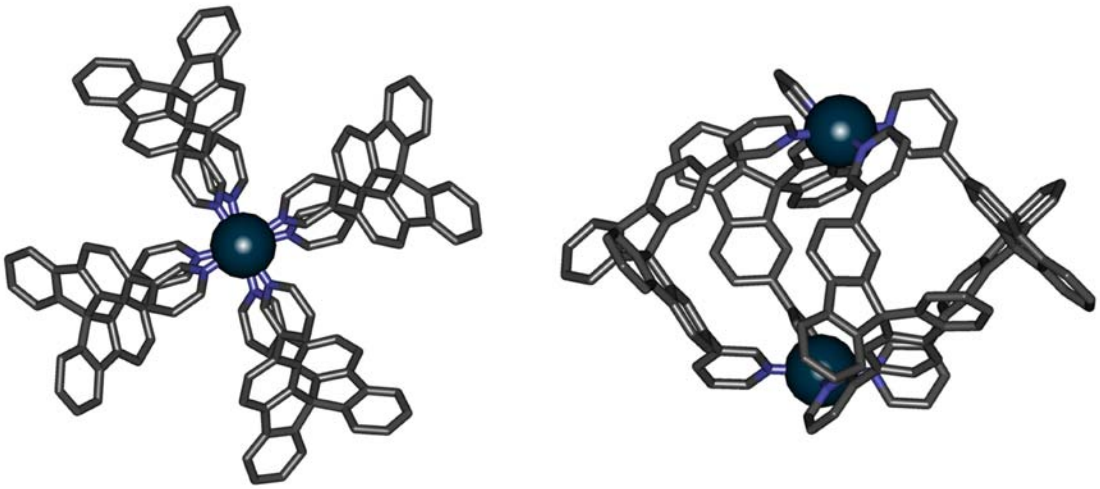

*Figure 5.5 PM6-minimized model of the M_2L_4-complex of ligand (R)-**22***

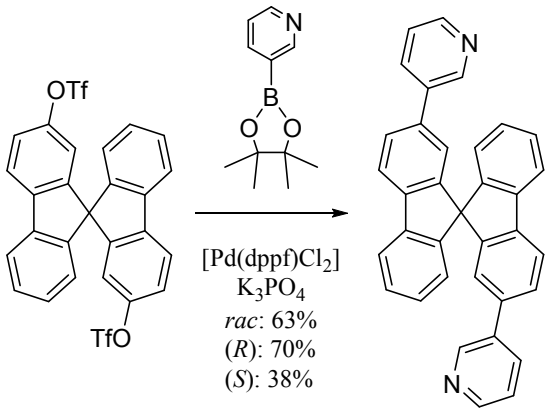

11 **22**

*Scheme 5.1 Synthesis of ligand **22***

The synthesis of ligand **22** was initially performed using three equivalents of 3-pyridineboronic acid and 7% Pd-catalyst. K_3PO_4 was added to increase the reactivity of the boronic acid ester, since PO_4^{3-} acts as a fourth ligand to the boron and the transmetallation to the palladium proceeds faster than without addition of base.[64,65] However, only the mono-substituted spirobiflourene was obtained. Even when adding five equivalents of the boronic acid product **22** could not be isolated. Instead, use of five equivalents of 3-pyridineboronic acid pinacol ester, while keeping the amount of catalyst constant at 7% resulted in racemic **22** in a yield of 63%. So even though the reaction was carried out under the exclusion of light it may be possible that the boronic acid was not stable enough to allow the reaction to continue until completion. The (*R*)- and (*S*)-enantiomers were obtained in yields of 70 and 38% respectively. The difference in yield between the enantiomers is not readily explained. Most likely presence of water reduced the outcome of the reaction to produce (*S*)-**22**.

5.3 Complexation

The complexations of ligands **12** and **22** were carried out in different solvents and the self-recognition abilities of the smaller M_2L_4-cage formed by ligand **22** were investigated.

Several attempts were made with both the racemic and the enantiopure ligand **22** mixed with $Pd(CH_3CN)_4(BF_4)_2$ in the following deuterated solvents: Acetone, DMSO, CH_3CN and CH_2Cl_2/CH_3CN (3:1). The experiments led to different results. The use of the racemic ligand generally resulted in peak broadening in the ^{1}H-NMR-spectra with one large "wave" spanning the entire aromatic region independent of the solvent (spectra not shown). The complex mixture of the racemic ligand with $Pd(CH_3CN)_4(BF_4)_2$ in CD_3CN gelated, sug-

gesting that polymerization had occurred. A mass spectrum of the racemic ligand **22** showed no significant signals other than the one belonging to the free ligand. The use of the enantiopure ligand (*R*)-**22** in DMSO-d_6 and acetone-d_6 again resulted in ^{1}H-NMR-spectra, indicating polymerization. We therefore concentrated on the investigation of (*R*)-**22** in CD_3CN and CD_2Cl_2/CD_3CN (3:1) which gave relatively well-resolved ^{1}H-NMR-spectra. Since we were using only the enantiopure ligand, it was not possible to investigate any potential self-sorting processes.

Complexation was performed at room temperature as well as at 65°C in a microwave vial. The heated solutions were heated in 3 hour intervals and ^{1}H-NMR-spectra were recorded after each 3 hour interval. For solutions that were stirred at room temperature, the spectra were recorded in intervals of one week. Several ^{1}H-NMR-spectra were recorded during the reaction time, the resulting spectra are shown in Figure 5.6.

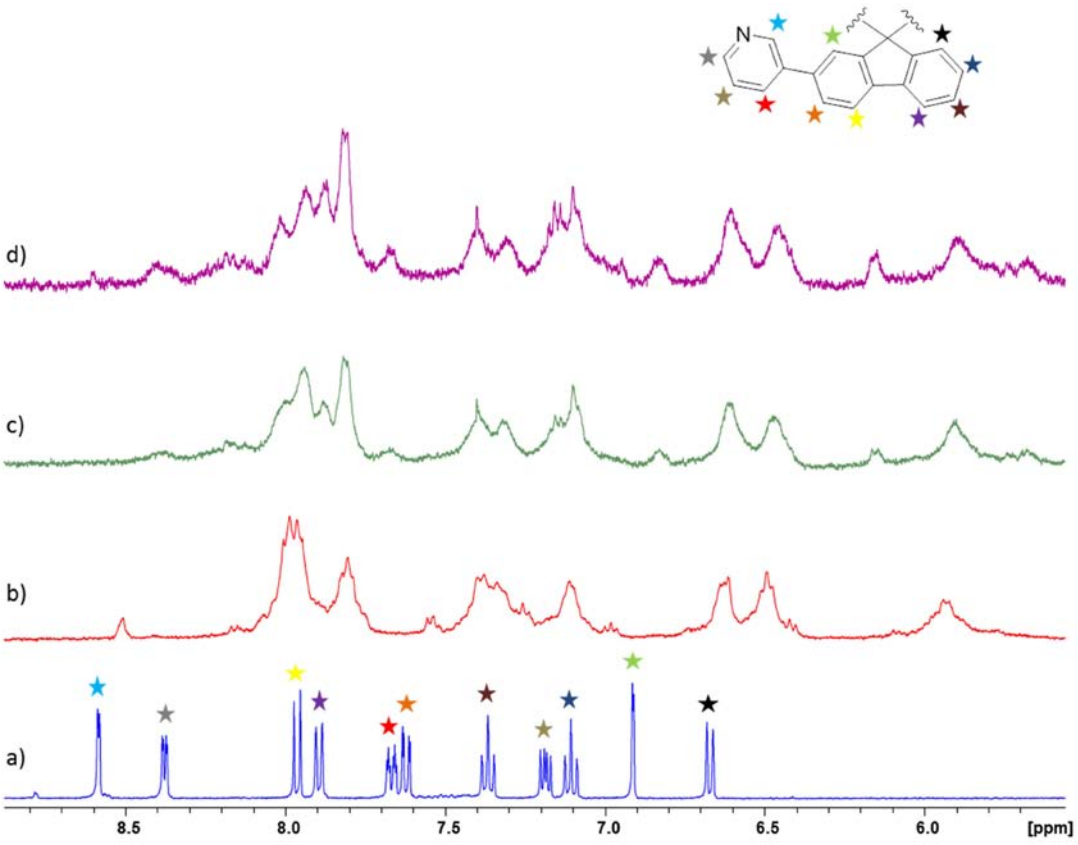

*Figure 5.6 ^{1}H-spectrum of a) ligand (R)-**22** b) ligand (R)-**22** with $Pd(CH_3CN)_4(BF_4)_2$ after 1 day c) ligand (R)-**22** with $Pd(CH_3CN)_4(BF_4)_2$ after 31 days d) ligand (R)-**22** with $Pd(CH_3CN)_4(BF_4)_2$ after 49 days all in CD_2Cl_2/CD_3CN (3:1).*

The complex spectra are all characterized by broad peaks and a low resolution, which made it difficult to compare the spectra and extract information from them. Also, it has not been possible to assign the protons using H,H-COSY.

Nevertheless, comparing the spectrum of the free ligand (Figure 5.6a) with the spectra of the complexes (Figure 5.6b, c and d) no free ligand is present in the spectra of the complexated ligand **22**. All peaks are shifted indicating the formation of a new species. From the ^{1}H-NMR-spectra it is not possible to conclude whether the M_2L_4-cage has been formed or not.

Diffusion-ordered spectroscopy (DOSY) was attempted in order to assess the size of the formed complex in solution. Unfortunately, it was not possible to obtain a DOSY-spectrum from which it was possible to derive the hydrodynamic radius. We therefore hoped to obtain more information from the mass spectra.

After ca. three weeks after the complexation, mass spectra were recorded in the mass spectrum showing the presence of large amounts of ligand and smaller, unidentified peaks. However, a small peak corresponding to the 2:4:1-complex was also present. After about one month of alternate stirring at RT and resting at 5°C of the same solution, another mass spectrum was recorded, which contained significant amounts of the desired 2:4-complex at 727.2, 1100.2 and 1134.3 m/z (Figure 5.7).

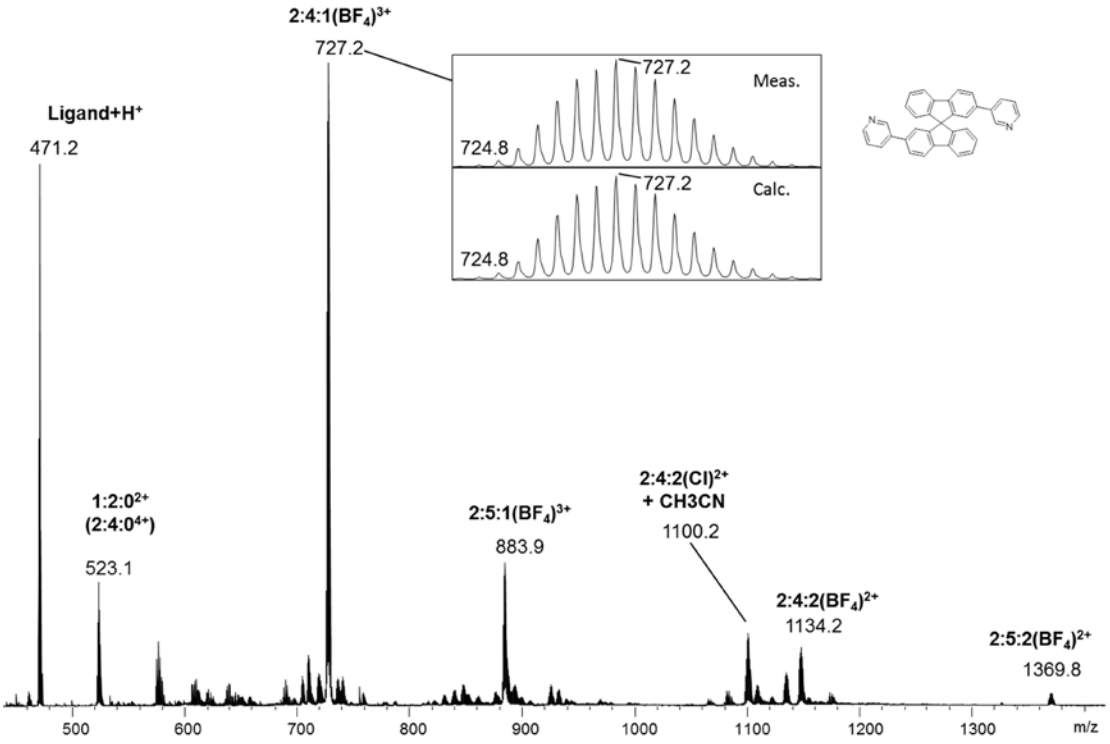

*Figure 5.7 ESI mass spectrum (positive mode) of ligand (R)-**22** in CH_2Cl_2/CH_3CN (3:1) at RT 49 days after mixing. The notation corresponds to Metal:Ligand:Anion.*

Although quite large amounts of free ligand are present, the base peak is the 727.2 m/z-peak corresponding to the desired 2:4:1^{3+}-complex. Furthermore, small peaks corresponding to half the M_2L_4-cage have been identified at 523.1 m/z and peaks attributed to

M_2L_5-complexes were seen at 883.9 and 1369.8 m/z. The latter are most likely a result of non-specific aggregates. The presence of the M_1L_2-complex is probably due to fragmentation of the M_2L_4-complex in the mass spectrometer. However, quite a large peak originating from the free ligand was present, indicating that the complexation had not been completed.

We therefore decided to investigate the effect of time on the complexation. To do so, an ESI mass spectrum of the complex five months after mixing in the same solvents (Figure 5.8) was recorded. Here significantly less of the free ligand was present and instead the largest peak in the spectrum was the one corresponding to the $2:4:1^{3+}$-complex. When investigating the complex mixture more closely, it was discovered that a layer of gel had formed at the bottom of the solution. It is possible that a fraction of the ligands has polymerized over time, leaving the M_2L_4 in solution but at a very low concentration. It is therefore not possible to estimate the concentration of the solution. However, this would explain why only solvent peaks were visible in the ^{1}H-NMR-spectrum (spectrum not shown).

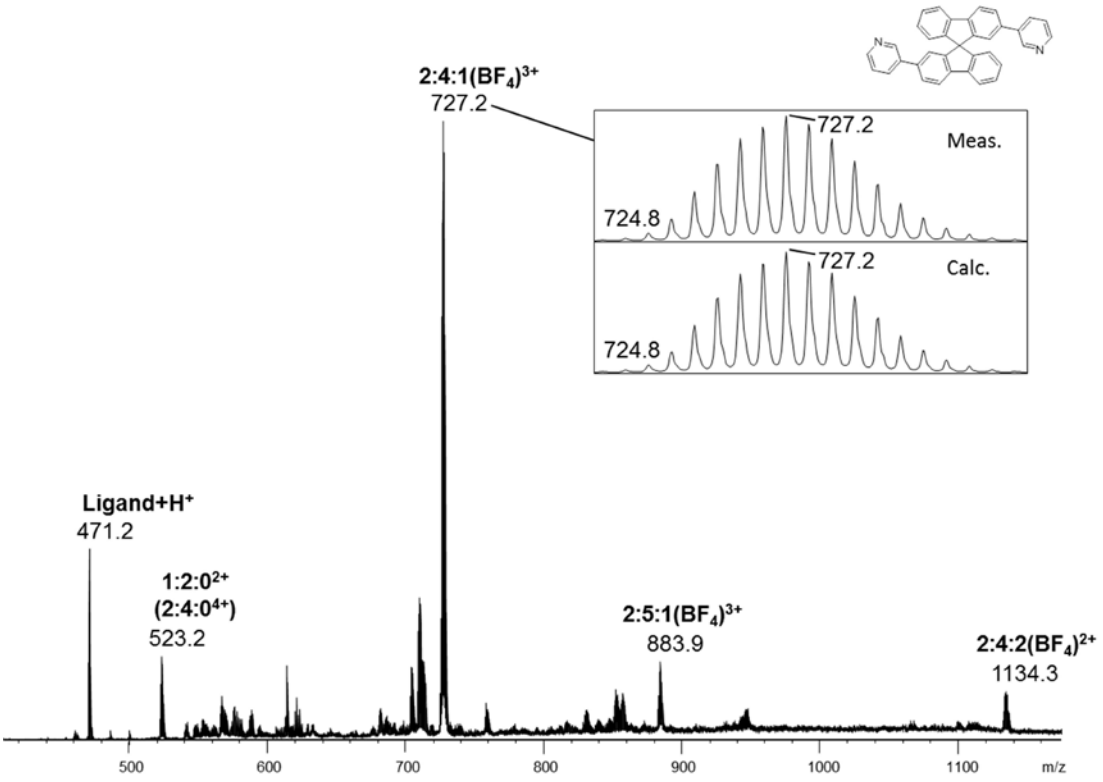

*Figure 5.8 ESI mass spectrum (positive mode) of ligand (R)-**22** in CH_2Cl_2/CH_3CN (3:1) at RT five months after mixing. The notation corresponds to Metal:Ligand:Anion.*

We therefore focused on investigating the complex in CD_3CN, which had also produced promising ^{1}H-NMR-spectra (Figure 5.9b). Additional heating produced the spectrum in Figure 5.9c. The change from spectrum b to c is pronounced, with one set of signals de-

creasing and another increasing. It was not possible to assign the protons, even for the well resoluted peaks. Also the integrals do not match the expected number of eleven protons, which could be due to the low signal-to-noise ratio. Again, all signals had shifted compared to the free ligand (Figure 5.9), so it is very likely that one or more complexes have formed. However, it was not possible to determine the identity of these complexes using only ^{1}H-NMR.

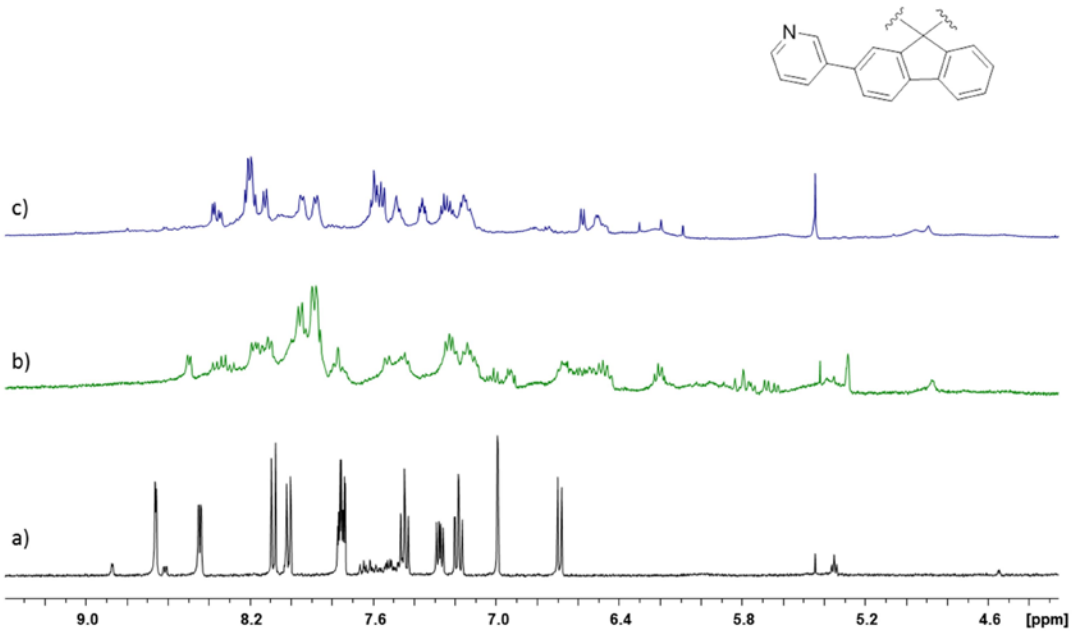

*Figure 5.9 ^{1}H-spectrum of a) ligand (R)-**22** b) ligand (R)-**22** with $Pd(CH_3CN)_4(BF_4)_2$ after 3h at 65°C and 3 days after mixing c) ligand (R)-**22** with $Pd(CH_3CN)_4(BF_4)_2$ after 7h at 65°C and 10 days after mixing all in CD_3CN.*

Therefore, a mass spectrum of ligand (*R*)-**22** in CH_3CN which has been heated for seven hours at 65°C after 10 days was recorded. The resulting spectrum is shown in Figure 5.10.

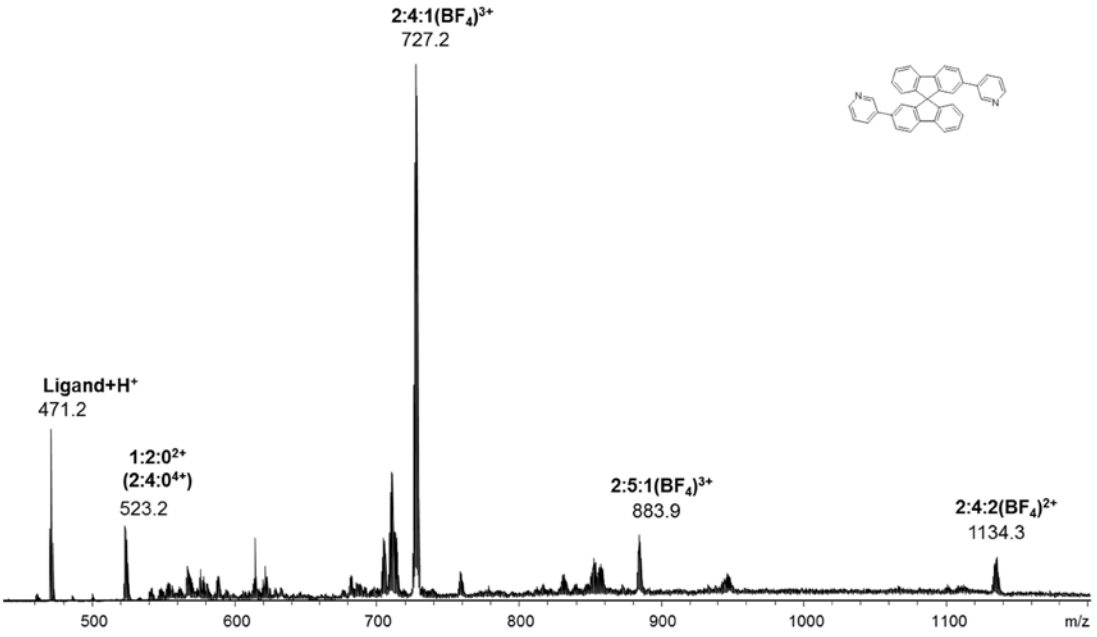

*Figure 5.10 ESI mass spectrum (positive mode) of ligand (R)-**22** in CH_3CN after 7h at 65°C and 10 days after mixing. The notation corresponds to Metal:Ligand:Anion.*

The mass spectrum is very similar to the spectrum of the complexation of (*R*)-**22** in CH_2Cl_2/CH_3CN (3:1) (See Figure 5.8). We see the base peak at 727.2 m/z corresponding to the desired 2:4-complex. Also, a peak corresponding to the free ligand is present in the mass spectrum, but since no free ligand is visible in the ^{1}H-NMR-spectrum (Figure 5.9), it is most likely a fragment. From the mass spectrum we expect the formation of one major complex, the 2:4-complex. Next, we tried to confirm the formation of the complex using ^{1}H-DOSY-NMR. The resulting spectrum is shown in Figure 5.11.

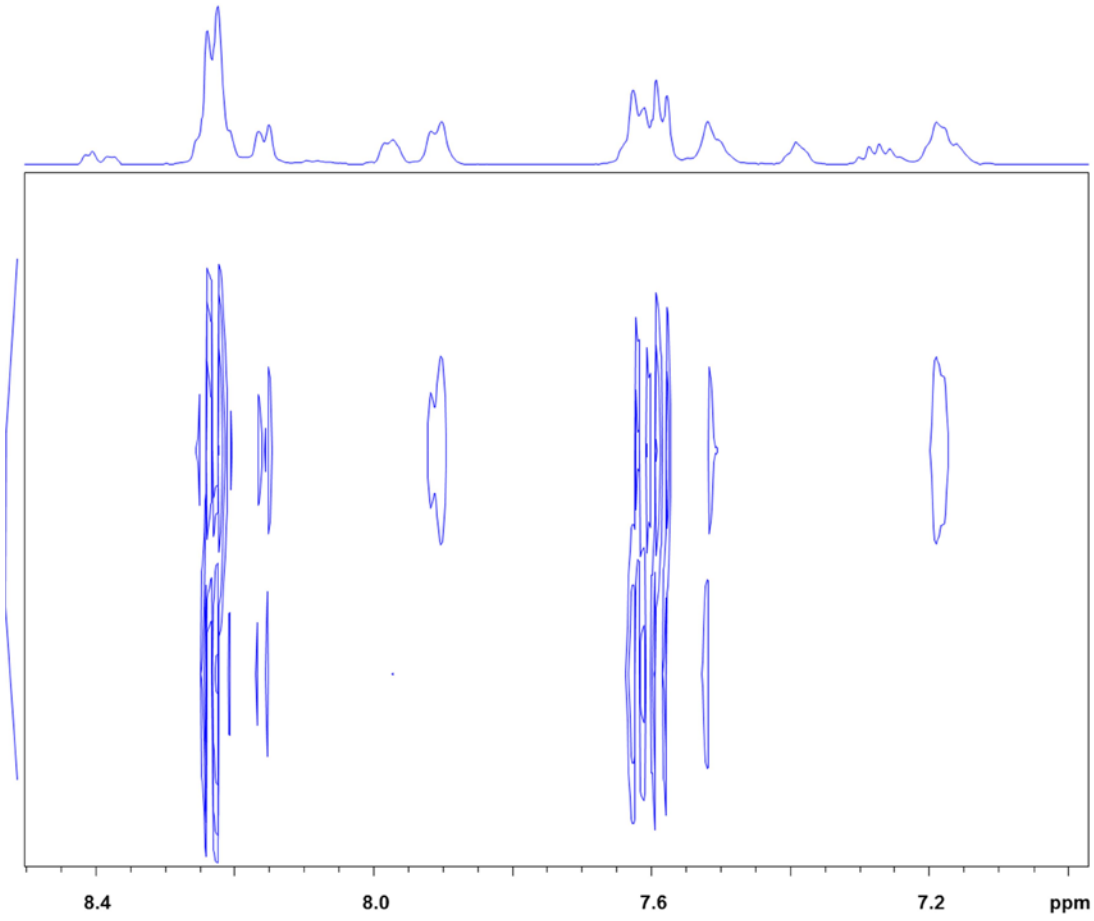

*Figure 5.11 ^{1}H-DOSY-NMR of ligand (R)-**22** with $Pd(CH_3CN)_4(BF_4)_2$ in CD_3CN*

At the top of the DOSY-spectrum the ^{1}H-NMR-spectrum is shown on the x-axis, while the diffusion coefficient is shown on the y-axis. Peaks with the same diffusion coefficient will have cross peaks (marked in blue) along the same horizontal line.

The DOSY-spectrum in Figure 5.11 clearly shows that two species of different size are present in the solution. We observed more than one set of signals in the ^{1}H-NMR-spectrum, so it is possible, that the solution has not yet equilibrated. Nevertheless, it was possible to calculate the hydrodynamic radius of the largest species in the solution. Using the *Stokes-Einstein* equation (Equation 4.1) the hydrodynamic radius was found to be ca. 25 Å. This compares well to the size measured on the modeled complex (Figure 5.5), which was found to be around 22 Å.

The data strongly suggests the formation of the desired 2:4-complex of ligand (*R*)-**22** in both CD_2Cl_2/CD_3CN (3:1) and CD_3CN. No free ligand is present in the complex ^{1}H-NMR-spectra, and the base peak of the mass spectra originates from the 2:4:1-peak. Also, the hydrodynamic radius could be calculated from the DOSY-spectrum of the solution in CD_3CN and was in the expected range. However, we also see indications of a second species in the spectra, which may be due to unfinished equilibration of the complex mixture. It

would therefore be interesting to stir and/or heat the complex mixture for a longer period of time recording ^{1}H-NMR-spectra after each interval. Moreover, investigation of the precipitate could contribute with valuable information about the complexation event.

It has not been possible to form distinct complexes using the *rac*-**22** in CD_2Cl_2/CD_3CN (3:1) and CD_3CN. Testing this racemic ligand in other solvents such as DMF and THF, could help work towards exploring possible self-sorting effects.

Complexation of ligand 12 into M_6L_{12}-cage

Next we focused on the formation of an even larger supramolecular complex. Ligand **12** is not only able to form rhombs, but also expected to be able to form a supramolecular M_6L_{12}-cube (See Figure 5.12) similar to the one synthesized by C. Gütz using a ligand derived from BINOL.[86] In this case only the enantiomerically pure (*R*)-ligand is used, since Gütz has experienced problems when using the racemic ligand. Gütz only obtained broad ^{1}H-NMR-spectra which showed no sign of formation of one specific aggregate when using racemic ligands.[86]

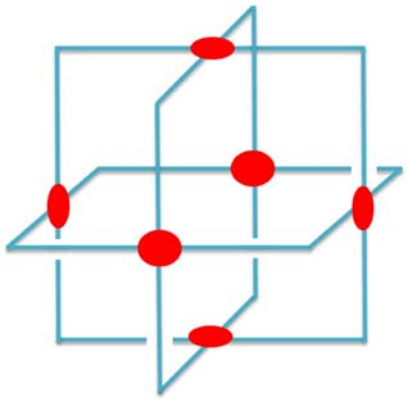

Figure 5.12 Stylized structure of the target M_6L_{12}-complex. Red: Metal. Blue: Ligand

The first complexation attempts were performed in DMSO, since Gütz had succeeded in forming a similar coordination cube using BINOL substituted with ethynylpyridine as the ligand in this solvent.

Ligand (*R*)-**12** was mixed with $Pd(CH_3CN)_4(BF_4)_2$ in DMSO and heated to 70°C for three hours. The resulting ^{1}H-NMR-spectrum is shown in Figure 5.13. All peaks had shifted in response to the complexation, so that no free ligand remains. The number of peaks is constant, indicating the formation of only one distinct species. However, all peaks are broad, indicating a dynamic behavior. This also made it difficult to assign the protons by H,H-COSY-NMR with certainty, and as a result the assignment is an assumption. Only the protons at the pyridine (green and light blue star in Figure 5.13) could be assigned with certainty due to their intensity. From the ^{1}H-NMR-spectrum it was difficult to determine if the desired M_6L_{12}-complex has formed. We therefore turned to ^{1}H-DOSY-experiments.

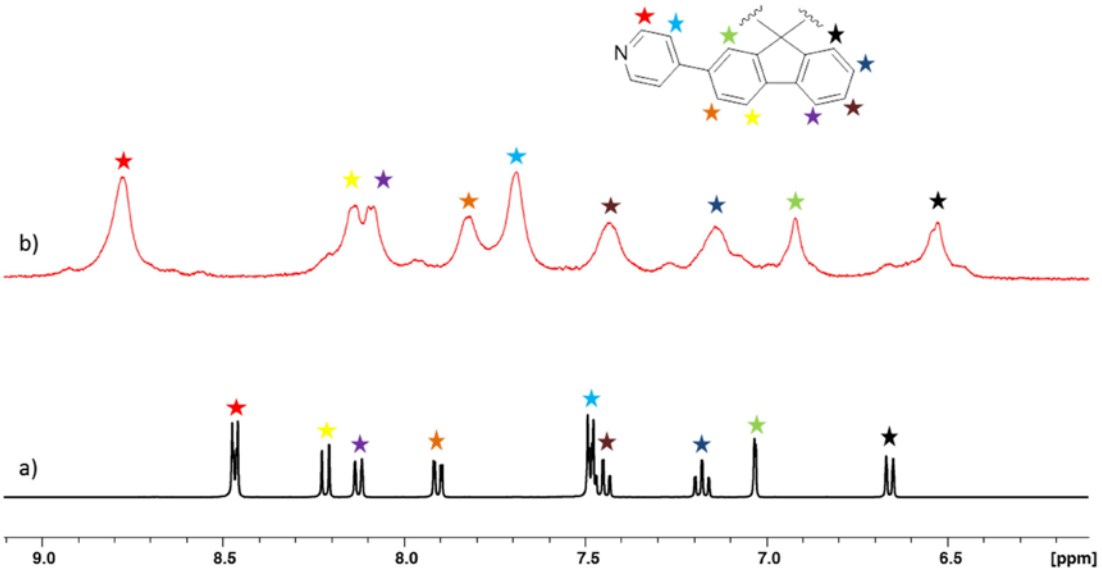

*Figure 5.13 ^{1}H-NMR-spectrum of a) ligand (R)-**12** in DMSO-d_6 b) ligand (R)-**12** with $Pd(CH_3CN)_4(BF_4)_2$ in DMSO-d_6*

During the first DOSY-experiment, the delay times of 150, 200 and 250 s were applied between the gradient pulses, since these were expected to fit well with the size of the supramolecular cube as well as the viscosity of the solvent. However, the relaxation did not reach zero in any of the three measurements and the delay times were therefore increased gradually. Surprisingly the relaxation time finally dropped to zero at a delay time of 1000 s. This suggested, that the formed complex is significantly larger than the 20 Å predicted from the modeled structure. The resulting DOSY-NMR-spectrum is shown below in Figure 5.14.

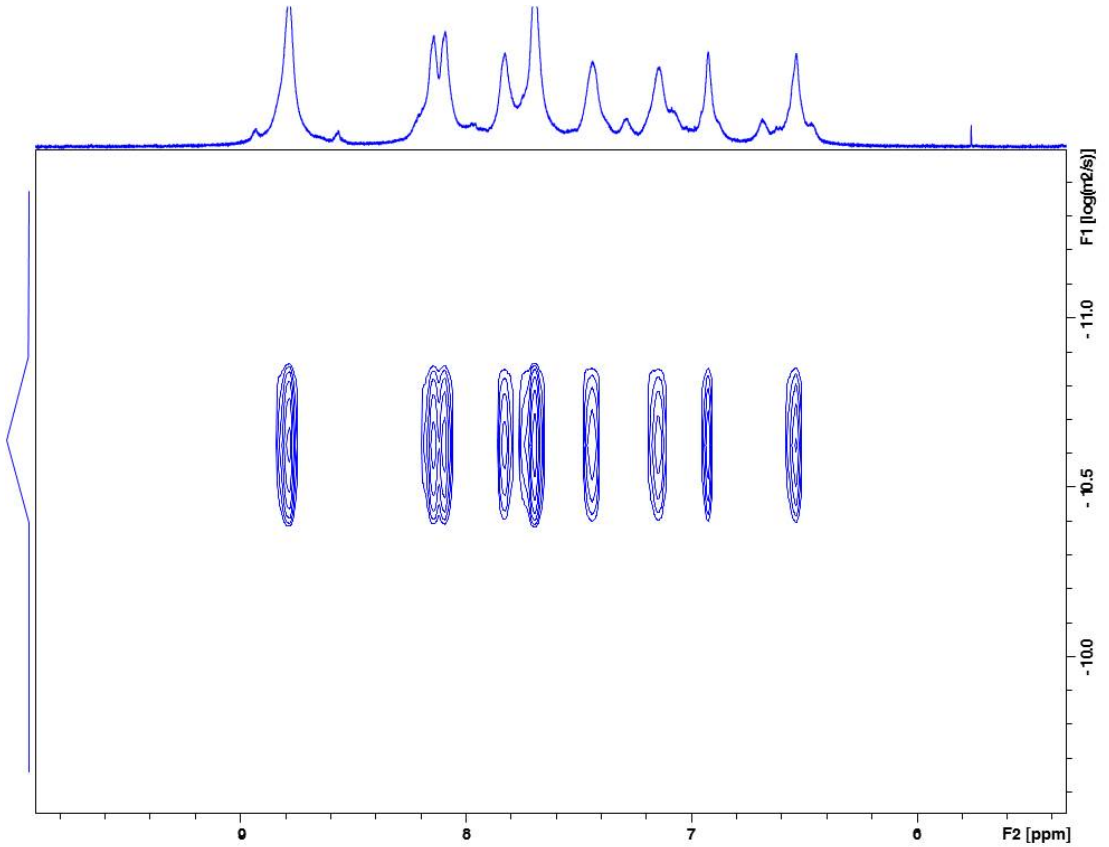

*Figure 5.14 ^{1}H-DOSY-NMR of ligand (R)-**12** with $Pd(CH_3CN)_4(BF_4)_2$ in DMSO-d_6.*

The ^{1}H-DOSY-NMR confirms that only one species is present in the solution. By inserting the diffusion coefficient of $2.61 \cdot 10^{-11}$ [$m^2 \cdot s^{-1}$] into the the *Stokes-Einstein* equation (Equation 4.1), we were able to calculate the hydrodynamic radius to 14 nm or 140 Å. This is significantly bigger than expected for the M_6L_{12}-cube, rendering the question what had formed in the solution. Similar observations have been made earlier by Fujita.[87,88] When trying to form a $M_{12}L_{24}$-cage with Pd(II) in DMSO, the ^{1}H-NMR-spectrum only produced broad signals and ^{1}H-DOSY-NMR revealed that the complex was much bigger than expected. Light scattering experiments showed that a vesicle had formed out of the $M_{12}L_{24}$-cage mediated by the counterions, and this was confirmed by TEM-measurements. Fujita et al. also observed that over days the single nano-cages formed a large vesicle, which was still in equilibrium with the single $M_{12}L_{24}$-cage.[87]

The ^{1}H-DOSY-NMR was therefore repeated 24 hours after mixing the complex, however, we didn't observe any difference. The large structure observed built by ligand (*R*)-**12** seems to form within 24 hours. Still, 140 Å is not enough to form a large vesicle from the M_6L_{12}-complex. As mass spectroscopy is unsuited for complexes this large, dynamic light scattering measurements (DLS) were performed.

DLS is an alternative method for measuring the hydrodynamic radius of particles in a solution based on the *Brownian* motion using the property of particles to scatter light. The in-

tensity of the scattered light is measured and correlated to the change of intensity over time. Large particles will diffuse slower than small and the change in intensity over time will be slower, making it possible to correlate the *Brownian* motion to size. Since it is still the hydrodynamic radius that is being measured, the same limitations apply to the measured size as in the DOSY-experiments. There are three different size distributions correlated either to the intensity, the volume or the number. Because the intensity of the scattered light of large particles is significantly larger than for small particles, it can be necessary to convert the intensity-distribution into a volume- or a number-distribution and thereby eradicating intensity-effects originating from small amounts of large particles.

The measurements were performed on the NMR-solutions in the lab of Prof. Dr. Carsten Schmuck with the help of Patryciusz Piotrowski. The intensity distribution showed a small peak around 2 nm and a very large peak at around 100 nm. Large particles generally result in a greater intensity even if they only make up a minority of all particles present. Therefore, it is advantageous to convert the intensity distribution into volume- or number-distribution, when several particles of different size are present in the solution. This gives a more accurate picture of the ratio of small and large particles in the mixture. When converting the intensity distribution obtained from the measurements only one peak at around 2 nm was obtained in both the volume- and number-distribution (Figure 5.15).

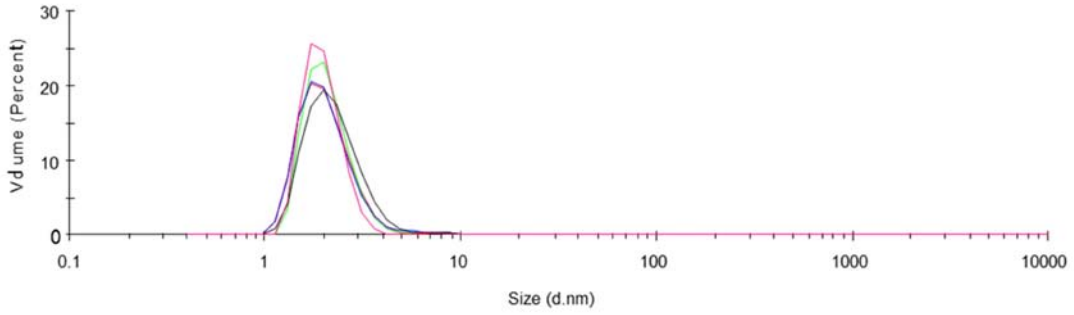

*Figure 5.15 Size distribution by volume from DLS-measurements of ligand (R)-**12** with $Pd(CH_3CN)_4(BF_4)_2$ in DMSO.*

Several measurements were performed which gave rise to very similar curves as can be seen in Figure 5.15. The size, as determined from the volume-distribution, varied from 2.045 to 2.416 nm and corresponds very well to the size expected for the M_6L_{12}-complex. However, certain reservations have to be made, since the solution was both colored and fluorescent. These two characteristics decrease the quality and reliability of the measurement, and consequently the results are not unambiguous. Nevertheless, it seems unlikely that particles around the size of 14 nm are present in solution after performing the DLS-measurements. Another ^{1}H-DOSY-experiment was performed on a different batch of the solution about one month after mixing. Here the hydrodynamic radius was calculated to be around 6 nm. It is not apparent how these different size-measurements come about.

Performing mass spectroscopy on the complexes turned out to be unfeasible. Since it is not possible to properly spray DMSO in the ESI-chamber, the solution was diluted in CH_3CN, although the complex may behave differently in a different solvent. The mass spectra (not shown) did not exhibit any peaks corresponding to the complete sphere. Instead, a base peak at 471.2 m/z was recorded, corresponding to the free ligand. Several other, smaller peaks were also found in the spectrum, but these could not be identified. Repeated measurements produced the same result. This can partly be explained with the structure of the sphere. The cage is not well suited for the mass spectrometer, since evaporation of the solvents from the cavity of the probe during the experiments would cause the sphere to collapse. However, even in this case it would be expected to see fragments from other species than the uncomplexed ligand. A possible solution to obtain a spectrum of the whole sphere structure could be addition of a guest molecule, which fits into the cavity and would be able to stabilize the sphere. Therefore, additional ^{1}H-DOSY-NMR as well as DLS-measurements of complex solutions after different times of mixing are necessary to confirm the formation of the M_6L_{12}-sphere.

Since identification the M_6L_{12}-complex in DMSO proved to be rather difficult, we instead turned to other solvents such as acetone-d_6, CD_3CN and CD_2Cl_2/CD_3CN (3:1) hoping for clearer results. As seen earlier with the ligand *rac*-**21** in acetone- d_6 the ^{1}H-NMR-spectrum of the complex of (*R*)-**12** indicated the formation of a polymeric species. Using CD_3CN as the solvent gave a similar spectrum and both solutions gelated after a few days. Only the solvent mixture CD_2Cl_2/CD_3CN (3:1) resulted in a well resoluted spectrum, but the number of signals in the complex did not correspond to the number of signals in the free ligand (Figure 5.16a and b). It is therefore likely, that there was more than one species in the solution. Proton assignment was not possible.

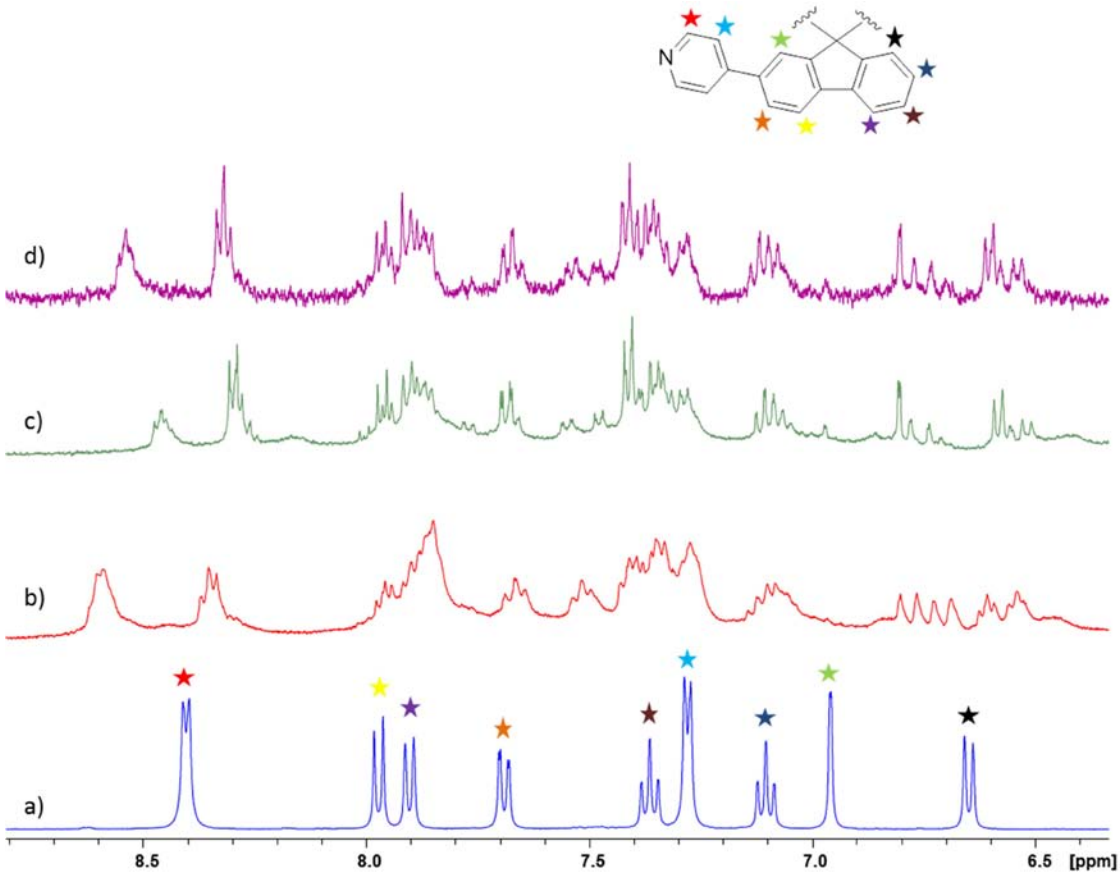

*Figure 5.16 ^{1}H-NMR-spectrum of a) ligand (R)-**12** in CD_2Cl_2/CD_3CN (3:1) b) ligand (R)-**12** with $Pd(CH_3CN)_4(BF_4)_2$ in CD_2Cl_2/CD_3CN (3:1) after 6h at 65°C c) ligand (R)-**12** with $Pd(CH_3CN)_4(BF_4)_2$ in CD_2Cl_2/CD_3CN (3:1) after 9h at 65°C d) ligand (R)-**12** with $Pd(CH_3CN)_4(BF_4)_2$ in CD_2Cl_2/CD_3CN (3:1) after 12h at 65°C.*

A ^{1}H-DOSY-NMR-experiment confirmed the presence of two species of different but similar size in the solution. The solution was therefore heated for another three hours, which resulted in the increase of intensity of some peaks and decrease of others. Encouraged by this, we heated the solution in three hour-intervals, recording a ^{1}H-NMR-spectrum after each interval. The result is shown in Figure 5.16c and d.

It can be seen that further heating changed the intensity relation between the peaks, one set becoming larger than the other. The change in shifts from Figure 5.16b to c and d is due to changes in the ratio of CD_2Cl_2 to CD_3CN, since the heating causes evaporation of the solvent. After 9 hours of heating, additional heating did not result in any change, and a ^{1}H-DOSY-experiment was performed after 12 hours of heating. The resulting DOSY-spectrum still showed the presence of two species, where the peaks at 8.6 and 8.3 ppm (Figure 5.16d) each belong to one of the two different species and have an intensity ratio of 1:1.4. It was not possible to make a calculation of the hydrodynamic radius because the solvent is a mixture of solvents and consequently the viscosity is not known. The mass spectra of the complex were also recorded by diluting the solution in CH_3CN. Again, the spectra only resulted in a peak corresponding to the free ligand along with several unidenti-

fiably peaks, confirming that mass spectrometry may not be the optimal method to investigate the M_6L_{12}-spheere.

DLS-measurements could have been made on the solution; however, the measurements would have been ambiguous, because of the presence of two different species of similar size in the solution. This makes it difficult to obtain one sharp and defined signal. To obtain only one species in the solution it could be tried to carry out the complexation in the microwave at low intensity.

5.4 Conclusion

Ligand **22** based on spirobifluorene has been synthesized and its ability to form an M_2L_4-cage has been tested in different solvents, were pure CH_3CN turned out to be the most promising. The formation of M_2L_4-cage using ligand (*R*)-**22** was established in CH_3CN and CH_2Cl_2/CH_3CN (3:1) by mass and ^{1}H-NMR-spectroscopy. Further experiments to obtain better ^{1}H- and DOSY-NMR-spectra are still to be made. However, we are optimistic that it is possible to produce the desired spectra and confirm the formation of one singular M_2L_4-species by NMR-spectroscopy.

We used ligand (*R*)-**12** in complexation experiments in different solvents aiming to produce an M_6L_{12}-sphere. Using ^{1}H-NMR-spectroscopy and DOSY-experiments it was confirmed, that only one species had been formed. The size was assessed using both DOSY-NMR-spectroscopy and DLS-measurements.

6 Multicomponent systems

The use of more than two components in a single complexation event adds complexity to the system and challenges the process of self-sorting adding more possibilities to the equilibrium. However, it also lets us investigate the how self-sorting proceeds when the conditions are more similar to conditions found in nature.

6.1 Background

The formation of smaller supramolecular 2:2-rhombs (Chapter 4.3.1, Page 31) as well as large self-assembled balls and cubes (Chapter 5.3, Page 68) has been presented. However, they are all composed of one ligand forming one distinct interaction with one specific metal-ion. Nature on the other hand is able to perform a much higher degree of self-sorting forming distinct complex structures from numerous different components. The replication of DNA is a good example of this ability to assemble a large, complicated molecule with a remarkably small margin of error. Such a high degree of accuracy in artificial systems is very difficult to achieve, and therefore not many examples of multicomponent self-assemblies exist.[79,89]

In order to achieve a more complex version of self-sorting including the application of different building blocks, it is crucial that the different interactions differ enough from each other to ensure effective self-sorting. To ensure the orthogonality of the different binding types and to prevent unwanted interactions one can use interactions of different strengths, but also steric effects or metals of different binding geometries.

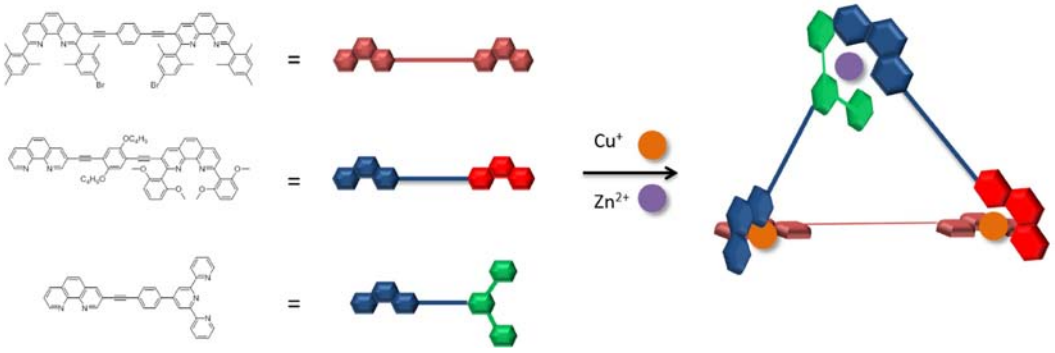

Figure 6.1 Synthesis of isoscelic triangle by Schmittel and Mahata.[90]

Schmittel and coworkers succeeded in the formation of a molecular triangle consisting of five components: three different ligands and two different metals (Figure 6.1).[90]

The methods employed in this case were the HETTAP (heterochiral terpyridine and phenanthroline complex formation)[91] and PHENLOCK[92] protocols, which are based on steric hindrance to prevent unwanted complexation events. The triangle was synthesized in a one pot reaction with all three ligands present in CH_3CN/CH_2Cl_2 (3:1) along with the two metal ions all in stoichiometric amounts. Reflux of the mixture for three hours resulted in exclusive formation of the triangle in Figure 6.1). Addition of excess amounts of metal-ions still resulted in the clean formation of the triangle.

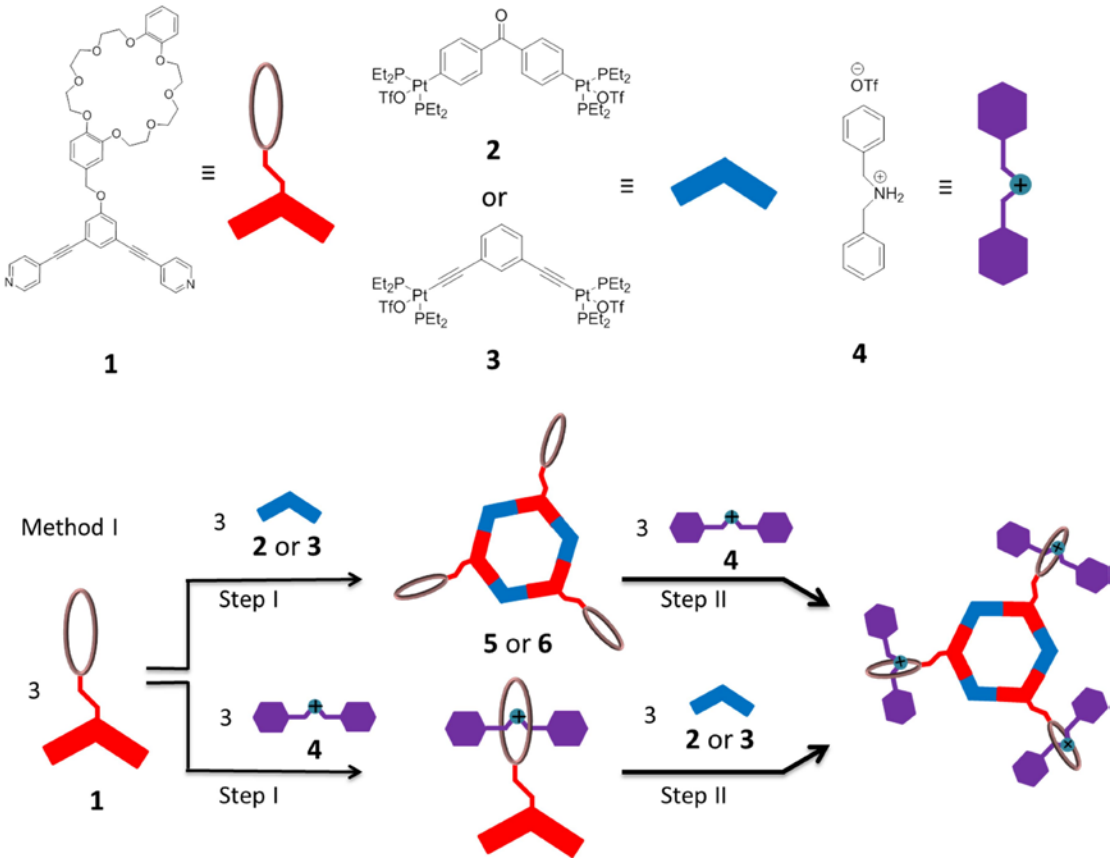

Figure 6.2 Formation of tris[2]pseudorotaxanes by Stang et al. adadpted from Stang et al.[93]

However, it is also possible to achieve selectivity between different recognition events using the orthogonality of different binding modes.[93,94] Stang and coworkers used the difference in strength between directional Pt-bonds and non-directional binding of ammonium-ions by crown-ethers to form two different tris[2]pseudorotaxanes (Figure 6.2).[93] Another approach is to use the different coordination geometries and the soft and hard nature of different metals. Employing Cu(I) and Zn(II), Lehn *et al*. were able to form a heterometallic grid together with ligand **LH** with incorporated soft and hard metal-binding sites (Figure 6.3).[95]

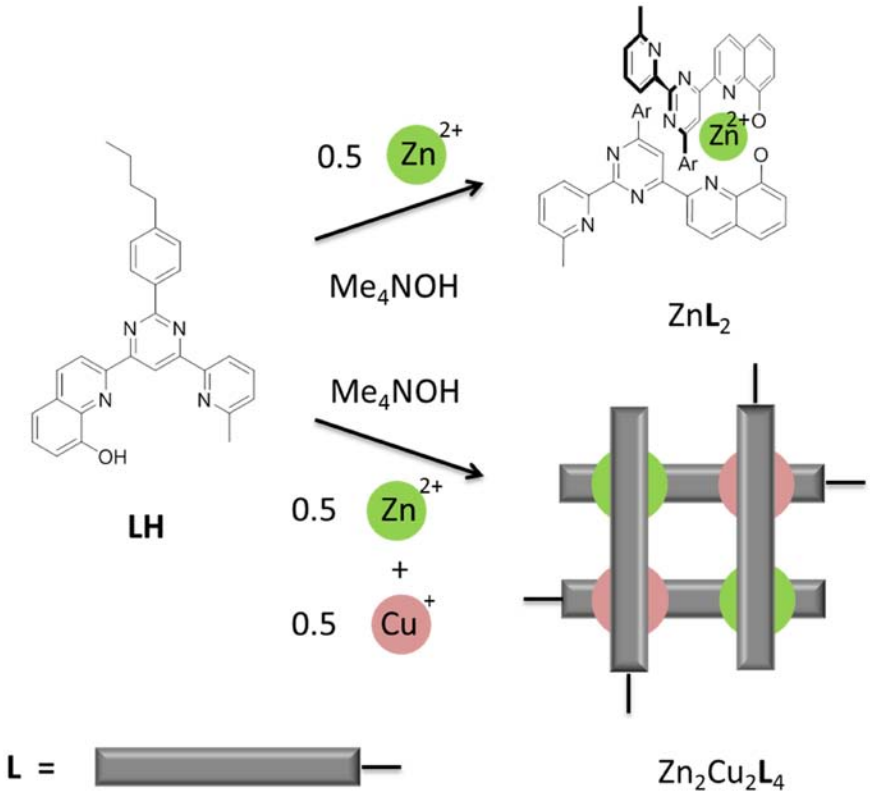

Figure 6.3 Synthesis of heterometallic grid by Lehn et al. adapted from Lehn et al.[95]

6.2 Synthesis of the ligands

As shown above there are many ways to achieve self-sorting in multicomponent systems. We decided to use the approach of Lehn *et al.*[95] incorporating soft and hard metal-binding sites into the ligand. However, we aimed at forming a larger structure, more exactly a supramolecular cage in the shape of a trigonal bipyramid.

Previously, Wang *et al* succeeded in the synthesis of a supramolecular trigonal bipyramid using the ligand shown in Figure 6.4.[96] The ligand can bind a hard oxophilic and a soft nitrophilic metal at either end. Using Al(III), the first complexation is carried out and results in the formation of a tripodal complex which can be further reacted with $ZnBr_2$ or $Pd(en)(NO_3)_2$ resulting in a trigonal bipyramidal and a capped octahedral complex respectively as shown in Figure 6.4.

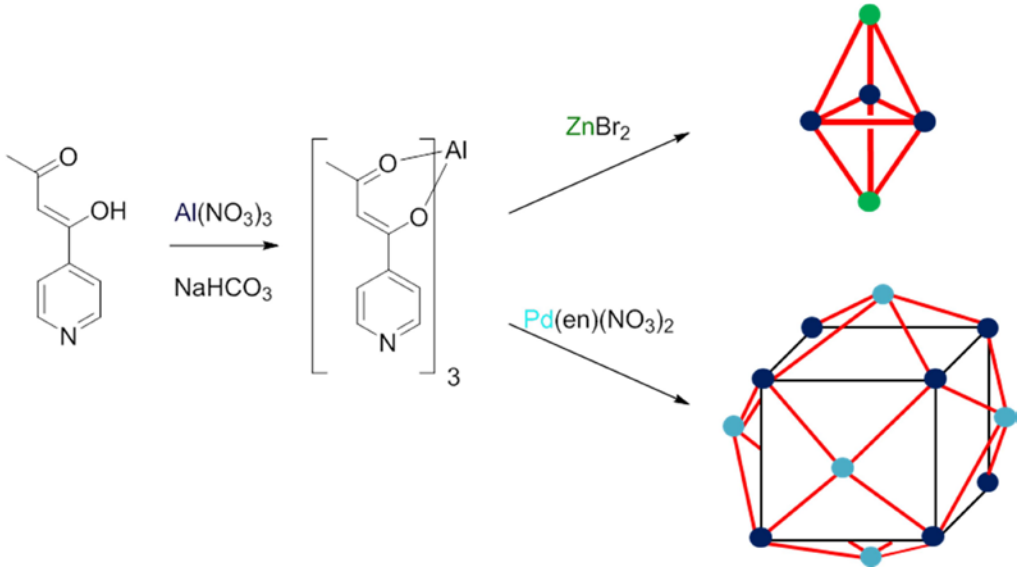

Figure 6.4 Synthesis of heterometallic trigonal bipyramid and capped octahedron by Wang et al.

Both complexes can be chiral due to the octahedral coordination geometry of Al(III).[97] The tripodal aluminum-complex forms both the *fac*- and the *mer*-isomers in solution, but when $ZnBr_2$ is added, the homochiral trigonal bipyramid is formed with all aluminum-centers either in the Λ – or the Δ-configuration. The capped octahedron resulting from reaction of the tripodal Al-complex with $Pd(en)(NO_3)_2$ consists of 38 components: 24 ligands, 8 Al(III)-ions and 6 Pd(II) ions. This large complex is also chiral since all eight Al(III)-ions are either in the Λ- or the Δ-configuration.[96]

Inspired by the work of Wang *et al.* a ligand was developed in order to produce a heteronuclear trigonal bipyramid-complex with a larger ligand than used previously in order to test the possibility of employing a chiral ligand. As the soft metal binding site 4-pyridine was used while the hard metal binding site was to be catechol. These two sites are engineered to bind Pd(II) and Ti(IV) respectively, with high selectivity.

The target molecule **34** is shown in Scheme 6.1 along with the retrosynthesis. We decided to use 1,4-diethynylbenzene as the central building block and substitute it with the iodo-derivatives of pyridine and catechol.

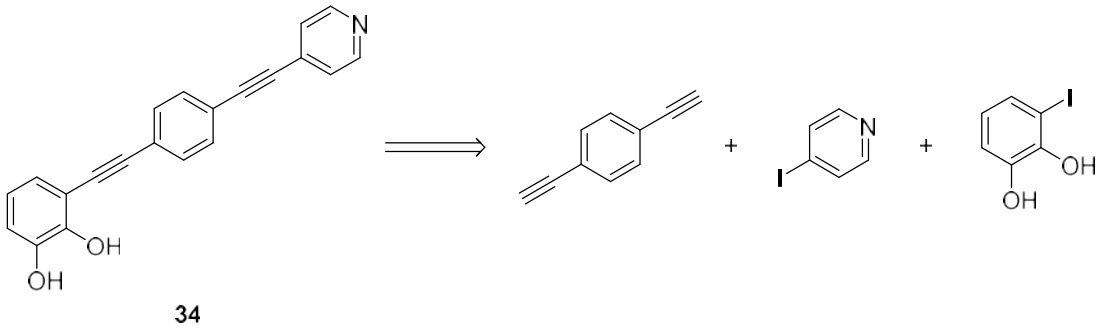

34

*Scheme 6.1 Retrosynthesis of ligand **34***

The 4-iodopyridine was tested again in this *Sonogashira*-reaction, since it is more reactive than the bromo-derivative. Even if the 4-iodopyridine decomposes to a certain extent, the higher reactivity could still lead to product formation.

4-iodopyridine is commercially available; however the price makes it feasible to synthesize the molecule. Two different methods were tested starting with the halogen exchange of the HCl-salt of 4-chloropyridine seen on the right in Scheme 6.2. The method was adapted from Wolf *et al*.[98] Refluxing the starting material with NaI over night gave the impure product **22** in a 34% yield. The low yield combined with low purity prompted the search for a different method. A variation of the *Sandmeyer*-reaction, which can be seen on the left of Scheme 6.2, was chosen as an alternative.[99]

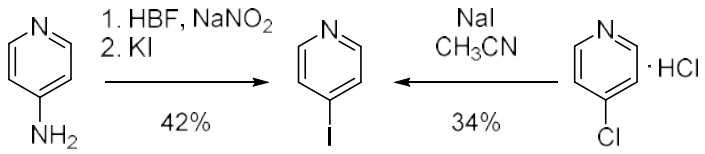

23

*Scheme 6.2 Synthesis of 4-Iodopyridine (**23**)*

The yield increased to 42% and after sublimation of the crude product, pure **23** was obtained as a white powder. However, **23** is both sensitive to both light and heat, and even stored at -18°C in the dark it slowly decomposed into a brown solid. It is therefore important to use 4-iodopyridine **23** shortly after its synthesis.

The catechol synthesis was performed after a protocol by U. Kiehne and is described in Scheme 6.3.[100]

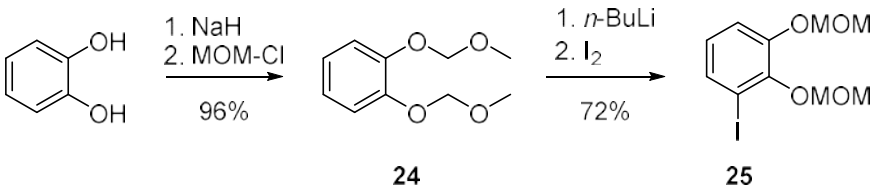

*Scheme 6.3 Synthesis of 2,3-bis(methoxymethyl)-1-iodobenzene (**25**)*

The hydroxyl groups are protected with methoxymethyl ether-groups (MOM) for several reasons. Firstly, addition of the protecting groups increases the solubility of the molecule in organic solvents. Secondly, the MOM-groups direct the *ortho*-metallation much better than a hydroxyl-group. Deprotection of the MOM-groups is performed with acid. Using NaH as a base, the hydroxyl groups of the catechol were deprotonated and methoxymethyl chloride was added resulting in **24** in an excellent yield of 96%. Substance **24** was then subjected to *ortho*-lithiation with *n*-butyllithium followed by addition of iodide resulting in **25**. First the *ortho*-lithiation only produced **25** in yields ranging from 10% to 40%. A closer examination of the byproduct revealed that significant amounts of unreacted starting material still remained in the reaction. Since incomplete *ortho*-lithiation had taken place, the amount of *n*-BuLi added was increased from 1.1 to 1.3 equivalents, resulting in a yield of 72%.

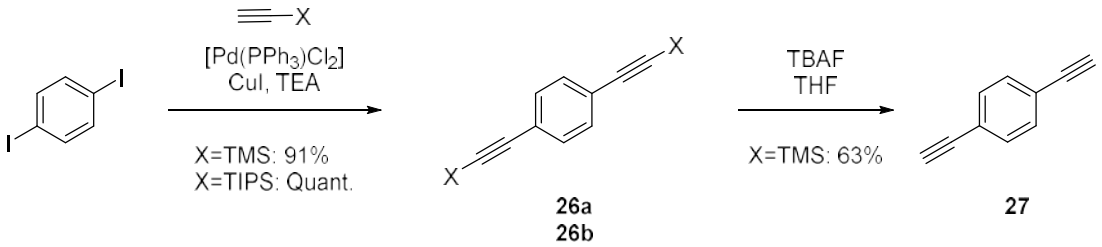

*Scheme 6.4 Synthesis of central building block **27**. **26a**: X = TMS, **26b**: X = TIPS*

The central building block of the ligand is synthesized starting from 1,4-iodobenzene in a *Sonogashira*-coupling Scheme 6.4).[67] Using TMS-acetylene as described previously, (Chapter 4.2) the doubly TMS-protected 1,4-diethynylbenzene **26a** was obtained in a yield of 91%. It was attempetd to partially deprotect **26a**, thereby obtaining a building block, which could be asymmetrically substituted. However, deprotection with tetra-*n*-butylammonium fluoride (TBAF) resulted in **27** without any traces of the mono-protected product. Instead, triisopropylsilyl-group (TIPS) was used to synthesize **26b**, since triisopropylsilyl is more stable towards deprotection than trimethylsilyl. The synthesis was performed analogous to the synthesis of **26a** and gave **26b** in a quantitative yield. The deprotection with TBAF in THF, however, did not result in the desired mono-protected product; instead no deprotection was observed at all

Still it was hoped that it would be possible to perform a single *Sonogashira*-reaction on **27** resulting in **28** as shown in Scheme 6.5.

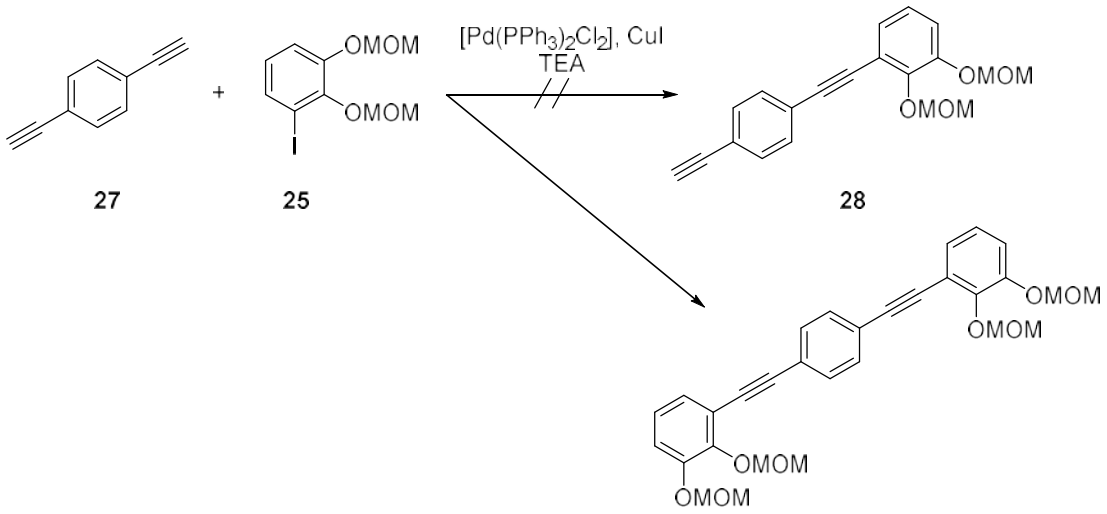

27 25 28

*Scheme 6.5 Synthesis of the mono-substituted building block **28***

Even though only 0.8 equivalents of **25** were added, only the doubly substituted product was obtained along with the starting material. After several attempts this approach was abandoned in favor of a synthesis based on the (3-cyanopropyl)diisopropylsilyl-protecting group (CPDIPS-group), introduced by Höger and Bonrad.[101] CPDIPS-acetylene (Figure 6.5) can be readily synthesized from (3-cyanopropyl)diisopropylsilyl-chloride via a *Grignard*-reaction. The CPDIPS-protecting group distinguishes itself from the TMS- and the TIPS-group in that it is somewhat more stable and more polar. Höger *et al*. used CPDIPS-acetylene and TMS-acetylene in a stepwise *Sonogashira*-reaction to obtain a hetero-functionalized product.[102] Having two different protecting groups makes it possible to deprotect selectively. It is also possible to perform this kind of reaction using TMS- and TIPS-acetylene. However, since the two protecting groups have very similar polarity, it is almost impossible to separate the hetero-substituted product from the two homo-substituted byproducts. The cyano-group adds enough polarity to the product and byproducts, to easily distinguish them by chromatography. Moreover, the difference in stability is greater between TMS and CPDIPS than between TMS and TIPS.

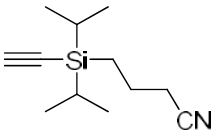

Figure 6.5 [(3cyanopropyl) diisopropylsilyl]-acetylene (CPDIPS-acetylene)

The first attempt was carried out using 1,4-diiodobenzene and self-made CPDIPS-acetylene and resulted in roughly equal amounts of the product **29** and the two byproducts **30** and **26a** (Scheme 6.6, X=I).

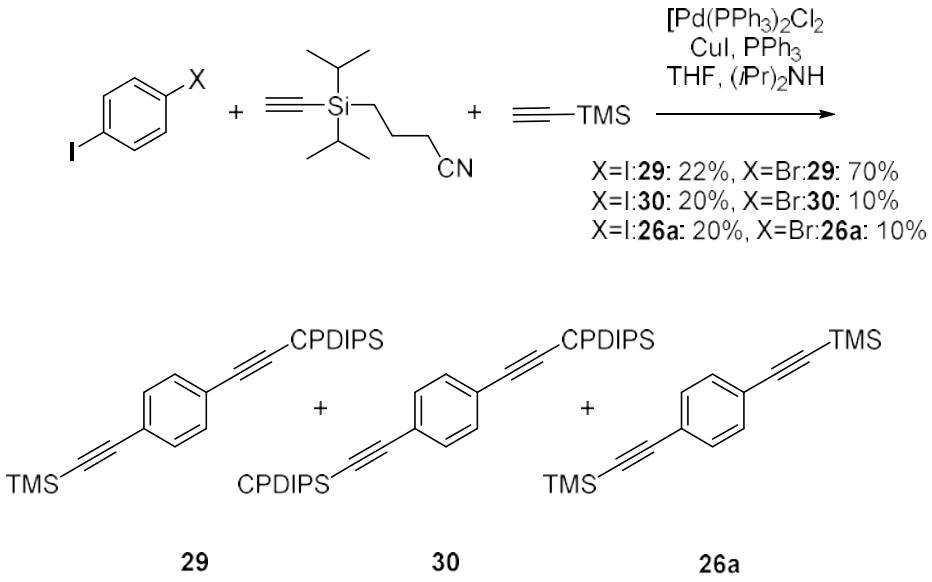

*Scheme 6.6 Synthesis of **29**, **30** and **26a** starting from 1,4-diiodobenzene (X=I) or 1-bromo-4-iodobenzene (X=Br)*

Even though it was possible to mono-deprotect **30** in a 40% yield, this result was still unsatisfying considering the extra steps involved in the synthesis The reaction with 1-bromo-4-iodobenzene was attempted, hoping that the difference in reactivity could help increase the yield of the desired unsymmetrical product **29** (Scheme 6.6, X=Br). Indeed, the yield of **29** improved considerably from 22% to 70%, prompting the further use of 1-bromo-4-iodobenzene for this reaction.

Next, **29** and **30** were deprotected to yield the mono-protected diethynylbenzene **31** (Scheme 6.7). Starting from the hetero-protected **29** the TMS-group can be selectively removed using K_2CO_3 in methanol and THF. In order to deprotect the mono-substituted **30**, one takes advantage of the fact, that the CPDIPS-group needs rather harsh conditions to be removed. Therefore TBAF in THF/H_2O was used according to the method by Höger *et al*.[102] The water is added to reduce the reactivity of the TBAF, making it possible to stop the reaction when only one of the CPDIPS-groups has been removed.

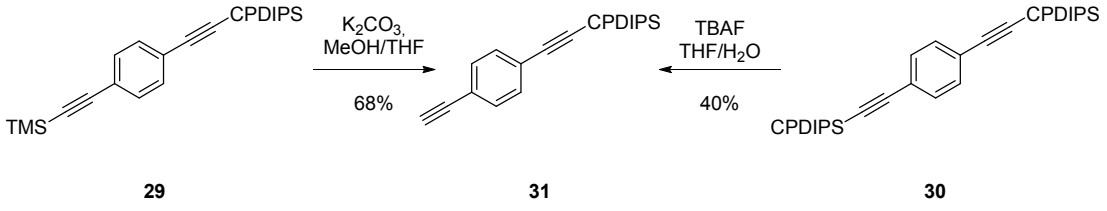

*Scheme 6.7 Deprotection of **29** and **30** respectively, yielding **31***

The yield for deprotection of the hetero-protected diethynylbenzene **29** (68%) is higher than for the deprotection of the homo-protected **30** (40%), reflecting the fact that the selectivity is difficult to control during the latter reaction.

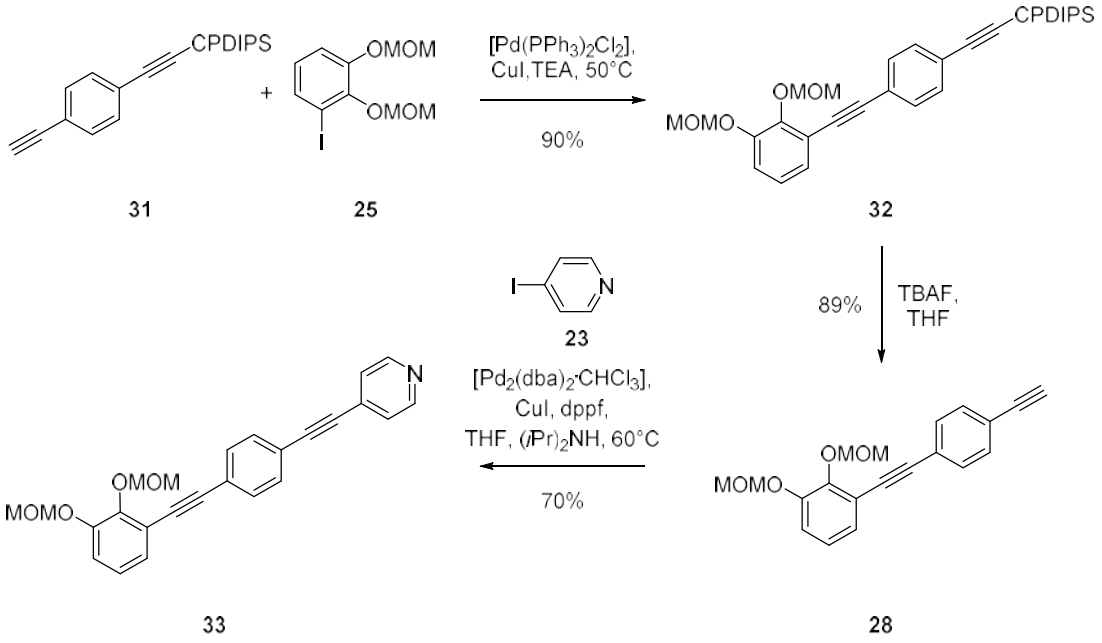

*Scheme 6.8 Synthesis of MOM-protected ligand **33***

With the mono-protected **31** it was now possible to add two different groups to either end of the ethynyl-ends. To this end we performed a *Sonogashira*-reaction using the catechol-derivative **25** resulting in **32** in a yield of 90% (Scheme 6.8). Compound **32** was subsequently deprotected with TBAF yielding **28** in a good yield of 89%.

Another *Sonogashira*-reaction with 4-iodopyridine **23** resulted in **33**, which was verified by ^{1}H – and ^{13}C-NMR. The signal originating from the ethynyl-proton had disappeared and the signals of the central benzene core shift together and overlap indicating, that the chemical and magnetic environment of the two seemingly different benzene protons has become very similar. This was surprising, since we had previously encountered problems performing *Sonogashira*-reactions with 4-iodopyridine and spirobifluorene (Chapter 4.2). However, the product could not be found by mass-spectrometry. ESI-MS spectra only showed peaks originating from 4-iodopyridine and the starting material **28**. Nevertheless, an attempt was made to remove the MOM-groups with HCl in ether to produce ligand **34**. Most likely, the coupling reaction did not work and instead obtained the deprotonated ligand **28**, and the salt of iodopyridine **23**.

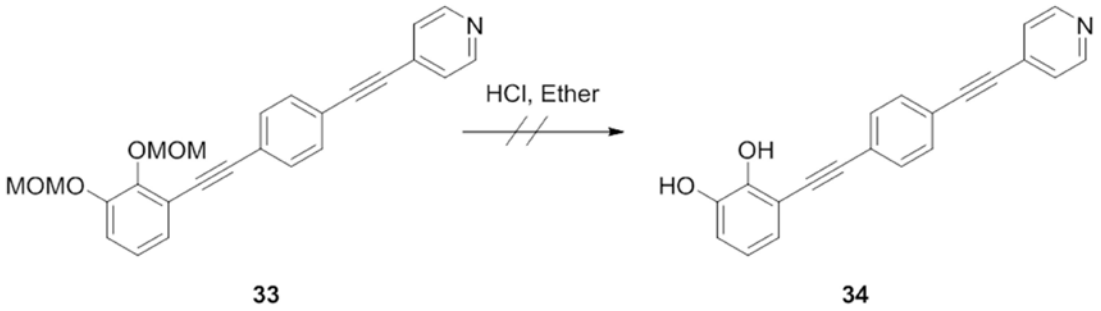

33 **34**

*Scheme 6.9 Attempted deprotection of **33***

The ^{1}H-NMR-spectrum of the crude product revealed the presence of the MOM-groups, and the pyridine protons seemed to have disappeared. The deprotection did not seem to have worked, and in addition compound **33** seemed to have disintegrated. Taking the results from the ESI-MS measurements into account, it is possible that the product **33** was never formed.

Deprotection of **28** into **35** was also attempted, since **35** could also be used as a ligand in complexation studies. The free ethynyl can be deprotonated and *cis*-directing Pt(II) can be complexated, which induces a defined angle into the complex. The catechol-unit was to be complexated to Ti(IV) in the same fashion as ligand **34**. According to modeling studies the ligand would be suitable forming a trigonal bipyramid with Pt(dppp) and Ti(IV) (Figure 6.6).

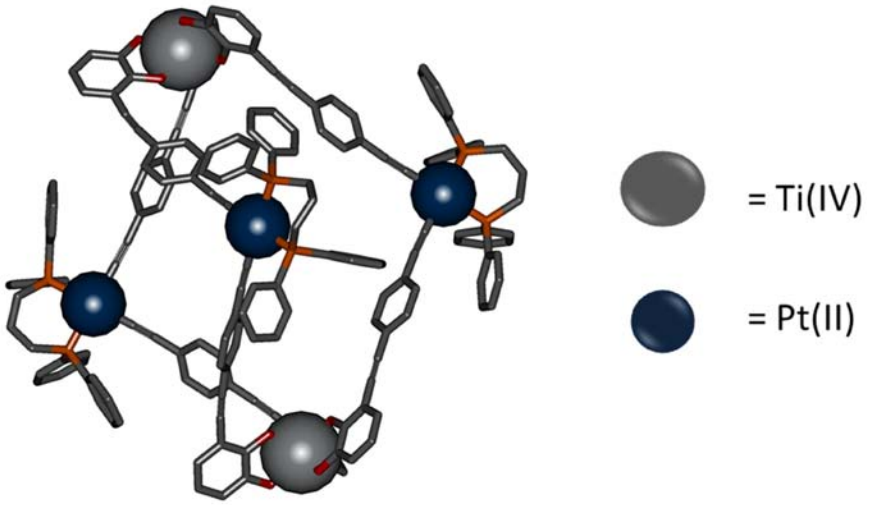

*Figure 6.6 Energy minimized structure of heterometallic complex of ligand **35***

However, deprotection of **28** to **35** with HCl also showed to be troublesome as shown in Scheme 6.10.

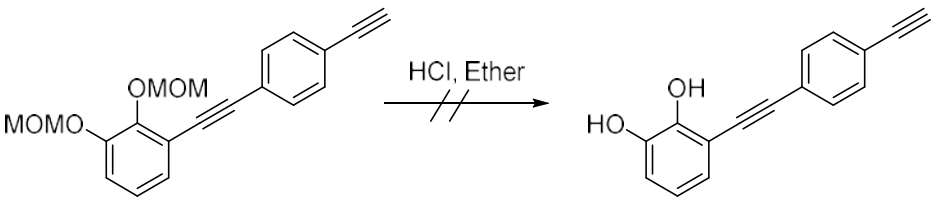

28 **35**

*Scheme 6.10 Deprotection of **28***

The ligand **35** was isolated but ^{1}H-NMR-spectroscopy indicated that it still contained impurities. However, the low solubility of **35** made purification by column chromatography very difficult and it was not possible to isolate the ligand in sufficient purity for the complexation-experiments. Instead, we decided to perform the deprotection after the initial complexation of ligand **27** with $Pt(dppp)Cl_2$ as described in chapter 0.

All in all, the synthetic efforts towards synthesizing ligand **34** did not compare with the outcome, so instead we decided to look at a smaller molecule, which was expected to be easier to synthesize. Ligand **39** (Figure 6.7) was chosen because we already had synthesized one of the building blocks (**25**), while the other (**37**, Scheme 6.11) should be easily prepared by a *Sonogashira*-reaction.

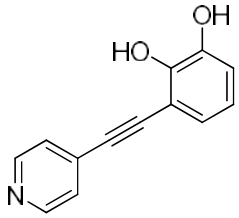

*Figure 6.7 Ligand **39***

36 was synthesized from **23** using $[Pd(PPh_3)_4]$ in Et_3N yielding 4-trimethylsilylethynylpyridine in a yield of 90% (Scheme 6.11). Apparently, the cross-coupling reaction is not a problem when using trimethylsilylethylene. Deprotection with KF and subsequent precipitation of the crude product with HCl resulted in the HCl-salt of 4-ethynylpyridine. This was done to increase the stability of **37**.

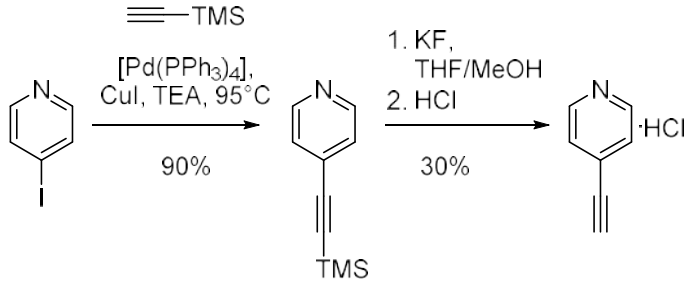

23 **36** **37**

*Scheme 6.11 Synthesis of 4-ethynylpyridine **37***

The following *Sonogashira*-reaction of **37** and **25** resulted in **38** in 58% yield (Scheme 6.12). Of 4-Ethynylpyridine **37** two equivalents were added since, in spite of the higher stability, it was still light- and heat-sensitive.

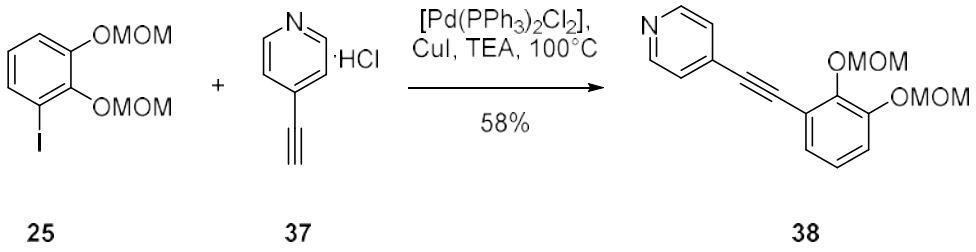

25 **37** **38**

*Scheme 6.12 Synthesis of **38** via Sonogashira-reaction of **25** and **37***

The attempted deprotection of **38** using HCl in ether (Scheme 6.13) did not afford the desired ligand **39** according to the ^{1}H-NMR-spectrum. This prompted the search for an alternative method to deprotect MOM-ethers. A method found in a protocol by Sharma *et al*. used the Lewis acid $ZrCl_4$ in dry isopropanol.[103]

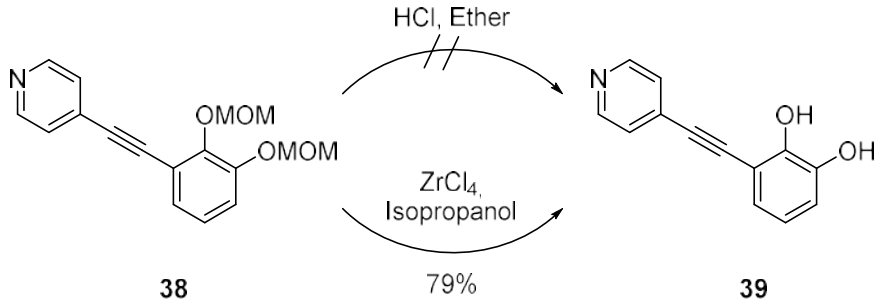

38 **39**

*Scheme 6.13 Deprotection of **38** with HCl in ether and $ZrCl_4$ in isopropanol resulting in **39***

The reaction was performed under argon and yielded crude ligand **39** which could be purified by column chromatography in ethanol resulting in a yield of 79%.

Even though deprotection of the MOM-groups posed several problems, a solution was found in form of the method of Sharma *et al*. and two ligands (**28** and **39**) were synthesized to be used in complexation studies.

6.3 Complexation

Multicomponent self-assembly was attempted with the two ligands **28** and **39**, which both contain a hard and a soft metal binding site (Figure 6.8).

*Figure 6.8 Ligands for multicomponent self-assembly **28** and **39***

To obtain a multicomponent self-assembly we first attempted to use ligand **28** together with Pt(dppp) via the ethynyl-functionality of **28**. The modeled structure of this complex is shown in Figure 6.6.

This complexation proceeds through several steps. We are using the protected ligand **28**, since deprotection of **28** was not possible (Chapter 6.2, Page 84). The complexation of the protected ligand **28** to the Pt(dppp) could increase the solubility of the complex enough to perform the deprotection. The deprotection of the MOM-groups is to be followed by the last complexation step including Ti(IV) (Figure 6.9). This method adds an extra step to the complexation since the MOM-groups would have to be removed first.

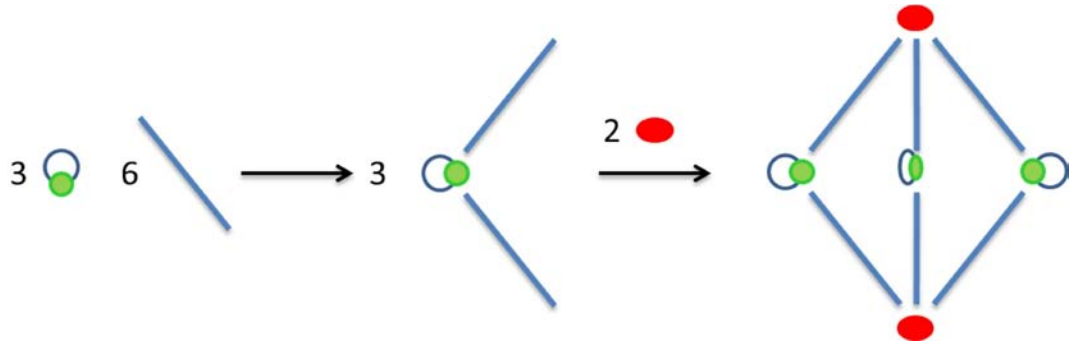

*Figure 6.9 Schematic representation of the complexation of ligand **28**. Green = Pt(dppp), blue = ligand **28**, red = Ti(IV).*

The complexation of **28** with Pt(dppp)Cl_2 was carried out in a similar fashion to the Sonogashira-reaction using Et_3N and CuI under argon. The reaction was stirred for 48 hours and the crude product was purified by column chromatography using neutral ALOX. The product was isolated in a yield of 51 %, while the unreacted starting material was recovered. The ^{1}H-NMR-spectrum of the product compared to the free ligand **28** is shown below in Figure 6.10.

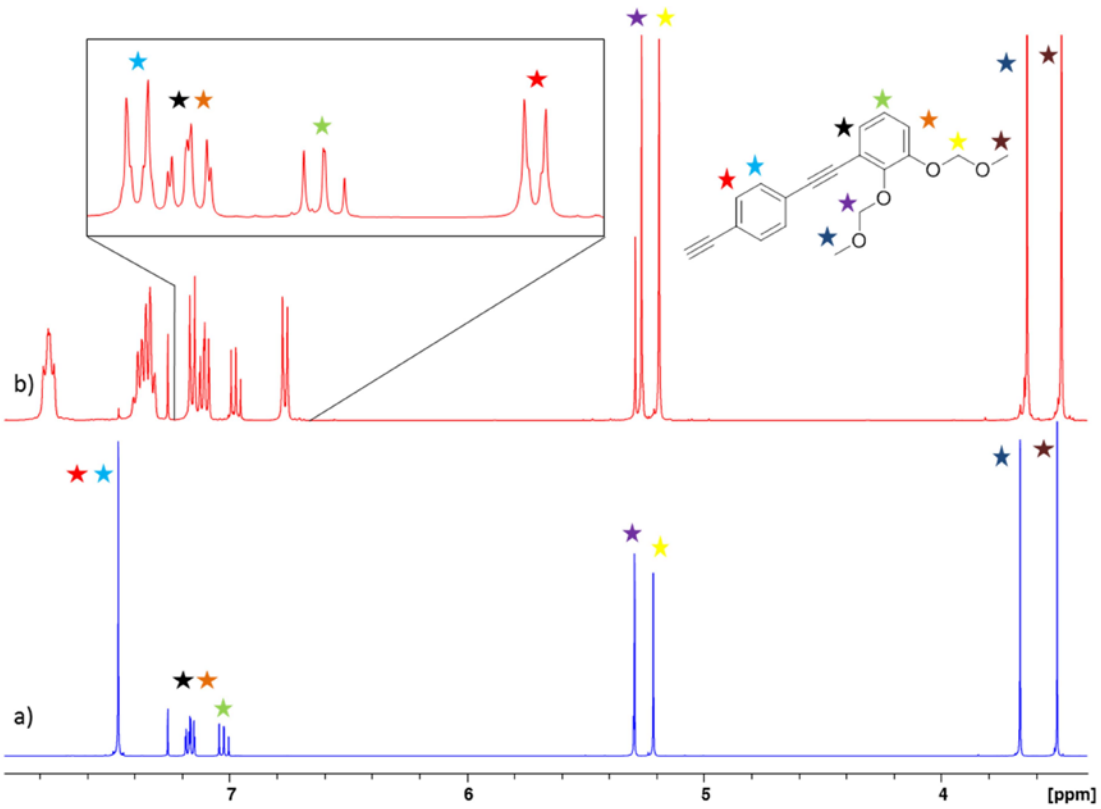

*Figure 6.10 ^{1}H-NMR-spectrum of a) ligand **27** in $CDCl_3$ b) ligand **28** with Pt(dppp)Cl_2 in $CDCl_3$*

All the aromatic signals have shifted significantly, while the signals of the MOM-ether have only shifted slightly, as could be expected. The alkyne-proton is no longer present (not shown). Also, the relation of the integrals is consistent with the formation of a 1:2-complex of $Pt(dppp)^{2+}$ and ligand **28** into a tweezer-like structure. The protons belonging to central phenyl-ring (marked with a red and light blue star respectively) split up in two after complexation, due to the change in environment imposed by the Pt(II). Another indication of the complexation is that the signal of the ethynyl-proton, previously at 3.17 ppm has disappeared. An ESI mass sprectroscopy (positive mode) was also recorded and showed the presence of $[Pt(dppp)\mathbf{28}_2Na]^+$. Interestingly, all following attempts to synthesize more of the complex $[Pt(dppp)(\mathbf{28})_2]$ failed. According to the reaction-TLC, the product had been formed but column chromatography only produced the $Pt(dppp)(OTf)_2$. The column material was extracted with CH_2Cl_2, because of the good solubility of the product in this solvent, but neither ^{1}H-NMR- nor mass spectra of the extract contained any signals corresponding to the desired complex. Lack of starting material prevented further attempts of purification.

Nevertheless, the deprotection was performed on the obtained amount of $[Pt(dppp)(\mathbf{28})_2]$ with $ZrCl_4$ as described earlier (Chapter 6.2). However, an ^{1}H-NMR-spectrum of the crude product still showed the presence of the MOM-groups. Even prolonged heating did not

deprotect the hydroxyl-groups. In the future, other methods with other Lewis acids such as $ZnBr_2$[104] or a heterogeneous catalyst such as silica supported $NaHSO_4$ could be tested.[105]

Complexation was also attempted with the second ligand **39** (Figure 6.8). The modeled structure of the complex is shown in Figure 6.11. Here, the pyridine can coordinate to the square planar $Pd(dppp)^{2+}$, while the deprotonated hydroxylgroups assemble around the octahedral Ti(IV).

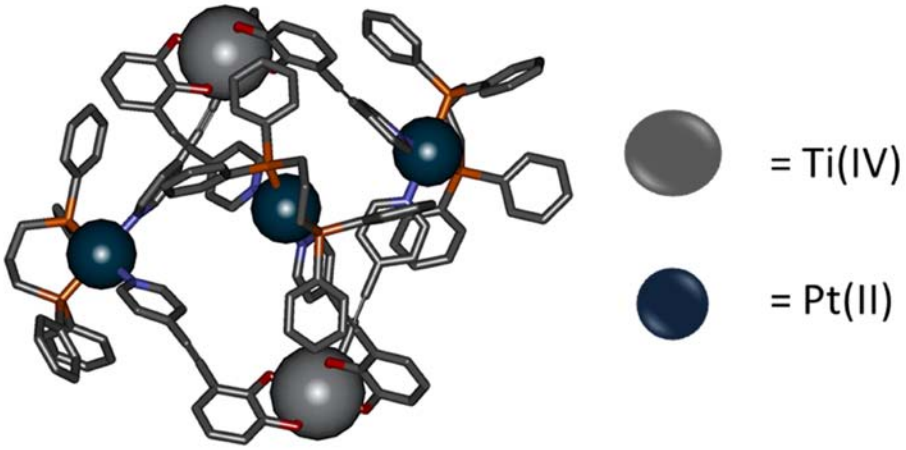

*Figure 6.11 Energy minimized structure of heterometallic complex of ligand **39***

Ligand **39** was mixed with $TiO(acac)_2$ and Li_2CO_3 in DMF while heating the solution to 80°C for 48 hours, which resulted in a dark brown solution. The resulting ^{1}H-NMR-spectrum is shown in Figure 6.13b. The complex spectrum is compared to a spectrum of the free ligand with Li_2CO_3 (Figure 6.13a). It is important to remember, that the ligands in the Ti(**39**)$_3$-complex can point either up or down and this leaves two possible configurations: All ligands in one direction (*fac*-diastereomer) or two ligands in one and one in the other direction (*mer*-diastereomer) as shown in Figure 6.12. At least three different sets of signals would be expected, one for the *fac*-diastereomer and two for the *mer*- diastereomer.

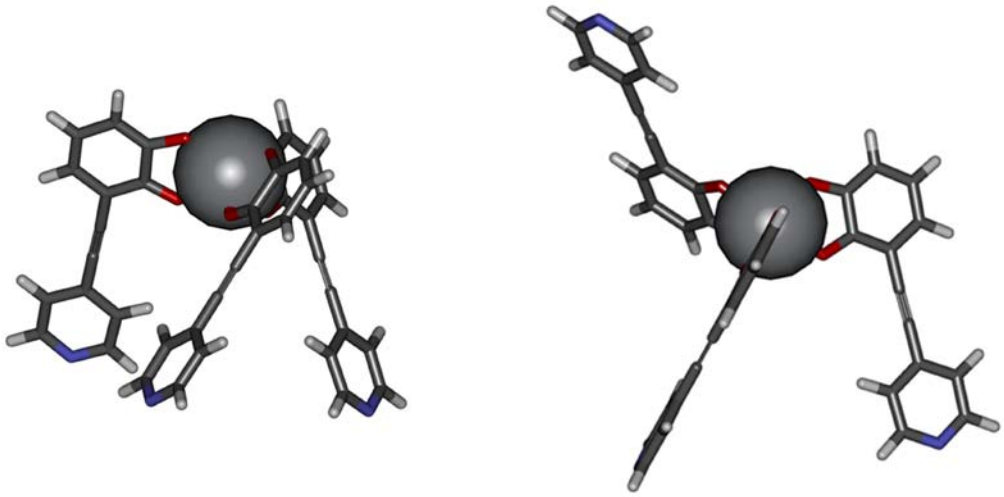

*Figure 6.12 PM6-modeled structure of the complex of ligand **39** and $TiO(acac)_2$ in the fac- (left) and mer-conformation (right)*

Indeed, when looking at the ^{1}H-NMR-spectra (Figure 6.13a and b) we see that more than one set of peaks is present, however, ten peaks are found in the spectrum, divided into only two sets; one with lower and one with a larger intensity. We did expect three sets, but it is possible that the two ligands in the *mer*-isomer pointing in one direction are not magnetically and chemically significantly different from the three ligands in the *fac*-isomer, resulting in the same shifts.

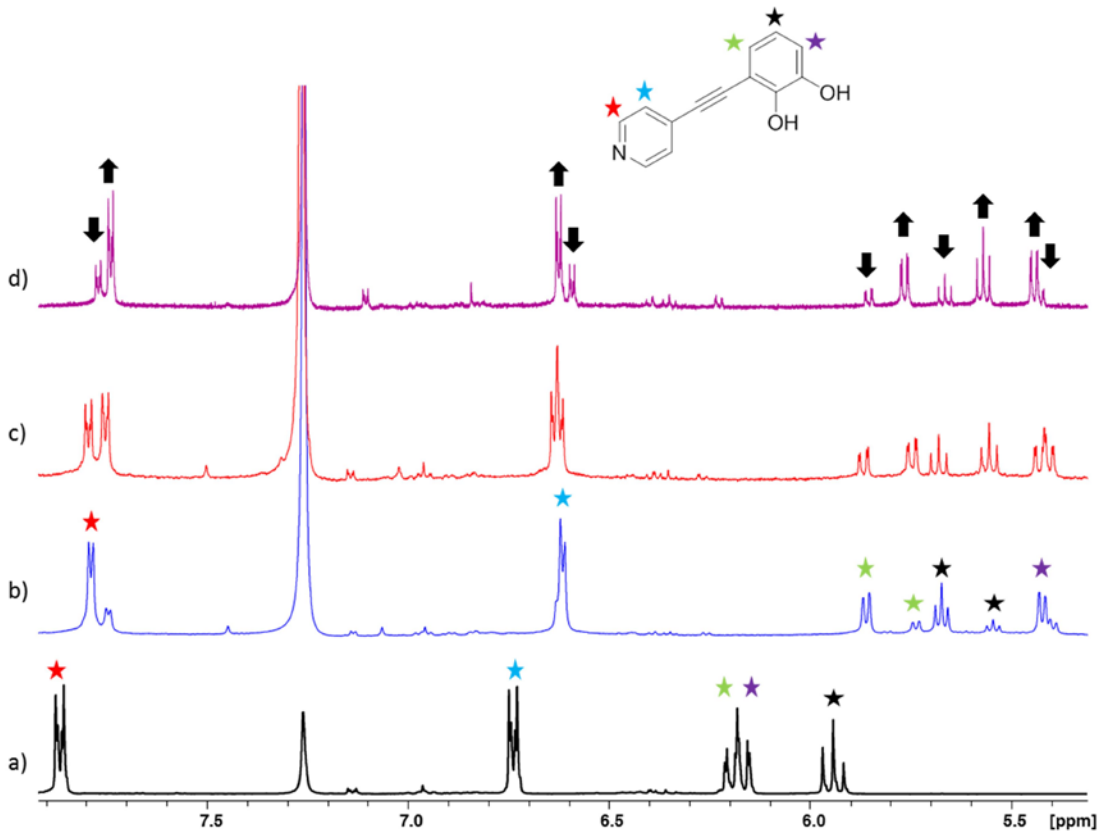

*Figure 6.13 ^{1}H-NMR-spectrum of a) ligand **39** with Li_2CO_3 in DMF-d_6 b) ligand **39** with Li_2CO_3 and $TiO(acac)_2$ in DMF-d_6 after 24h at 80°C c) ligand **39** with Li_2CO_3 and $TiO(acac)_2$ in DMF-d_6 after 48h at 80°C d) ligand **39** with Li_2CO_3 and $TiO(acac)_2$ in DMF-d_6 after 72h at 80°C*

We further observe a change in the relative intensities of the peaks depending on the heating time. The complex-mixtures were heated at 80°C and depending on the duration of the heating, the set of peaks initially smaller increases while the set initially larger, decreases (Figure 6.13b to d). This process was not reversible. To confirm this, a ^{1}H-DOSY-NMR was recorded.

The ^{1}H-DOSY-experiment shows a slight difference in size between the two sets of signals. From the diffusion coefficient the hydrodynamic radii are calculated, and for the set, with an increasing intensity over time, the diameter is ca. 14.5 Å, while the diameter for the other set is ca. 13.5 Å. The difference is not large, but it is consistent for every peak in the spectrum. The obtained hydrodynamic diameters are compared to the diameters measured on the modeled structures (Figure 6.12), which are 13 and 19 Å for the *fac*- and *mer*-isomers respectively. The measured and calculated values for the *fac*-isomer match very well, while the calculated value for the *mer*-isomer is somewhat smaller than the measured value.

As mentioned earlier, the hydrodynamic radius of a molecule depends on how fast the molecule moves through the solvent, and therefore the shape of the molecule can change

the measurement. While the *fac*-isomer is relatively globular, this is not the case for the *mer*-isomer, which can have the effect, that it looks smaller in the DOSY-experiment than it actually is. This could explain the discrepancy between the calculated and measured value.

An ESI negative mass spectrum was also recorded and showed very large amounts of free ligand (Figure 6.14). Also, a small peak corresponding to the fragment $[Ti(\mathbf{39})_2(acac)]^-$ was found. Two peaks corresponding to $[TiH(\mathbf{39})_3]^-$ and $[Ti(\mathbf{39})_3Li]^-$ were found in the spectrum. Since we don't observe any free ligand in the ^{1}H-NMR-spectrum, it is likely that the complex fragments during the measurements.

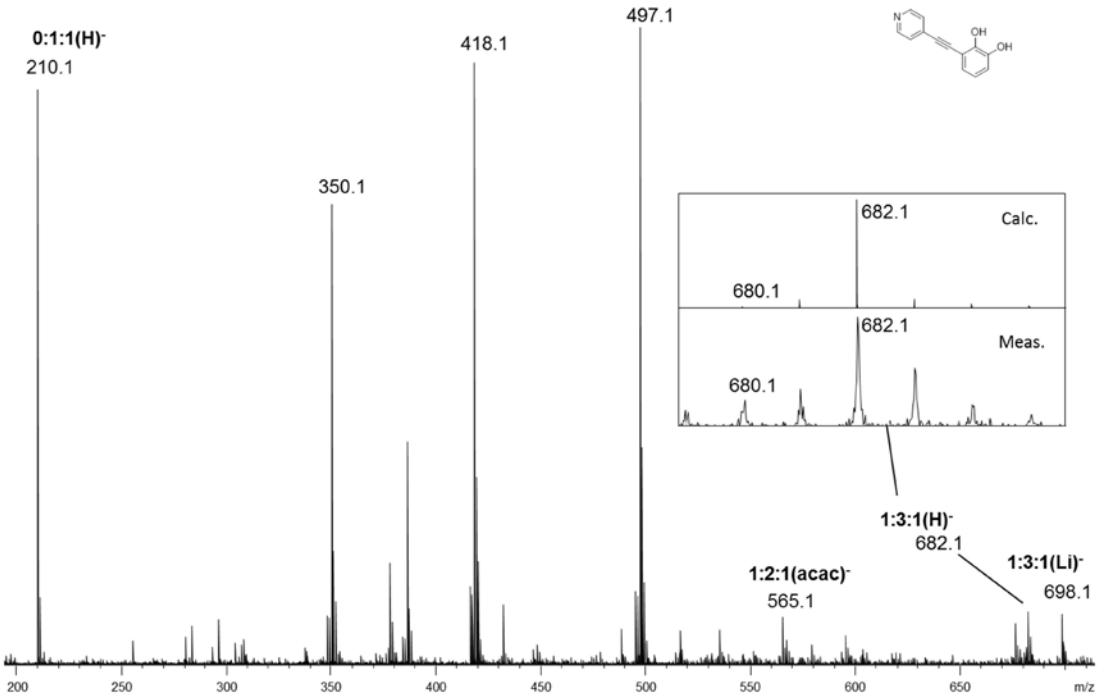

*Figure 6.14 ESI mass spectrum (negative mode) of ligand **39** with $TiO(acac)_2$ in DMF-d_6. The notation corresponds to Metal:Ligand:Cation.*

The DOSY-experiment strongly indicates that two different species, the *fac*- and *mer*-isomers, are present in the solution. The ^{1}H-NMR-spectra recorded after different heating intervals show that one of the two species is thermodynamically more stable than the other. By the help of the diffusion constant obtained from the DOSY-experiment, it is likely that the *mer*-isomer is increasingly formed during heating. This can cause difficulties in the following complexation with Pd(II) or Pt(II), since the *mer*-isomer is not able to form the desired trigonal bipyramidal complex. This assumption was confirmed when the metal salts $Pd(dppp)(OTf)_2$ or $Pt(dppp)(OTf)_2$ were added to the $Ti(\mathbf{39})_3$-complex 24 hours after mixing. The metal-salts were dissolved in DMF and added to the solution of $Ti(\mathbf{39})_3$ and the complex solution was heated over night. However, in neither case a change in shifts of the peaks was observed in ^{1}H-NMR-spectrum compared to the $Ti(\mathbf{39})_3$-complex. It was

also attempted to heat the Ti(**39**)$_3^{2-}$-complex for only 3 hours, followed by addition of either the Pd- or the Pt-corner in DMF-d_6. The resultant mixtures were subsequently stirred at room temperature over night to avoid isomerization of the *fac*-isomer into the *mer*-isomer. The resultant ^{1}H-NMR-spectrum shows the presence of the Pd- or Pt-corner along with only the *fac*-isomer. However, none of the signals has shifted even the slightest compared to the ^{1}H-NMR-spectrum of the pure Ti(**39**)$_3^{2-}$-complex, strongly indicating that no complexation steps beyond Ti(**39**)$_3^{2-}$ have occurred. The short heating time is probably the reason why only the *fac*-isomer is present, since the *mer*-isomer only forms upon prolonged heating. An ESI mass spectrum (positive mode) of the complex solution showed only Pd- and Pt-corner with chloride as the anion along with several unidentified peaks, while only one peak at 565.1 m/z was observed for both solutions in the ESI mass spectrum (negative mode) corresponding to Ti(**39**)$_2$(acac)$^-$. Prolonged stirring of the mixtures did not result in any changes in neither the ^{1}H-NMR- nor the mass spectrum. We have confirmed the formation of the Ti(**39**)$_3^{2-}$-complex, and it is therefore difficult to explain, why the subsequent complexations with Pd(II) and Pt(II) are not proceeding. The *fac*/*mer*-isomerism can halter complexation, however, it is unlikely that it will prevent it completely.

Since the complexation of Pd(II) and Pt(II) with Ti(**39**)$_3^{2-}$ had not succeeded, we therefore decided to investigate the complexation of free ligand **39** to Pd(II) and Pt(II). Starting the complexation with Pd(II) and Pt(II) it should be possible to avoid the formation of different isomers and preorganize the ligand for the following complexation with Ti(IV). Therefore ligand **39** was complexated with Pt(dppp)(OTf)$_2$ and Pd(dppp)(OTf)$_2$ in the solvents CD_2Cl_2/CD_3CN (3:1), acetone-d_6 and DMF-d_6.

In DMF-d_6, no change in the ^{1}H-NMR-spectra was seen for the mixture of ligand **39** with Pd(dppp)(OTf)$_2$ compared to the free ligand even after heating at 60°C. Mass spectra of the solution only showed peaks belonging to the Pd(dppp)(OTf)$_2$. Mixing ligand **39** with the Pt(dppp)(OTf)$_2$ and heating it to 60°C resulted in the ^{1}H-NMR-spectra shown below (Figure 6.15).

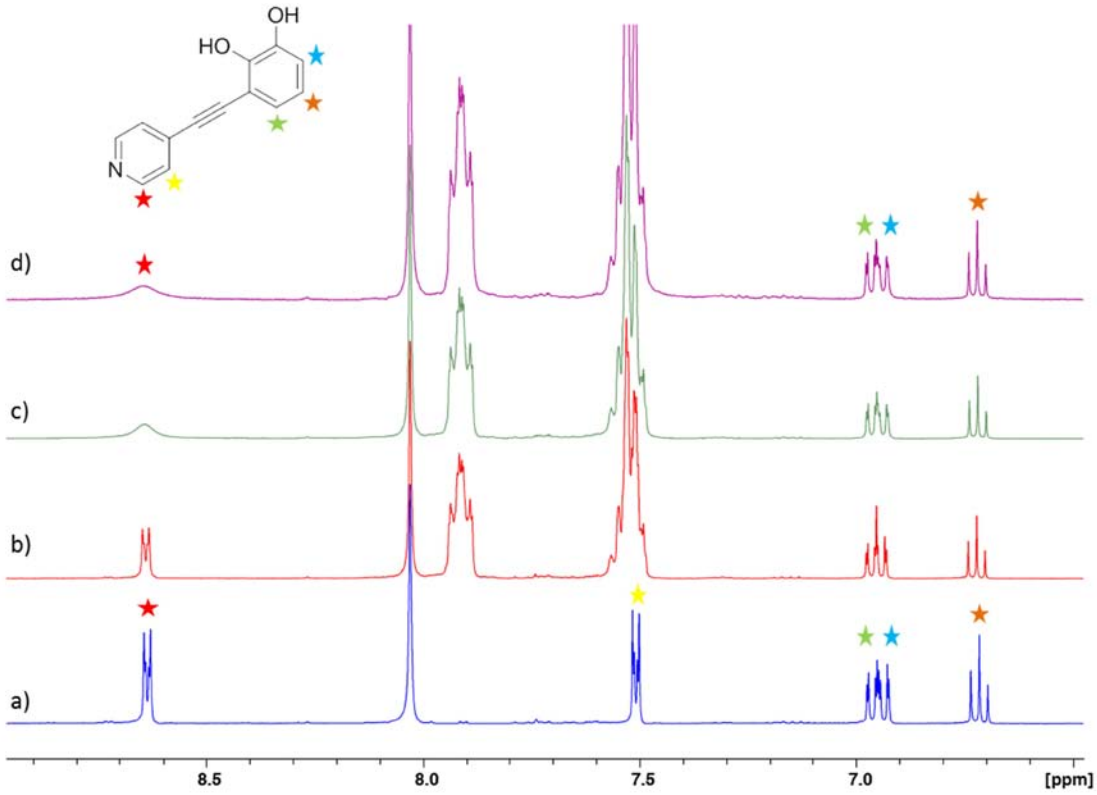

*Figure 6.15 ^{1}H-NMR-spectra of a) ligand **39** b) ligand **39** with Pt(dppp)(OTf)$_2$ after 3 days at RT c) ligand **39** with Pt(dppp)(OTf)$_2$ after 4h at 60 °C d) ligand **39** with Pt(dppp)(OTf)$_2$ after 3days at 60°C all in DMF-d_6.*

The signal belonging to the proton 2 of the pyridine (marked with a red star) exhibits broadening upon heating (Figure 6.15c). Additional heating beyond 4 hours did not produce any significant change in the spectrum (Figure 6.15d). Also, the signal did not shift as would be expected in the case of a complexation event at the pyridine. After three days of heating the DMF-solution was diluted in CH_3CN and a mass spectrum was recorded (Figure 6.16). The base peak of the spectrum at 853.2 m/z corresponds to the monosubstituted Pt(dppp)(OTf)$_2$ (1:1-complex). Two other peaks were not identified, but the isotope patterns suggest that one Pt-ion is present in the peak at 700.1 m/z while at least two Pt ions must constitute the peak at 1379.1 m/z. Fragments containing two Pt(dppp)(OTf)$_2$ but no ligand have been observed before. It seemed that the complex has fragmented, facilitated by the presence of chloride ions. The complexations were performed again with new batches of solvents; however, this did not change the spectra.

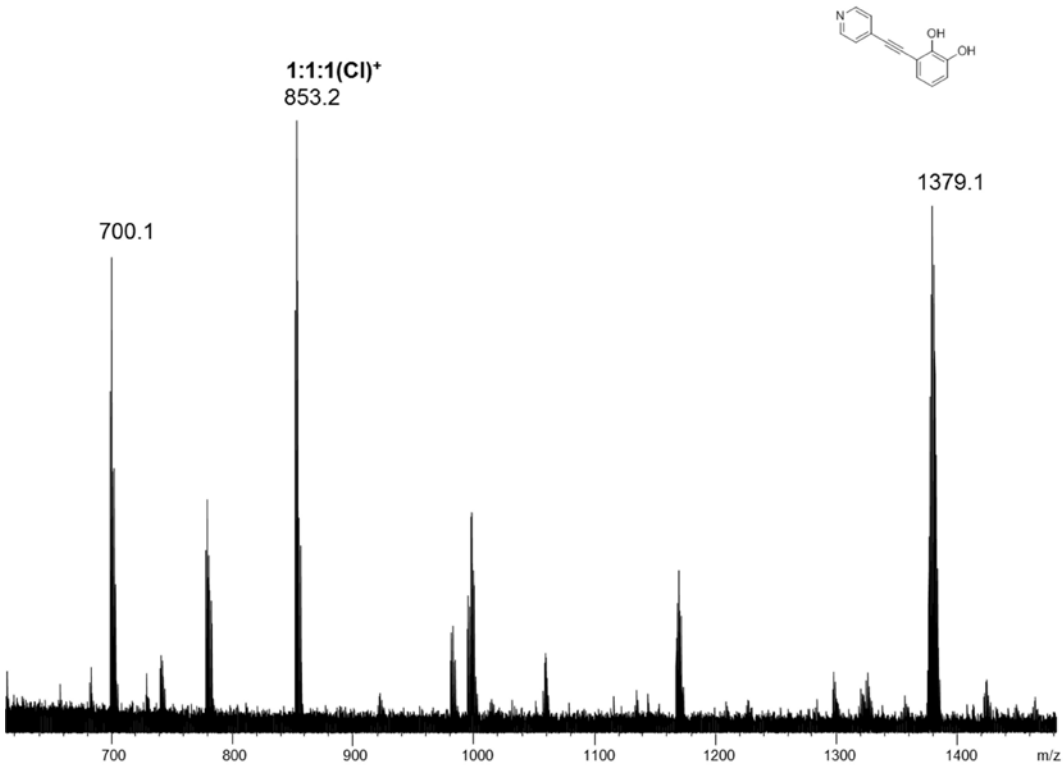

*Figure 6.16 ESI mass spectrum (positive mode) of ligand **39** with Pt(dppp)(OTf)$_2$ in DMF-d$_6$ after 3 days at 60° . The notation corresponds to Metal:Ligand:Anion.*

As previously mentioned, the complexation of ligand **39** was also carried out in two other solvent mixtures: acetone-d_6 and CD_2Cl_2/CD_3CN (3:1). In both cases mixing with the Pd(dppp)(OTf)$_2$ resulted in broadening of the signals in the ^{1}H-NMR-spectra belonging to the pyridine and the bis(diphenylphosphino)propane. The mass spectra exemplified by the one in CH_2Cl_2/CH_3CN (3:1) showed the presence of a peak corresponding to the 1:1:1(Cl)$^+$-complex as well as peaks belonging to the 1:0:1(Cl)+CH_3CN^- and the 2:0:3(Cl)$^+$-complexes (Figure 6.17). Again, only fragments with Cl^- were obtained.

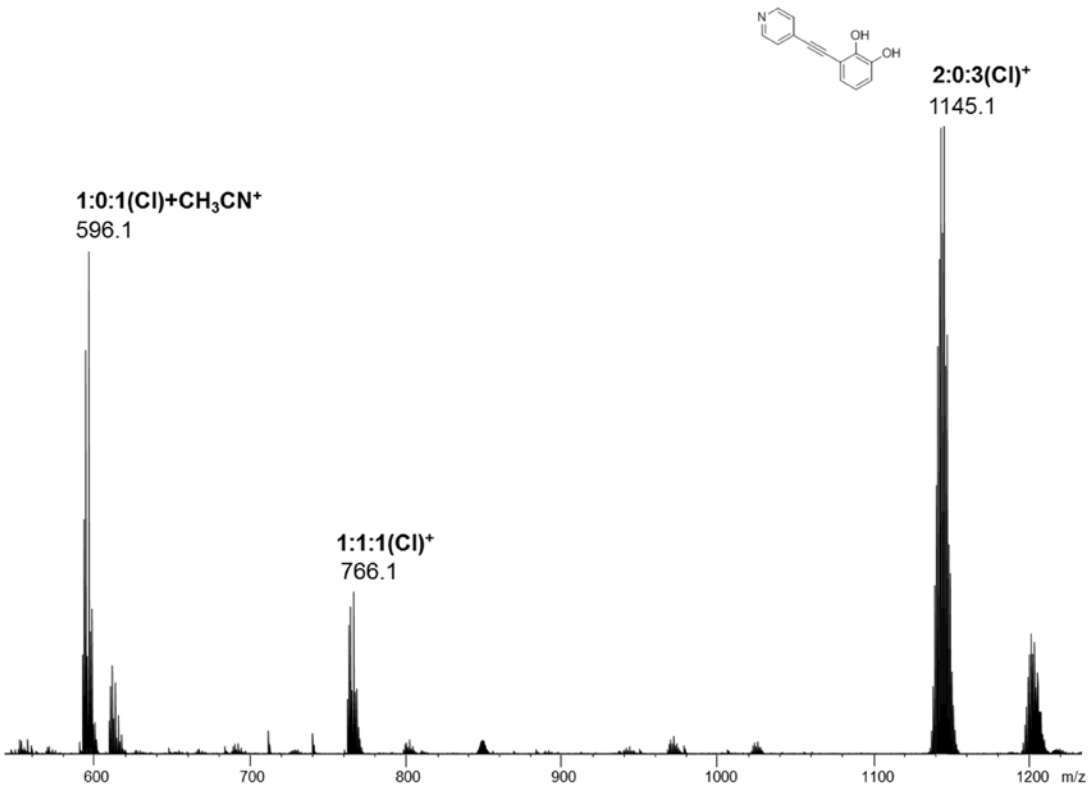

*Figure 6.17 ESI mass spectrum (positive mode) of ligand **39** with Pd(dppp)(OTf)$_2$ in CH_2Cl_2/CH_3CN (3:1) after 3h at 60°. The notation corresponds to Metal:Ligand:Cation.*

Using Pt(dppp)(OTf)$_2$ on the other hand resulted in well resolved ^{1}H-NMR-spectra, but the number of signals demonstrated that several species containing ligand **39** had been formed in both solvents. The ^{1}H-NMR-spectrum of the complexation in CD_2Cl_2/CD_3CN (3:1) is shown in Figure 6.18. Stirring at room temperature yielded a spectrum showing more than one species and it was hoped that heating could help overcome kinetic barriers to produce the desired Pt(dppp)(**39**)$_2^{2-}$-complex. Instead, more peaks appeared, suggesting that adding more kinetic energy to the complexation process brings about undesired coordination events (Figure 6.18b and c).

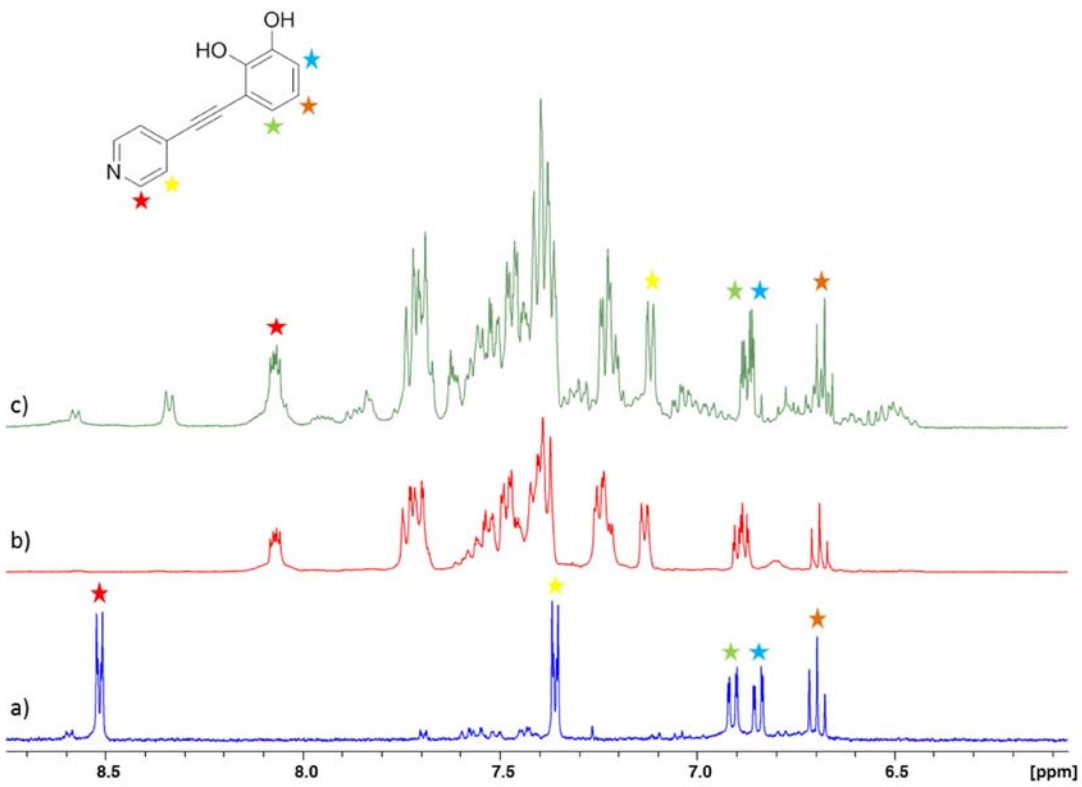

*Figure 6.18 ^{1}H-NMR-spectra of a) ligand **39** b) ligand **39** with Pt(dppp)(OTf)$_2$ after 3 days at RT c) ligand **39** with Pt(dppp)(OTf)$_2$ after 3h at 60°C all in CD_2Cl_2/CD_3CN (3:1)*

The ESI mass spectrum (positive mode) of the solution was recorded and the resultant spectrum is shown in Figure 6.19. Here, only the peak at 853.2 m/z can be identified, which contains ligand **39**. In addition, the peaks at 1231.1, 1379.2, 1495.3, 1531.3 and 2174.4 m/z were not identified as well as many smaller peaks. All of the peaks mentioned above are singly charged and contain more than one Pt-ion according to the isotope pattern. Nevertheless, none of them belong to the expected Pt(dppp)(**39**)$_2^{2-}$-complex or its fragments. Again, we only see Cl^- as the anion, where we would have expected OTf^- to be the dominant anion.

In addition, the complexation of Pt(dppp)(OTf)$_2$ with ligand **39** in CD_2Cl_2/CD_3CN (3:1) was performed again but was only stirred at room temperature. This could help investigate the complex solution of the ^{1}H-NMR-spectrum in Figure 6.18b. However, the ESI mass spectrum (positive) did not show any identifiable peaks (spectrum not shown).

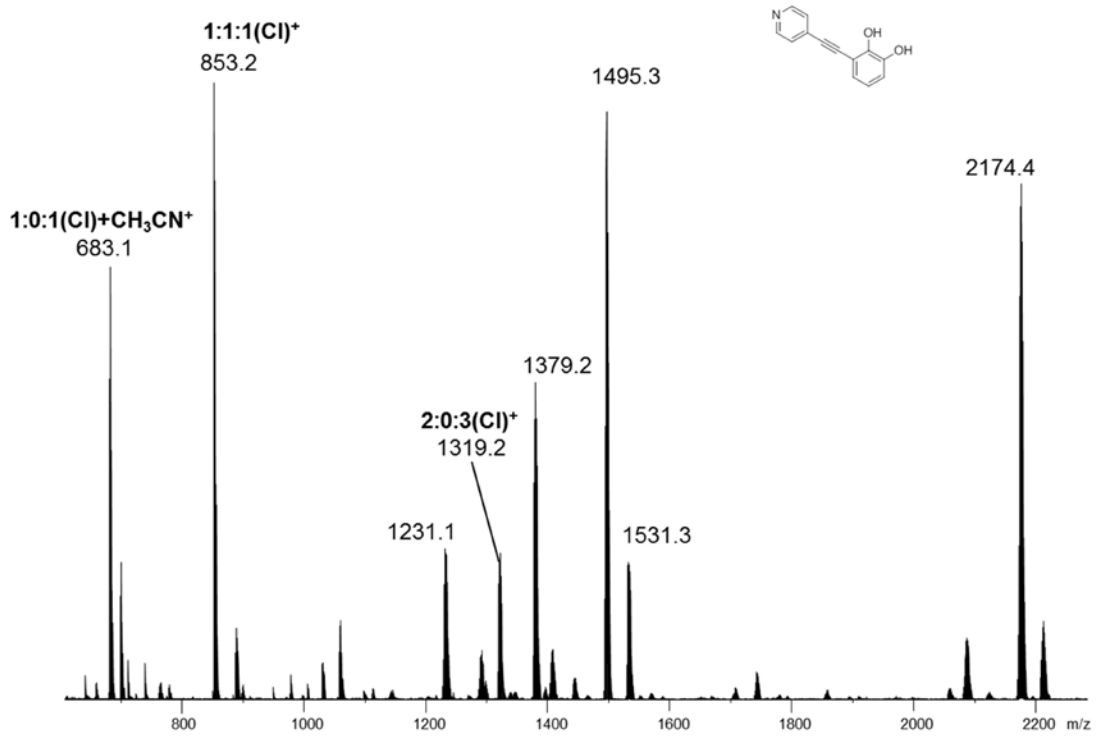

*Figure 6.19 ESI mass spectrum (positive mode) of ligand **39** with Pt(dppp)(OTf)$_2$ after 3h at 60°C in CD_2Cl_2/CD_3CN (3:1). The notation corresponds to Metal:Ligand:Cation.*

In acetone-d_6, without heating, a similar result as in CD_2Cl_2/CD_3CN (3:1) was obtained in the ^{1}H-NMR-spectrum (Figure 6.20). The mass spectrum of the acetone solution also showed the three peaks corresponding to the 1:1:1(Cl)$^+$-, 1:0:1+CH_3CN^- and the 2:0:3(Cl)$^+$-complexes as seen previously (spectrum not shown). This does not correspond well with the ^{1}H-NMR-spectra, from which we would expect several species containing the ligand **39**.

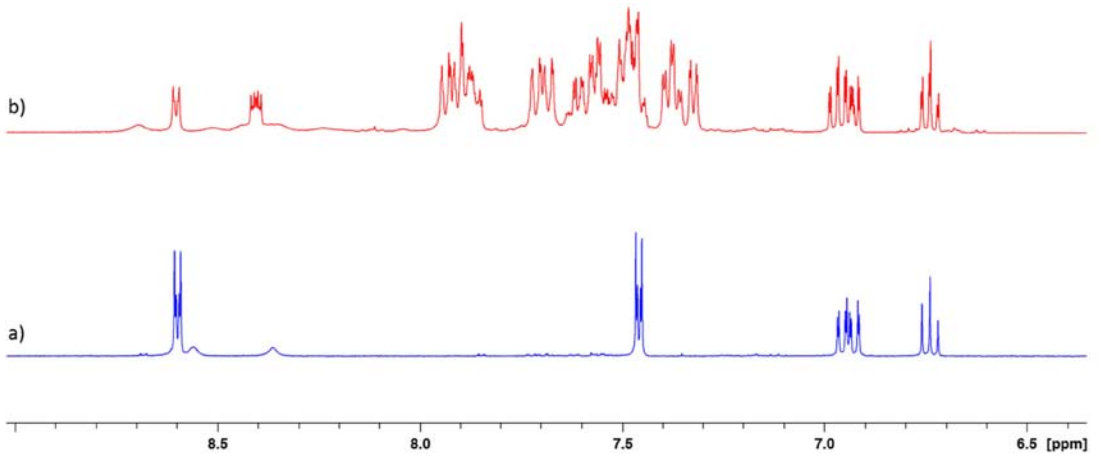

*Figure 6.20 ^{1}H-NMR-spectra of a) ligand **39** b) ligand **39** with Pt(dppp)(OTf)$_2$ after 3 days at RT both in acetone-d_6.*

It was possible to confirm the formation of the monosubstituted Pt(dppp)(**39**)- and Pd(dppp)(**39**)-complex in the mass spectra in acetone and CH_2Cl_2/CH_3CN (3:1), and the

Pt(dppp)(**39**)-complex in DMF. However, the ^{1}H-NMR-spectra suggest that more than one species containing ligand **39** is present, so the question remains why we do not see these in the mass spectra. An answer to that could be the unidentified peaks at 1495.3, 1379.1 and 700.1 m/z (Figure 6.16) which display the isotope pattern of the Pt-ion. It is possible that the desired complex [Pt(dppp)(**39**)$_2$]$^{2-}$ fragments during the measurements.

6.4 Conclusion

The two ligands **28** and **39** have been synthesized and used in complexation experiments towards forming a multicomponent supramolecular system.

The first step in the complexation of **28** resulting in [Pt(dppp)(**28**)$_2$] has been performed and the product has been characterized by ^{1}H-NMR- and mass spectrometry.

Ligand **39** has been complexated with Pd(dppp)(OTf)$_2$ and Pt(dppp)(OTf)$_2$ resulting in the monosubstituted [Pd(dppp)(**39**)]$^{2-}$ and [Pt(dppp)(**39**)]$^{2-}$ respectively. The desired complex [Pd(dppp)(**39**)] was not obtained. Testing other solvents such as THF-d_8 or CD_3CN could help obtain the desired complex, which then could be complexes with Ti(IV).

The ability of ligand **39** to bind to Ti(IV) has been successfully tested in this thesis, and we are therefore expect to obtain a supramolecular self-assembled multicomponent trigonal bipyramid in the near future.

7 Outlook

The 2:3-helix with thiophene ligand **10** and $Fe(BF_4)_2 \bullet 6H_2O$ was not able to undergo spin crossover. In order to form a complex able to undergo spin transition, other ligands based on bipyridine with 2,4- and 2,5-thiazole as the core could be tested. Also, modification of ligand **10** with hexyloxygroups which increase the solubility could help solubilize the complex in CH_2Cl_2/DMSO. Moreover, changing the angle in ligand **10** by using 2,4-thiophene as the core could change the coordination geometry in the complex with Fe(II) and possibly lead to a high spin complex. Investigation of the spin-transition abilities of these ligands is a promising approach to obtain a supramolecular spin-crossover metal-complex.

We have confirmed that racemic spirobifluorene ligand **12** has a preference towards formation of heterochiral supramolecular rhombs in CD_3Cl/CD_3CN (3:1), and the next step would be to investigate self-sorting effects in different solvents such as acetone, DMF and CH_3CN using the pseudo-enantiomer ligand **21**.

The catenane from spirobifluorene ligand (*R*)-**15** has been confirmed by crystal structure. Since the crystal was obtained from the enantiomerically pure ligand it is not possible to determine if any self-sorting is working on the formation of the catenane. The use of the pseudo-enantiomer (*S*)-**20** was not able to resolve this, because ligand **20** is not able to form a catenane. Instead, the complexation could be carried out with *rac*-**15** and subsequently crystallized. Considering that we already know how to crystallize (*R*)-**15**, this approach is very promising.

Further investigation of the selectivity of the ligands (*R*)-**15** and (*S*)-**20** in different solvents could possibly result in the discovery of solvent dependency. The production of crystals and the resulting structures are essential for the characterization of the complexes.

The larger M_2L_4- and M_6L_{12}-aggregates formed from ligand (*R*)-**22** and (*R*)-**12** respectively need to be characterized further. New ^{1}H-NMR-spectra of the M_2L_4-cage should be recorded at higher concentrations along with ^{1}H-DOSY-spectra to assess the size of the formed aggregate and fully confirm its formation. Further investigation of the assumed M_6L_{12}-sphere should be made, to assess the identity of the formed species. In both cases getting a crystal structure would be of great importance to the identification of the complexes.

The aspect of multicomponent self-assembly should be approached, starting with the synthesis of [Pt(dppp)(**28**)$_2$]. The work-up has to be optimized in order to gain enough starting

material for the following deprotection. Also, different deprotection methods should be tested, since the use of $ZrCl_4$ in isopropanol did not result in the desired deprotected product. When deprotection has been achieved, the complexation with Ti(IV) can be performed resulting in a supramolecular heterometallic trigonal pipyramid.

The complex $[Ti(\mathbf{39})_3]^{2-}$ was obtained, however, changing the spraying solvent could help gain better mass spectra. Complexation of ligand **39** with the Pd- and Pt-corner resulted in $[M(dppp)(\mathbf{39})Cl]^-$- complexes (M = Pt(II) of Pd(II)) exclusively. Complexations in other solvents are to be made in order to obtain the desired complex.

These additional experiments could contribute with valuable information about the rules that govern the self-sorting of chiral ligands. Obtaining the trigonal bipyramid using ligands **28** and **39** paves the way to performing multicomponent self-assembly with chiral ligands and investigate self-sorting with more than two components present. Modifying ligand **10** could help produce a self-assembled supramolecular complex able to undergo spin crossover further elucidating how distortion of the ligand field of Fe(II) affects its electronic properties. Ultimately, supramolecular spin crossover-complexes could be used as switches in computing and memory storage.

8 Conclusion

During this thesis self-assembly and self-sorting of metallo-supramolecular aggregates have been investigated starting with small M_2L_2-rhombs based on spirobifluorene. To this end both the racemic and the enantiomerically pure ligand **12** with pyridine as the recognition unit was synthesized. Ligand **12** was used in complexation studies with Pt(dppp)$(OTf)_2$ and Pd(dppp)$(OTf)_2$ in CD_3Cl/CD_3CN (3:1) and the formation of the rhombs was confirmed by ^{1}H-NMR- and mass spectroscopy. It was confirmed by NMR- and mass spectroscopy (using pseudoenantiomer ligand **21**) that ligand **12** self-assembles preferably in a narcissistic way. Furthermore, a crystal structure of the homochiral rhomb was obtained from the racemic complex mixture confirming the tendency for ligand **12** towards self-recognition.

A M_2L_2-rhomb with a larger internal cavity was formed using the Pd- or Pt-corners together with spirobifluorene ligand **15**, which has a ethynyl-spacer between the spirobifluorene and the pyridine. Ligand **15** was synthesized both racemically and in its enantiomerically pure (*R*)-form. The spectra of the complexes in CD_3Cl/CD_3CN (3:1) indicated the formation of a 4:4-catenane in addition to the expected 2:2-rhomb. The formation of the catenane was confirmed by a crystal structure of the catenane from ligand (*R*)-**15**. To investigate the selectivity of ligand (*R*)-**15** the pseudo-enantiomer (*S*)-**20** was synthesized and complexations of each of the ligands and the mixed ligand were performed in different solvents. It was found that the elongation of the linker resulted in loss of selectivity during self-assembly of the rhomb.

Furthermore, the complexations of both ligand **12** and **15** was studied in several other solvents and further experiments could determine if the self-sorting behavior of the spirobifluorene ligands is solvent dependent.

In order to form a self-assembled multicomponent system with two different metal centers ligand **28** with an ethynyl- and a MOM-protected catechol-group and ligand **39** with a pyridine- and a catechol-group were synthesized. Ligand **28** was mixed with Pt(dppp)$(OTf)_2$ resulting in a well-defined tweezer-like structure. Deprotection of the MOM-groups was attempted with the Lewis acid $ZrCl_4$ without success, however it is expected, that testing of other deprotection methods will result in the desired product. Ligand **39** was first complexated with Ti(IV) resulting in *fac*- and *mer*-isomers of Ti(**39**)$_3$. The *mer*-isomer is the thermodynamically stable isomer, making the following complexation with Pd(II) or Pt(II) difficult. Instead, ligand **39** was complexated with Pd(II) and Pt(II) in different solvents and the respective [M(dppp)(**39**)Cl]$^-$-complexes (M = Pt(II) of Pd(II)) were obtained.

In order to form a self-assembled supramolecular complex able to undergo spin crossover with Fe(II), ligand **10** was synthesized starting from 2,5-diiodothiophene. In spite of the problems with the solubility of the ligand, it was possible to form a triple helix with Fe(II) in CH_2Cl_2/CH_3CN (3:1). The formation of the complex was confirmed by ^{1}H-NMR-spectroscopy as well as by mass spectrometry. Testing of the complex abilities to undergo spin transition turned out with negative results. However, first steps towards modification of the ligand, changing the angle between the metal binding pyridines, have been made and future complexation experiments will determine their potential in spin crossover.

All in all, seven different ligands belonging to three different ligand systems were synthesized in this thesis. Several complexation experiments on the ligand systems have been performed on the ligand systems while varying the solvents and the metal-centers and have given us valuable knowledge about metallosupramolecular self-assembly. Self-sorting effects have been investigated thoroughly, steps have been made towards the formation of a heterometallic aggregate via multicomponent self-assembly and a first complex of a potential system for spin crossover has been made. In the future, additional experiments will add to the information already obtained in this thesis, and help complete the picture of self-assembly in supramolecular chemist.

9 Experimentals

NMR-Spectroscopy:

^{1}H – and ^{13}C-NMR-spectra were recorded on either an *Avance 300* (^{1}H: 300.1 MHz, ^{13}C: 125.5 MHz), an *AM 400* (^{1}H: 400.1 MHz, ^{13}C: 100.6 MHz) or a *DMX 500* (^{1}H: 500.1 MHz, ^{13}C: 125.8 MHz) by *Bruker*. Chemical shifts (δ) are given relative to the ^{1}H-signals of undeuterated solvents or the ^{13}C-signals of the undeuterated solvent as internal standards respectively. The coupling constants (J) are given in Hz. Assignment of the ^{1}H – and ^{13}C-NMR-spectra are based on H,H-COSY, C,H-correlated HMQC-spectra and HMBC-spectra.

The evaluation of the spectra was performed using either *Top Spin 3.0* by *Bruker* or *Spin Works*.

Mass-Spectroscopy:

The EI-mass spectra were recorded on a *MAT 95 XL* or a *MAT 90* spectrometer by *Thermo Finnigan*. The ESI-mass spectra were recorded either on a *micrOTOF-Q*-spectrometer or an *Apex IV FT-ICR*-spectrometer both by *Bruker*.

Angle of rotation:

The specific optical rotation was recorded on a *Jasco P-1020* Polarimeter using a 10 cm cuvette from *Jasco*.

CHN-analysis:

The CHN-analysis was performed on a *Vario EL* by *Hereaus*.

Thin Layer Chromatography:

The reactions were monitored using TLC by *Merck* silica gel plates or Aluminum oxide plates.

Column Chromatography:

Column chromatography was performed by hand using silica gel 60 (0.040-0.063 mm) by *Merck* or ALOX neutral 60A (50-200 μm) by *Acros*.

Syntheses with water or air sensitive substances were performed under argon applying the *Schlenck technique* using dry solvents. The solvents were dried and distilled using standard methods and stored under dry argon in an airtight *Schlenck* flask.

THF, acetonitrile, diisopropylamine, dichloromethane, diethyl ether and toluene were dried according to standard methods.[106] Dry DMF and dry isopropanol were purchased at *Acros* or *Sigma Aldrich*. The solvents used for chromatography (except methanol and ethanol) were all distilled before use.

The following substances, whose synthesis are not described but are mentioned in the thesis, were purchased at one of the following companies *Alfa Aesar*, *ABCR*, *Sigma Aldrich*, *Merck* or *TCI Europe*:

CPDIPS-Cl, ethynyl magnesiumbromide, 4-pyridineboronic acid pinacol ester, 3-pyridineboronic acid pinacol ester, K_3PO_4, 4-brompyridine hydrochloride, *n*-BuLi, $B(OMe)_3$, TMS-acetylene, TIPS-acetylene CuI, Na_2SO_4, $MgSO_4$, $NaHCO_3$, 1,4-diiodobenzene, 1-bromo-4-iodobenzene, 2,5-Diiodothiophene, Tetra-*n*-butylammonium fluoride (TBAF), PPh_3, KF, $ZrCl_4$.

Following substances were available in the laboratory of Prof. Dr. Lützen:

$[Pd(dppp)Cl_2]$, $[Pd(dppf)Cl_2]$, $[PdCl_2(PPh_3)_2]$, $[Pd_2(dba)_2]\cdot CHCl_3$, $[Pd(PPh_3)_4]$, dppf.

9.1 Synthesis

The following molecules were synthesized according to protocols known from the literature:

Ditriflate(1,3-bis(diphenylphosphino)propane)palladium[44], Dichloro(1,3-bis (diphenylphosphino)propane)platinum[44], bis(triphenylphosphine)palladium(II)dichloride[44] and ((3-cyanopropyl)dimethylsilyl)acetylene[102].

9.1.1 Ligands for spin crossover

The following molecules were synthesized according to protocols known from the literature:

2-bromothiazole (**1**)[36,107], 2,5-dibromo-1,3-thiazole (**2**)[36,108], 2-iodothiazole (**3**)[36,109], 2,4-dibromo-1,3-thiazole (**4**)[36,108], 4-iodo-2-aminopyridine (**5**)[37–39], 2-bromo-4-iodopyridine (**6**)[37–39], 2-brom-4-(trimethylsilylethynyl)pyridine (**7**)[34], 5-carboxymethyl-5'-[(trimethylsilyl)ethynyl]-2,2'-bipyridine (**8**)[34], 5-carboxymethyl-5'-ethynyl-2,2'-bipyridine (**9**)[34],

Synthesis of 2,5-bis(5-ethynyl-5'-carboxymethyl-2,2'-bipyridyl)-thiophene (10)

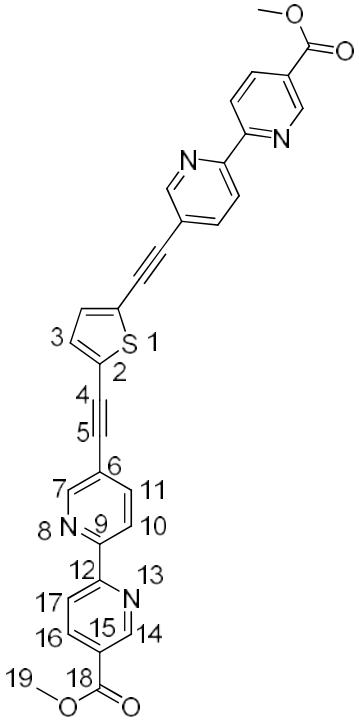

2,5-Diiodothiophene (64 mg, 0.191 mmol), **9** (82 mg, 0.366 mmol), CuI (5 mg, 0.026 mmol), and $Pd(PPh_3)_4$ (9 mg, 0.008 mg) were added to a dry *Schlenck* flask and the flask was evacuated. Next, dry THF (10 mL) and dry Et_3N (12 mL) was added and the reaction was heated to 35°C for 120 h.

The solution was cooled to room temperature and the resulting yellow precipitate was filtered off and washed with CH_2Cl_2. The crude product was purified by refluxing it in THF and filtering it off while warm resulting in a yellow solid.

Yield: 68 mg (67%)

^{1}H-NMR (400 MHz, CF_3COOD): δ 9.68-9.67 (m, 1 H, H-14), 9.17-9.15 (m, 2 H, H17 and H-7), 8.75-8,69 (m, 3 H, H-10 and H-11 and H-16), 7.59 (s, 1 H, H-3), 4.53 (s, 3H, H-19)*

*Assignment not unambiguous

Due to low solubility it was not possible to obtain a ^{13}C-NMR-spectrum.

EI-MS: m/z (556.1 $[M]^{+\bullet}$)

9.1.2 Spirobifluorene ligands

The following molecules were synthesized according to protocols known from the literature:

(*R*)-bis(trifluoromethylsulfoxyl)-9,9'-spirobifluorene ((*R*)-**11**)[59], (*S*)-bis (trifluoromethylsulfoxyl)-9,9'-spirobifluorene ((*S*)-**11**)[59], (*R*)-2,2'-bis(trimethylsilylethynyl)-9,9'-spirobifluoren (*R*)-**13**[59], *rac*-2,2'-diethynyl-9,9'-spirobifluoren (*rac*-**14**)[59], (*R*)-2,2'-diethynyl-9,9'-spirobifluoren ((*R*)-**14**)[59], *rac*-2,2'-dimethyl-9,9'-spirobifluorene (*rac*-**16**)[59], (*R*)-2,2'-dimethyl-9,9'-spirobifluoren ((*R*)-**16**)[59], (*S*)-2,2'-dimethyl-9,9'-spirobifluoren ((*S*)-**16**)[59], (*R*)-2,2'-dibromo-7,7'-dimethyl-9,9'-spirobifluorene ((*R*)-**17**)[59], (*S*)-2,2'-dibromo-7,7'-dimethyl-9,9'-spirobifluorene ((*S*)-**17**)[59].

Crystal structures were obtained of spirobifluorenes (*R*)-**11** from *rac*-**11** and (*S*)-**14** from *rac*-**14**.

Crystal data for (*R*)-**11**:

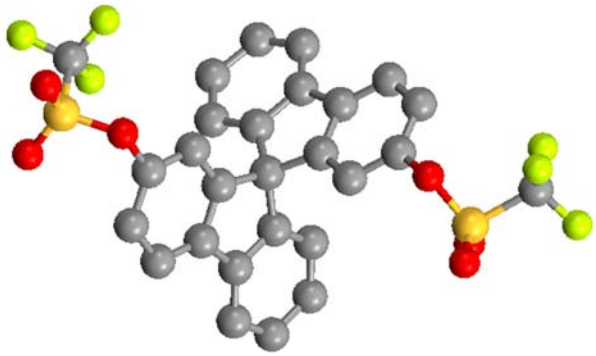

Empirical formula:	$C_{27}H_{14}F_6O_6S_2$	
Molecular weight:	612.50 g/mol	
Space group:	Monoclinic, P 21/c	
Unit cell dimensions:	a = 9.2475(2) Å	α = 90 deg.
	b = 22.9592(7) Å	β = 113.555(2) deg.
	c = 13.1192(4) Å	γ = 90 deg.
Volume:	2553.32(13) $Å^3$	
Absorption coefficient:	0.296 mm^{-1}	

F(000):	1240
Crystal Size:	0.18 x 0.08 x 0.06 mm
Θ-range for data collection:	1.91 to 28.00 deg.
Limiting Indices:	-12<=h<=12, -30<=k<=30, -17<=l<=17
Reflexions collected:	43760
Unique reflexions:	6149 [R(int) = 0.0790]
Completeness to theta:	28.00 99.9 %
Absorption correction:	Semi-empirical
Max. and min. Transmission:	0.9825 and 0.9487
Refinement method:	Full-matrix least-squares on F^2
Data/Restraints/Parameters:	6149 / 1 / 370
Goodness-of-fit on F^2:	0.898
Final R indices [I>2sigma(I)]:	R1 = 0.0385, wR2 = 0.0815
R indices (all data):	R1 = 0.0855, wR2 = 0.0940
Largest diff. peak and hole:	0.266 and -0.421 e×A^{-3}

Crystal data for (*S*)-**14**:

Empirical formula:	$C_{29}H_{16}$
Molecular weight:	364.42 g/mol
Space group:	Orthorhombic, Pbna
Unit cell dimensions:	a = 7.9400(3) Å α = 90 deg.
	b = 15.5848(4) Å β = 90 deg.
	c = 15.8501(6) Å γ = 90 deg.
Volume:	1961.34(12) $Å^3$
Absorption coefficient:	0.070 mm^{-1}
F(000):	760
Crystal Size:	0.38 x 0.26 x 0.20 mm
Θ-range for data collection:	2.57 to 28.00 deg.
Limiting Indices:	-10<=h<=10, -18<=k<=20, -20<=l<=20
Reflexions collected:	27874
Unique reflexions:	2374 [R(int) = 0.0758]
Completeness to theta:	28.00 100.0 %
Absorption correction:	Semi-empirical

Max. and min. Transmission: 0.9861 and 0.9739

Refinement method: Full-matrix least-squares on F^2

Data/Restraints/Parameters: 2374 / 0 / 132

Goodness-of-fit on F^2: 1.011

Final R indices [I>2sigma(I)]: R1 = 0.0455, wR2 = 0.1125

R indices (all data): R1 = 0.0715, wR2 = 0.1228

Largest diff. peak and hole: 0.154 and -0.235 eA^{-3}

Synthesis of substances known from the literature:

Synthesis of (*R*)- or (*S*)-2,2'-Bis(trimethylsilylethynyl)-7,7'-dimethyl-9,9'-spirobifluorene (18)[59]

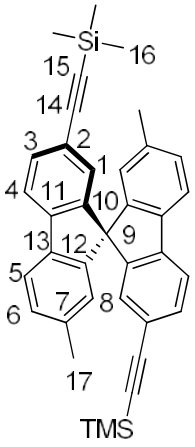

TMS-acetylene (1.9 mL, 13.7 mmol) was mixed with dry THF (29 mL) and cooled to -78°C. A solution of *n*-BuLi (8.5 mL, 1.6 M in *n*-Hexane) in dry THF (20 mL) was added dropwise. Subsequently $B(OMe)_3$ (1.54 mL, 2.3 mmol) was dissolved in dry THF (4.75 mL) and added drop wise to the TMS-acetylene solution. The reaction was stirred at room temperature. Next **(*R*)-** or **(*S*)-17** (257 mg, 0.512 mmol) and $[Pd(PPh_3)_4]$ (59 mg, 0.051 mmol) were dissolved in dry toluene (25 mL) and 10.25 mL of the TMS-acetylene solution was added. Subsequently an aqueous solution of Na_2CO_3 (2 M, 1.7 mL) was added to the reaction which was the heated to 110°C and stirred for 48 h after which TMS-acetylene solution (13.5 mL, 2.8 mmol) was added. The reaction was stirred for 72 h after which TMS-acetylene solution (10 mL, 2,1 mmol) was again added. The reaction was stirred for 24 h.

When finished, the reaction was cooled to room temperature and the organic phase was washed twice with H_2O and once with brine. Subsequently, the organic phase was dried over $MgSO_4$. The solvents were removed *in vacuo*. The crude product was purified by repeated column chromatography on silica gel, first with *n*-hexane/ethylacetate (5:1) as the eluent, secondly with (cyclohexane → (cyclohexane/CH_2Cl_2 (1:1) as the eluent affording the title product as a yellow oil.

Yield:

(*R*): 92 mg (34%)

(*S*): 192 mg (71%)

R_f: 0.63 (*n*-hexane/ethylacetate (5:1))

^{1}H-NMR (400 MHz, $CDCl_3$): δ 7.72-7.68 (m, 2 H, H-4 and H-6), 7.47 (dd, 1 H, $J_{3,4}$ = 7.9 Hz, $J_{3,1}$ = 1.4 Hz, H-3), 7.18 (d, 1 H, $J_{5,6}$ = 7.7 Hz, H-5), 6.79 (d, 1 H, $J_{1,3}$ = 1.4 Hz, H-1), 6.50 (s, 1 H, H-8), 2.20 (s, 3 H, H-17), 0.15 (s, 9 H, H-16)

EI-MS: m/z (536.2 [$M^{+\bullet}$])

Synthesis of (*R*)- or (*S*)-2,2'-diethynyl-7,7'-dimethyl-9,9'-spirobifluorene ((*R*)-19)[59]

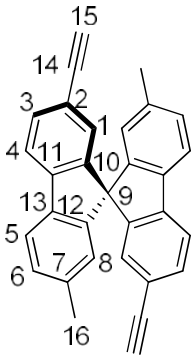

(*R*)- or **(*S*)-18** (92 mg, 0.171 mmol) was dissolved in THF and methanol (1:1, 20 mL) and K_2CO_3 (230 mg, 1.6 mmol) was added. The reaction was stirred at room temperature for 2 h. When finished the reaction was poured onto CH_2Cl_2 (90 mL) and the organic phase was washed twice with H_2O and subsequently dried over Na_2SO_4. The solvents were removed *in vacuo*.

The crude product was purified by column chromatography on silica gel using *n*-hexane/ethylacetate (5:1) as the eluent affording the title product as a yellow solid.

Yield:

(*R*): 30 mg (45%)

(*S*): 25 mg (38%)

R_f: 0.42 (*n*-hexane/ethylacetate (5:1))

^{1}H-NMR (400 MHz, $CDCl_3$): δ 7.73-7.69 (m, 2 H, H-6 and H-4), 7.51 (dd, 1 H, $J_{3,4}$ = 7.9 Hz, $J_{3,1}$ = 1.4 Hz, H-3), 7.20 (d, 1 H, $J_{5,6}$ = 7.8 Hz, H-5), 6.83 (s, 1 H, H-1), 6.54 (s, 1 H, H-8), 2.97 (s, 1 H, H-15), 2.22 (s, 3 H, H-16)

^{13}C-NMR (101 MHz, $CDCl_3$): δ 148.8 (C-12), 128.3 (C-10), 142.4 (C-11), 138.6 (C-13), 138.2 (C-7), 132.0 (C-3), 128.9 (C-5), 127.7 (C-1), 124.7 (C-8), 120.5 (C-2), 120.1 (C-4), 119.5 (C-6), 83.9 (C-14), 77.1 (C-15), 65.2 (C-9), 21.5 (C-16)

Synthesis of the spirobifluorene ligands:

Synthesis of *rac*- or (*R*)-2,2'-di-4-pyridyl-9,9'-spirobifluorene (12)

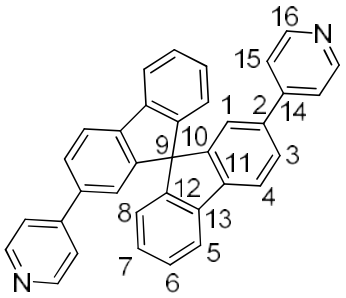

***Rac*- or (*R*)-11** (151 mg, 0.246 mmol), 4-pyridineboronic acid pinacol ester (145 mg, 0.707 mmol), K_3PO_4 (224 mg, 1.041 mmol) and [Pd(dppf)Cl_2] (12 mg, 0.0147 mmol) were added to a flame dried round bottomed flask, which was subsequently evacuated. Dry THF (5 mL) was added and the reaction was heated to 65°C for 24 h. After the reaction was cooled to RT the solvent was removed *in vacuo* and the residue was taken up in CH_2Cl_2 and H_2O and the phases were separated. The aqueous phase was extracted with CH_2Cl_2 and the collected organic phases were washed with H_2O and brine and subsequently dried over $MgSO_4$. The solvent was removed *in vacuo*.

The crude product was purified by column chromatography on silica gel using methanol/ethylacetate (1:1) as the eluent. After purification all fractions were dried, dissolved in CH_2Cl_2, and filtered affording the title product as a light brown oil.

Yield:

(*R*): 116 mg (100%)
rac: 116 mg (100%)

R_f: 0.79 (methanol/ethylacetate (1:1))

^{1}H-NMR (400 MHz, $CDCl_3$): δ 8.51 (dd, 4 H, $J_{16,15A}$ = 4.6 Hz, $J_{16,15B}$ = 1.6 Hz, H-16), 7.97 (d, 2 H, $J_{4,3}$ = 7.9 Hz, H-4), 7.91 (d, 2 H, $J_{5,6}$ = 7.6 Hz, H-5), 7.69 (dd, 2 H, $J_{3,4}$ = 7.9 Hz, $J_{3,1}$ = 1.6 Hz, H-3), 7.42 (ddd, 2 H, $J_{6,5}$ = 7.6 Hz, $J_{6,7}$ = 7.5 Hz, $J_{6,8}$ = 1 Hz, H-6), 7.33 (dd, 4 H, $J_{15,16A}$ = 4.6 Hz, $J_{15,16B}$ = 1.6 Hz, H-15), 7.16 (ddd, 2 H, $J_{7,6}$ = 7.5 Hz, $J_{7,8}$ = 7.6 Hz, $J_{7,5}$ = 1 Hz, H-7), 7.02 (d, 2 H, $J_{1,3}$ = 1.6 Hz, H-1), 6.78 (d, 2 H, $J_{8,7}$ = 7.6 Hz, H-8)

^{13}C-NMR (100 MHz, $CDCl_3$): δ 150.0 (C-16), 149.4 (C-10), 148.8 (C-12), 147.8 (C-14), 142.8 (C-11), 140.8 (C-13), 137.7 (C-2), 128.5 (C-7), 128.1 (C-6), 127.0 (C-3), 124.1 (C-8), 122.4 (C-1), 121.5 (C-15), 120.7 (C-4), 120.4 (C-5), 66.0 (C-9)

ESI-MS(+): m/z (471.2 $[M+H]^+$)

HR-ESI: Calculated for $C_{35}H_{22}N_2$: 471.1861

Found: 471.1856

CHN-analysis: $C_{35}H_{22}N_2 \cdot 1$Methanol$\cdot 2/3$Cyclohexane

Calculated [%]: C 85.74; H 5.33; N 5.36

Measured [%]: C 85.99; H 6.13; N 5.01

Specific rotation: R_a: $[\alpha]_D^{20} = +213$ ° mL dm^{-1} g^{-1} (c = 0.56; THF)

Synthesis of *rac*- or (*R*)-2,2'-bis(4-ethindiylpyridyl)-9,9'-spirobifluorene ((*rac*)-15)

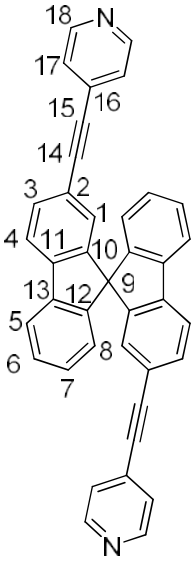

***Rac*-** or **(*R*)-14** (96 mg, 0.26 mmol), $[Pd_2(dba)_2]\cdot CHCl_3$ (11 mg, 0.010 mmol), dppf (9 mg, 0.16 mmol), and CuI (4 mg, 0.02 mmol) were added to a round bottomed flask, which was subsequently evacuated. Next, 4-brompyridine hydrochloride (205 mg, 1.05 mmol) was added and the flask was shaded from light. Dry THF (7 mL) and dry diiso-propylamine (1.2 mL) were added and the reaction was heated to 60°C overnight.

The reaction was cooled to room temperature and the reaction mixture was quenched with brine and was subsequently filtered. The filter was rinsed with CH_2Cl_2. The phases were separated and the aqueous phase was extracted thoroughly with CH_2Cl_2. The collected organic phases were washed with saturated aqueous $NaHCO_3$ and dried over Na_2SO_4. The solvents were removed *in vacuo*.

The crude product was purified by column chromatography on silica gel using cyclohex-ane/ethylaceate (1:1) + 0.5% Et_3N → ethylacetate + 0.5% Et_3N as the eluent, affording the title product as a yellow foam.

Yield:

Rac: 129 mg (54%)
(*R*): 105 mg (44%)

R_f: 0.66 (ethylacetate)

^{1}H-NMR (400 MHz, $CDCl_3$): δ 8.52 (dd, 2 H, $J_{18,17}$ = 4.6 Hz, $J_{18,18'}$ = 1.6 Hz, H-18), 7.87 (2d, 2 H, $J_{4,3}$ = 7.9 Hz, $J_{5,6}$ = 7.7 Hz, H-4 and H-5), 7.58 (dd, 1 H, $J_{3,4}$ = 7.9 Hz, $J_{3,1}$ = 1.2 Hz, H-3), 7.41 (ddd, 1 H, $J_{6,5}$ = 7.6 Hz, $J_{6,7}$ = 7.6 Hz, $J_{6,8}$ = 0.9 Hz, H-6), 7.24 (dd, 2 H, $J_{17,18}$ = 4.6 Hz, $J_{17,17'}$ = 1.6 Hz, H-17), 7.17 (ddd, 1 H, $J_{7,8}$ = 7.6 Hz, $J_{7,6}$ = 7.6 Hz, $J_{7,5}$ = 0.9 Hz, H-7), 6.94 (d, 1 H, $J_{1,3}$ = 1.2 Hz, H-1), 6.76 (d, 1 H, $J_{8,7}$ = 7.6 Hz, H-8).

^{13}C-NMR (101 MHz, $CDCl_3$): δ 149.6 (C-18), 148.4 (C-10 or C-12), 148.3 (C-10 or C-12), 142.8 (C-19), 140.8 (C-13), 131.9 (C-3), 131.2 (C-16), 128.7 (C-7), 128.2 (C-6), 127.4 (C-1), 125.3 (C-17), 124.4 (C-8), 121.2 (C-2), 120.5 (C-5), 120.2 (C-4), 94.2 (C-14), 87.1 (C-15), 65.6 (C-9).

ESI-MS(+): m/z (519.3 $[M+H]^+$)

HR-ESI: calculated for $C_{39}H_{22}N_2$: 518.1783

Found: 518.1778

CHN-analysis: $C_{39}H_{22}N_2 \cdot 1/6$ethylacetate

Calculated [%]: C 89.34; H 4.41; N 5.25

Measured [%]: C 89.40; H 4.68; N 5.45

Specific rotation: R_a: $[\alpha]_D^{20}$ = + 621 ° • mL dm^{-1} g^{-1} (c = 0.49; THF)

Synthesis of (*R*) or (*S*)-2,2'-bis(4-ethindiylpyridyl)-7,7'-dimethyl-9,9'-spirobifluorene (20)

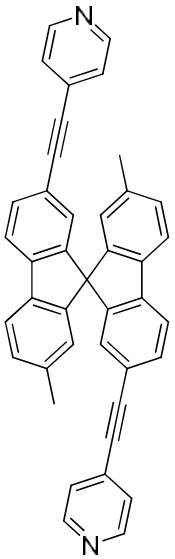

(*S*)- or **(*R*)-19** (113 mg, 0.288 mmol), 4-bromopyridine hydrochloride (344 mg, 1.770 mmol), $[Pd_2(dba)_2]\cdot CHCl_3$ (16 mg, 0.015 mmol), dppf, (20 mg, 0.036 mmol), and CuI (8 mg, 0.042 mmol) were added to a round bottomed flask and dissolved in dry THF (8 mL) and dry diisopropylamine (1.2 mL). The reaction was heated to 60°C over night and shielded from light. When finished the reaction was quenched with brine and CH_2Cl_2. The phases were separated and the aqueous phase was extracted thoroughly with CH_2Cl_2. The collected organic phases were washed with saturated aqueous $NaHCO_3$ and dried over Na_2SO_4. The solvents were removed *in vacuo*.

The crude product was purified by column chromatography on silica gel using *n*-hexane/ethylacetate (1:1) + 0.5% Et_3N as the eluent affording the title product as a yellow solid.

Yield:

(*S*): 69 mg (44%)

(*R*): 39 mg (25%, impure)

R_f: 0.18 (*n*-hexane/ethylacetate (1:1) + 0.5% Et_3N)

^{1}H-NMR (400 MHz, $CDCl_3$): δ 8.53 (d, 4 H, $J_{18,17}$ = 4.6 Hz, H-18), 7.82 (dd, 2 H, $J_{4,3}$ = 7.9 Hz, $J_{4,1}$ = 0.5 Hz, H-4), 7.76 (d, 2 H, $J_{6,5}$ = 7.8 Hz, H-6), 7.58 (dd, 2 H, $J_{3,4}$ = 7.9 Hz, $J_{3,1}$ = 1.5 Hz, H-3), 7.27-7.25 (m, 4 H, H-17), 7.23 (d, 2 H, $J_{5,6}$ = 7.8 Hz, H-5), 6.91 (d, 2 H, $J_{1,3}$ = 1.5 Hz, H-1), 6.65 (s, 2 H, H-8), 2.23 (s, 6 H, H-19)

^{13}C-NMR (101 MHz, $CDCl_3$): δ 149.2 (C-18), 148.8 (C-12), 148.4 (C-10), 143.0 (C-11), 139.0 (C-7), 138.1 (C-13), 131.9 (C-3), 131.7 (C-16), 129.1 (C-5), 127.4 (C-1), 125.4 (C-17), 124.7 (C-8), 120.5 (C-6), 120.3 (C-4), 119.8 (C-2), 94.8 (C-14), 86.8 (C-15), 65.2 (C-9), 21.5 (C-19)

ESI-MS(+): m/z (547.2 $[M+H]^+$)

HR-ESI: Calculated for $C_{41}H_{27}N_2$: 547.2169

Found: 547.2167

CHN-analysis: $C_{41}H_{26}N_4 \cdot 1/6$Ethylacetate$\cdot 1/6$H2O$\cdot 1/3$cyHEX$\cdot 1/3CH_2Cl_2$

Calculated [%]: C 85.14; H 5.25; N 4.51

Measured [%]: C 85.29; H 5.26; N 4.62

Specific rotation: S_a: $[\alpha]_D^{25}$ = + 505 ° • mL dm^{-1} g^{-1} (c = 0.264; CH_2Cl_2)

Synthesis of *rac*-, (*R*)- or (*S*)-2,2'-bis(3-pyridyl)-9,9'-spirobifluorene (21)

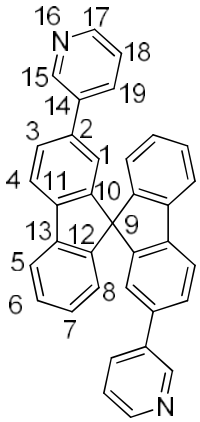

***Rac*-, (*R*)-** or **(*S*)-11** (130 mg, 0.212 mmol), 3-pyridineboronic acid pinacol ester (214 g, 1.044 mmol), K_3PO_4 (184 mg, 0.866 mol), $[PdCl_2(PPh_3)_2]$ (10 mg, 0.014 mmol), and dppf (8 mg, 0.014 mmol) were added to a round bottomed flask and evacuated twice. Next, dry THF (5 mL) was added and the reaction was heated to 65°C overnight. When finished, the reaction mixture was cooled to RT and subsequently quenched with a saturated aqueous $NaHCO_3$. The aqueous phase was extracted three times with CH_2Cl_2 and the collected organic phases were washed with H_2O and brine and dried over $MgSO_4$. The solvents were removed *in vacuo*.

The crude product was purified by column chromatography on silica gel using cyclohexane/ethylacetate (20:1)+0.5% Et_3N as the eluent, affording the title product as a brown solid.

Yield:

Rac: 63 mg (63%)

(*R*): 108 mg (70%)

(*S*): 61 mg (38%)

R_f: 0.78 (cyclohexane/ethylacetate (20:1)+0.5% Et_3N)

^{1}H-NMR (400 MHz, $CDCl_3$): δ 8.69 (br s, 2 H, H-15), 8.48 (br s, 2 H, H-17), 7.98 (d, 2 H, $J_{4,3}$ = 7.9 Hz, H-4), 7.91 (d, 2 H, $J_{5,6}$ = 7.9 Hz, H-5), 7.73 (br d, 2 H, $J_{19,18}$ = 7.8 Hz, H-19), 7.63 (dd, 2 H, $J_{3,4}$ = 7.9 Hz, $J_{3,1}$ = 1.2 Hz, H-3), 7.42 (ddd, 2 H, $J_{6,5}$ = 7.5 Hz, $J_{6,7}$ = 7.5 Hz, $J_{6,8}$ = 0.9 Hz, H-6), 7.28 (br s, 2 H, H-18), 7.16 (ddd, 2 H, $J_{7,6}$ = 7.5 Hz, $J_{7,8}$ = 7.5 Hz, $J_{7,5}$ = 0.9 Hz, H-7), 6.95 (s, 2 H, H-1), 6.79 (d, 2 H, $J_{8,7}$ = 7.5 Hz, H-8)

^{13}C-NMR (101 MHz, $CDCl_3$): δ 149.5 (C-11), 148.7 (C-13), 141.9 (C-10), 141.0 (C-12), 137.3 (C-14), 134.5 (C-19), 128.3 (C-7), 128.0 (C-6), 127.0 (C-3), 124.1 (C-8), 122.6 (C-1), 120.7 (C-4), 120.3 (C-5), 66.0 (C-9), C-15, C-17, C-18 could not be found.

EI-MS: m/z (470.2 $[M]^{+\bullet}$)

HR-EI: calculated for $C_{39}H_{21}N_2$: 469.1710

Found: 469.1704

Specific rotation: S_a: $[\alpha]_D^{25}$ = - 242 ° • mL dm^{-1} g^{-1} (c = 0.15; CH_2Cl_2)

R_a: $[\alpha]_D^{25}$ = + 233 ° • mL dm^{-1} g^{-1} (c = 0.253; CH_2Cl_2)

9.1.3 Ligands for multicomponent self-assembly

The following molecules were synthesized according to protocols known from the literature:

4-Iodopyridine (**23**) from 4-aminopyridine[99], 1,2-bis(methoxymethyl)benzene (**24**)[100], 2,3-bis(methoxymethyl)-1-iodobenzene (**25**)[100], and 4-(trimethylsilyl)ethynylpyridine (**36**)[110,111],

Synthesis of substances known from the literature:

Synthesis of 4-Iodopyridine (23) from 4-chloropyridine[98]

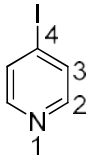

NaI was dried at 120°C under vacuum prior to the synthesis.

4-Chloropyridine·HCl (0.517 g, 3.47 mmol) and NaI (2.173 g, 14.50 mmol) were dissolved in dry CH_3CN (13 mL) and heated to 75°C, and a color change to green was observed. The reaction was stirred for 20h at 75°C. The reaction was cooled to room temperature and a solution of 10% K_2CO_2 and 5% $NaHSO_3$ in water was added. The aqueous phase was extracted with ethyl acetate and the collected organic phases were dried over $MgSO_4$.

The crude product was purified by column chromatography on silica gel using methanol/ethylacetate (1:1) as the eluent, and affording the title product as a brown solid.

Yield: 240 mg (34 %)

R_f: 0.63

^{1}H-NMR (400 MHz, $CDCl_3$): δ 8.24-8.23 (m, 2H, H-2), 7.88-7.87 (m, 2H, H-3) (In agreement with literature data[99])

Synthesis of 4-ethynylpyridine (37)[111]

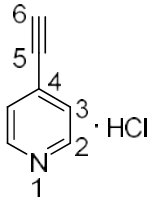

36 (497 mg, 2.835 mmol) was dissolved in THF (5 mL) and methanol (1.5 mL) and KF (205 mg, 3.528 mmol) was added and the reaction was stirred at room temperature overnight. When the reaction was finished the solvents were carefully removed. The residue was extracted with Et_2O and the organic phase was treated with HCl (2 M in diethyl ether) until no

more precipitate formed. The solid was filtered off and dried affording the title product as a a white solid.

Yield: 117 mg (30%)

^{1}H-NMR (400 MHz, DMSO-d_6): δ 8.86 (d, 2 H, $J_{1,2}$ = 5.3 Hz, H-2), 7.96 (d, 4 H, $J_{2,1}$ = 5.3 Hz, H-3), 5.18 (s, 1 H, H-6) (In agreement with literature data[111])

Synthesis of 1,4-bis(trimethylsilylethynyl)benzene (26a)[112]

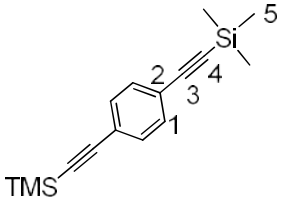

1,4-Diiodobenzene (513 mg, 1.555 mmol), CuI (15 mg, 0.078 mmol) and $PdCl_2(PPh_3)_2$ (72 mg, 0.102 mmol) were added to a Schlenck flask followed by dry Et_3N (17 mL) as the solvent. Trimethylsilylacetylene (0.50 mL, 3.023 mmol) was added drop wise to the reaction. The reaction was stirred at room temperature for 24 h followed by removal of solvent *in vacuo*. The crude product was boiled twice in cyclohexane (12 mL) and filtered resulting in a brown solid. The solid was purified by column chromatography on silica gel using cyclohexane/ethylacetate (10:1) as the eluent.

Yield: 383 mg (91%)

R_f: 0.71 (cyclohexane/ethylacetate (9:1))

^{1}H-NMR (300 MHz, $CDCl_3$): δ 7.38 (s, 4 H, H1), 0.24 (s, 18 H, H5)

^{13}C-NMR (75 MHz, $CDCl_3$): δ 131.9 (C-1), 123.1 (C-2), 104.5 (C-3), 96.2 (C-4), -0.11 (C 5) (In agreement with literature)[112]

EI-MS: m/z (270.1 $[M]^{+\bullet}$, 255.1 $[M\text{-}CH_3]^{+\bullet}$)

Synthesis of 1,4-bis(triisopropylsilylethynyl)benzene (26b)

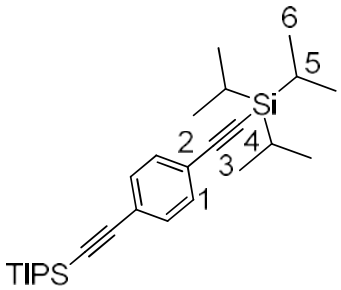

1,4-Diiodobenzene (93 mg, 0.612 mmol), CuI (6.9 mg, 0.036 mmol), and $[PdCl_2(PPh_3)_2]$ (41 mg, 0.059 mmol) were added to a Schlenck flask and dry Et_3N (7 mL) was added. TIPS-acetylene (0.27 mL, 1.211 mmol) was added dropwise to the reaction. The reaction was stirred at 50°C for 24 h followed by removal of solvent *in vacuo*.

The crude product was boiled twice in cyclohexane (5 mL)

and filtered yielding an orange oil.

Yield: 268 mg (100 %)

R_f: 0.58 (cyHEX/Ethylacetate (9:1))

^{1}H-NMR (300 MHz, $CDCl_3$): δ 7.38 (s, 4 H, H-1), 1.12-1.09 (m, 42 H, H-5 and H-6)

^{13}C-NMR (75 MHz, $CDCl_3$): δ 131.3 (C-1), 122.9 (C-2), 106.2 (C-4), 92.2 (C-3), 18.2 (C-5), 10.9 (C-6)

Synthesis of 1,4-ethynylbenzene (27)[112]

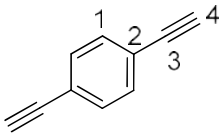

26b (93 mg, 0.344 mmol) was dissolved in THF (4 mL) and TBAF (1000 mg, 1.031 mmol) was added. The reaction was run at room temperature for 3 h. When finished the solvent was removed *in vacuo* and the crude product was purified by column chromatography on silica gel using cyclohexane/ethylacetate (9:1) as the eluent affording the title product as a white solid.

Yield: 28 mg (65%)

R_f: 0.45 (cyclohexane/ethylacetate (9:1))

^{1}H-NMR (300 MHz, $CDCl_3$): δ 7.44 (s, 2 H, H-1), 3.17 (s, 1 H, H-4)

^{13}C-NMR (75 MHz, $CDCl_3$): δ 131.9 (C-1), 122.5 (C-2), 83.0 (C-3), 79.0 (C-4) (In agreement with literature)[112]

Synthesis of the ligands for multicomponent self-assembly:

Synthesis of 1,4-bis(trimethylsilylethynyl)benzene (26a) 1-((3-cyanopropyl)dimethylsilyl)ethynyl-4-trimethylsilylethynyl)benzene (29) and 1,4-(bis-((3-cyanopropyl)dimethylsilyl)ethynyl)-benzene (30)

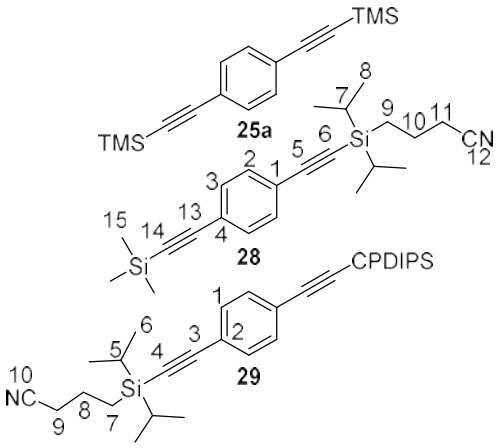

Diiodobenzene (999 mg, 4.60 mmol), $[Pd(PPh_3)_2Cl_2]$ (60 mg, 0.08 mmol), CuI (31 mg, 0.16 mmol), and PPh_3 (106 mg, 0.41 mmol) were added to a dry *Schlenck* flask and were dissolved in dry diisopropylamine (5 mL). CPDIPS-acetylene (945 mg, 4.60 mmol) was added and the reaction was run over night at room temperature.

The next day TMS-acetylene (1.1 mL, 6.81 mmol) was added and the reaction was heated to 50°C for two hours. Next the reaction was cooled to room temperature and poured into Et_2O (150 mL) and H_2O (48 mL). The organic phase was washed with H_2O (3 × 50 mL) and brine (1 × 50 mL) and was subsequently dried over $MgSO_4$. The solvents were removed *in vacuo*.

The crude product was purified by column chromatography on silica gel using first cyclohexane/CH_2Cl_2 (1:1) next cyclohexane/CH_2Cl_2 (1:2) as the eluent.

26a:

Yield: 242 mg (20 %)

R_f: 0.74 (cyclohexane/CH_2Cl_2 (1:1))

29:

Yield: 376 mg (22%)

R_f: 0.44 (cyclohexane/CH_2Cl_2 (1:1))

^{1}H-NMR (400 MHz, $CDCl_3$): δ 7.39 (s, 4 H, H-1 + H-2), 2.42 (t, 2 H, $J_{14,13}$ = 6.9 Hz, H-14), 1.88-1.83 (m, 2 H, H-13), 1.11-1.07 (m, 14 H, H-10 + H-11), 0.85-0.80 (m, 2 H, H-12), 0.25 (s, 9 H, H-7)

^{13}C-NMR (75 MHz, $CDCl_3$): δ 131.8 (C-2 or C-3), 131.7 (C-2 or C-3), 123.3 (C-1 or C-14), 122.9 (C-1 or C-14), 119.7 (C-12), 107.3 (C-5), 104.4 (C-13), 96.4 (C-14), 91.4 (C-6), 21.2 (C-11), 20.7 (C-10), 18.7 (C-8 or C-8'), 17.9 (C-8 or C-8'), 11.6 (C-7), 9.5 (C-9), -0.1 (C-15)

ESI-MS(+): m/z (402.2 $[M+Na]^+$)

30:

Yield: 457 mg (20%)

R_f: 0.21 (cyclohexane/CH_2Cl_2 (1:1))

^{1}H-NMR (400 MHz, $CDCl_3$): δ 7.39 (s, 4 H, H-1), 2.42 (t, 4 H, $J_{9,8}$ = 6.9 Hz, H-9), 1.87-1.83 (m, 4 H, H-8), 1.11-1.07 (m, 28 H, H-5 + H-6), 0.85-0.80 (m, 2 H, H-7)

^{13}C-NMR (75 MHz, $CDCl_3$): δ 131.5 (C-1), 122.7 (C-2), 119.3 (C-10), 106.8 (C-3), 91.3 (C-4), 20.8 (C-5 or C-8), 20.3 (C-5 or C-8), 17.8 (C-9 or C-6), 17.5 (C-9 or C-6), 11.3 (C-7)

ESI-MS(+): m/z (511.3 $[M+Na]^+$)

Synthesis of 1-((3-cyanopropyl)dimethylsilyl)ethynyl-4-trimethylsilylethynyl)benzene (29)

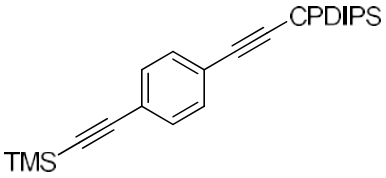

A *Schlenck* flask was evacuated twice and flushed with argon. 1-bromo-4-iodobenzene (216 mg, 0.763 mmol), $[PdCl_2(PPh_3)_2]$ (39 mg, 0.055 mmol), CuI (11 mg, 0.057 mmol), PPh_3 (10 mg, 0.038 mmol), and CPDIPS-acetylene (140 mg, 0.675 mmol) was added. The reagents were dissolved in dry THF (2 mL) and dry diisopropylamine (1 mL) and the reaction mixture was stirred at room temperature under Argon for 3 h resulting in a yellow mixture. TMS-acetylene (0.16 mL, 1.144 mmol) was added to the reaction mixture resulting in a colour change to brown. The reaction mixture was stirred at room temperature under argon for 96 h. Subsequently the reaction was poured onto a mixture of Et_2O and H_2O and the phases were separated. The organic phase was washed with H_2O (3x) and brine and dried over $MgSO_4$. The solvent was removed *in vacuo*.

The crude product was purified by column chromatography on silica gel using cyclohexane/CH_2Cl_2 (1:1) as the eluent.

Yield: 180 mg (70%)

R_f: 0.18 (cyclohexane/CH_2Cl_2 (1:1))

^{1}H-NMR (400 MHz, $CDCl_3$): δ 7.39 (s, 4 H, H-1 + H-2), 2.42 (t, 2 H, $J_{14,13}$ = 6.9 Hz, H-14), 1.88-1.83 (m, 2 H, H-13), 1.11-1.07 (m, 14 H, H-10 + H-11), 0.85-0.80 (m, 2 H, H-12), 0.25 (s, 9 H, H7)

^{13}C-NMR (75 MHz, $CDCl_3$): δ 131.8 (C-2 or C-3), 131.7 (C-2 or C-3), 123.3 (C-1 or C-14), 122.9 (C-1 or C-14), 119.7 (C-12), 107.3 (C-5), 104.4 (C-13), 96.4 (C-14), 91.4 (C-6), 21.2 (C-11), 20.7 (C-10), 18.7 (C-8 or C-8'), 17.9 (C-8 or C-8'), 11.6 (C-7), 9.5 (C-9), -0.1 (C-15)

ESI-MS(+): m/z (402.2 $[M+Na]^+$)

HR-EI: Calculated for $C_{23}H_{33}NSi_2$: 379.2151

Found: 379.2137

Synthesis of 1-(2-((3-cyanopropyl)diisopropyl)-4-ethynylbenzene (31) from 1-((3-Cyanopropyl)dimethylsilyl)ethynyl-4- trimethylsilylethynyl)benzene (29)

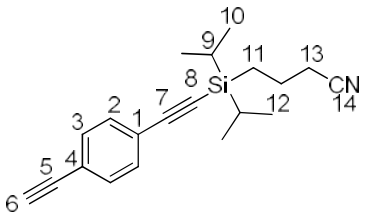

29 (337 mg, 0.887 mmol) was dissolved in methanol (2 mL) and THF (2 mL) and K_2CO_3 (606 mg, 4.384 mmol) was added. The reaction was run for 3 h. The reaction mixture was poured into Et_2O (40 mL) and H_2O (40 mL) and the phases were separated. The organic phase was washed with H_2O (3 × 15 mL) and brine (15 mL) and dried over $MgSO_4$. The solvent was removed *in vacuo* resulting in a brown oil. The crude product was purified by column chromatography on silica gel using cyclohexane/CH_2Cl_2 (2:1) as the eluent.

Yield: 185 mg (68%)

R_f: 0.21 (cyclohexane/CH_2Cl_2 2:1)

^{1}H-NMR (400 MHz, $CDCl_3$): δ 7.42 (s, 4 H, H-2 + H-3), 3.17 (s, 1 H, H-6), 2.42 (t, 2 H, $J_{12,13}$ = 6.9 Hz, H-13), 1.88-1.83 (m, 2 H, H-12), 1.11-1.06 (m, 14 H, H-9 and H-10), 0.85 0.81 (m, 2 H, H-11)

^{13}C-NMR (75 MHz, $CDCl_3$): δ 132.0 (C-2 or C-3), 131.9 (C-2 or C-3), 123.3 (C-1), 122.3 (C-4), 119.6 (C-14), 107.1 (C-7), 91.6 (C-8), 83.1 (C-5), 79.0 (C-6), 21.2 (C-13), 20.7 (C-12), 18.1 (C-10 or C-10') 17.9 (C-10 or C-10'), 11.6 (C-9), 9.5 (C-11)

Synthesis of 1-(2-((3-cyanopropyl)diisopropyl)-4-ethynylbenzene (31) from 1,4-(bis-((3-cyanopropyl)dimethylsilyl)ethynyl)-benzene (30)

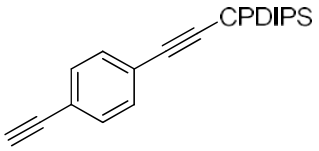

30 (527 mg, 1.08 mmol) was dissolved in THF (14 mL) and H_2O (1.4 mL) and cooled to 0°C. TBAF (0.70 mL, 1 M in THF, 0.70 mmol) was added and the reaction was stirred at room temperature for 3 h. The reaction was quenched with H_2O and poured into Et_2O. The phases were separated and the organic phase was washed three times with H_2O and once with brine and subsequently dried over $MgSO_4$. The solvents were removed *in vacuo*. The crude product was purified by column chromatography on silica gel using cyclohexane/CH_2Cl_2 (2:1) as the eluent affording the title product as a brown oil.

Yield: 133 mg (40%)

Analytical data described above.

Synthesis of 4-(((2',3'-bis(methoxymethoxy)biphenyl-4-yl)ethynyl)diisopropylsilyl)-butannitrile (32)

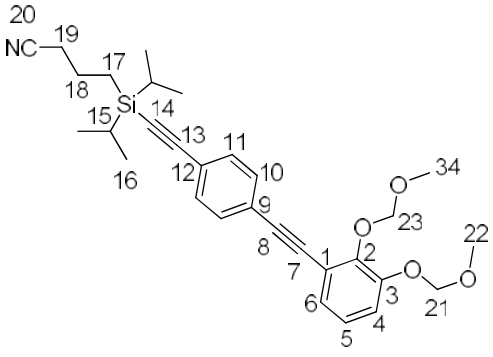

CuI (6 mg, 0.032 mmol) and $[PdCl_2(PPh_3)_2]$ (29 mg, 0.041 mmol) were added to a twice evacuated *Schlenck*-flask. 2,3-bis(methoxymethyl)-1-iodobenzene (**25**) (204 mg, 0.629 mmol) was dissolved in dry Et_3N (3 mL) and added to the flask. 1-(2-((3-cyanopropyl)diisopropyl)-4-ethynyl benzene (**30**) (174 mg, 0.565 mmol) was dissolved in dry Et_3N (5 mL) and added. The reaction mixture was heated to 50°C under argon overnight. The reaction was cooled to room temperature and poured onto Et_2O (40 mL) and H_2O (10 mL) and the phases were separated. The organic phase was washed three times with H_2O, once with brine and dried over $MgSO_4$. The solvents were removed *in vacuo*. The crude product was purified by column chromatography on silica gel using

first cyclohexane/ethylacetate (1:1) then CH_2Cl_2/cyclohexane (10:1) as the eluent affording the title product as a brown oil.

Yield: 257 mg (90%)

R_f: 0.51 (cyclohexane/Ethylacetate (1:1))

^{1}H-NMR (400 MHz, $CDCl_3$): δ 7.45-7.44 (m, 4 H, H-10 and H-11), 7.26-7.16 (m, 2 H, H-4 and H-6), 7.03 (dd, 1 H, $J_{5,6}$ or $J_{5,4}$ = 7.8 Hz, $J_{5,6}$ or $J_{5,4}$ = 8.2 Hz, H-5), 5.28 (s, 2 H, H-21), 5.21 (s, 2 H, H-23), 3.66 (s, 3 H, H-22), 3.51 (s, 1 H, H-24), 2.43 (t, 2 H, $J_{19,18}$ = 6.9 Hz, H-19), 1.91-1.83 (m, 2 H, H-18), 1.12-1.08 (m, 14 H, H-15 and H-16), 0.86-0.81 (m, 2 H, H-17)

^{13}C-NMR (75 MHz, $CDCl_3$): 150.2 (C-2), 147.7 (C-3), 132.0 (C-10 or C-11), 131.3 (C-10 or C-11), 126.7 (C-5), 124.3 (C-4), 123.5 (C-9 or C-12), 122.8 (C-9 or C-12), 119.7 (C-20), 118.4 (C-7), 117.5 (C-6), 107.4 (C-13), 98.8 (C-21), 95.2 (C-23), 95.2 (C-8), 92.8 (C-14), 88.0 (C-1), 57.5 (C-24), 56.3 (C-22), 21.2 (C-18), 20.7 (C-19), 18.2 (C-16), 17.9 (C-16'), 11.7 (C-15), 9.6 (C-17)

ESI-MS(+): m/z (526.2 $[M+Na]^+$, 521.3 $[M+NH_4]^+$, 504.2 $[M+H]^+$)

HR-ESI: calculated for $C_{30}H_{37}NNaO_4Si^+$: 526.2390

Found: 526.2385

Synthesis of 1-((4-ethynylphenyl)ethynyl)-2,3-bis(methoxymethoxy)benzene (28)

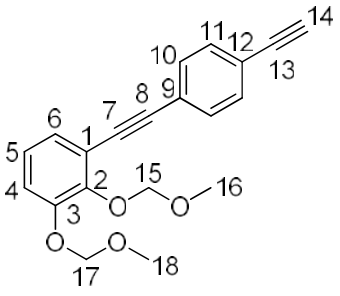

32 (474 mg, 0.942 mmol) was dissolved in THF (10 mL). TBAF (1.03 ml, 1.04 mmol, 1 M in THF) was added and the reaction was stirred at room temperature for 3 h. The reaction was quenched with H_2O and poured onto Et_2O. The phases were separated and the organic phase was washed with H_2O (3x) and brine and dried over $MgSO_4$. The solvents were removed *in vacuo*. The crude product was purified by column chromatography on silica gel using CH_2Cl_2/cyclohexane (10:1) as the eluent affording the title product as a brown oil.

Yield: 269 mg (89%)

R_f: 0.44 (CH_2Cl_2/cyclohexane (10:1))

^{1}H-NMR (400 MHz, $CDCl_3$): δ 7.46 (s, 1 H, H-10 and H-11), 7.18-7.14 (m, 2 H, H-4 and H-6), 7.10 (dd, 1 H, $J_{6,4}$ = 1.49 Hz, $J_{6,5}$ = 7.65 Hz, H-6), 7.15 (dd, 1 H, $J_{4,6}$ = 1.49 Hz, $J_{4,5}$ = 7.65 Hz, H-4), 7.02 (dd, 1 H, $J_{5,6}$ = $J_{5,4}$ = 7.65 Hz, H-5), 5.29 (s, 2 H, H-15 or H-17), 5.21 (s, 2 H, H-15 or H-17), 3.66 (s, 3 H, H-18), 3.51 (s, 3 H, H-16), 3.17 (s, 1 H, H-14)

^{13}C-NMR (75.47 MHz, $CDCl_3$): δ 150.2 (C-2), 147.7 (C-3), 132.0 (C-10 or C-11), 131.3 (C-10 or C-11), 126.6 (C-5), 124.2 (C-4), 123.7 (C-9 or C-12), 121.9 (C-9 or C-12), 118.4 (C-1), 117.5 (C-6), 98.8 (C-21 or C-23), 95.2 (C-21 or C-23), 92.6 (C-8), 87.9 (C-7), 83.2 (C-13), 78.9 (C-14), 57.4 (C-22 or C-24), 56.2 (C-22 or C-24)

ESI-MS(+): m/z (345.1 $[M+Na]^+$, 340.2 $[M-CH_3+Na]^+$, 323.1 $[M+H]^+$)

HR-ESI: calculated for $C_{20}H_{18}NaO_4^+$: 345.1103

Found: 345.1096

CHN-analysis: $C_{20}H_{16}O_4 \cdot 2/3THF$

Calculated [%]: C 73.49; H 6.35

Measured [%]: C 73.24; H 6.34

Synthesis of 4-((4-((2,3-bis(methoxymethoxy)phenyl)ethynyl)phenyl)ethynyl)pyridine (33)

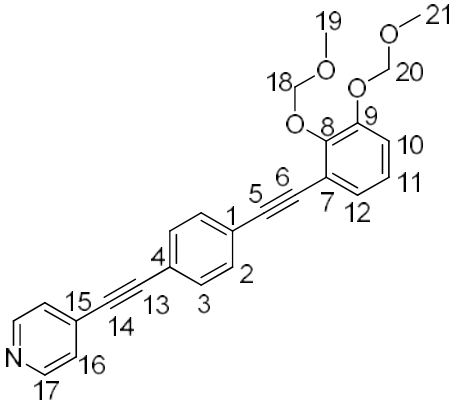

28 (482 mg, 1.50 mmol) was added to a dry two-neck round bottomed flask. $Pd_2(dba)_3 \cdot CHCl_3$ (54 mg, 0.052 mmol), CuI (16 mg, 0.084 mmol), and dppf (47 mg, 0.084 mmol) were added and the flask was evacuated. 4-Iodopyridine (342 mg, 1.668 mmol) was added followed by dry THF (75 mL) and dry *i*Pr_2NH (25 mL). The reaction was heated to 60°C and stirred for 19 h. The reaction was cooled to room temperature and saturated aqueous solutions of EDTA and Na_2CO_3 were added until the solution was basic. CH_2Cl_2, brine and H_2O was added and the phases were separated. The aqueous phase was extracted three times with CH_2Cl_2 and the collected organic phases were washed with saturated aqueous $NaHCO_3$ and dried over $NaSO_4$. The solvents were removed *in vacuo.*

The crude product was purified by column chromatography on silica gel using first CH_2Cl_2/cyclohexane (10:1) and next CH_2Cl_2/cyclohexane (20:1) as the eluent affording the title product as a dark green solid.

Yield: 86 mg (70%)

R_f: 0.11 (CH_2Cl_2/ cyclohexane (10:1))

^{1}H-NMR (400 MHz, $CDCl_3$): δ 8.27 (d, 2 H, $J_{17,16}$ = 6 Hz, H-17), 7.68 (dd, 2 H, $J_{16,17}$ = 6 Hz, H-16), 7.50-7.49 (m, 4 H, H-10 + H-11), 7.18-7.15 (m, 2 H, H-4 + H-6), 7.02 (dd, 1 H, H-5), 5.29 (s, 2 H, H-18 or H-20), 5.21 (s, 1 H, H-18 or H-20), 3.66 (s, 3 H, H-19 or H-21), 3.51 (s, 3 H, H-19 or H-21)

^{13}C-NMR (100 MHz, $CDCl_3$): δ 150.2 (C-2), 150.1 (C-17), 147.7 (C-3), 133.1 (C-16), 132.4 (C-10 or C-11), 131.4 (C-10 or C-11), 126.7 (C-5), 124.3 (C-4), 124.2 (C-12), 121.4 (C-9), 118.3 (C-1), 117.6 (C-6), 105.3 (C-15), 98.8 (C-18 or C-20), 95.2 (C-18 or C-20), 92.7 (C-8), 66.7 (C-7), 82.0 (C-13), 75.6 (C-14), 57.5 (C-19 or C-21), 56.2 (C-19 or C-21)

Mass spectra were measured but the product **33** was not found.

Synthesis of 4-((2,3-bis(methoxymethoxy)phenyl)ethynyl)pyridine (38)

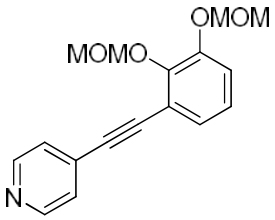

25 (250 mg, 0.768 mmol), CuI (6 mg, 0.031 mmol), and $[PdCl_2(PPh_3)_2]$ (23 mg, 0.032 mmol) were added to a dry round bottomed flask which was subsequently shielded from light. Next **28** (190 mg, 1.361 mmol) was added followed by dry Et_3N (5 mL). The reaction was heated to 80°C for 72 h. When finished, the reaction was cooled to room temperature and CH_2Cl_2 was added. The organic phase was washed three times with H_2O and dried over $MgSO_4$. The solvents were removed *in vacuo*.

The crude product was purified via column chromatography on silica gel using ethylacetate as the eluent affording the title product as a yellow oil.

Yield: 133 mg (58%)

R_f: 0.56 (ethylacetate)

^{1}H-NMR (400 MHz, $CDCl_3$): δ 8.60 (dd, 2 H, $J_{11,10}$ =4.4 Hz, $J_{11,10'}$ =1.6 Hz, H-11), 7.37 (dd, 2 H, $J_{10,11}$ = 4.4 Hz, $J_{10,11'}$ = 1.6 Hz, H-10), 7.21-7.19 (m, 1 H, H-6), 7.19-7.17 (m, 1 H, H-4), 7.04 (dd, 1 H, $J_{5,6}$ = 7.96 Hz, $J_{5,4}$ = 7.96 Hz, H-5), 5.28 (s, 2 H, H-14), 5.21 (s, 2 H, H-12), 3.66 (s, 3 H, H-13), 3.51 (s, 3 H, H-15)

^{13}C-NMR (101 MHz, $CDCl_3$): δ 150.1 (C-1), 149.7 (C-11), 148.0 (C-2), 131.4 (C-9), 126.7 (C-4), 125.3 (C-10), 124.3 (C-5), 118.1 (C-6), 117.6 (C-3), 98.8 (C-14), 95.2 (C-12), 90.6 (C-7), 90.3 (C-8), 57.5 (C-13), 56.3 (C-15)

ESI-MS(+): m/z (300.1 $[M+H]^+$, 256.1 $[M-CH_3OCH_2+H]^+$)

HR-ESI: Calculated for $C_{17}H_{17}NaNO_4^+$: 322.1055

Found: 322.1049

Synthesis of 3-(Pyridine-4-ylethynyl)benzene-1,2-diol (39)

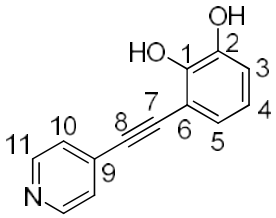

38 (113 mg, 0.378 mmol) were added to a dry roundbottomed flask and dissolved in dry isopropanol (2 mL). Next, $ZrCl_4$ (49 mg, 0.210 mmol) was added and the reaction was heated to reflux for 2 h. The reaction was cooled to room temperature and the solvent was removed *in vacuo*. The crude product was purified by column chromatography on silica gel using ethanol as the eluent, affording the title product as a brown solid.

Yield: 73 mg (91%)

R_f: 0.80 (ethanol)

^{1}H-NMR (400 MHz, CD_3OD): δ 8.54-8.53 (m, 2 H, H-11), 7.65-7.54 (m, 2 H, H-10), 6.93 (dd, 1 H, $J_{6,5}$ = 7.7 Hz, $J_{6,4}$ = 1.3 Hz, H-6), 6.87 (dd, 1 H, $J_{4,5}$ = 7.7 Hz, $J_{4,6}$ = 1.3 Hz, H-4), 6.72 (dd, 1 H, $J_{5,6}$ = 7.7 Hz, $J_{5,6}$ = 7.7 Hz, H-5)

^{13}C-NMR (100 MHz, CD_3OD): δ 150.2 (C-11), 148.7 (C-1), 146.9 (C-2), 134.6 (C-9), 127.2 (C-10), 125.0 (C-5), 120.9 (C-4), 117.8 (C-3), 110.7 (C-6), 93.0 (C-8), 90.8 (C-7)

ESI-MS(+): m/z (212.1 $[M+H]^+$)

HR-ESI: Calculated for $C_{13}H_{10}NO_2^+$: 212.0706

Found: 212.0708

9.2 Complexations

The general methods for assembly of the different complexes are described in this chapter. For solutions to be measured by NMR-spectroscopy, deuteriated solvents were used.

9.2.1 Complexes for spin crossover

The complexation of ligand **10** was carried out in two different solvent mixtures as described below.

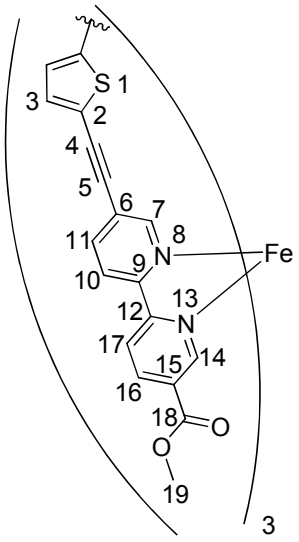

$[Fe_2(10)_3](BF_4)_4$ in CD_2Cl_2/DMSO-d_6 (3:1)

Ligand **10** (11.37 mg, 0.020 mmol), $Fe_2(BF_4)_2 \cdot 6H_2O$ (5.22 mg, 0.015 mmol) was mixed in CD_2Cl_2/DMSO-d_6 (3:1, 1.5 ml) resulting in a yellow suspension which was stirred at room temperature over night.

No NMR-spectra obtained

$[Fe_2(10)_3](BF_4)_4$ in CD_2Cl_2/CD_3CN (3:1)

Ligand **10** (10.77 mg, 0.029 mmol), $Fe_2(BF_4)_2 \cdot 6H_2O$ (4.44 mg, 0.013 mmol) was mixed in CD_2Cl_2/CD_3CN (3:1, 1.5 mL) resulting in a red suspension which was stirred at room temperature overnight.

^{1}H-NMR (400 MHz, CD_2Cl_2/CD_3CN (3:1)): δ 8.78-8.73 (m, 3 H)*, 8.36-8.35 (m, 1 H)*, 7.78-7.61 (m, 2 H)*, 7.40-7.31 (m, 1 H)*, 3.88 (s, 3 H, H-19)

* Protons could not be assigned unambiguously

ESI-MS: m/z (445.3 $[Fe_2\mathbf{10}_3]^{4+}$)

9.2.2 Complexes with spirobifluorene derivatives

The complexation of the M_2L_2-rhombs of ligand **12**, **15** and **20** are exemplified by the complexation of ligand (*R*)-**12** with Pd(dppp)$(OTf)_2$:

(*R*)-**12** (4,70 mg, 0.01 mmol) was dissolved in CD_2Cl_2 (1 mL) and 250 µL were drawn from the solution and filled up to 750 µL with CD_2Cl_2. Pd(dppp)$(OTf)_2$ (9.71 mg, 0.01 mmol) was dissolved in CD_3CN (1 mL) and 250 µL were drawn from the solution and added to the diluted solution of (*R*)-**12**. The solution was stirred at room temperature for 24 h.

$[Pd_2(dppp)_2((R)\text{-}12)_2](OTf)_2$ from (*R*)-12

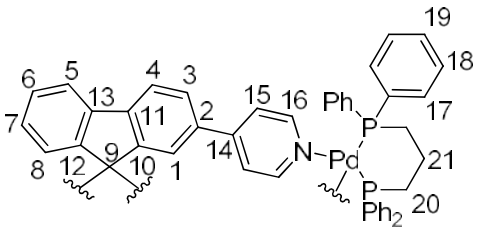

^{1}H-NMR (400 MHz, CD_2Cl_2/CD_3CN (3:1)): δ 8.40-8.38 (m, 4 H, H-16), 7.89-7.85 (m, 4 H, H-4 and H-5), 7.43-7.41 (m, 18 H, H-18 and H-6), 7.19-7.08 (m, 26 H, H-7, H-17 and H-19), 7.04 (d, 4 H, $J_{3,4}$ = 6.9 Hz, H-3) 6.84 (br s, 4 H, H-15), 6.63 (d, 4 H, $J_{8,7}$ = 7.5 Hz, H-8), 6.46 (s, 2 H, H-1), 3.02-2.95 (m, 8 H, H-20), 2.09-2.02 (m, 4 H, H-21).

ESI-MS: m/z (707.8 $[Pd_2\mathbf{12}_2OTf]^{3+}$; 1136.2 $[Pd_2\mathbf{12}_2(OTf)_2]^{2+}$)

$[Pt_2(dppp)_2((R)\text{-}12)_2](OTf)_2$ from (*R*)-12

^{1}H-NMR (400 MHz, CD_2Cl_2/CD_3CN (3:1)): δ 8.44 (br s, 4 H, H-16), 7.90-7.86 (m, 4 H, H-4 and H-5), 7.49-7.29 (m, 18 H, H-18 and H-6), 7.21-7.10 (m, 26 H, H-7, H-17 and H-19), 7.04 (d, 4 H, $J_{3,4}$ = 7.0 Hz, H-3) 6.88 (br s, 4 H, H-15), 6.65 (d, 4 H, $J_{8,7}$ = 7.5 Hz, H-8), 6.46 (s, 2 H, H-1), 3.12-3.05 (m, 8 H, H-20), 2.14-1.98 (m, 4 H, H-21).

ESI-MS: m/z (538.4 8 $[Pt_2\mathbf{12}_2]^{4+}$; 767.5 8 $[Pt_2\mathbf{12}_2OTf]^{3+}$; 1225.2 $[Pt_2\mathbf{12}_2(OTf)_2]^{2+}$)

Crystal Data for $[Pt_2(dppp)_2((R)\text{-}\mathbf{12})_2](OTf)_2$

Empirical formula:	$C_{144}\,H_{128}\,F_{12}\,N_4\,O_{20}\,P_4\,Pd_2\,S_4$
Molecular weight:	2927.42 g/mol
Space group:	Monoclonic, C 2/c

Unit cell dimensions:	a = 18.8830(5) Å	α = 90 deg.
	b = 23.7387(5) Å	β = 101.585 deg.
	c = 35.9013(6) Å	γ = 90 deg.
Volume:	15765.2(6) $Å^3$	
Absorption coefficient:	0.395 mm^{-1}	
F(000):	6016	
Reflexions collected:	27330	
Unique reflexions:	14210 [R(int) = 0.0193]	
Completeness to theta:	99.4 %	
Restraints/Parameters:	669 / 942	
Goodness-of-fit on F^2:	1.061	
Final R indices [I>2sigma(I)]:	R1 = 0.0505, wR2 = 0.1399	
Largest diff. peak and hole:	1.548 and -0.653 eA^{-3}	

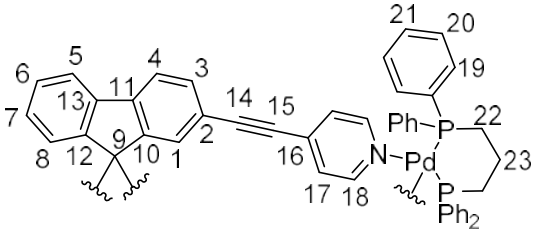

$[Pd_2(dppp)_2((R)\text{-}15)_2](OTf)_2$ from (*R*)-15 in CD_2Cl_2/CD_3CN (3:1)

(*R*)-**15** (5.2 mg, 0.01 mmol) was dissolved in CD_2Cl_2 (1 mL) and 250 µL were taken out and filled up to 750 µL. $Pd(dppp)(OTf)_2$ (10.1 mg, 0.01 mmol) was dissolved in CD_3CN (1 mL) and 250 µL were taken out and added to the solution of (*R*)-**15**. The solution was stirred at room temperature for 24 h.

^{1}H-NMR (400 MHz, CD_2Cl_2/CD_3CN (3:1)): δ 8.53 (d, 8 H, $J_{18,17}$ = 5.1 Hz, H-18), 7.88 (d, 4 H, $J_{5,6}$ = 7.5 Hz, H-5), 7.84 (d, 4 H, $J_{4,3}$ = 7.9 Hz, H-4), 7.48-7.43 (m, 8 H, H-20), 7.39 (dd, 4 H, $J_{6,5}$ = 7.5 Hz, $J_{6,7}$ = 7.5 Hz, H-6), 7.33-7.19 (m, 16 H, H-3, H-19 and H-21), 7.14 (dd, 4 H, $J_{7,6}$ = 7.5 Hz, $J_{7,8}$ = 7.5 Hz, H-7), 6.82 (d, 8 H, $J_{17,18}$ = 5.1 Hz, H-17), 6.69 (s,

4 H, H-1), 6.64 (d, 4 H, $J_{8,7}$ = 7.5 Hz, H-8), 3.07-2.98 (m, 8 H, H-22), 2.18-2.11 (m, 4 H, H-23).

ESI-MS: m/z (1186.2 $[Pd_2\mathbf{15}_2(OTf)_2]^{2+}$; 2522.6 $[Pd_2\mathbf{15}_2(OTf)_3]^{+}$)

$Pd_4(dppp)_4((R)\text{-}\mathbf{15})_4](OTf)_4$ from (*R*)-**15** in CD_2Cl_2/CD_3CN (3:1)

The complexation was described above, by the complexation of $[Pd_2(dppp)_2((R)\text{-}15)_2](OTf)_2$ from (*R*)-15 in CD_2Cl_2/CD_3CN (3:1).

No proper ^{1}H-NMR-data was obtained.

ESI-MS: m/z (1631.7 $[Pd_4\mathbf{15}_4(OTf)_5]^{3+}$; 2522.4 $[Pd_4\mathbf{15}_4(OTf)_6]^{4+}$)

Kristallstruktur: daten fehlen noch

$[Pd_2(dppp)_2((R)\text{-}\mathbf{15})_2](OTf)_2$ from (*R*)-**15** in acetone-d_6

(*R*)-**15** (5.2 mg, 0.01 mmol) was dissolved in acetone-d_6 (1 mL) and 250 µL were drawn from the solution and filled up to 750 µL with acetone-d_6. $Pd(dppp)(OTf)_2$ (10.1 mg, 0.01 mmol) was dissolved in acetone-d_6 (1 mL) and 250 µL was drawn from the solution and added to the solution of (*R*)-**15**. The solution was stirred at room temperature for 24 h.

^{1}H-NMR (400 MHz, $(CD_3)_2CO$): δ 8.82 (d, 8 H, $J_{18,17}$ = 5.4 Hz, H-18), 8.09-8.07 (m, 16 H, H-4 and H-5), 7.75-7.70 (m, 4 H, H-21), 7.61 (dd, 4 H, $J_{3,4}$ = 7.9 Hz, $J_{3,1}$ = 1.4 Hz, H-3), 7.52-7.46 (m, 8 H, H-19 or H-20), 7.41-7.33 (m, 8 H, H-19 or H-20), 7.26 (dd, 4 H, $J_{7,6}$ = 7.5 Hz, $J_{7,8}$ = 7.5 Hz, H-7), 7.09 (d, 8 H, $J_{17,18}$ = 5.4 Hz, H-17), 6.79 (d, 4 H, $J_{1,3}$ = 1.4 Hz, H-1), 6.74 (d, 4 H, $J_{8,7}$ = 7.5 Hz, H-8), 3.60-3.63 (m, 8 H, H-22), 3.35-3.29 (m, 4 H, H-23).

$Pd_4(dppp)_4((R)\text{-}15)_4](OTf)_4$ from (*R*)-15 in acetone-d_6

The complexation is described above, by the complexation of $[Pd_2(dppp)_2((R)\text{-}\mathbf{15})_2](OTf)_2$ from (*R*)-**15** in acetone-d_6).

^{1}H-NMR (400 MHz, $(CD_3)_2CO$): δ 8.72-8.70 (m, 16 H, H-18)*, 8.04 (d, 8 H, J = 7.6 Hz), 7.98 (d, 8 H, J = 8.0 Hz), 8.85 (d, 8 H, J = 8.0 Hz), 7.16 (d, 8 H, J = 5.8 Hz), 7.05-7.02 (m,

8 H), 6.68 (s, 8 H), 6.58 (s, 8 H), 5.95 (dd, 8 H, J_1 = 7.0 Hz, J_2 = 7.0 Hz), 5.62 (dd, 8 H, J_1 = 4.3 Hz, J_2 = 4.3 Hz), 4,80 (dd, 8 H, J_1 = 7.5 Hz, J_2 = 7.5 Hz).

* Protons could not be assigned unambiguously.

ESI-MS: m/z (1631.7 $[Pd_4\mathbf{15}_4(OTf)_5]^{3+}$; 2522.4 $[Pd_4\mathbf{15}_4(OTf)_6]^{4+}$)

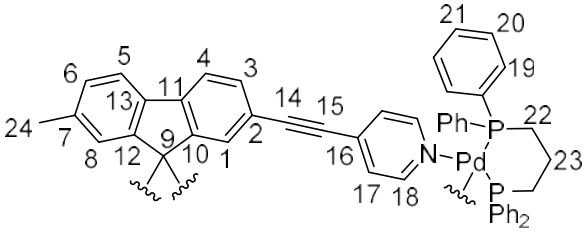

$[Pd_2(dppp)_2((S)\text{-}20)_2](OTf)_2$ and from (*S*)-20 in CD_2Cl_2/CD_3CN (3:1)

(*S*)-**20** (5.46 mg, 0.01 mmol) was dissolved in CD_2Cl_2 (1 mL) and 250 µL were drawn from the solution and filled up to 750 µL with CD_2Cl_2. Pd(dppp)$(OTf)_2$ (8.17 mg, 0.01 mmol) was dissolved in CD_3CN (1 mL) and 250 µL was drawn from the solution and added to the solution of (*S*)-**20**. The solution was stirred at room temperature for 24 h.

^{1}H-NMR (400 MHz, CD_2Cl_2/CD_3CN (3:1)): δ 8.56-8.55 (d, 8H, $J_{18,17}$ = 5.5 Hz, H-18), 7.79-7.74 (m, 8H, H-4 and H-6), 7.49-7.44 (m, 8H, H-20), 7.33-7.27 (m, 8H, H-3 and H-5), 7.25-7.20 (m, 12H, H-19 and H-21), 6.82-6.21 (d, 8H, $J_{17,18}$ = 5.5 Hz, H-17), 6.68-6.67 (s, 4H, H-1), 6.47 (s, 4H, H-8), 3.07-3.02 (m, 8H, H-22), 2.85-2.83 (m, 4H, H-23), 2.16 (s, 6H, H-24).

$[Pd_2(dppp)_2((S)\text{-}20)_2](OTf)_2$ from (*S*)-20 in acetone-d_6

(*S*)-**20** (5.46 mg, 0.01 mmol) was dissolved in acetone-d_6 (1 mL) and 250 µL were drawn from the solution and filled up to 750 µL with acetone-d_6. Pd(dppp)$(OTf)_2$ (8.17 mg, 0.01 mmol) was dissolved in acetone-d_6 (1 mL) and 250 µL were drawn from the solution and added to the diluted solution of (*S*)-**20**. The solution was stirred at room temperature for 24 h.

^{1}H-NMR (400 MHz, $(CD_3)_2CO$): δ 8.82 (d, 8 H, $J_{18,17}$ = 5.4 Hz, H-18), 8.01 (d, 4 H, $J_{4,3}$ = 7.9 Hz, H-4), 7.95 (d, 4 H, $J_{4,3}$ = 7.8 Hz, H-5), 7.75-7.70 (m, 16 H, H-20), 7.67 (d, 4 H, $J_{3,4}$ = 7.9 Hz, H-3), 7.48-7.31 (m, 24 H, H-19 and H-21), 7.08 (d, 8 H, $J_{18,17}$ = 5.4 Hz, H-17), 6.75 (d, 4 H, $J_{1,3}$ = 1.3 Hz, H-1), 6.55 (s, 4 H, H-8), 3.34-3.29 (m, 8 H, H-22), 3.22-3.15 (m, 4 H, H-23), 2.23 (s, 6 H, H-24).

The complexation of ligand **21** into M_2L_4-complexes was carried out in two different solvent mixtures as described below:

$[Pd_2((R)\text{-}21)_4](BF_4)_2$ in CD_3CN

(*R*)-**21** (4.70 mg, 0.01 mmol) and $[Pd(CH_3CN)_4](BF_4)_2$ (2.33 mg, 0.005 mmol) were dissolved in CD_3CN (1.52 mL) and either stirred at room temperature or heated at 65°C.

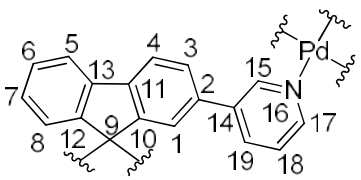

^{1}H-NMR (400 MHz, CD_3CN (3:1)): δ 8.21-8.19 (m, 8 H, H-4), 8.13-8.12 (m, 8 H, H-5), 7.98-7.96 (m, 8 H, H-3), 7.93-7.86 (m, 8 H, H-19), 7.56-7.54 (d, 8 H, H-17), 7.49-7.45 (m, 8 H, H-6), 7.27-7.22 (m, 8 H, H-18), 7.18-7.10 (m, 8 H, H-7), 6.47-6.47 (m, 8 H, H-8), H-1 and H-15 could not be found.

ESI-MS: m/z (523.1 $[Pd_2\mathbf{21}_4]^{4+}$; 727.2 $[Pd_2\mathbf{21}_4BF_4]^{3+}$; 1134.2 $[Pd_2\mathbf{21}_4(BF_4)_2]^{2+}$)

$[Pd_2((R)\text{-}21)_4](BF_4)_4$ in CD_2Cl_2/CD_3CN (3:1)

(*R*)-**21** (4.70 mg, 0.01 mmol) and $[Pd(CH_3CN)_4](BF_4)_2$ (2.33 mg, 0.005 mmol) were dissolved in CD_3CN (0.52 mL) and CD_2Cl_2 (1 mL) and either stirred at room temperature or heated at 65°C.

^{1}H-NMR (400 MHz, CD_2Cl_2/CD_3CN (3:1)): δ 8.02-7.80 (m, 32H, H-4, H-5, H-15 and H-17),* 7.43-7.37 (m, 8H, H-19),* 7.16-7.09 (m, 16H, H-3 and H-6),* 6.83 (m, 4H, H-1),* 6.63-6.57 (m, 8H, H-18),* 6.50-6.40 (m, 8H, H-7),* 6.15 (m, 4H, H-1),* 5.90-5.89 (m, 8H, H-8).*

* Protons could not be assigned unambiguously.

ESI-MS: m/z (523.1 $[Pd_2\mathbf{21}_4]^{4+}$; 727.2 $[Pd_2\mathbf{21}_4BF_4]^{3+}$; 1100.2 $[Pd_2\mathbf{21}_4Cl_2]^{2+}$; 1134.2 $[Pd_2\mathbf{21}_4(BF_4)_2]^{2+}$)

Complexation of ligand (*R*)-**12** into M_6L_{12}-complexes was carried out in the different solvent mixtures as described below:

$[Pd_6((R)\text{-}12)_{12}](BF_4)_{12}$ in DMSO-d_7

(*R*)-**12** (4.76 mg, 0.01 mmol) and $[Pd(CH_3CN)_4](BF_4)_2$ (2.52 mg, 0.006 mmol) were mixed in DMSO-d_7 (1.5 mL) and heated for three hours at 65°C.

$[Pd_6((R)\text{-}12)_{12}](BF_4)_{12}$ in CD_2Cl_2/CD_3CN (3:1)

(*R*)-**12** (4,76 mg, 0.01 mmol) and $[Pd(CH_3CN)_4](BF_4)_2$ (2.52 mg, 0.006 mmol) were mixed in CD_2Cl_2/CD_3CN (3:1, 1.5 mL) and heated for 12 h at 65°C.

9.2.3 Complexes of multicomponent self-organizing ligands

The complexation of ligand **39** and **28** were performed as described below.

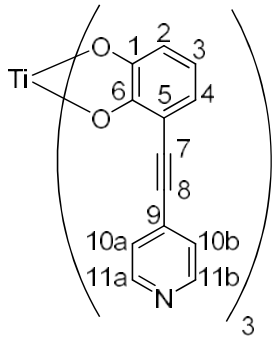

$[Ti(39)_3]Li_2$

Ligand **39** (5.85 mg, 0.28 mmol), Li_2CO_3 (8.52 mg, 0.115 mmol), and $TiO(acac)_2$ (4.80 mg, 0.18 mmol) were mixed in DMF-d_7 (1.5 mL) and heated over night at 80°C.

Fac-[Ti**39**$_3$]$^{2-}$ (after 24 h):

^{1}H-NMR (400 MHz, DMF-d_7): δ 8.56 (dd, 2 H, $J_{11,10a}$ = 6.0 Hz, $J_{11,10b}$ = 1.5 Hz, H-11a and H-11b), 7.40 (dd, 2 H, $J_{10,11a}$ = 6.0 Hz, $J_{10,11b}$ = 1.5 Hz, H-10a and H-10b), 6.62 (dd, 1 H, $J_{2,3}$ = 7.8 Hz, $J_{2,4}$ = 1.4 Hz, H-2), 6.44 (dd, 1 H, $J_{3,2}$ = 7.8 Hz, $J_{3,4}$ = 7.8 Hz, H-3), 6.19 (dd, 1 H, $J_{4,3}$ = 7.8 Hz, $J_{4,2}$ = 1.4 Hz, H-4).

ESI-MS: m/z (565.1 [Ti**39**$_3$$C_5H_8O_2$]$^-$; 676.1 [Ti**39**$_3$H]$^-$)

^{1}H-DOSY-NMR: (500 MHz, DMSO-d_6, 300 K):

D [$m^2 \cdot s^{-1}$] = $4.134 \cdot 10^{-10}$

Mer-[Ti**39**$_3$]$^{2-}$ (after 24h):

^{1}H-NMR (400 MHz, DMF-d_7): δ 8.52 (dd, 2H, $J_{11,10a}$ = 5.0 Hz, $J_{11,10b}$ = 1.5 Hz, H-11a and H-11b), 7.38 (dd, 2H, $J_{10,11a}$ = 5.0 Hz, $J_{10,11b}$ = 1.5 Hz, H-10a and H-10b), 6.51 (dd, 1 H, $J_{2,3}$ = 7.8 Hz, $J_{2,4}$ = 1.4 Hz, H-2), 6.31 (dd, 1 H, $J_{3,2}$ = 7.8 Hz, $J_{3,4}$ = 7.8 Hz, H-3), 6.17 (dd, 1 H, $J_{4,3}$ = 7.8 Hz, $J_{4,2}$ = 1.4 Hz, H-4).

^{1}H-DOSY-NMR: (500 MHz, DMSO-d_6, 300 K):

D [$m^2 \cdot s^{-1}$] = $3.823 \cdot 10^{-10}$

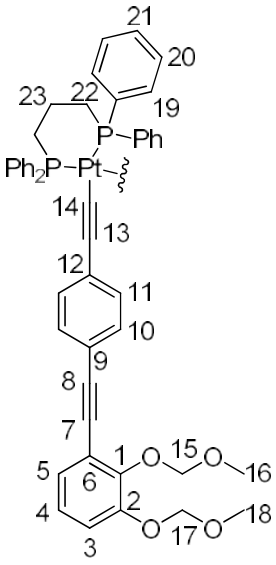

[Pt(dppp)(28)$_2$]

Ligand **28** (29 mg, 0.089 mmol), Pt(dppp)Cl_2 (32 mg, 0.471 mmol), and CuI (1.5 mg, 0.008 mmol) were added to a dry *Schlenck*-flask and dry Et_3N (10 mL) was added. The reaction was stirred for 48 h under argon and with exclusion of light. When finished the solvent was removed *in vacuo* and the residue was extracted with CH_2Cl_2. The organic phase was washed with H_2O and dried over $MgSO_4$. The solvent was removed *in vacuo*. The crude product was purified by column chromatography on neutral ALOX using CH_2Cl_2/cyclohexane (10:1) as the eluent affording the title product as a brown solid.

Yield: 28 mg (52%)

R_f: 0.62 (CH_2Cl_2/cyclohexane (10:1))

^{1}H-NMR (400 MHz, $CDCl_3$): δ 7.78-7.73 (m, 8 H, H-20), 7.38-7.31 (m, 12 H, H-19 and H-21), 7.15 (dd, 4 H, $J_{10,11a}$ = 8.1 Hz, $J_{10,11b}$ = 1.7 Hz, H-10), 7.12-7.08 (m, 4 H, H-5 and H-3), 6.97 (dd, 2 H, $J_{4,5}$ = 8.2 Hz, $J_{4,3}$ = 8.2 Hz, H-4), 6.76 (dd, 4 H, $J_{11,10a}$ = 8.2 Hz, $J_{11,10b}$ = 1.7 Hz, H-11), 5.26 (s, 4 H, H-15), 5.18 (s, 4 H, H-17), 3.63 (s, 6 H, H-16), 3.49 (s, 6 H, H-18), 2.54-2.48 (m, 4 H, 22), 2.21-1.98 (m, 2 H, H-23)

ESI-MS: m/z (1273.4 $[M+Na]^+$)

Literature

(1) Gade, L. H. *Koordinationschemie*; 1st ed.; Wiley-VCH, 1998.

(2) Werner, A. *Z. Anorg. Chem.* **1893**, *3*, 267–330.

(3) Lehn, J.-M. *Rep. Prog. Phys.* **2004**, *67*, 249–265.

(4) Lehn, J.-M. *Pure Appl. Chem.* **1978**, *50*, 871–892.

(5) Pedersen, C. J. *J. Am. Chem. Soc.* **1967**, *89*, 2495–2496.

(6) Vögtle, F. *Supramolekulare Chemie*; 2. Edition.; Teubner: Stuttgart, 1992.

(7) Lehn, J.-M. *Supramolecular Chemistry*; VCH: Weinheim, 1995.

(8) Balzani, V.; Venturi, M.; Credi, A. *Molecular Devices and Machines*; Wiley-VCH, 2003.

(9) *Supramolecular Catalysis*; van Leeuwen, P. W. N. M., Ed.; Wiley-VCH, 2008.

(10) Ariga, K.; Kunitake, T. *Supramolecular Chemistry - Fundamentals and Applications*; Springer, 2006.

(11) *Molecular Encapsulation*; Brinker, H. U.; Mieusset, J.-L., Eds.; 1st ed.; Wiley, 2010.

(12) Steed, J. W.; Atwood, J. L. *Supramolecular Chemistry*; Wiley, 2000.

(13) Philp, D.; Stoddart, J. F. *Angew. Chem.* **1996**, *108*, 1242–1286; Philp, D.; Stoddart, J. F. *Angew. Chem. Int. Ed.* **1996**, *35*, 1154-1196.

(14) Berg, J. M.; Tymoczyko, J. L.; Stryer, L. *Biochemistry*; 5th ed.; W.H. Freeman: New York, 2002.

(15) Lodish, H.; Berk, A.; Matsudaira, P.; Kaiser, C. A.; Krieger, M.; Scott, M. P. *Molecular Cell Biology*; 5th ed.; W.H. Freeman: New York, 2003.

(16) Voet, D.; Voet, J. G.; Pratt, C. W. *Lehrbuch der Biochemie*; Wiley, 2002.

(17) Leininger, S.; Olenyuk, B.; Stang, P. J. *Chem. Rev.* **2000**, *100*, 853–908.

(18) Ercolani, G. *J. Am. Chem. Soc.* **2003**, *125*, 16097–16103.

(19) Garrett, T. M.; Koertt, U.; Lehn, J.-M. *J. Phys. Org. Chem.* **1992**, *5*, 529–532.

(20) Hamacek, J.; Borkovec, M.; Piguet, C. *Chem. Eur. J.* **2005**, *11*, 5227–5237.

(21) Canard, G.; Piguet, C. *Inorg. Chem.* **2007**, *46*, 3511–3522.

(22) Kiehne, U.; Weilandt, T.; Lützen, A. *Org. Lett.* **2007**, *9*, 1283–1286.

(23) Dalla Favera, N.; Kiehne, U.; Bunzen, J.; Hytteballe, S.; Lützen, A.; Piguet, C. *Angew. Chem.* **2010**, *122*, 129–132; Dalla Favera, N.; Kiehne, U.; Bunzen, J.; Hytteballe, S.; Lützen, A.; Piguet, C. *Angew. Chem. Int. Ed.* **2010**, *49*, 125-128.

(24) Yoshizawa, M.; Klosterman, J. K.; Fujita, M. *Angew. Chem.* **2009**, *121*, 3470–3490; Yoshizawa, M.; Klosterman, J. K.; Fujita, M. *Angew. Chem.* **2009**, *48*, 3418–3438.

(25) Sunatsuki, Y.; Ohta, H.; Kojima, M.; Ikuta, Y.; Goto, Y.; Matsumoto, N.; Iijima, S.; Akashi, H.; Kaizaki, S.; Dahan, F.; Tuchagues, J.-P. *Inorg. Chem.* **2004**, *43*, 4154–4171.

(26) Bilbeisi, R. a; Zarra, S.; Feltham, H. L. C.; Jameson, G. N. L.; Clegg, J. K.; Brooker, S.; Nitschke, J. R. *Chem. Eur. J.* **2013**, 1–6.

(27) Tuna, F.; Lees, M. R.; Clarkson, G. J.; Hannon, M. J. *Chem. Eur. J.* **2004**, *10*, 5737–5750.

(28) Cambi, L.; Malatesta, L. *Ber. Dtsch. Chem. Ges.* **1937**, *70*, 2067–2078.

(29) Gütlich, P.; Goodwin, H. A. *Top. Curr. Chem.* **2004**, *233*, 1–47.

(30) Chappert, C.; Fert, A.; Van Dau, F. N. *Nat. Mat.* **2007**, *6*, 813–823.

(31) Kahn, O.; Martinez, C. J. *Science,* **1998**, *279*, 44–48.

(32) Nihei, M.; Shiga, T.; Maeda, Y.; Oshio, H. *Coord. Chem. Rev.* **2007**, *251*, 2606–2621.

(33) Duriska, M. B.; Neville, S. M.; Moubaraki, B.; Cashion, J. D.; Halder, G. J.; Chapman, K. W.; Balde, C.; Létard, J.-F.; Murray, K. S.; Kepert, C. J.; Batten, S. R. *Angew. Chem.* **2009**, *121*, 2587–2590; Duriska, M. B.; Neville, S. M.; Moubaraki, B.; Cashion, J. D.; Halder, G. J.; Chapman, K. W.; Balde, C.; Létard, J.-F.; Murray, K. S.; Kepert, C. J.; Batten, S. R. *Angew. Chem.* **2009**, *14*, 2428-2431.

(34) Bunzen, J. Synthese enantiomerenreiner BINOL-Liganden zur Darstellung helicaler mehrkerniger Metallkomplexe, Dissertation, Rheinische Friedrich-Wilhelms-Universität Bonn, 2009.

(35) Volbach, L. Y. Synthese von zweifach funktionalisierten aromatischen 5-Ring-Heterozyklen als Einstieg zur Darstellung von Eisen(II)-Spin-Cross-Over-Komplexen, Bachelor Thesis, Rheinischen Friedrich-Wilhelms-Universität Bonn, 2012.

(36) Grubb, A.; Schmidt, M.; Seed, A.; Sampson, P. *Synthesis* **2012**, *44*, 1026–1029.

(37) Dolci, L.; Dolle, F.; Valette, H.; Vaufrey, F.; Fuseau, C.; Bottlaender, M.; Crouzel, C. *Bioorg. Med. Chem.* **1999**, *7*, 467–479.

(38) Hama, Y.; Nobuhara, Y.; Aso, Y.; Otsubo, T. *Bull. Chem. Soc. Jpn.* **1988**, *61*, 1683–1686.

(39) Bouillon, A.; Lancelot, J.-C.; Collot, V.; Bovy, P. R.; Rault, S. *Tetrahedron* **2002**, *58*, 2885–2890.

(40) King, A. O.; Okado, N.; Negishi, E.-I. *Chem. Commun.* **1977**, 683–684.

(41) Shivanyuk, A.; Rebek, J. *J. Am. Chem. Soc.* **2002**, *124*, 12074–12075.

(42) Mukhopadhyay, P.; Wu, A.; Isaacs, L. *J. Org. Chem* **2004**, *69*, 6157–6164.

(43) Kramer, R.; Lehn, J.; Marquis-Rigault, A. *Proc. Nat. Acad. Sci. USA.* **1993**, *90*, 5394–5398.

(44) Stang, P. J.; Cao, D. H.; Saito, S.; Arif, A. M. *J .Am. Chem. Soc.* **1995**, *117*, 6213–6283.

(45) Weilandt, T.; Kiehne, U.; Bunzen, J.; Schnakenburg, G.; Lützen, A. *Chem. Eur. J.* **2010**, *16*, 2418–2426.

(46) Tröger, J. *J. Prakt. Chem.* **1887**, *36*, 225–245.

(47) Dolenský, B.; Elguero, J.; Král, V.; Pardo, C.; Valík, M. *Adv. Heterocycl. Chem.* **2007**, *93*, 1–56.

(48) Dolenský, B.; Havlík, M.; Král, V. *Chem. Soc. Rev.* **2012**, *41*, 3839–3858.

(49) Spielman, M. A. *J. Am. Chem. Soc.* **1935**, 583–585.

(50) Valík, M.; Strongin, R. M.; Král, V. *Supramol. Chem.* **2005**, *17*, 347–367.

(51) Goldberg, Y.; Alper, H. *Tetrahedron Lett.* **1995**, *36*, 369–372.

(52) Cowart, M. D.; Sucholeiki, I.; Bukownik, R. R.; Wilcox, C. S. *J .Am. Chem. Soc.* **1988**, *110*, 6204–6210.

(53) Gomberg, M.; Clarkson, R. G. *J. Am. Chem. Soc.* **1930**, *52*, 2881–2891.

(54) Prelog, V. *Pure Appl. Chem.* **1978**, *50*, 893–904.

(55) Prelog, V.; Bedekovit, D. *Helv. Chim. Acta.* **1979**, *62*, 2285–2302.

(56) Prelog, V. V.; Kovaeevik, M.; Egli, M. *Angew. Chem.* **1989**, *101*, 1173–1178; *Angew. Chem. Int. Ed.* **1989**, *28*, 2274-2278

(57) Prelog, V.; Mutak, S. *Helv. Chim. Acta.* **1983**, *66*, 2274–2278.

(58) Haas, G.; Prelog, V. *Helv. Chim. Acta.* **1969**, *52*, 1202–2018.

(59) Thiemann, F.; Piehler, T.; Haase, D.; Saak, W.; Lützen, A. *Eur. J. Org. Chem.* **2005**, *2005*, 1991–2001.

(60) Weisburger, J. H.; Weisburger, E. K.; Ray, F. E. *J .Am. Chem. Soc.* **1950**, *72*, 4253–4255.

(61) Sutcliffe, F. K.; Shahidi, H. M.; Patterson, D. *J. Soc. Dye. Colour* **1978**, 306–309.

(62) Huang, X.; Buchwald, S. L. *Org. Lett.* **2001**, *3*, 3417–3419.

(63) Stobe, C. Ein neuer synthetischer Zugang zum Hamilton-Phosphonat, Diplomarbeit, Rheinischen Friedrich-Wilhelms-Universität Bonn, 2010.

(64) Miyaura, N.; Yamada, K.; Suzuki, A. *Tetrahedron Lett.* **1979**, *36*, 3437–3440.

(65) Miyaura, N.; Suzuki, A. *Chem. Commun.* **1979**, *19*, 866–867.

(66) Brückner, R. *Reaktionsmechanismen*; 3rd ed.; Elsevier, 2004.

(67) Sonogashira, K.; Tohda, Y.; Hagihara, N. *Tetrahedron Lett.* **1975**, *50*, 4467–4470.

(68) Tamao, K.; Sumitani, K.; Kumada, M. *J .Am. Chem. Soc.* **1972**, *94*, 4374–4376.

(69) Hovorka, R.; Hytteballe, S.; Piehler, T.; Meyer-Eppler, G.; Topic, F.; Rissanen, K.; Lützen, A. *Beilstein J. Org. Chem.* **2014**, *10*, 432–411.

(70) Hovorka, R.; Meyer-Eppler, G.; Piehler, T.; Hytteballe, S.; Engeser, M.; Topić, F.; Rissanen, K.; Lützen, A. *Chem. Eur. J.* **2014**, *20*, 13253–13258.

(71) Wasserman, E. *J. Am. Chem. Soc.* **1960**, *496*, 4433–4434.

(72) Fujita, M.; Yazaki, J.; Ogura, K. *J .Am. Chem. Soc.* **1990**, *112*, 5645–5647.

(73) Fujita, M.; Ibukuro, F.; Seki, H.; Kamo, O.; Imanari, M.; Ogura, K. *J. Am. Chem. Soc.* **1996**, *118*, 899–900.

(74) Fujita, M.; Aoyagi, M.; Ibukuro, F.; Ogura, K.; Yamaguchi, K. *J. Am. Chem. Soc.* **1998**, *120*, 611–612.

(75) Hori, A.; Kumazawa, K.; Kusukawa, T.; Chand, D. K.; Fujita, M.; Sakamoto, S.; Yamaguchi, K. *Chem. Eur. J.* **2001**, *7*, 4142–4149.

(76) Fujita, M.; Tominaga, M.; Hori, A.; Therrien, B. *Acc. Chem. Res.* **2005**, *38*, 369–378.

(77) Seidel, S. R.; Stang, P. J. *Acc. Chem. Res.* **2002**, *35*, 972–983.

(78) Fujita, M.; Nagao, S.; Ogura, K. *J .Am. Chem. Soc.* **1995**, 1649–1650.

(79) Baxter, P.; Lehn, J.-M.; DeCian, A.; Fischer, J. *Angew. Chem. Int. Ed.* **1993**, *32*, 69–72; *Angew. Chem.* **1993**, *105,* 92–95

(80) Caulder, D. L.; Powers, R. E.; Parac, T. N.; Raymond, K. N. *Angew. Chem.* **1998**, *110*, 1996–1999; *Angew. Chem. Int. Ed.* **1998**, *37*, 1840–1843.

(81) Yoshizawa, M.; Takeyama, Y.; Kusukawa, T.; Fujita, M. *Angew. Chem.* **2002**, *114*, 1403–1405; *Angew. Chem.* **2002**, *114*; *Angew. Chem. Int. Ed.* **2002**, *41*, 1347–1349.

(82) Takashima, Y.; Hatanaka, S.; Otsubo, M.; Nakahata, M.; Kakuta, T.; Hashidzume, A.; Yamaguchi, H.; Harada, A. *Nat. Commun.* **2012**, *3*, 1–8.

(83) Coskun, A.; Banaszak, M.; Astumian, R. D.; Stoddart, J. F.; Grzybowski, B. a. *Chem. Soc. Rev.* **2012**, *41*, 19–30.

(84) Amabilino, D. B.; Stoddart, J. F. *Chem. Rev.* **1995**, *95*, 2725–2828.

(85) Bunzen, J.; Iwasa, J.; Bonakdarzadeh, P.; Numata, E.; Rissanen, K.; Sato, S.; Fujita, M. *Angew. Chem.* **2012**, *124*, 3215–3217; *Angew. Chem. Int. Ed.* **2012**, *51*, 3161-3163.

(86) Gütz, C. Synthese von Liganden mit unterschiedlichen Metallkoordinationseinheiten und deren Selbstorganisation zu metallosupramolekularen Aggregaten, Dissertation, Rheinischen Friedrich-Wilhelms-Universität Bonn, 2013.

(87) Li, D.; Zhou, W.; Landskron, K.; Sato, S.; Kiely, C. J.; Fujita, M.; Liu, T. *Angew. Chem. Int. Ed.* **2011**, *50*, 5182–5187. *Angew. Chem.* **2011**, *123*, 5288-5293.

(88) Li, D.; Zhang, J.; Landskron, K.; Liu, T. *J. Am. Chem. Soc.* **2008**, *130*, 4226–4227.

(89) Saha, M. L.; Schmittel, M. *Org. Biom. Chem.* **2012**, *10*, 4651–4684.

(90) Schmittel, M.; Mahata, K. *Chem. Commun.* **2010**, 4163–4165.

(91) Schmittel, M.; Kalsani, V.; Mal, P.; Bats, J. W. *Inorg. Chem.* **2006**, *45*, 6370–6377.

(92) Schmittel, M.; Mahata, K. *Chem. Commun.* **2008**, 2550–2552.

(93) Yang, H.-B.; Ghosh, K.; Northrop, B. H.; Zheng, Y.-R.; Lyndon, M. M.; Muddiman, D. C.; Stang, P. J. *J. Am. Chem. Soc.* **2007**, *129*, 14187–14189.

(94) Kishore, R. S. K.; Paululat, T.; Schmittel, M. *Chem. Eur. J.* **2006**, *12*, 8136–8149.

(95) Petitjean, A.; Kyritsakasb, N.; Lehn, J.-M. *Chem. Commun.* **2004**, 1168–1169.

(96) Wu, H.-B.; Wang, Q.-M. *Angew. Chem.* **2009**, *121*, 7479–7481; *Angew. Chem. Int. Ed*. **2009**, *48*, 7343-7345

(97) Seeber, G.; Tiedemann, B. E. F.; Raymond, K. N. *Top. Curr. Chem.* **2006**, *265*, 147–183.

(98) Wolf, C.; Tumambac, G. E.; Villalobos, C. N. *Synlett* **2003**, 1801–1804.

(99) Coudret, C. *Synth. Commun.* **1996**, *26*, 3543–3547.

(100) Kiehne, U. Synthese dissymmetrischer Liganden und deren Nutzung zum Aufbau mehrkerniger helicaler Metallkomplexe, Dissertation, Rheinischen Friedrich-Wilhelms-Universität Bonn, 2007.

(101) Höger, S.; Bonrad, K. *J . Org. Chem* **2000**, *65*, 2243–2245.

(102) Gaefke, G.; Höger, S. *Synthesis* **2008**, *2008*, 2155–2157.

(103) Sharma, G. V. M.; Reddy, K. L.; Sree Lakshmi, P.; Radha Krishna, P. *Tetrahedron Lett.* **2004**, *45*, 9229–9232.

(104) Han, J. H.; Kwon, Y. E.; Sohn, J.-H.; Ryu, D. H. *Tetrahedron* **2010**, *66*, 1673–1677.

(105) Ramesh, C.; Ravindranath, N.; Das, B. *J. Org. Chem.* **2003**, *68*, 7101–7103.

(106) Hünig, S.; Märkl, G.; Sauer, J. *Einführung in die apparativen Methoden in der Organischen Chemie*; Institut für Organische Chemie der Universität Regensburg: Regensburg, 1994.

(107) Katritzky, A. R.; Law, K. W. *Magn. Reson. Chem.* **1988**, *26*, 129–133.

(108) Stanetty, P.; Schnu, M.; Mihovilovic, M. D. *J. Org. Chem.* **2006**, *71*, 3754–3761.

(109) L'Helgoual'ch, J.-M.; Seggio, A.; Chevallier, F.; Yonehara, M.; Jeanneau, E.; Uchiyama, M.; Mongin, F. *J. Org. Chem.* **2008**, *73*, 177–183.

(110) Gao, W.-Y.; Yan, W.; Cai, R.; Williams, K.; Salas, A.; Wojtas, L.; Shi, X.; Ma, S. *Chem. Commun.* **2012**, *48*, 8898–8900.

(111) Grunder, S.; Huber, R.; Horhoiu, V.; González, M. T.; Schönenberger, C.; Calame, M.; Mayor, M. *J. Org. Chem.* **2007**, *72*, 8337–8344.

(112) Plater, M. J.; Sinclair, J. P.; Aiken, S.; Gelbrich, T.; Hursthouse, M. B. *Tetrahedron* **2004**, *60*, 6385–6394.